ADA041321

RADC-TR-77-160

FINAL TECHNICAL REPORT
April 1977

DESIGN AND ANALYSIS OF BIFURCATED TWIN DIELECTRIC SLAB LOADED RECTANGULAR WAVEGUIDE DUAL FREQUENCY ARRAY ELEMENTS

RAYTHEON COMPANY
MISSILE SYSTEMS DIVISION
Bedford, Mass.

This research was partially supported by
the Air Force In-House Laboratory
Independent Research Fund

Approved for Public Release
Distribution Unlimited

ROME AIR DEVELOPMENT CENTER
AIR FORCE SYSTEMS COMMAND
Griffiss Air Force Base, NY 13341

This report has been reviewed by the RADC Information Office (OI) and is releasable to the National Technical Information Service (NTIS). At NTIS it will be releasable to the general public, including foreign nations.

This technical report has been reviewed and approved for publication.

APPROVED: Robert J. Mailloux

ROBERT J. MAILLOUX
Project Engineer

APPROVED: Allan C. Schell
ALLAN C. SCHELL
Acting Chief,
Electromagnetic Sciences Division

FOR THE COMMANDER: John P. Huss

Plans Office

UNCLASSIFIED

SECURITY CLASSIFICATION OF THIS PAGE (When Data Entered)

REPORT DOCUMENTATION PAGE

READ INSTRUCTIONS BEFORE COMPLETING FORM

1. REPORT NUMBER: RADC-TR-77-160	2. GOVT ACCESSION NO.
3. RECIPIENT'S CATALOG NUMBER	
4. TITLE (and Subtitle): Design and Analysis of Bifurcated Twin Dielectric Slab Loaded Rectangular Waveguide Dual Frequency Array Elements	5. TYPE OF REPORT & PERIOD COVERED: Final Jan 76 — Feb 77
	6. PERFORMING ORG. REPORT NUMBER: BR-9674
7. AUTHOR(s): J. H. Pozgay, M. Fassett, L. R. Lewis	8. CONTRACT OR GRANT NUMBER(s): F19628-75-C-0197
9. PERFORMING ORGANIZATION NAME AND ADDRESS: Raytheon Company, Missile Systems Division, Bedford, Massachusetts 01730	10. PROGRAM ELEMENT, PROJECT, TASK AREA & WORK UNIT NUMBERS: ILIR5B01
11. CONTROLLING OFFICE NAME AND ADDRESS: Deputy for Electronic Technology (RADC), Hanscom AFB, Massachusetts 01731, Contract Monitor: R. J. Mailloux/ETER	12. REPORT DATE: 1 March 1977
	13. NUMBER OF PAGES: 248
14. MONITORING AGENCY NAME & ADDRESS (if different from Controlling Office)	15. SECURITY CLASS (of this report): Unclassified
	15a. DECLASSIFICATION/DOWNGRADING SCHEDULE

16. DISTRIBUTION STATEMENT (of this Report)

Approved for public release; distribution unlimited.

17. DISTRIBUTION STATEMENT (of the abstract entered in Block 20, if different from Report)

18. SUPPLEMENTARY NOTES

This research was partially funded by the Air Force In-House Laboratory Independent Research Fund.

19. KEY WORDS (Continue on reverse side if necessary and identify by block number)

Dual Frequency Array Element
Stripline Fed Notch Exciter
Infinite Array Analysis

20. ABSTRACT (Continue on reverse side if necessary and identify by block number)

The design and analysis of a unique dual frequency array element and three probe element exciter for aperture sharing at two widely separated frequency bands is presented. The bifurcated twin dielectric slab loaded rectangular waveguide element simultaneously supports a single low frequency band phase center and four independently controllable high frequency phase centers, resulting in the formation of an independent radiating beam in each band. The principle element design objective is to minimize the

247 680

20. Abstract (Cont.)

element count while maximizing the rejection of high frequency grating lobes. It is shown that the slab loaded element results in 21 percent fewer phase and frequency control per unit array area than an alternate diplexed wide band element dual frequency concept for a scanning array operated over 15 percent bands centered at 4 and 8 GHz.

The radiation and coupling properties of the array element are developed from a scattering formulation of the feedguide - free space discontinuity for the fully excited infinite array. Comparison of theoretical performance for triangular and rectangular grid configurations shows that considerable improvement in high frequency grating lobe rejection is obtained from the triangular lattice.

To characterize the transverse aperture fields, a complete modal description of propagation in the inhomogeneously loaded guide is obtained through a component-by-component comparison of the degenerate eigenfunctions of the structure.

Simulator measurement of an element designed to provide 60° scan coverage over 15 percent bands centered at 4 and 8 GHz shows excellent agreement with theoretical predictions for main beam gain loss in the measurement bands 4. - 4.32 GHz and 7.36 - 8.08 GHz. Over the remainder of the operating bands, the agreement is assumed to be equally close.

Initial experimental design data for unidirectional stripline fed notch is presented. The notch probe is shown to result in better than 2:1 mismatch over greater than 10 percent measurement bands when looking into load terminated twin slab feedguides, and greater than 50 dB probe isolation over the 4 GHz band. Over the 8 GHz, probe isolation is approximately 12 dB and remains a problem for future design efforts.

EVALUATION

1. This report is the Final Report of Contract F19628-75-C-0197. It covers the analytical and experimental investigations of the bifurcated twin dielectric slab loaded rectangular waveguide dual frequency array element. The report describes analytical studies of the infinite array and documents operation at two 15% frequency bands centered at 4GHz and 8GHz. In addition, the report presents the experimental results and examination of the strip-line fed notch exciter which is used at both frequency ranges.

Robert J. Mailloux

ROBERT J. MAILLOUX
Project Engineer

ACKNOWLEDGEMENT

The authors would like to extend their appreciation to Ms. Joni Bursey for her considerable help in the preparation of this manuscript.

TABLE OF CONTENTS

Table of Contents (Cont.)

List of Illustrations

List of Illustrations (Continued)

List of Illustrations (continued)

List of Illustrations (continued)

List of Tables

1. INTRODUCTION AND SUMMARY

This report summarizes the analytical and experimental investigations of the infinite array radiation and coupling properties of bifurcated twin dielectric slab loaded rectangular waveguide dual frequency array elements[1] conducted under Contract F19628-75-C-0197. Specifically, the report presents:

- The complete analysis of the element in infinite array configurations.
- Theoretically determined element/grid design trade-off conclusions, leading to a proposed configuration for operation over 15% bands centered at 4GHZ and 8GHZ.
- Experimental verification of the analytical results and the examination of a unique strip-line fed notch antenna mode exciter.
- The computational details and computer programs developed during the study.

The bifurcated twin dielectric slab loaded rectangular waveguide dual frequency array element shown in Figure 1 is a unique concept for providing simultaneous aperture usage at two widely separate frequency bands. At low frequency both upper and lower halves of the waveguide are excited in-phase with equiamplitude signals. For moderate slab loading (assuming relatively thin slabs) this array will behave similarly to a rectangular waveguide array excited in the TE_{10} mode with scan behavior associated with these elements in the basic lattice (either rectangular or triangular). At the high frequency the first odd and even half-waveguide modes can be independently specified such that four phase centers are defined; within a single low frequency cell the fields are confined predominately to the slab regions.

For practical array designs, the low and high frequency lattice cells are identifical, and the principal element/grid design trade-off is to minimize the number of phase centers (or phase shifters) while maintaining main beam purity and gain over a specified scan volume, particularly in the high frequency band. Consequently the lattice is selected such that element spacing is not optimum for either band, but presents the best compromise of element count versus grating

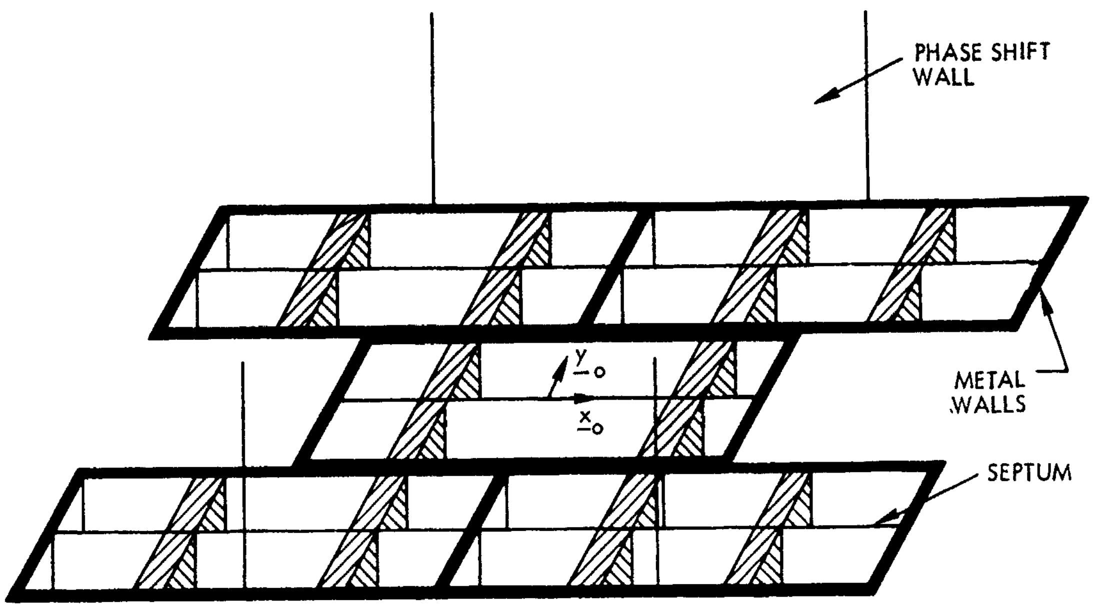

Figure 1. Bifurcated Twin Dielectric Slab Loaded Rectangular Waveguide Element in Triangular Grid

lobe free scan volume in the high frequency band. At scan conditions for which high frequency grating lobes are entering or present, the multimode aperture excitation is adjusted (slightly) to cancel the grating lobe. These considerations are treated fully in Section 2 which gives details of the analysis of array performance, and section 4 which summarizes design tradeoffs and experimental results.

The application of the twin dielectric slab loaded element to dual frequency aperture sharing follows from the unique propagation properties of the inhomogeneously loaded structure. The symmetric loaded guide, shown in Figure 2, is inherently wideband. At sufficiently low frequency, a single guide mode (the LSE_{10} mode) propogates and has an electric field distribution somewhat broader than the homogeneously loaded guide TE_{10} distribution. As frequency is increased, the LSE_{20} mode enters, having electric field distribution similar to the TE_{20} distribution of the homogeneously loaded guide. Concurrently, the LSE_{10} distribution begins to develop a minimum along the guide mid-plane. At sufficiently high frequency, the distributions become essentially identical, except for symmetry about the mid-plane, and the ratio of longitudinal wavenumbers approaches unity.

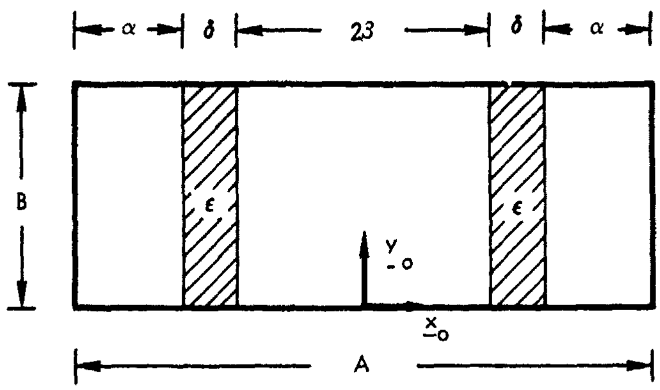

Figure 2. Symmetric Inhomogeneously Loaded Rectangular Waveguide

By appropriate selection of guide, slab permittivity, and operating points such that only the two modes propagate, the guide will simultaneously support a single propagating low frequency mode with phase center at the midplane, and a conglomerate high frequency distribution with two independent phase centers at (roughly) the slab centers. The analysis of propagation in the inhomogenously loaded guide is given in Section 3.

In general, he dispersion in the inhomogeneously loaded guide is not linear in frequency. Consequently, the use of a bidirectional exciter requires load terminations at the back of the guide to ensure the proper aperture field phase at both frequencies, and results in a 3 dB power loss. This difficulty is alleviated by a unique unidirectional exciter consisting of three stripline fed flared notch antennas[2,3,4] inserted into the back of the feedguide in suc h a manner as to provide a minimum of 25 dB frequency band isolation. Preliminary experimental investigation of this exciter design concept was begun during this study, and is discussed in Section 5.

Four appendices are included. Appendices A, B, and C give the details of the analysis. Explicit expansions of modal coupling coefficient integrals are given in Appendix A. In Appendix B, the derivation of the differential equations relating feedguide modal fields is given. And in Appendix C, explicit expressions for feedguide mode orthonormalization integrals are given. The remaining appendix gives complete listings of all programs required to reproduce the numerical results given in this report.

A time dependence $e^{j\omega t}$ is assumed throughout.

2.0 ANALYSIS OF INFINITE PHASED ARRAYS OF BIFURCATED TWIN DIELECTRIC SLAB LOADED RECTANGULAR WAVEGUIDE DUAL FREQUENCY ELEMENTS

In this section, the formal solution for the radiation properties of the element in infinite array configuration is presented. The unique property of the bifurcated twin dielectric slab loaded rectangular waveguide dual frequency array element is that it possesses five phase centers: one, associated with the low frequency band operation; and the remaining four, with a high frequency band. By appropriate exciter design, the element can simultaneously operate over both bands.

The basic element is shown in Figure 3. Arrays are formed by stacking these elements in rectangular or triangular grid configuration. The element consists of a rectangular waveguide bifurcated in the E-plane by a septum of thickness δ. Outer dimensions are D_x and D_y, and inner dimensions, A and B', where D_x and A are associated with the x coordinate. Four half height lossless dielectric slabs of thickness δ and relative dielectric constant ε_r are located at distance $\alpha + \delta/2$ (on center) from the narrow

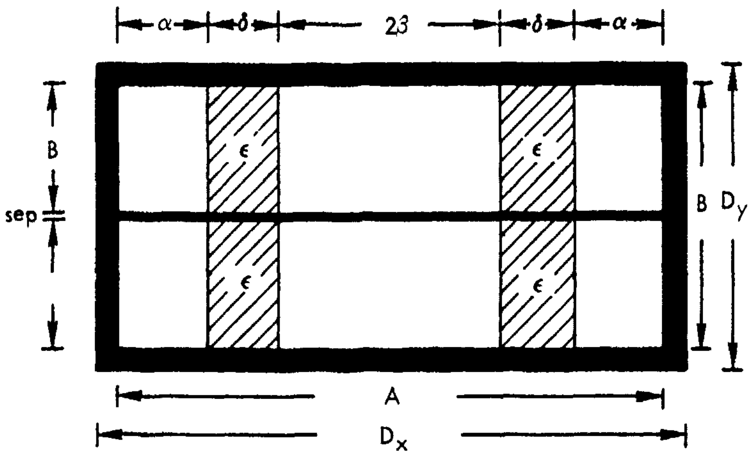

Figure 3. Dual Frequency Element

walls. At low frequency, a phase center is maintained at the element center (i.e., over the septum) by exciting the LSE_{10} mode equally in the two half guides. At high frequency, four independent phase centers, at roughly the four slab centers, are formed by appropriately exciting the LSE_{10} and LSE_{20} modes in each half guide.

When the elements are arrayed in a rectangular grid the element lattice vectors, $\underline{s}_1$ and $\underline{s}_2$ are as shown in Figure 4a, provided the septum thickness, δ, is not equal to $(D_y - B')/2$. When $\delta = (D_y - B')/2$, the low frequency lattice is as shown in Figure 4a, and the high frequency lattice is as shown in Figure 4b, When arrayed in a triangular grid, the lattice vectors are defined as in Figure 5, regardless of operating frequency or septum thickness.

In section 2.1, the formal solution for active array element pattern is given. The method of solution is similar to that developed by Lewis, et al[5] for the analysis of a parallel plate array with protruding dielectric. In the present work, the formalism is extended to two dimensional array cells, and the unique dual frequency unit cell geometry is accounted for. In section 2.2 numerical results are presented and particular attention is given to the disposition of high frequency band grating lobes. Discussion of grating lobe suppression is deferred

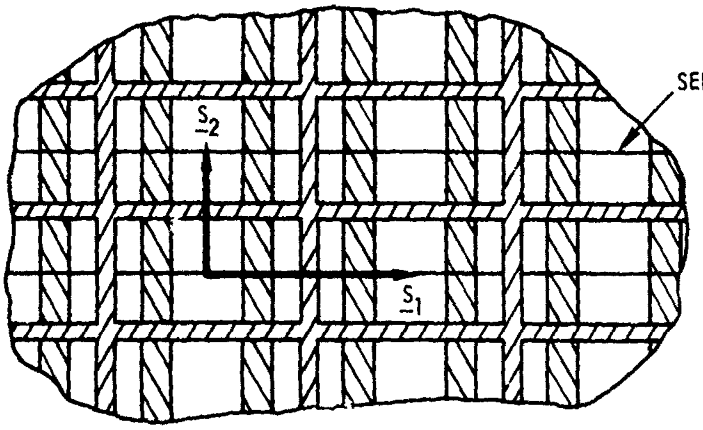

(a) Septum Thickness, s = Dy - B', High and Low Frequencies

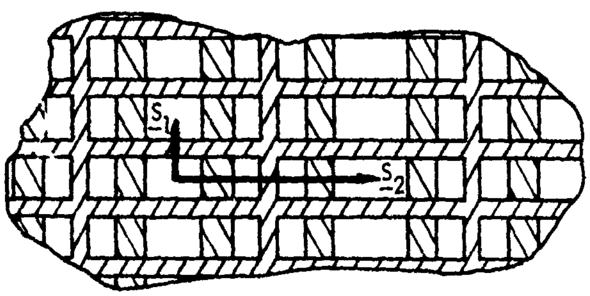

(b) Septum Thickness gs = Dy - B', High Frequency

Figure 4. Lattice Definitions for Rectangular Grids

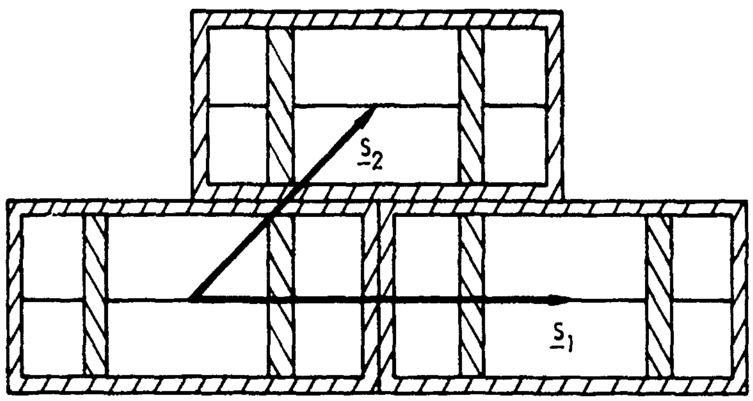

Figure 5. Lattice Definitions for Triangular Grid - Either Frequency Band

to section 4.1. In section 2.3, numerical results are checked against published data for several limiting geometries.

2.1 Active Array Element Pattern

The active array element pattern is determined from a unit cell formulation of scattering at the feedguide free space interface. The interface is taken as coincident with the $z = 0$ plane, with the array elements occupying the $z < 0$ half space. The scattering matrix, $\underline{\underline{S}}$, which relates feedguide modal voltages to the modal voltages of the space harmonics, in the manner indicated by the network in Figure 6, is obtained by matching the transverse-to-z fields in the cell across the interface. The field matching is accomplished *via* Galerkin's method, from which the scattering formalism follows directly. Active array transmission coefficient is then obtained from the network. In the following discussion, the assumed cell configuration is that shown in Figure 4a. The extension of these results to either of the other two cases is straight forward.

For the configuration of Figure 4a, the unit cell perimeter may be taken as coincident with the element outside perimeter. Thus, the unit cell overlays two

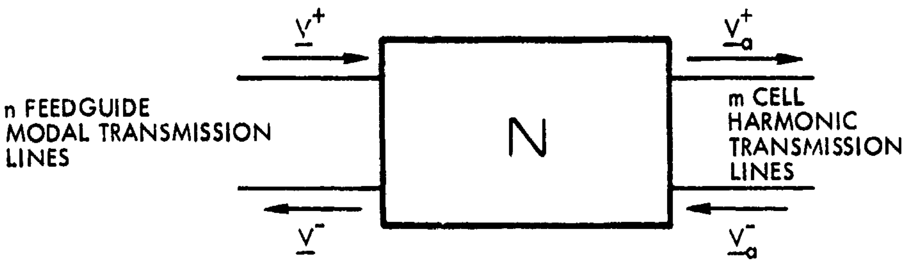

Figure 6. Network Representation of Unit Cell Discontinuity

independent aperture regions and the modal representation of total transverse-to-z electric and magnetic fields at $z = 0^-$ is given as

$$\underline{E}_t^-(\underline{s}) = U(y)\sum_i V_{>i}\underline{e}_i^>(\underline{s}) + U(-y)\sum_j V_{<j}\underline{e}_i^<(\underline{s}) \tag{1}$$

$$\underline{H}_t^-(\underline{s}) = U(y)\sum_i I_{>i}\underline{h}_i^>(\underline{s}) + U(-y)\sum_j I_{<j}\underline{h}_i^<(\underline{s}) \tag{2}$$

where

$$U(\xi) = \begin{cases} 1, \xi>0 \\ 0, \xi>0 \end{cases} \tag{3}$$

The subscripts > and < are used to distinguish the two aperture regions. $V_{\gtrless i}$ and $I_{\gtrless i}$ are modal voltage and current coefficients, and are related by

$$I_{\gtrless i} = Y_{\gtrless i}\, V_{\gtrless i} \tag{4}$$

where $Y_{\gtrless i}$ is the modal admittance of the i^{th} aperture mode, and the single ordering index i is used to simplify notation. The mode functions $\underline{e}$ and $\underline{h}$ are given in section 3.1.

At $z = 0^+$, the unit cell guide representation of transverse-to-z fields, over the full cell, is

(5) $$\underline{E}_t^+(\underline{s}) = \sum_{pqr} V_{apqr}\underline{e}_{apqr}(\underline{s})$$

(6) $$\underline{H}_t^+(\underline{s}) = \sum_{pqr} I_{apqr}h_{apqr}(\underline{s})$$

where (6)

(7) $$\underline{h}_{apqr}(\underline{s}) = \underline{z}_o x \underline{e}_{apqr}(\underline{s})$$

(8) $$\underline{e}_{apqr}(\underline{s}) = \frac{e^{-j\underline{k}_t \cdot \underline{s}}}{\sqrt{c}|\underline{k}_{tpq}|}[(2-r)\underline{k}_{tpq}+(r-1)\underline{k}_{tpq}x\underline{z}_o]$$

(9) $$r = \begin{cases} 1, \text{ for E modes with respect to z} \\ 2, \text{ for H modes with respect to z} \end{cases}$$

(10) $$\underline{k}_{tpq}=k_{xpq}\underline{x}_o+k_{ypq}\underline{y}_o=k\sin\theta_o(\cos\phi_o\underline{x}_o+\sin\phi_o\underline{y}_o)$$
$$+p\underline{t}_1+q\underline{t}_2$$

(11) $$k_{xpq} = k\sin\theta_o\cos\phi_o+pt_{1x} + qt_{2x}$$

(12) $$k_{ypq} = k\sin\theta_o\sin\phi_o + pt_{1y} + qt_{2y}$$

(13) $$\underline{t}_i \cdot \underline{s}_j = 2\Pi\delta_{ij},\ i,j = 1,2$$

(14) $$c = |\underline{s}_1 x \underline{s}_2|$$

δ_{ij} is Kronecker's delta, $\underline{s}_j$ are the lattice vectors, as shown, for example, in Figures 4 a,b, and 5, and θ_o and ϕ_o are the spatial look angles. The mode function normalization is taken such that $V_{apqr}I^*_{apqr}$ is power, and such that the modal voltage and current are related by

(15) $$I_{apqr} = Y_{apqr}V_{apqr}$$

where Y_{apqr} is a modal admittance, given as

(16) $$Y_{apqr} = \begin{cases} k_o/k_{zpq}\eta_o, & r = 1 \\ k_{zpq}/k_o\eta_o, & r = 2 \end{cases}$$

$k_o = 2\Pi/\lambda$ is the free space wavenumber and η_o is the free space impedance 377 ohms. The indices pqr and pq, which appear explicitly in equations (5) through (12) will henceforth be replaced by the single index σ.

Matching transverse fields at the aperture plane of the unit cell gives

$$(17)\qquad \sum_{\sigma} V_{a\sigma}\underline{e}_{a\sigma}(s) = \begin{cases} U(y)\sum_{i} V_{>i}\underline{e}_{i}^{>}(\underline{s}) + U(-y)\sum_{j} V_{<j}\underline{e}_{j}^{>}(s), & \text{in the aperture} \\ 0, \text{ elsewhere} & \end{cases}$$

and

$$(18)\qquad \sum_{\sigma} I_{a\sigma}\underline{h}_{a\sigma}(\underline{s}) = U(y)\sum_{i} I_{>i}\underline{h}_{i}^{>}(s) + U(-y)\sum_{j} I_{<j}\underline{h}_{j}^{<}(\underline{s}), \quad \text{in the aperture}$$

Approximate solutions for the parameters of the network in Figure 6 are obtained when the modal series are truncated. As a result of the truncation, the continuity equations (i.e., equations (17) and (18) can no longer be exactly satisfied, and vector error terms $\underline{\Delta}_1$ and $\underline{\Delta}_2$ must be inserted to restore the equality. These error terms are given as

$$(19)\qquad \underline{\Delta}_1 = \begin{cases} \sum_{\sigma}^{M} V_{a\sigma}\underline{e}_{a\sigma}(\underline{s}) - U(y)\sum_{i}^{I} V_{>i}\underline{e}_{i}^{>}(\underline{s}) + U(-y)\sum_{j}^{J} V_{<j}\underline{e}_{j}^{<}(\underline{s}), & \text{in the apertures} \\ \sum_{\sigma}^{M} V_{a\sigma}\underline{e}_{a\sigma}(\underline{s}), \text{ elsewhere} & \end{cases}$$

and

$$(20)\qquad \underline{\Delta}_2 = \sum_{\sigma}^{M} I_{a\sigma}\underline{h}_{a\sigma}(s) - U(y)\sum_{i}^{I} I_{>i}\underline{h}_{i}^{>}(\underline{s}) - U(-y)\sum_{j}^{J} I_{<j}\underline{h}_{j}^{<}(\underline{s}), \quad \text{in the apertures.}$$

It is now required that the projections of $\underline{\Delta}_1$ and $\underline{\Delta}_2$ onto the appropriate modal spaces be zero.

The domain of definition of $\underline{E}_t^+(\underline{s})$ is over the entire unit cell, and the domain of $\underline{E}_t^-(\underline{s})$ may be artificially extended over the metalic portions of the cell. Thus, the domain of $\underline{\Delta}_1$ is the unit cell, and the modal subset spanning the space are the $\underline{h}_{a\sigma}(\underline{s})$. Requiring orthogonality of $\underline{\Delta}_1$ to the $\underline{h}_a(\underline{s})$ and performing the inner products over the cell results, after manipulation, in

$$\underline{V}_a = \underline{\underline{E}}^{>}\underline{V}_{>} + \underline{\underline{E}}^{<}\underline{V}_{<} \tag{21}$$

where $\underline{\underline{E}}^{\gtrless}$ is a matrix of coupling coefficients, the elements of which are given as

$$E^{\gtrless}_{\sigma,i} = \int_{1/2 \text{ cell } \gtrless} dA\, \underline{e}_i^{\gtrless}(\underline{s}) \cdot (\underline{h}^*(\underline{s}) \times \underline{z}_o) \tag{22*}$$

The elements of the column vectors $\underline{V}_{\gtrless}$ are the feedguide modal voltages.

The domain of definition of $\underline{\Delta}_2$ is over the aperture only. Therefore, the appropriate basis spanning this space is formed by the concatination of the trunicated modal

*Complete expressions for $E^{\gtrless}_{\sigma,i}$ are given in Appendix A sets which individually span only one or the other f the aperture region spaces. Such a basis may be represented by the partitioned vector $\underline{B}(\underline{s})$, given as

$$(23) \qquad \underline{B}(\underline{s}) = \left\{ \begin{array}{c} U(y) e_i^{>}(\underline{s}) \\ \vdots \\ \hline U(-y) \underline{e}_j^{<}(\underline{s}) \\ \vdots \end{array} \right\}$$

Requiring orthogonality of $\underline{\Delta}_2$ on the space spanned by $\underline{B}(\underline{s})$ results in

$$(24) \qquad \underline{I} = \left\{ \begin{array}{c} \underline{I}_{>i} \\ \cdots\cdots \\ \underline{I}_{<j} \end{array} \right\} = \left\{ \begin{array}{c} \underline{\underline{\lambda}}^{>} \\ \hline \underline{\underline{\lambda}}^{<} \end{array} \right\} \underline{I}_a$$

where $\underline{\underline{\lambda}}^{\gtrless}$ are submatrices of coupling coefficients, the elements of which are given as

$$(25) \qquad \lambda_{i\sigma}^{\gtrless} = \int_{1/2 \text{ aperture } \gtrless} dA [\underline{h}_{a\sigma}(\underline{s}) x \underline{z}_o] \cdot \underline{e}_i^{\gtrless} * (\underline{s})$$

Since the $\underline{e}_i^{>}(s)$ and $\underline{e}_j^{<}(\underline{s})$ may be artificially extended to individually span the appropriate entire half cell,

$$(26) \qquad \lambda_{i,\sigma}^{\gtrless} = E_{\sigma,n}^{\gtrless *}$$

It is convenient, then, to define the partitioned vector $\underline{V}$ such that

$$(27) \qquad \underline{V} = \left\{ \frac{\underline{V}^{>}}{\underline{V}^{<}} \right\}$$

and the partitioned matrix $\underline{\underline{E}}$ as

$$(28) \qquad \underline{\underline{E}} = (\underline{\underline{E}}^{>} | \underline{\underline{E}}^{<})$$

Then, the voltage and current equations, (3-21) and (3-24), respectively, take the form

$$(29) \qquad \underline{V}_a = \underline{\underline{E}}\ \underline{V}$$

$$(30) \qquad \underline{I} = \underline{\underline{E}}^{*t} \underline{I}_a$$

where the asterisk denotes conjugation and the t denotes the transpose operation.

The vectors $\underline{V}$, $\underline{V}_a$, $\underline{I}$, and $\underline{I}_a$ in equations (29) and (30) are total modal voltages and currents. Using the conventions established for the network in Figure 6, assuming that all external sources are zero (i.e. $\underline{V}_a^- \equiv 0$), and manipulating equations (29) and (30) results in an expression for feedguide reflected field voltage coefficients, $\underline{V}^-$, in terms of the active modal excitations, $\underline{V}^+$, given as

$$(31) \qquad \underline{V}^- = \{2[\underline{\underline{Y}} + \underline{\underline{E}}^{*t}\underline{\underline{Y}}_a\underline{\underline{E}}]^{-1}\underline{\underline{Y}}-\underline{\underline{1}}\}\underline{V}^+$$

where $\underline{\underline{1}}$ is the identity matrix.

Let the scattering matrix of the network be defined by

$$(32) \qquad \frac{\underline{V}^-}{\underline{V}_a^+} = \begin{pmatrix} \underline{\underline{S}}_{11} & \underline{\underline{S}}_{12} \\ \underline{\underline{S}}_{21} & \underline{\underline{S}}_{22} \end{pmatrix} \begin{Bmatrix} \underline{V}^+ \\ \hline 0 \\ \vdots \end{Bmatrix}$$

where the scattering blocks have the usual meaning. Then, from equation (31)

$$(33) \qquad \underline{\underline{S}}_{11} = 2[\underline{\underline{Y}} + \underline{\underline{E}}^{*t}\,\underline{\underline{Y}}_a\underline{\underline{E}}]^{-1}\underline{\underline{Y}} - \underline{\underline{1}}$$

and from equation (29)

$$(34) \qquad \underline{\underline{S}}_{21} = \underline{\underline{E}}(\underline{\underline{1}} + \underline{\underline{S}}_{11})$$

with $\underline{V}_a^- \equiv \underline{0}$.

In more standard array configurations, the feedguide and aperture are designed for single feedguide mode propagation in a single frequency band. In these configurations, the active array reflection coefficient is simply the one element of $\underline{\underline{S}}_{11}$ corresponding to reflections in the dominant mode. Defining that matrix element as $T(\theta_0, \phi_0)$, normalized active array element gain pattern is

$$g_e(\theta_0,\phi_0) = (1 - |\Gamma(\theta_0,\phi_0)|)^2 \cos\theta_0 \tag{35}$$

provided no grating lobes have entered real space. Following the entrance of the first grating lobe, it is necessary to track the propagating beams individually, and the relative power in the σ^{th} beam due to the single excited mode (i=1) is

$$P_\sigma(\theta_\sigma,\phi_\sigma) = |T_\sigma(\theta_0,\phi_0)|^2 Y_{a\sigma}/Y_1 \tag{36}$$

where $T_\sigma(\theta,\phi)$ is the (σ,i)th element of the partitioned block $\underline{\underline{S}}_{21}$, and θ_σ and ϕ_σ are the actual location angles of the σ^{th} beam.

Active array element pattern is defined in a different manner for the array of bifurcated twin dielectric slab loaded rectangular waveguides. In this instance, the aperture is always considered to be multimode. In the low frequency range, the LSE_{10} mode (ordered as the i^{th}) is excited equally, in amplitude and phase, in both regions of the aperture. Consequently, for an I-mode feedguide aperture field approximation in both upper and lower regions, the power in the main beam, σ=m, is given, for principle plane scan*, as

$$(37) \qquad P_m(\theta_0,\phi_0) = 1/2\left|S_{21}^{m,i}(\theta_0,\phi_0) + S_{21}^{m,i+I}(\theta_0,\phi_0)\right|^2 Y_{am}/Y_i$$

where $S_{21}^{m,i}(\theta,\phi)$ is the (m,i)th element of $\underline{\underline{S}}_{21}$, and the i^{th} feedguide mode is the propagating LSE_{10} mode. By the definitions in equations (27), (32), and (34), $S_{21}^{m,i}(\theta_0,\phi_0)$ is the voltage transmission coefficient for coupling from the i^{th} mode in the upper aperture region to the m^{th}

---

*Equation (3-37) is strictly valid only for $\theta_0 \neq 0$ and in the principle planes (ϕ=0,Π, or ϕ=Π/2, 3Π/2). For all other scan planes (and at broadside), the total power in the main beam is the sum of the powers in the dominant (p=q=o) E and H modes.

beam in free space; and $S_{21}^{m,i+I}$ is the voltage transmission from the i^{th} mode of the lower aperture region to the m^{th} beam*.

Active array reflection coefficient is also obtained via superposition. For the multimode aperture configuration, it is necessary to independently track all propagating waves in the feedguide. Hence, for low frequency excitation, the total reflected power in the LSE_{10} mode of the upper aperture region is given, for any scan angle, as

$$R^{>}(\theta_0,\phi_0) = 1/2\left|S^{i,i}(\theta_0,\phi_0) + S_{11}^{i,i+I}(\theta_0,\phi_0)\right|^2 \tag{38}$$

For the lower aperture region, the reflected power is

$$R^{<}(\theta_0,\phi_0) = 1/2\left|S_{11}^{i+I,i}(\theta_0,\phi_0) + S_{11}^{i+I,i+I}(\theta_0,\phi_0)\right|^2 \tag{39}$$

where $S_{11}^{r,t}(\theta_0,\phi_0)$ is the voltage scattering coefficient from the r^{th} aperture region mode to the t^{th} aperture region mode. It is evident from these two equations that the reflected powers in the two regions are not necessarily equal. Indeed, it is found that for low frequency excitation, $R^{>}(\theta_0,\phi_0)$ equals $R^{<}(\theta_0,\phi_0)$ only in the H plane of scan.

*It is assumed that the mode ordering in the two aperture regions is the same. This assumption will carry through the remainder of the report.

As an example, reflected power is shown versus E plane scan angle in Figure 7. The element is a WR187 guide with .250" thick slabs of $\varepsilon_r=9$ dielectric located .450", on center, from either narrow wall and with a .032" septum. The operating frequency is 2.5 GHz. There is considerable difference in reflected power between upper and lower regions throughout the scan range $.17 < \sin\theta < .95$. Consequently, low frequency excitation of the upper and lower regions of the element from a common post phase shifter feed point, as is desireable for several low frequency feed concepts, will produce an imbalance at the outputs of the power divider network. Since the impact of this effect on feed and exciter design is beyond the scope of this study, it will be given no further consideration in this report.

At the high frequency band, the element is excited such that four independently controllable phase centers are distributed in the aperture. To maintain this phase center distribution, four propagating modes, two in each region, are excited. The modes are LSE_{10} and LSE_{20}. For sufficiently high frequency and dielectric constants, these two modes have nearly equal dispersion. In addition, to a crude approximation, the modal field distributions, e''_{y10} and e''_{y20} differ

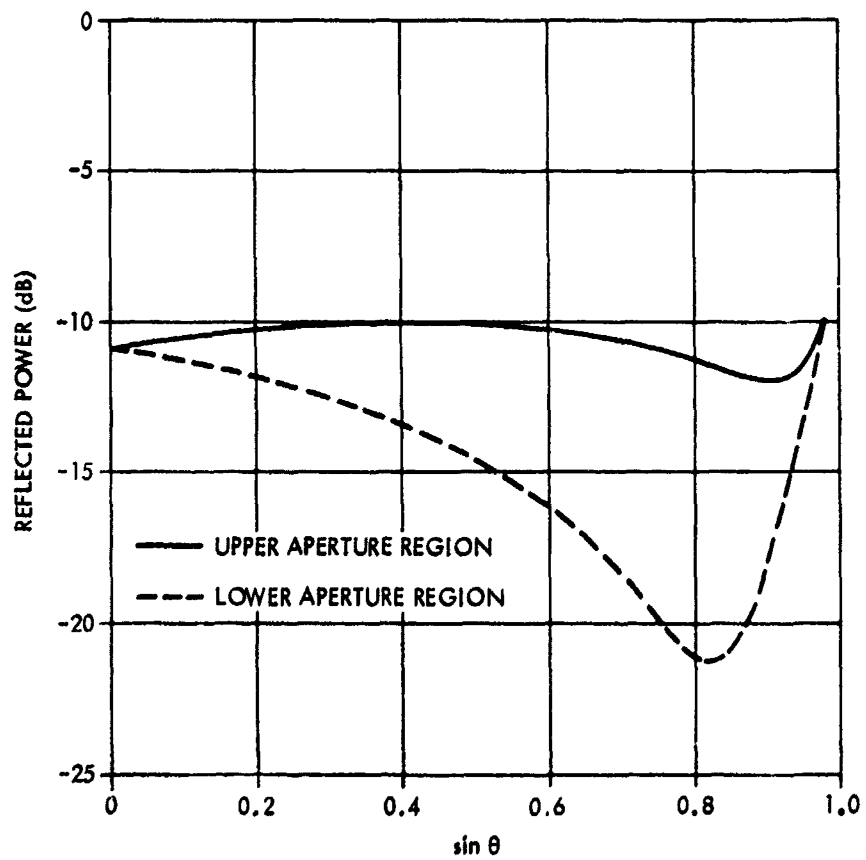

Figure 7. Reflected Power in Upper and Lower Element Halves - E Plane Scan

only in symmetry and behave like $|\sin(2\Pi x/A)|$ and $\sin(2\Pi x/A)$, respectively. By exciting the LSE_{10} and LSE_{20} modes of the upper aperture region with voltages

$$(40) \qquad V_1 = V_1^{>} = \cos(.25k_o D_x \sin\theta_o \cos\phi_o)$$

and

$$(41) \qquad V_2 = V_2^{>} = j\sin(.25k_o D_x \sin\theta_o \cos\phi_o)$$

respectively, and the modes of the lower aperture region with voltages

$$(42) \qquad V_3 = V_1^{<} = V_1^{>} \exp[j\, 0.5k_o B \sin\theta_o \sin\phi_o]$$

and

$$(43) \qquad V_4 = V_2^{<} = V_2^{>} \exp[j\, 0.5k_o B \sin\theta_o \sin\phi_o]$$

the four phase centers are established a roughly, $x = \pm A/4$ in each region. The beam is scanned to (θ_o, ϕ_o).

As for low frequency, the normalized power in the high frequency propagating beams is determined via superposition (i.e., using equation (29)). The total power delivered is

$$(44) \qquad P = 2[Y_1|V_1^{>}|^2 + Y_2|V_2^{>}|^2] = 2[Y_1+Y_2]$$

The power in the σ^{th} beam is therefore, given as

$$(45)^* \qquad P_\sigma(\theta_\sigma,\phi_\sigma) = |\sum_{i=1}^{4} S_{21}^{\sigma,i}(\theta_o,\phi_o)V_i|^2 Y_{a\sigma}/P$$

where the ordering of the elements of $\underline{V}^+$ has been altered to simplify the equation. Taking the same liberty with mode ordering, the power reflected in the jth mode ($j = 1,2,3,4$) is given as

$$(46) \qquad R_j(\theta_o,\phi_o) = |\sum_{i=1}^{4} S_{11}^{j,i}(\theta_o,\phi_o)V_i|^2 Y_j/P$$

2.2 Numerical Results

In this section, numerical results are presented for several element and grid geometries to illustrate the principle performance characteristics of the bifurcated

*See footnote to equation (37) .

twin dielectric slab loaded rectangular waveguide dual frequency array element. Element/grid design is discussed more fully in section 4.

For purpose of discussion, it is convenient to present performance data in a somewhat unusual format. Rather than present realized gain pattern, (i.e., normalized directive gain) power transmission coefficient is given for each radiating beam. The advantage gained by this form of presentation is that it allows a direct comparison of the power in the radiated beams. If $P_\sigma(\theta_\sigma,\phi_\sigma)$ is the power associated with the σ^{th} beam when the main beam is scanned to (θ_0,ϕ_0), then the directive gain of this beam is proportional to $P_\sigma(\theta_\sigma,\phi_\sigma)\cos\theta_\sigma$. Consequently, for a given scan angle, comparison of beam directive gains includes the comparison of projected aperture at the various beam locations.

Data are presented for rectangular and triangular grid configurations. Two elements are discussed: a WR187 guide with .250", ε_r=9 slab loading; and a WR137 guide with .125", ε_r= 4.75 slab loading. The former is operated at 2.5 GHz (kA/2=1.246) and 6.0 GHz (kA/2=2.990). The later is operated at 4 GHz (kA/2=1.463) and 8 GHz (kA/2=2.926). The dimensions of the elements are given in Table 1. In the following, the elements will be distinguished by the WR number of the rectangular guides.

	WR187 $\varepsilon_r = 9$	WR137 $\varepsilon_r = 4.75$
D_x	2.000	1.500
D_y	1.000	.750 or .960
A	1.872	1.374
B'	.872	.622 or .832
Δ	.032	.032
B	.420	.295 or .400
α	.325	.281
β	.361	.281
δ	.250	.125

Table 1

Dimensions (in.) of WR187 and WR137 Elements

The grating lobe diagrams for the four grids are shown in Figures 8a,b,c,d. Each diagram shows the near in grating lobe locations for the two operating points. Low frequency grating lobes are indicated by solid boxes, and high frequency lobes, by solid dots. What is immediately obvious from the figures is that the triangular grid provides a grating lobe free scan region for all directions in the plane at high frequency. One consequence of this is improved high frequency broadside match, as is shown below.

Figures 9 through 12 show power transmission coefficientin the principle planes at low frequency for each of the four grids. In the scan range $\sin\theta_0 < .95$, no grating lobes enter, as can be seen from the grating lobe diagrams in Figure 8. In general, the performance of the four configurations is the same. There is some improvement in scan coverage of the WR137 element over the WR187 element, but the difference is not large enough to show up on the scale of the figures. In the E-plane ($\sin\phi = 1.0$), the fall off is nearly $\cos^{1/2}\theta$, out to 60^o - the WR187 element shows slightly greater scan loss. In the H-plane, the scan loss exceeds $\cos^{1/2}\theta$ by approximately .5 db at $\theta=60^o$. As might be expected, the performance of the rectangular and triangular grid configurations, as measured by power trans-

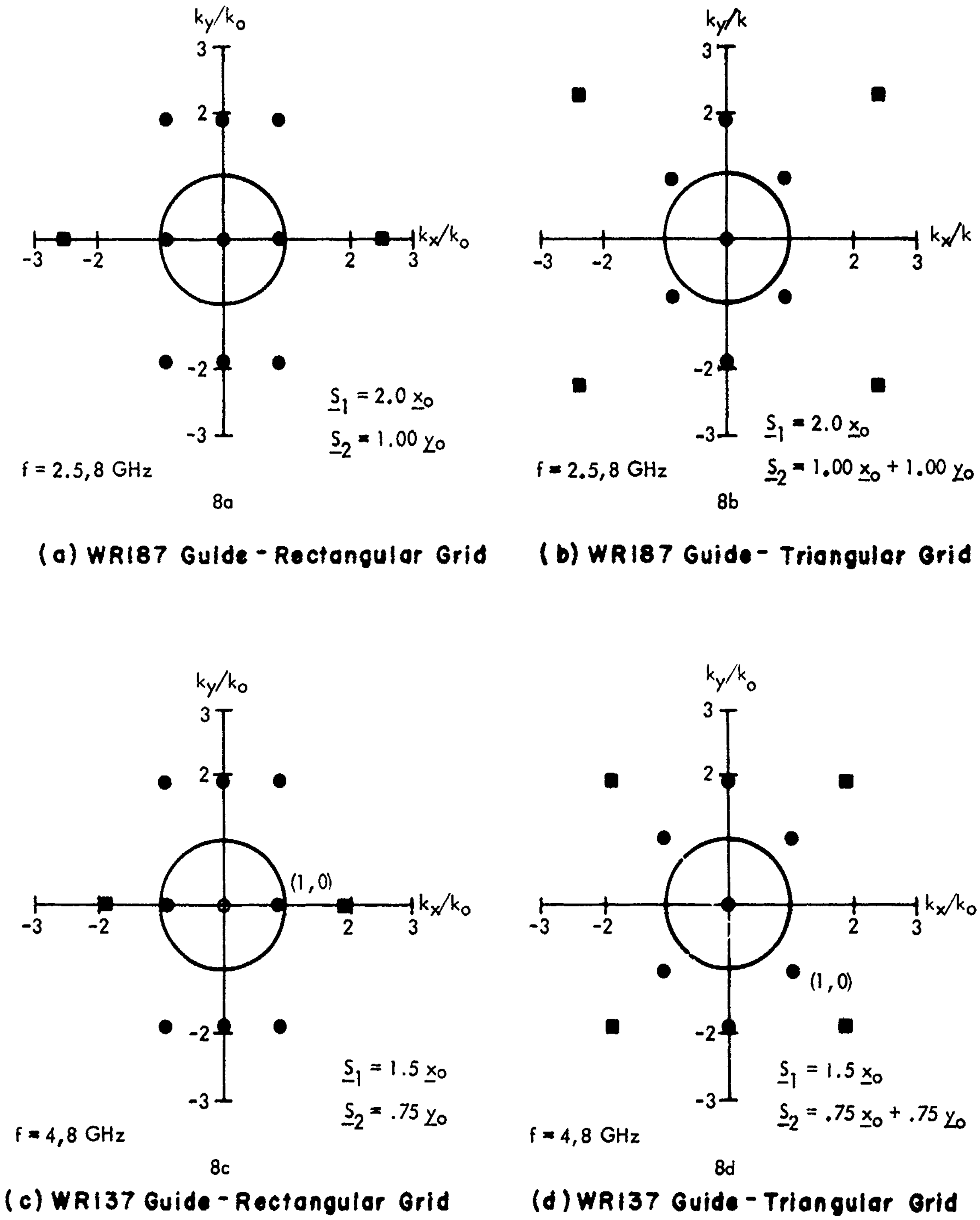

Figure 8. Grating Lobe Diagrams for WR187 and WR137 Elements in Rectangular and Triangular Configurations

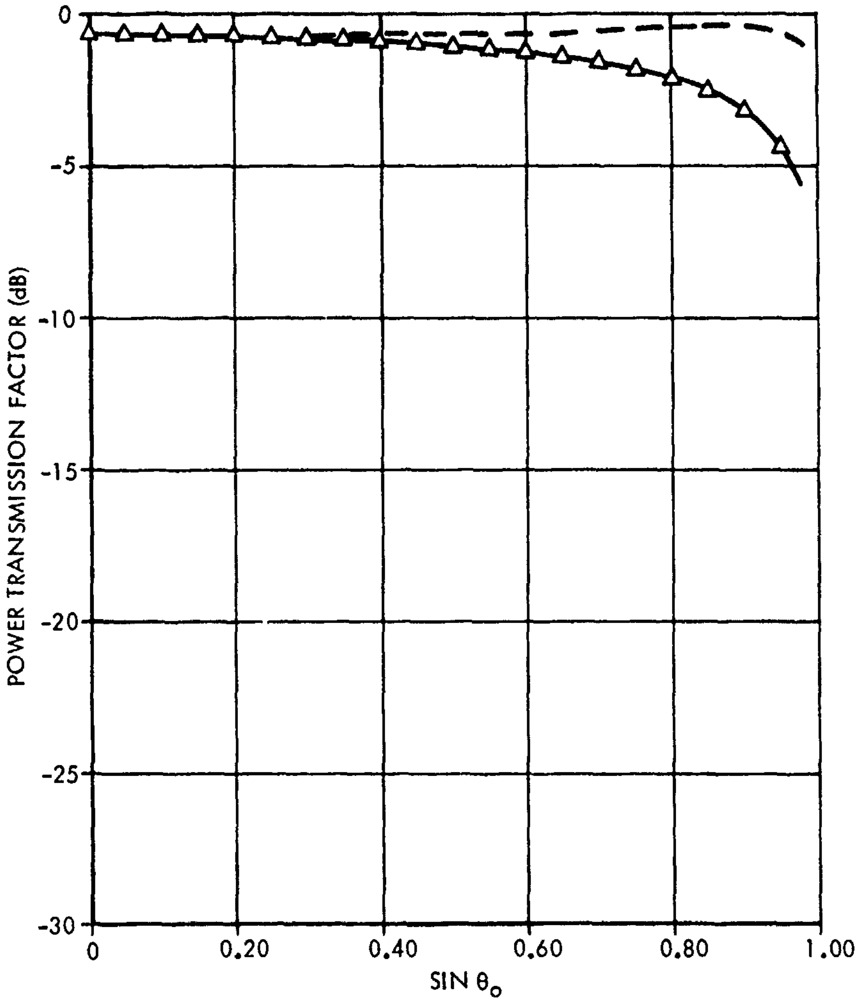

F	=	2.50 GHz	A	=	1.872 in.
α	=	0.325 in.	B	=	0.420 in.
β	=	0.361 in.	D_x	=	2.000 in.
δ	=	0.250 in.	D_y	=	1.000 in.
ϵ	=	9.00	SEP	=	0.032 in.

LEGEND

Δ H - PLANE
— — — E - PLANE

Figure 9. WR187 Element Power Transmission Coefficient - Rectangular Grid, Low Frequency (=2.5GHz)

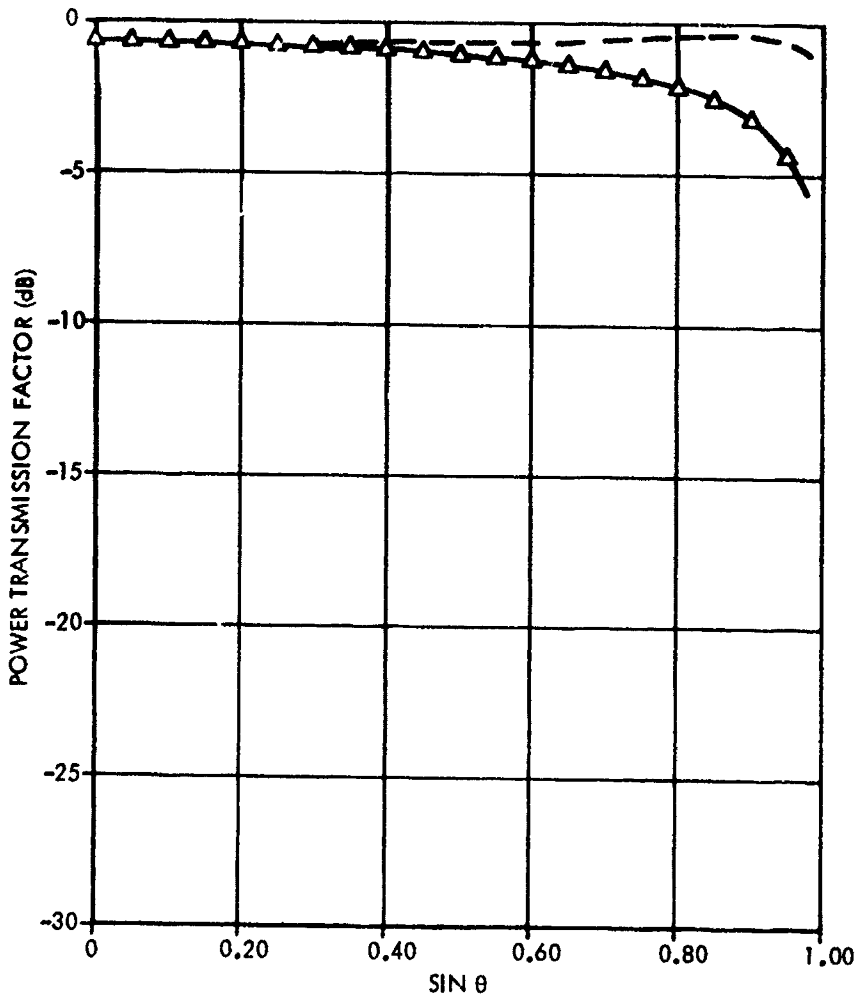

F	= 2.50 GHz	A	= 1.872 in.
α	= 0.325 in.	B	= 0.420 in.
β	= 0.361 in.	D_x	= 2.000 in.
δ	= 0.250 in.	D_y	= 1.000 in.
ε	= 9.00	SEP	= 0.032 in.

LEGEND

Δ H - PLANE
— — — E - PLANE

Figure 10. WT187 Element Power Transmission Coefficient - Triangular Grid, Low Frequency (=2.5GHz)

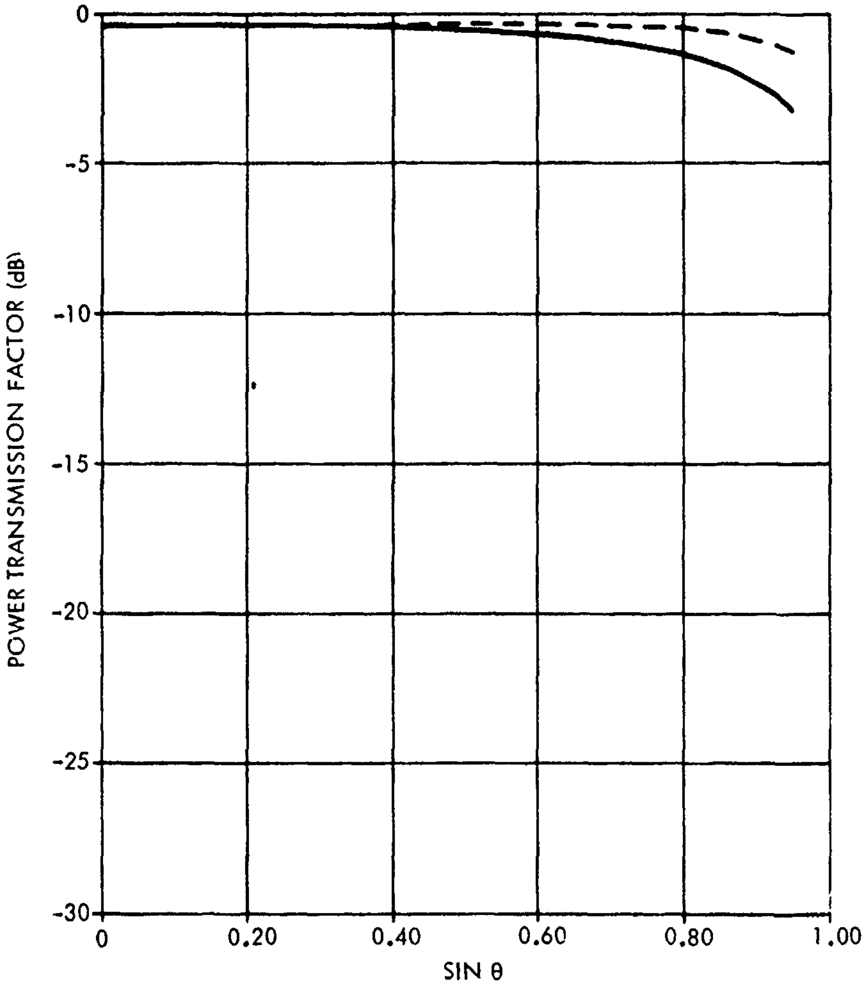

F	=	4.00 GHz	A	=	1.374 in.
α	=	0.278 in.	B	=	0.295 in.
ß	=	0.278 in.	D_x	=	1.500 in.
δ	=	0.132 in.	D_y	=	0.750 in.
ϵ	=	4.75 in.	SEP	=	0.032 in.

LEGEND

——— H - PLANE

– – – E - PLANE

Figure 11. WR137 Element Power Transmission Coefficient - Rectangular Grid, Low Frequency (=4 GHz)

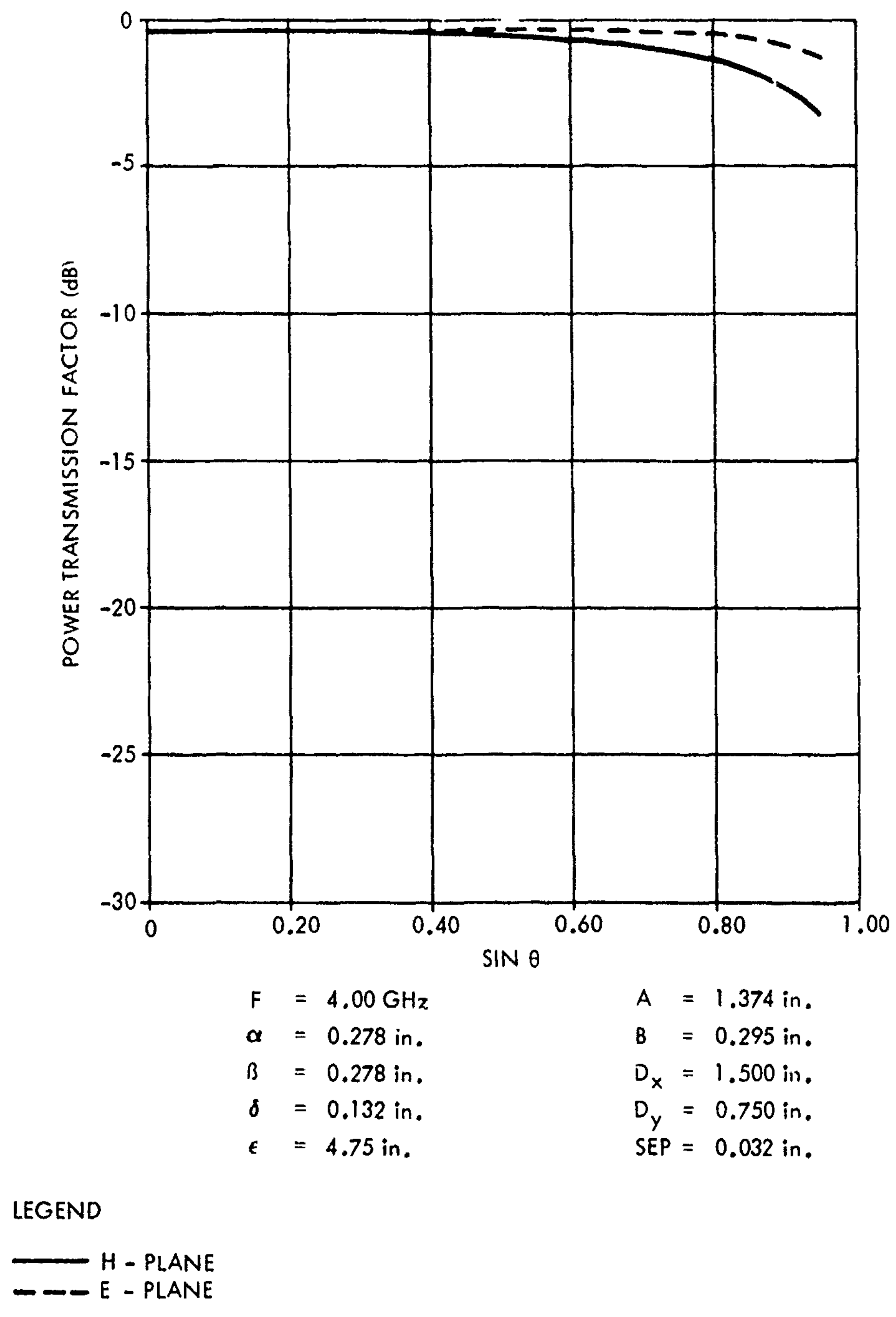

Figure 12. WR137 Element Power Transmission Coefficient - Triangular Grid, Low Frequency (=4 GHz)

mission coefficient, is not distinguishable, one grid from the other.

In Figures 8a and 8c, the high frequency grating lobes of the rectangular grid configurations are shown residing in real space for the no scan condition. In this situation, a broadside power loss occurs, and a high farout sidelobe condition is created. To a certain extent, the power delivered to these lobes can be reduced by introducing a complex, multiplicative correction for the voltage excitation coefficients, V_2 and V_4, given by equations (41) and (43).[7] Ideally, this correction is independent of scan and frequency (for small bandwidths). Typical grating lobe levels, with and without the correction, are shown in Figure 13 for a thin walled element in a rectangular grid. Without correction, grating lobe levels reach -16.7 db. With the multiplier 1.164 - j.291*, the maximum grating lobe level is -20.4 db, and beyond $\sin\theta_0=.3$, the level is below -25 db. Differences in the main beam due to the two excitations are too small to be represented in the figure.

*The case shown here is supplied by R. Mailloux, the multiplier 1.164 - j.291 was also found suitable for the WR187 element in a rectangular grid.

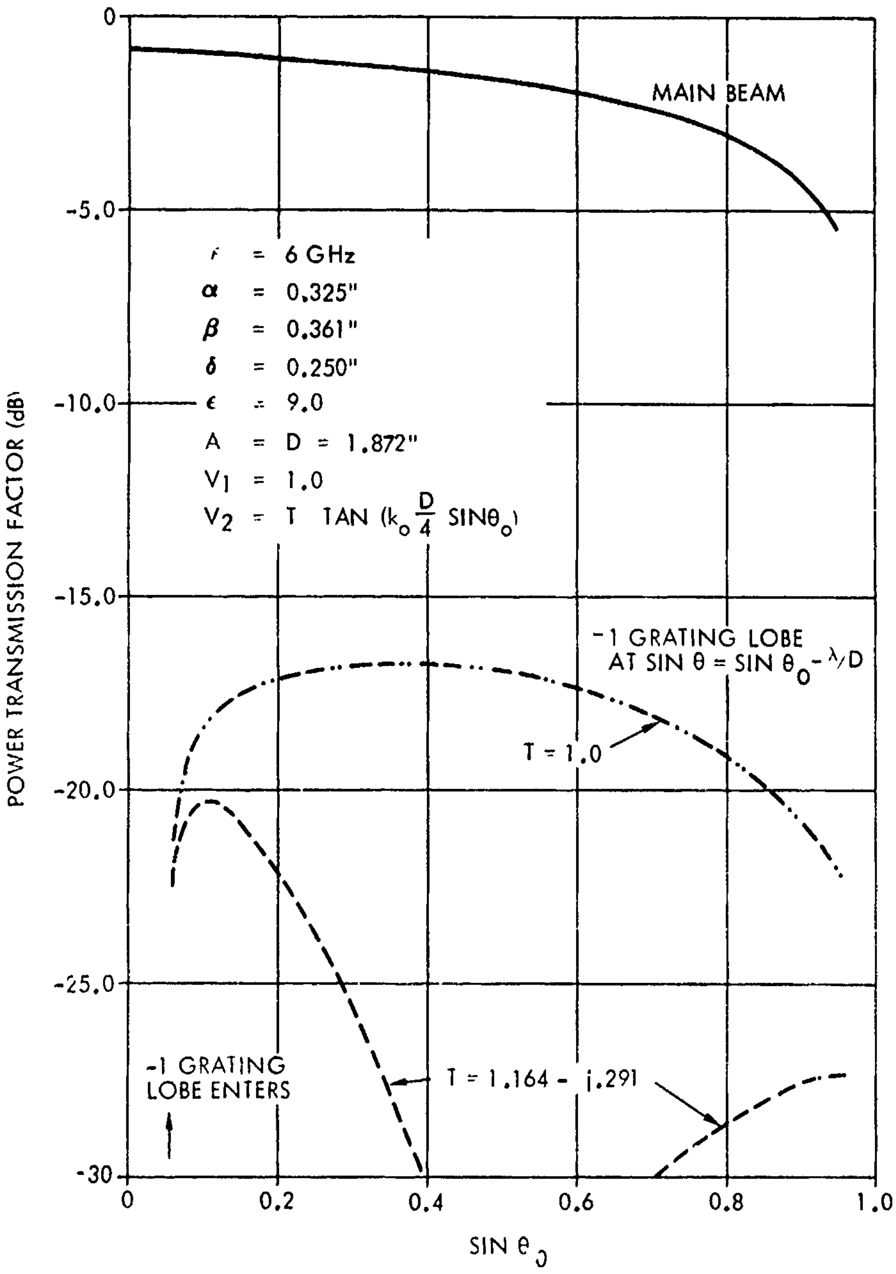

Figure 13. Effects of Grating Lobe Correction

By configuring the WR187 and WR137 elements in triangular lattice, the difficulties encountered due to the location of the high frequency grating lobes are largely eliminated. Figures 8b and 8d, show the disposition of high frequency grating lobes for triangular grid. No grating lobes enter real space along any cut plane for $\sin\theta_0 < .391$. In the principle cut planes, only the main beam is propagating out to $\sin\theta_0 = .820$, or nearly 60° scan.

For wide angle scan applications, the triangular grid configuration does not fully eliminate the necessity for the type of excitation correction described above. Consider Figures 8c and 8d. The (1,0) harmonics of the structures follow the same track for E plane scan, and while they are in real space, one is the image of the other, reflected about the k_{xr}/k_o axis. Hence, for the same voltage correction term, roughly the same amount of power will be dumped in the triangular and rectangular grid lobes when the E plane scan sines, $\sin\theta_t$ and $\sin\theta_r$, respectively are related by

$$(47) \qquad \sin\theta_r = \lambda/D_y - \sin\theta_t$$

This is illustrated in Figure 14 for the WR137 element operating at 8.64 GHz. Both E and H mode space harmonics are shown. It is clear from the high power levels shown in the figure that grating lobe control is required for either

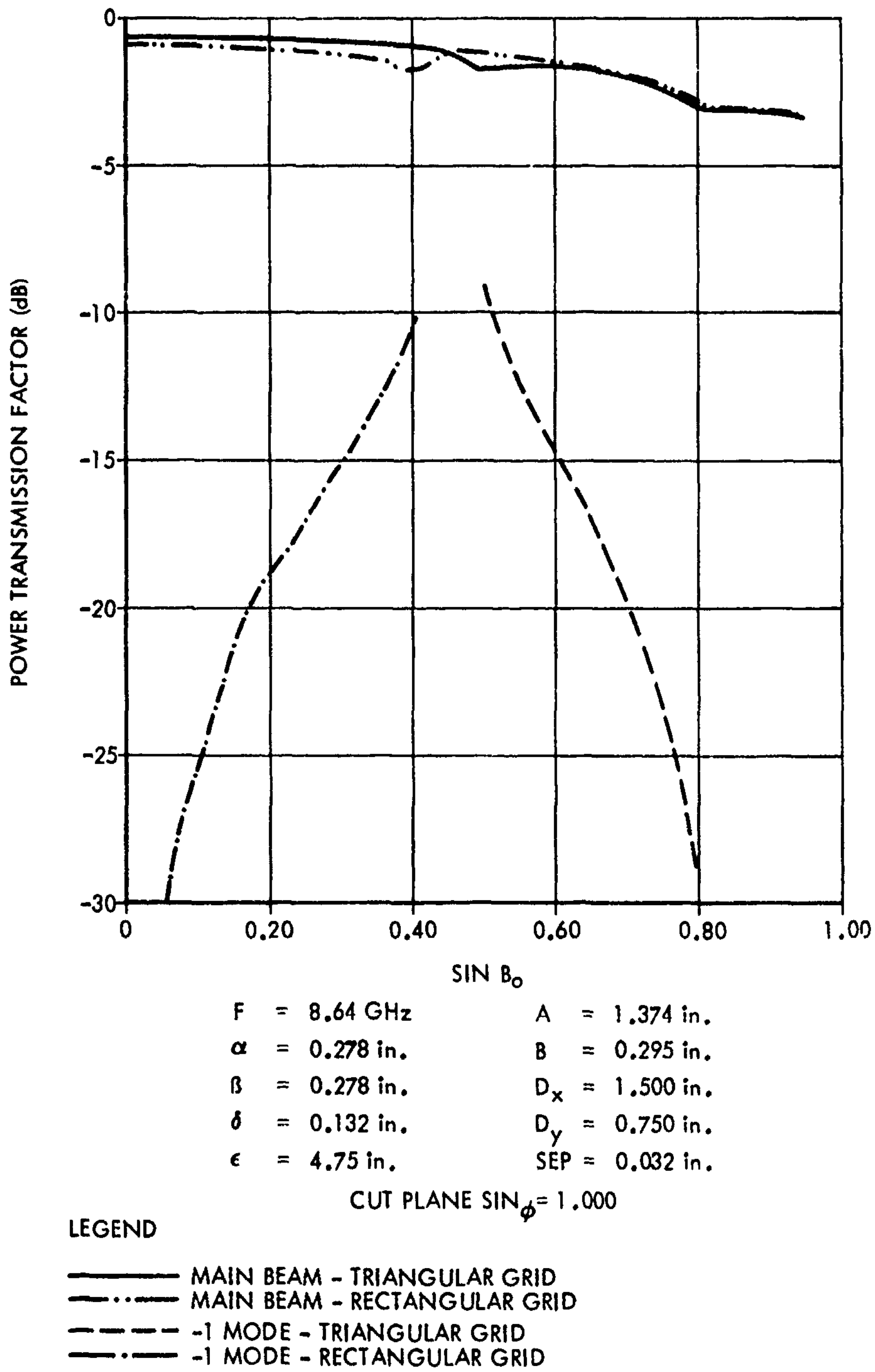

Figure 14. Grating Lobe Levels Obtained from Rectangular and Triangular Grid Configurations of WR137 Elements

grid type, even though the $\cos\theta_\sigma$ beam broadening factor is less than .4 throughout the scan range.

Because of the high grating lobe levels obtained for the rectangular grids, there is significant (approximately .1 db) main beam loss at broadside relative to main beam levels obtained for the triangular grid. For the WR137 element, the difference is .13 db. A comparison of principle plane main beam levels for the two grids is shown in Figures 15 and 16 . The operating point is 8 GHz. In the H plane, Figure 15 , the beams show the .13 db difference at broadside, and smoothly coalesce. In the E plane, Figure 16 , there are sharp jogs in the curves. For the rectangular grid, the jog occurs as the grating lobe pair exits from real space. For the triangular grid, the sudden power loss at $\sin\theta_0$ = .82 is due to the grating lobe pair entering real space. The main beam falloff is slightly greater than $\cos^{1/2}\theta_0$ for both grids in either plane.

2.3 Comparison with Limiting Cases

To check the analysis, and in particular the details of the computational procedure, several limiting cases have been examined. For these cases, the slab dielectric constant is set to ε_r=1 and the LSE_{10} mode is independently

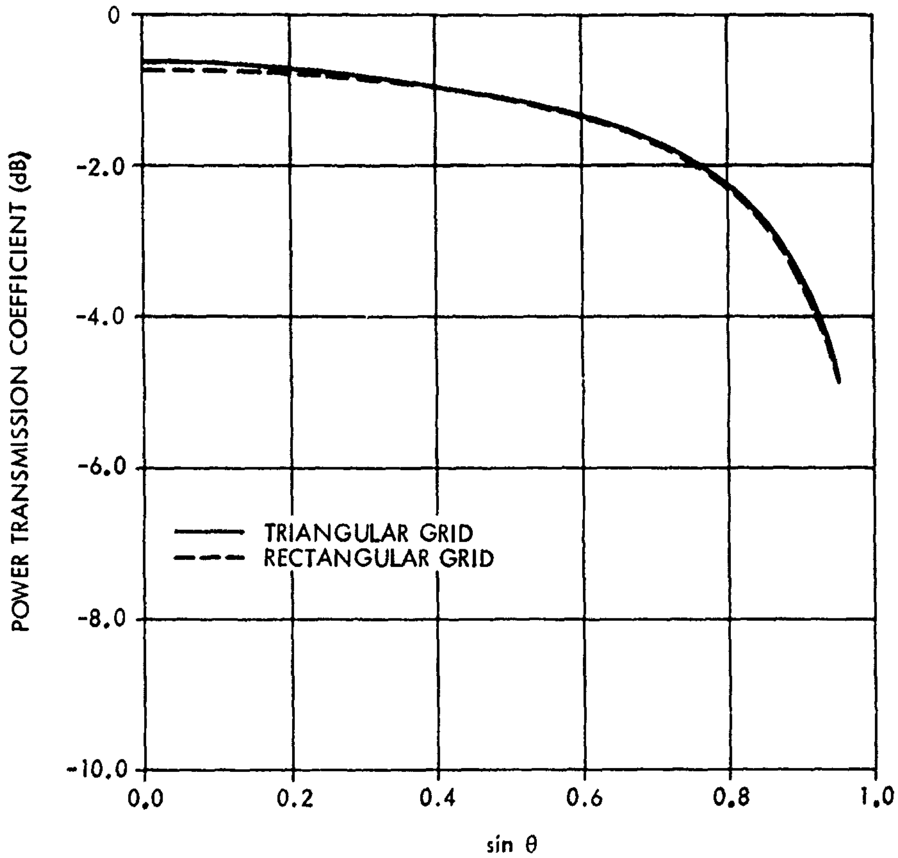

Figure 15. Comparison of Main Beam Power Levels for Rectangular and Triangular Grid Configurations of WR137 Elements - H Plane

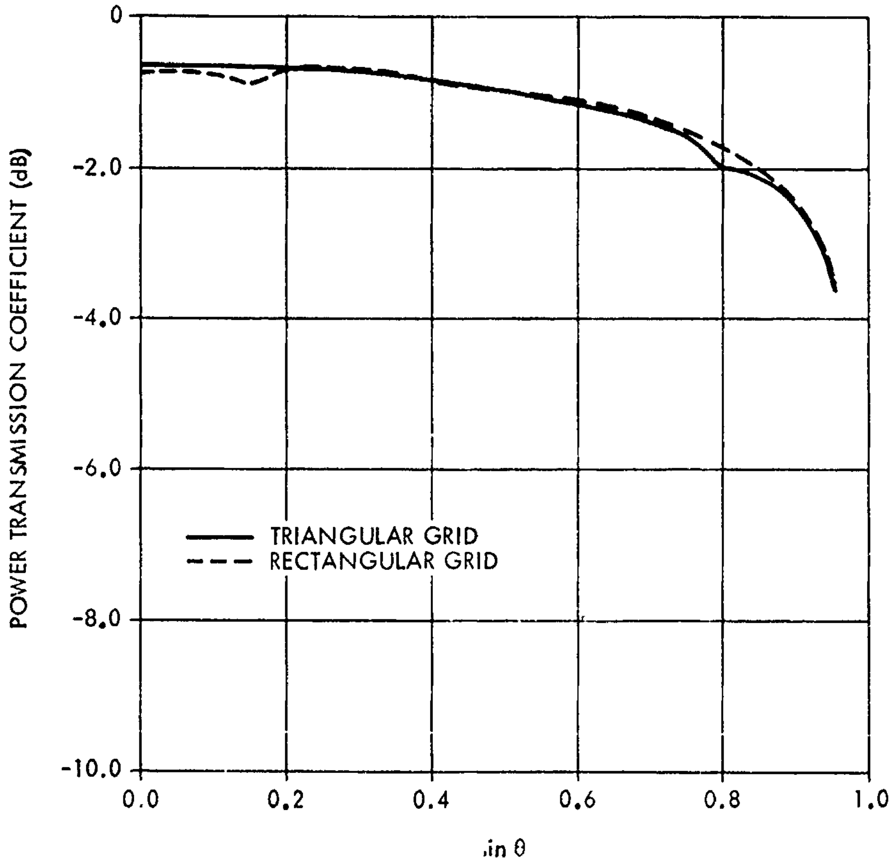

Figure 16. Comparison of Main Beam Power Levels for Rectangular and Triangular Grid Configurations of WR137 Elements - E Plane

excited in the upper and lower aperture regions.

For $\varepsilon_r=1$, the LSE_{no} modes degenerate to the TE_{no} modes of empty rectangular waveguide. Therefore, an appropriate set of check cases include H plane scanned thin wall rectangular grid arrays of rectangular elements and special triangular grid examples which have appeared in the literature. Thick wall rectangular grid cases can also be used as checks provided the wall thickness is not too great.

The geometry for the rectangular grid examples is shown in Figure 17. The aperture dimensions are A and B, and the lattice vectors are

$$\underline{S}_1 = d_x \underline{x}_o \tag{48}$$

and

$$\underline{S}_2 = d_y \underline{y}_o \tag{49}$$

For $A=d_x$ and $B=d_y$, exact solutions for E and H plane element patterns have been obtained using function theoretic techniques to construct the reflection coefficient of the driven TE_{10} mode.[8] Figures 18 through 20 show magnitude and phase of active reflection coefficient, Γ, of the TE_{10} mode of square waveguide in thin-wall square lattice configuration for H

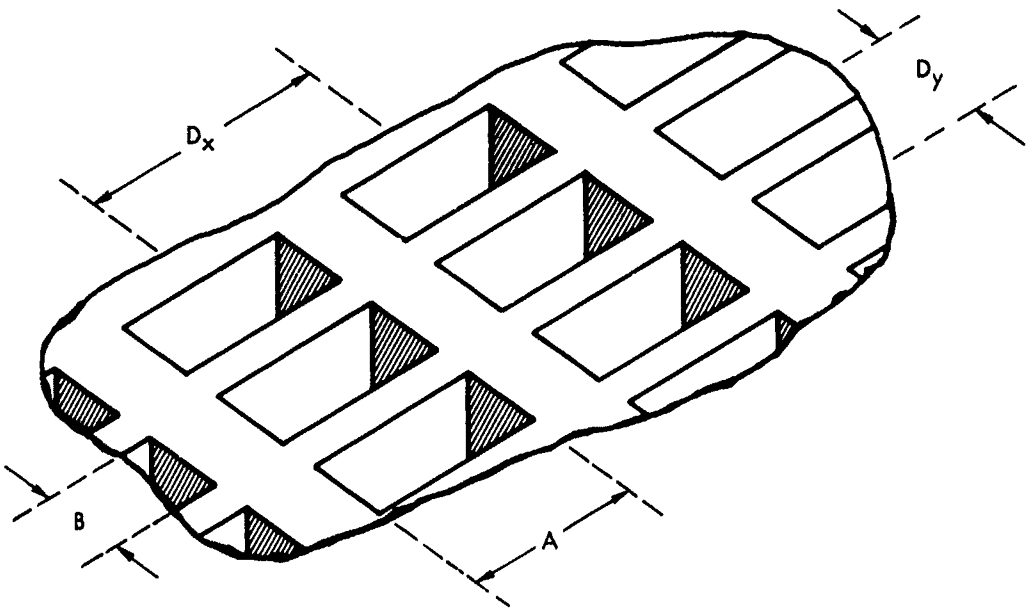

Figure 17. Rectangular Grid of Rectangular Waveguides

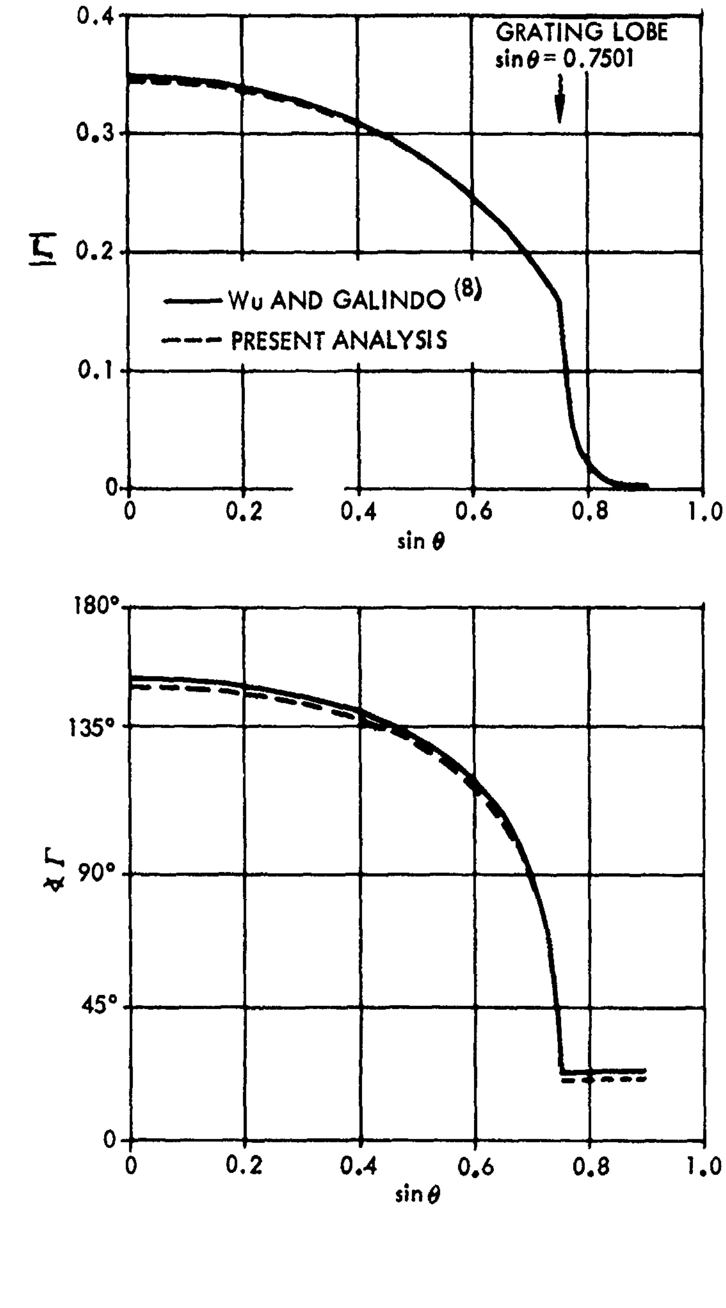

Figure 18. Comparison of Exact[8] and Approximate Modal Solutions for Active TE_{10} Reflection Coefficients - Thin Walled Square Elements H-Plane $D_x/\lambda = .5714$

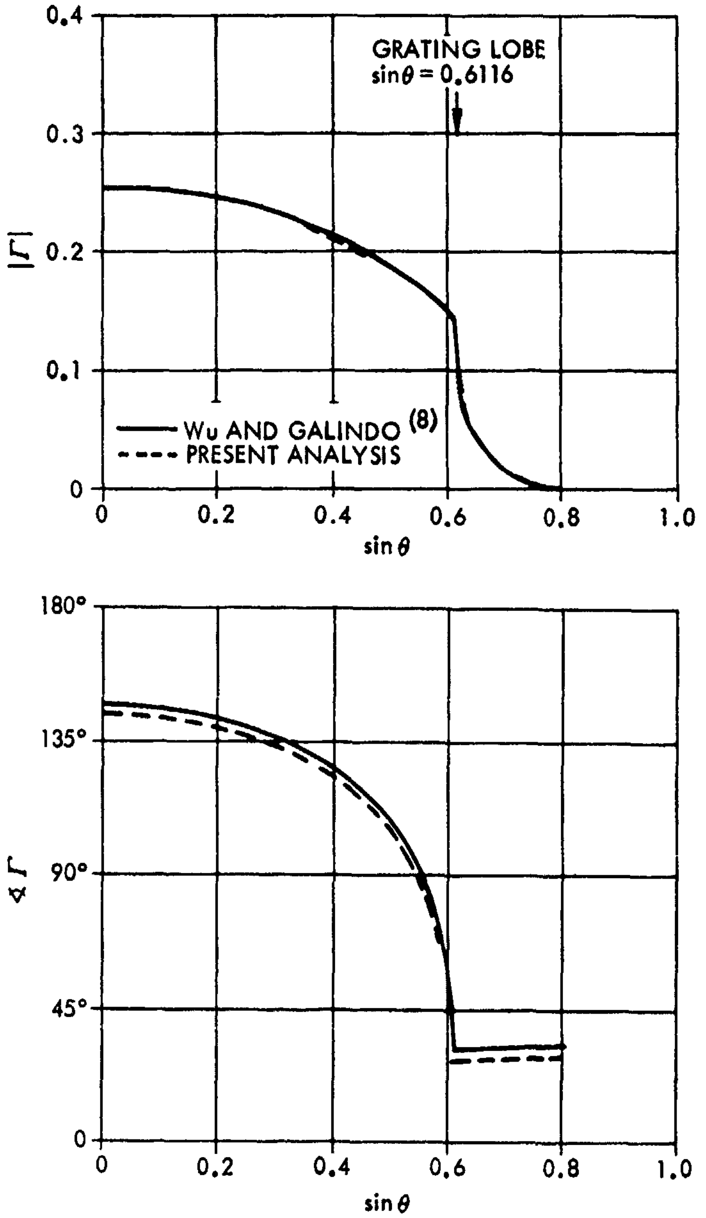

Figure 19. Comparison of Exact[8] and Approximate Modal Solutions for Active TE_{10} Reflection Coefficient - Thin Walled Square Elements H-Plane $D_x/\lambda = .6205$

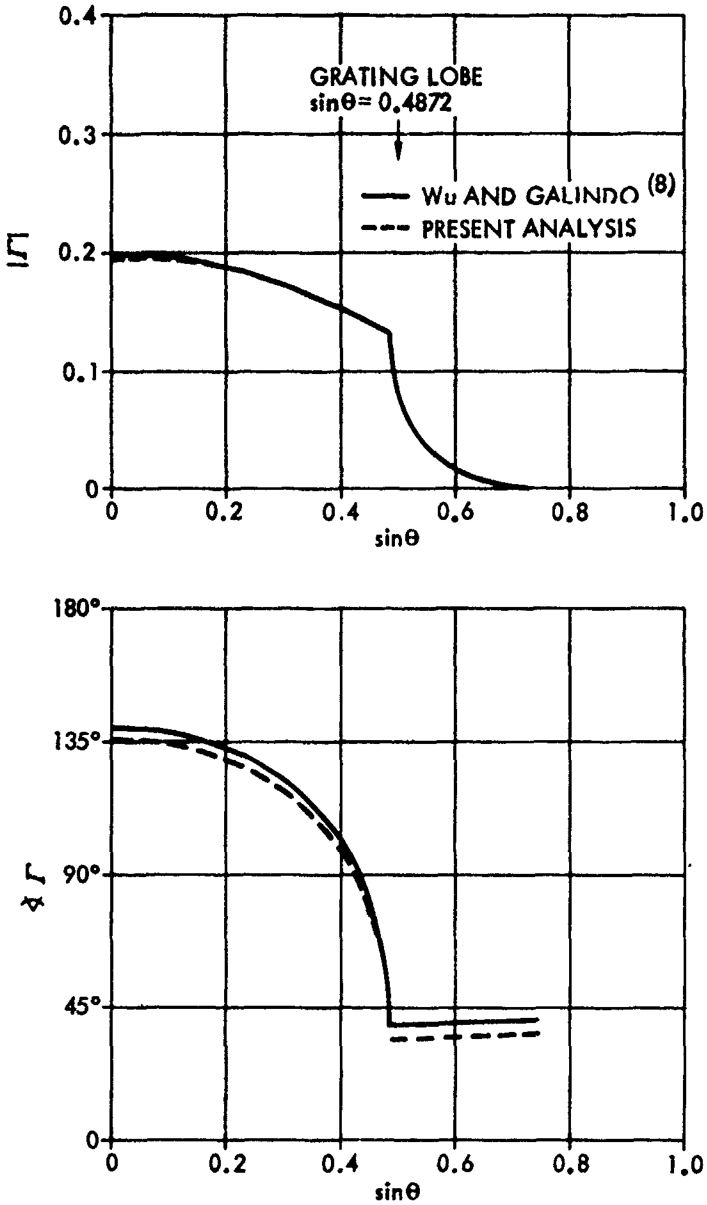

Figure 20. Comparison of Exact[8] and Approximate Modal Solutions For Active TE_{10} Reflection Coefficient - Thin Walled Square Elements H-Plane D_x/λ = .6724

plane scan. The solid curves are the exact solution, as obtained by Wu and Galindo.[8] The dashed curves are obtained from the current formalism using the first five TE_{no} modes to approximate the aperture field distrubution. The minor discrepancies between the results are removable by including additional higher order modes in the modal computations.

Figures 21 through 23 show magnitude of Γ as a function of H plane scan angle when the H plane metalic walls have finite thickness, $t = .1d_x$. The lattice remains square. The solid curves were obtained by Galindo and Wu[9] using 30 feedguide modes to represent the aperture field. The dashed curves are from the present analysis using the first nine TE_{no} modes. The agreement is excellent.

Aperture field approximations consisting of the first few TE_{no} mode functions may be used to compute H plane element patterns of triangular grid arrays of rectangular apertures.

Figures 24 and 25 show H plane element pattern, $[1 - |\Gamma|^2]\cos\theta$, as computed by Amitay, Galindo, and Wu[10] and using the approximate limiting case of the present analysis.

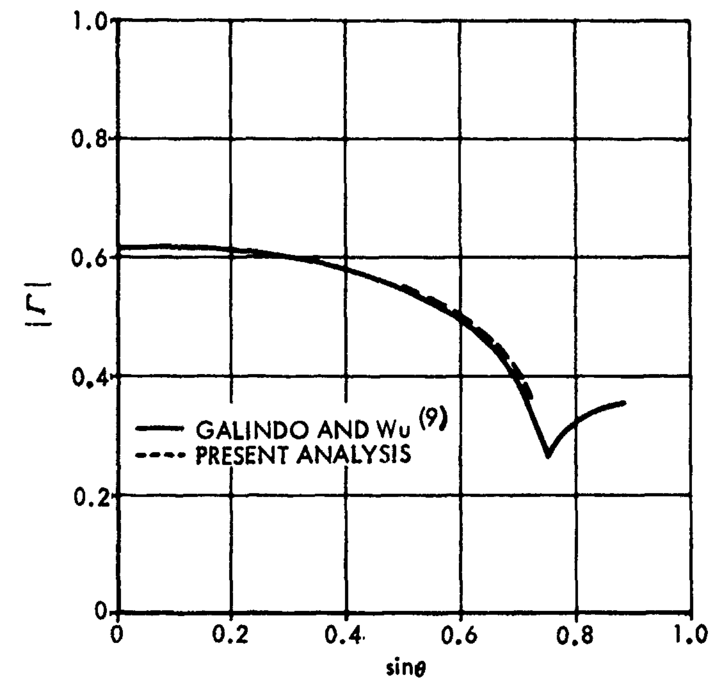

Figure 21. Comparison of Modal Solutions for Active TE_{10} Reflection Coefficient - Thick Walled Square Elements - H-Plane $D_x/\lambda = .5714$, $t = .1D_x$

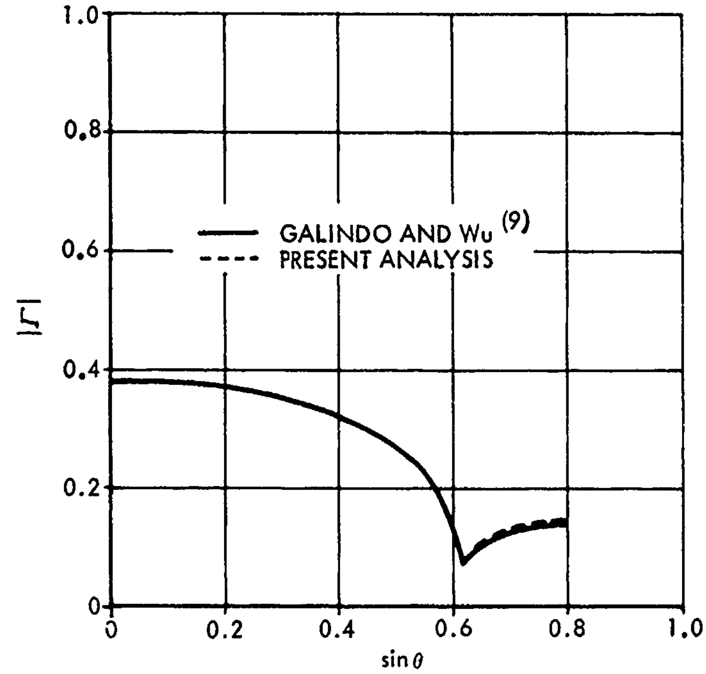

Figure 22. Comparison of Modal Solutions for Active TE_{10} Reflection Coefficient - Thick Walled Square Elements - H-Plane $Dx/\lambda = .6205$, $t = .1D_x$

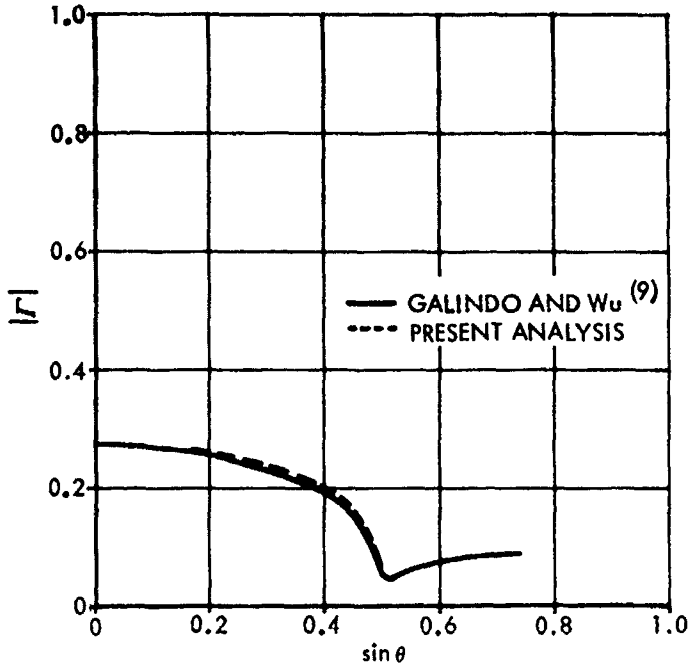

Figure 23. Comparison of Modal Solutions for Active TE_{10} Reflection Coefficient - Thick Walled Square Elements - H-Plane $Dx/\lambda = .6724$, $t = .1D_x$

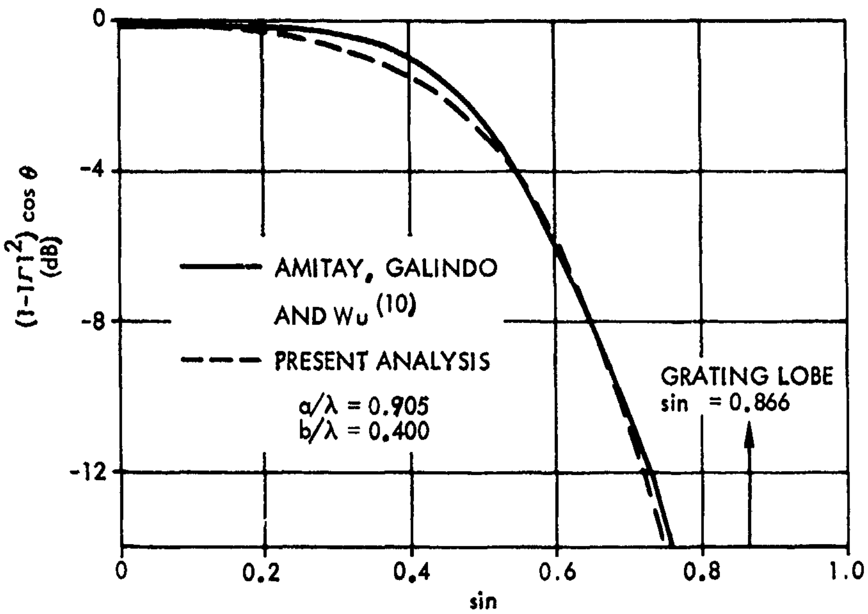

Figure 24. Comparison of Modal Solutions for H-Plane Element Pattern When Aperture Field is Approximated by TE_{10} Mode

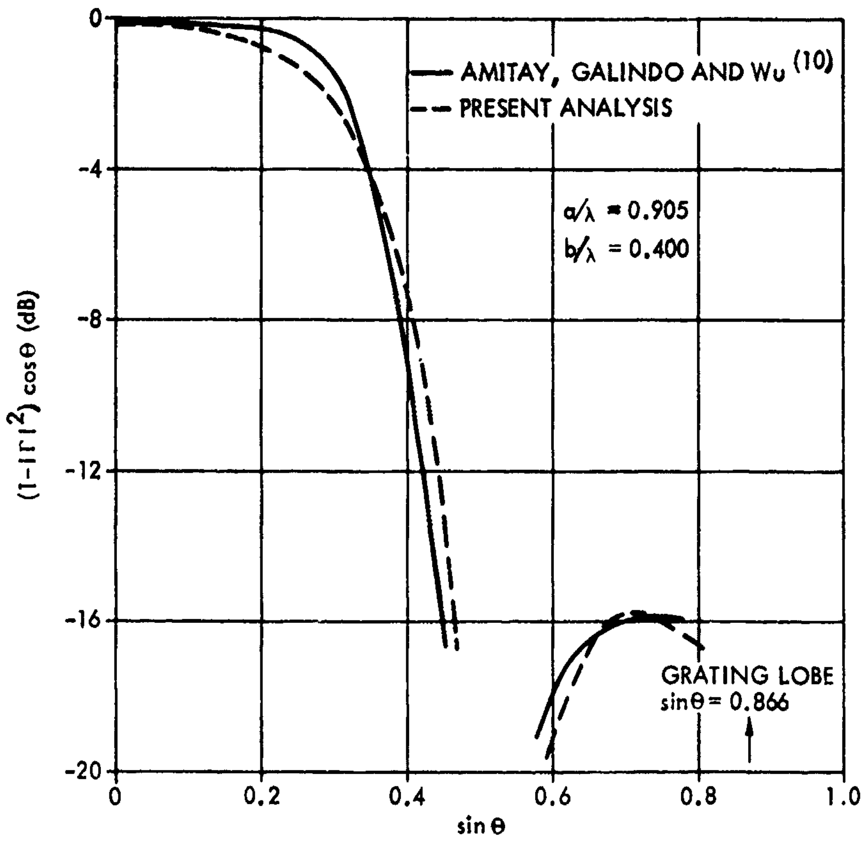

Figure 25. Comparison of Modal Solutions for H-Plane Element Pattern When Aperture Field is Approximated by TE_{10} + TE_{20} Modes

The lattice is 45° triangular, with lattice vectors

$$\underline{S}_1 = 1.008\lambda\underline{x}_o \tag{50}$$

and

$$\underline{S}_2 = .504\lambda\underline{x}_o + .504\lambda\underline{y}_o \tag{51}$$

The rectangular apertures are .905λ by .4λ. In figure 24, the aperture field is approximated using only the TE_{10} feedguide mode. For Figure 25, the TE_{20} mode is added. Again, the comparison is quite good. The resonance, near sinθ=.6, was found experimentally by Diamond(11) in an investigation of the central element pattern of a 95 element array.

The deviation of computed results in Figures 24 and 25 arise from two sources. The first is an inability to read the published curves to sufficient accuracy. The second source of error is number of space harmonics used to obtain the published curves and the present results.

2.4 Convergence of Numerical Results

From the results of the previous section, it is event that the numerical solution implemented here converges uniformly as the numer of aperture modes, space modes or both is increased. However, to ensure that the convergence is indeed uniform, the array properties of the WR187 element were examined as the mode count was varied in the aperture and free space regions. One to eight aperture modes were considered and the circle of convergence was varied from k_o (= $2\pi/\lambda$) to $13.9K_o$ at 2.5GHZ and $33.4k_o$ at 6 GHZ.

For maximum circle of convergence, the solution converged rapidly as the number of aperture modes was increased. At both frequencies, four or five aperture modes were found to be sufficient.

With the number of aperture modes held fixed, the circle of convergence was uniformly increased. Beyond roughly $5k_o$ at 2.5GHZ and $10k_o$ at 6GHZ, the solution became stable.

Except for the usual effect of truncating the modal series at an inordinately premature point, no convergence anomalies were evident in the computations.

3.0 PROPAGATION CHARACTERISTICS OF TWIN DIELECTRIC SLAB LOADED RECTANGULAR WAVEGUIDE

The analysis of the radiation properties of an infinite array of dual band elements requires a complete description of wave propagation in the inhomogeneously loaded feedguide. The geometry of the dual band element is shown in Figure 26. The element consists of a rectangular waveguide bifurcated in the E-plane by a septum of thickness, Δ, and symmetrically loaded with full height slabs of lossless dielectric parallel to the guide narrow wall. Both slab thickness and spacing are arbitrary in the ranges $0 < 2\delta/A < 1$, $0 < 2\beta/A < 1$, and ε_r, the relative dielectric constant may take on any real value, $\varepsilon_r > 1$.

Several investigators[12-14] have studied wave propagation in similar guiding structures, primarily to provide bases for perturbation calculations of ferrite phase shifter properties. Collin[15] has obtained general expressions for mode functions and modal propagation constants for the asymmetric single slab case. These results are equivalent to the symmetric twin slab results for short-circuit symmetry in x. Seckelmann[12] has obtained general expressions for LSE_{no} (i.e., TE_{no}) mode functions and propagation

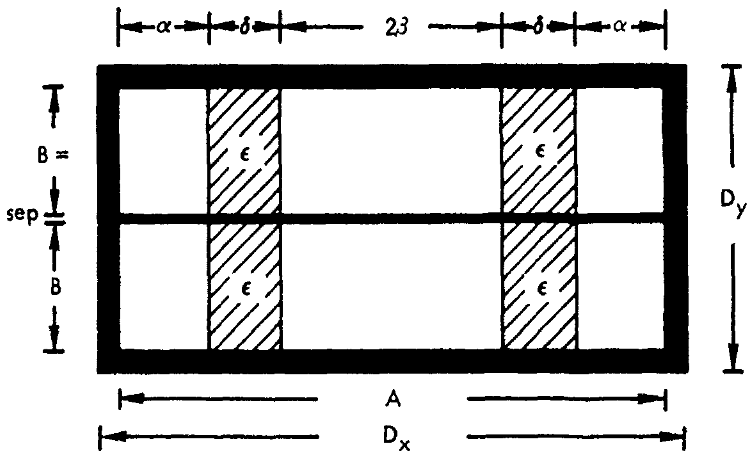

Figure 26. Dual Band Element

constants of the symmetric twin slab case.

The modal fields of the inhomogeneously loaded rectangular waveguide shown in Figure 26 are obtained in a straightforward manner. Recognizing that E and H modes with respect to $\underline{x}_o$ remain decoupled at the dielectric interfaces, arbitrary waveguide fields can be decomposed into E-type (LSM) and H-type (LSE) modes with respect to $\underline{z}_o$. Thus, an arbitrary field may be expressed in terms of either complete mode set. A one-to-one correspondence exists between the modes of each set (i.e., eigenvalues of the E and H mode set are eigenvalues of the type mode set for the given boundary value problem). The LSE and LSM modal fields are then obtained via a component-by-component comparison of the modal fields in either set corresponding to a particular eigenvalue. The components of the type mode functions are then proportional to either the voltage or current distributions of the equivalent circuit.

The modal spectrum for the structure is obtained via a transverse resonance technique.

3.1 Mode Functions

It is well known that E and H modes with respect to surface normals remain decoupled at planar interfaces between dielectrics.[15] Thus, in the inhomogeneously (in x) loaded guide shown in Figure 26 , decoupled modes of the structure will be E and H with respect to x, or, equivalently, E-type (LSM) and H-type (LSE) with respect to z.

For the infinite phased array of dual frequency elements, the aperture fields are expressed as the superposition of transverse-to-z mode functions which satisfy the vector equations (see Appendix B).

$$(52) \qquad \underline{y}_o \gamma Y_i' h_{yi}'(x,y) = \omega\varepsilon[\bar{I} + \frac{\nabla_t \nabla_t}{k^2}] \cdot (\underline{z}_o \times \underline{e}_i'(x,y))$$

$$(53) \qquad \underline{h}_o \gamma_i Z'' e_{yi}''(x,y) = \omega\mu[\bar{I} + \frac{\nabla_t \nabla_t}{k^2}] \cdot (\underline{h}_i''(x,y) \times \underline{z}_o)$$

In equations (52) and (53), γ_i is the longitudinal (z directed) wavenumbers; Y' and Z" are modal immittances; $\bar{I}$ is the unit transverse-to-Z diadic,

$$(54) \qquad I = \underline{x}_o\underline{x}_o + \underline{y}_o\underline{y}_o;$$

and ∇_t is the tranverse-to-z gradient operator,

$$\nabla_t = \underline{x}_o \frac{\partial}{\partial x} + \underline{y}_o \frac{\partial}{\partial y} \tag{55}$$

The prime (') is used to denote LSM modes [for which $h_x(x,y) \equiv 0$]; the double prime, to denote LSE modes [for which $e_x(x,y) \equiv 0$]; and single index is used rather than a double index.

The desired modal representation of transverse fields is

$$\underline{E}_t(x,y,z) = \sum_i V_i'(z)\underline{e}_i'(x,y) + \sum_j V_j''(z)\underline{e}_j''(x,y) \tag{56}$$

$$\underline{H}_t(x,y,z) = \sum_i I_i'(z)\underline{h}_i'(x,y) + \sum_j I_j''(z)\underline{h}_j''(x,y) \tag{57}$$

where $V_n^{\alpha}(z)$ and $I_n^{\alpha}(z)$ (α = ',") are z dependent modal voltages and currents satisfying the transmission line equations

$$\frac{d}{dz} V_i(z) = -j\gamma_i Z_i I_i(z) \tag{58}$$

$$\frac{d}{dz} I_i(z) = -jY_i \gamma_i V_i(Z) \tag{59}$$

Since the guide is uniform (and assumed infinite) in z, the z dependence of the modal voltages and currents is

$\exp[-j\gamma_i z]$, hence

$$V_i(z) = V_i e^{-j\gamma z} \tag{60}$$

$$I_i(z) = I_i e^{-j\gamma z} \tag{61}$$

Equations (52) and (53) may be solved to obtain relationships between the mode components. For LSM modes, the x component of $\underline{h}'(x,y)$ is taken as zero ($h'_x \equiv 0$), and equation (52) results in:

$$\underline{h}'_i(x,y) = \varepsilon_r(x)\; e'_{xi}(x,y)\underline{y}_o \tag{62}$$

$$\underline{e}'_i(x,y) = e'_{xi}(x,y)\underline{x}_o + \frac{1}{k^2\varepsilon_r(x) - \kappa_i^2(x)} \frac{\partial^2}{\partial x\,\partial y} e'_{xi}(x,y)\underline{y}_o \tag{63}$$

$$Z'_i = \frac{k^2\varepsilon_r(x) - \kappa_i^2(x)}{\gamma'_i \omega \varepsilon_o} \tag{64}$$

where $e'_{xi}(x,y)$ is a solution of the scalar wave equation

(65) $\quad (\nabla_t^2 + k_{ti}^2(x))\ e'_{xi}(x,y) = 0$

with $k_{ti}^2 = \kappa_i^2(x) + k_{yi}^2 = k_o^2\varepsilon_r(x) - \gamma_i^2$, subject to the boundary conditions of the guide cross-section. $\varepsilon_r(x)$ is the x-dependent dielectric constant of the cross-section. For LSE modes, the x component of $\underline{e}''(x,y)$ is zero ($e''_x \equiv 0$), and solution of (53) gives:

(66) $\quad \underline{e}''_i(x,y) = -h''_{xi}(x,y)\underline{y}_o$

(67) $\quad \underline{h}''_i(x,y) = h''_{xi}(x,y)\underline{x}_o$

$$+ \frac{1}{k^2\varepsilon_r(x) - \kappa_i^2(x)} \frac{\partial^2}{\partial x\,\partial y} h''_{xi}(x,y)\underline{y}_o$$

(68) $\quad Y''_i = \dfrac{k^2\varepsilon_r(x) - \kappa_i^2(x)}{\omega\mu\gamma_i}$

with $h''_{xi}(x,y)$ satisfying

(69) $\quad (\nabla_t^2 + k_{ti}^2(x)\ h''_{xi}(x,y) = 0$

over the cross-section. The wave immittances given by equations (64) and (68) are defined such that the direct proportionalities of equations (62) and (66) are obtained. It is shown in Appendix C that the type modes possess the following orthonormality property for the bounded cross-section (CS) of Figure 26.

$$(70) \qquad \int\!\!\int_{CS} dxdy\,\underline{e}_n^{\alpha} \cdot (\underline{h}_m^{\beta *} x\ \underline{z}_o) = \delta_{\alpha\beta}\delta_{nm}$$

where $\alpha,\beta = (',")$.

Equations (62) through (69) , with appropriate boundary conditions, are the complete formal solution for the mode functions of the symmetric twin dielectric slab loaded rectangular guide shown in Figure 26. However, due to the complexity of boundary conditions along x, the scalar wave equations (65) and (69) are difficult to solve. If the transmission line direction is temporarily taken along x, the fields in the guide may be put in a representation of E and H modes with respect to x. Due to the degeneracy of the rectangular cross-section, eigenvalues of the E(H) mode set are also eigenvalues of the LSM (LSE) mode set. Thus, corresponding to each eigenvalue of the structure, there are two expressions for total field. These expressions are compared component-by-component, resulting in particular expressions for LSE and LSM mode functions in the symmetric twin dielectric slab loaded rectangular waveguide.

The transverse-to-x modes of the twin slab loaded guide are obtained in standard fashion and are given as:

E modes $(\hat{h}'_x \equiv 0)$

(71) $$\hat{\underline{e}}_i(y,z) = -\frac{\hat{\nabla}_t \psi_E}{\hat{k}_{ti}}$$

$$= -\frac{Ae^{-j\gamma_i z}}{\hat{k}_{ti}}\left[\frac{m\Pi}{b}\cos\frac{m\Pi y}{b}\,\underline{y}_o - j\gamma_i \sin\frac{m\Pi y}{b}\,\underline{z}_o\right]$$

(72) $$\hat{\underline{h}}'_i(y,z) = \underline{x}_o \times \hat{\underline{e}}'_i(y,z)$$

(73) $$Z'_i = \frac{\kappa_i(x)}{\omega\varepsilon_o\varepsilon_r(x)}$$

(74) $$\psi_E = Ae^{-j\gamma_i z}\sin\frac{m\Pi y}{b}$$

H Modes $(\hat{e}''_x \equiv 0)$

(75) $$\hat{\underline{h}}''_i(y,z) = -\frac{\hat{\nabla}_t \psi_H}{\hat{k}_{ti}}$$

$$= \frac{Be^{-j\gamma_i z}}{\hat{k}_{ti}} \left[\frac{m\Pi}{b} \sin \frac{m\Pi y}{b}\, \underline{y}_o + j\gamma_i \cos\frac{m\Pi y}{b}\, \underline{z}_o\right]$$

(76) $$\hat{\underline{e}}''_i(y,z) = \hat{\underline{h}}''_i(y,z) \times \underline{x}_o$$

(77) $$\hat{Y}''_i = \frac{\kappa_i(x)}{\omega\mu}$$

(78) $$\psi_H = Be^{-j\gamma_i z} \cos \frac{m\Pi y}{b}$$

In the above equations, ^ is used to indicate results in the transverse-to-x representation, and $\hat{k}_{ti} = \sqrt{(\frac{m\Pi}{b})^2 + \gamma_i^2}$.

The modal representation of tranverse-to-x fields is

(79) $$\hat{\underline{E}}_t(x,y,z) = \sum_i V'_i(x)\hat{\underline{e}}_i(y,z) + \sum_j V''_j(x)\underline{e}''_j(y,z)$$

(80) $$\hat{\underline{H}}_t(x,y,z) = \sum_i \hat{I}_i(x)\hat{\underline{h}}'_i(y,z) + \sum_j \hat{I}''_j(x)\hat{\underline{h}}''_j(y,z)$$

where $\hat{V}_i^\alpha(x)$ and $\hat{I}_i^\alpha(x)$ are modal voltages an' currents which satisfy the transmission line equations:

$$\frac{d}{dx}\hat{V}_i^\alpha(x) = -j\kappa_i(x)\ Z_i I_i^\alpha(x) \tag{81}$$

$$\frac{d}{dx}\hat{I}_i^\alpha(x) = -j\kappa_i(x)\ \hat{Y}_i \hat{V}_i^\alpha(x) \tag{82}$$

The single mode tranverse-to-z magnetic field corresponding to eigenvalue γ_i of the LSM and E modal subsets must be equal. Thus, since $h'_x(x,y) = \hat{h}'_x(y,z) \equiv 0$,

$$\hat{I}'_i(x)\hat{h}'_{yi}(y,z)\underline{y}_o = I'\ e^{-j\gamma z}\varepsilon_r(x)e'_{xi}(x,y)\underline{y}_o \tag{83}$$

Using (71) in (72) , and letting $A = I'_i\hat{k}_{ti}/N'_i\gamma_i$ results in an expression for $e'_{xnm}(x,y)$ in terms of the x dependent modal current distribution $\hat{I}'_n(x)$:*

$$e'_{xnm}(x,y) = -j\frac{1}{N'_{nm}\varepsilon_r(x)}\ \hat{I}'_n(x)\sin\frac{m\Pi y}{b} \tag{84}$$

*in equations (84) and (86) , the double subscript is used to explicitly indicate x and y dependence.

Note that for m = 0, the LSM mode does not exist. Similarly, the single mode tranverse-to-z electric field corresponding to eigenvalue γ of the LSE and H modal subsets are equal giving

$$(85) \qquad \hat{V}''_{\ell}(x)\hat{e}''_{y\ell}(y,z)\underline{y}_o = -V''_{\ell}e^{-j\gamma_{\ell}z}h''_{x\ell}(x,y)\underline{y}_o$$

Letting $B_{\ell} = V''_{\ell}\hat{k}_{t\ell}/N''_{\ell}\gamma_{\ell}$ and using (75) in (76) results in

$$(86) \qquad h''_{xnm}(x,y) = -j\frac{1}{N''_{nm}}\hat{V}''_{n}(x)\cos\frac{m\Pi y}{b}$$

The coefficients N'_{nm} and N''_{nm} appearing in equations (84) and (86) are normalization constants determined by application of equation (70). Complete expressions for the normalizations are given in Appendix C.

Since the inhomogeneously (in x) loaded guide is symmetric about the midplane (x = 0), the modes will be either: symmetric, corresponding to an open circuit plane at x = 0 for LSE modes, or short circuit plane for LSM modes; or anti-symmetric, for the converse. Consider the equivalent transmission line representation of wave propagation in x shown in Figure 27. The complete current and voltage distributions may be written down by inspection for either of the indicated terminations. The resultant distributions are then appropriately inserted in (84) or (86) to obtain the cross-sectional dependence of the x components of LSM electric and LSE magnetic mode functions. The vector mode functions are summarized in Figures 28 and 29.

In normal operation as a dual frequency phased array element, the excited (propagating) modes of the symmetric twin dielectric slab loaded rectangular waveguide will be the LSE_{10} mode in the low frequency band, and LSE_{10} and LSE_{20} modes in the high frequency band. At either band, the tendency will be for the field strength interior to the dielectric slabs to exceed the field strength elsewhere. This characteristic is clearly evident in the equations of Figure 29 for slow wave propagation. Examination of the modal voltage expressions shows that for $\kappa_n = -j|\kappa_n|$, $e''_{y10}(x,y)$ is proportional to $\cosh(|\kappa_n x|)$ in $-\beta<x<0$, and to $\sinh |\kappa_n|(x+a/2)$ in $-a/2<x<-\beta-\delta$. Thus, for greatly slowed waves, i.e., $\gamma_{nm} \approx k\sqrt{\varepsilon_r}$, the $e''_{y10}(x,y)$ is nearly exponential in the air regions, and nearly constant in the dielectric. Similar characteristics

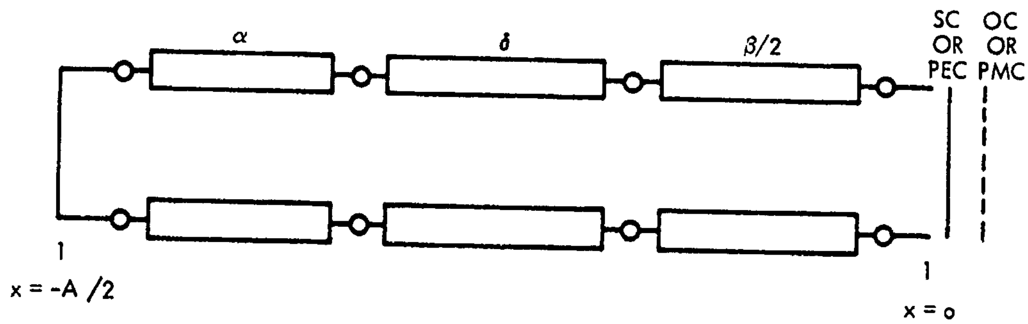

Figure 27. Equivalent Transmission Line Representation of Wave Propagation in x.

I. Transverse-to-z Mode Function

$$\underline{h}'_{nm}(x,y) = \varepsilon_r(x) e'_{xnm}(x,y)\underline{y}_o$$

$$\underline{e}'_{nm}(x,y) = e'_{xnm}(x,y)\underline{x}_o + \frac{1}{k^2\varepsilon_r(x)-\kappa_n^2(x)} \frac{\partial^2}{\partial x \partial y} e'_{xnm}(x,y)\underline{y}_o$$

$$Z'_{nm} = \frac{k^2\varepsilon_r(x)-\kappa_n^2(x)}{\gamma_{nm} j\omega\varepsilon_o}$$

where

$$\kappa_n^2(x) = k^2\varepsilon_r(x) - \left(\frac{m\pi}{b}\right)^2 - \gamma^2 = \begin{cases} \kappa_{\varepsilon n}^2, & \varepsilon_r(x)=\varepsilon_r \\ \kappa_n^2, & \varepsilon_r(x)=1 \end{cases}$$

$$e'_{xnm}(x,y) = -j\frac{1}{N'_{nm}\varepsilon_r(x)} \hat{I}'_n(x)\sin\frac{m\pi y}{b}$$

$$N'^2_{nm} = \frac{b}{2}\int_{-a/2}^{a/2} \frac{1}{\varepsilon_r(x)} |\hat{I}'_n(x)|^2 dx$$

$$\varepsilon_r(x) = \begin{cases} 1, & |x|<\beta,\ \beta+\delta<|x|<a/2 \\ \varepsilon_r, & \beta<|x|<\beta+\delta \end{cases}$$

II. Longitudinal Modal Currents, $\hat{I}'_n(x)$*

symmetric: $h'_{ynm}(|x|,y) = h'_{ynm}(-|x|,y)$

antisymmetric: $h'_{ynm}(|x|,y) = -h'_{ynm}(-|x|,y)$

$$I'_n(x) = \begin{cases} \cos\kappa_n x & , -\beta < x < 0 \\ B'_1\cos\kappa_{\varepsilon n}(x+\beta) + B'_2\sin\kappa_{\varepsilon n}(x+\beta) & , -\beta-\delta < x < -\beta \\ C'\cos\kappa_n(x+a/2) & , -a/2 < x < -\beta-\delta \end{cases}$$

$$\hat{I}'_n(x) = \begin{cases} \sin\kappa_n x & , -\beta < x < 0 \\ E'_1\cos\kappa_{\varepsilon r}(x+\beta) + E'_2\sin\kappa_{\varepsilon r}(x+\beta) & , -\beta-\delta < x < -\beta \\ F'\cos\kappa_n(x+a/2) & , -a/2 < x < -\beta-\delta \end{cases}$$

*The coefficients $B'_1, B'_2, C', E'_1, E'_2$, and F' are given in Appendix C.

Figure 28

LSM$_{nm}$ Mode Functions

I. Transverse-to-z Mode Functions

$$\underline{e}''_{nm}(x,y) = -h''_{xnm}(x,y)\underline{y}_o$$

$$\underline{h}''_{nm}(x,y) = \hat{h}''_{xnm}(x,y)\underline{x}_o + \frac{1}{k^2_{\varepsilon r}(x) - \kappa^2_n(x)} \frac{\partial^2}{\partial x \, \partial y} h''_{xnm}(x,y)\underline{y}_o$$

$$Y''_{nm} = \frac{k^2_{\varepsilon r}(x) - \kappa^2_n(x)}{\omega\mu \; \gamma_{nm}}$$

where

$$\kappa^2_n(x) = k^2_{\varepsilon r}(x) - \frac{m\Pi}{b}^2 - \gamma^2_{nm} = \begin{cases} \kappa^2_{\varepsilon n}, \varepsilon_r(x) = \varepsilon_r \\ \kappa^2_n, \varepsilon_r(x) = 1 \end{cases}$$

$$h''_{xnm}(x,y) = -j\frac{1}{N''_{nm}} \hat{V}''_n(x) \cos \frac{m\Pi y}{b}$$

$$N''^2_{nm} = \frac{r_m b}{2} \int_{-a/2}^{a/2} |\hat{V}''_n(x)|^2 dx, \quad r_m = \begin{matrix} 2, m=0 \\ 1, m \neq 0 \end{matrix}$$

II. Longitudinal (in x) Modal Voltages, $\hat{V}''_n(x)$ *

Symmetric: $e''_{ynm}(|x|,y) = e''_{ynm}(-|x|,y)$ Antisymmetric: $e''_{ynm}(|x|,y) = -e''_{ynm}(-|x|,y)$

$$\hat{V}''_n(x) = \begin{cases} \cos\kappa_n x & , -\beta < x < 0 \\ B''_1 \cos\kappa_{\varepsilon r}(x+\beta) + B''_2 \sin\kappa_{\varepsilon n}(x+\beta) & , -\beta-\delta < x < -\beta \\ C'' \sin\kappa_n(x+a/2) & , -a/2 < x < -\beta-\delta \end{cases}$$

$$V''_n(x) = \begin{cases} \sin\kappa_n x & , -\beta < x < 0 \\ E''_1 \cos\kappa_{\varepsilon n}(x+\beta) + E''_2 \sin\kappa_{\varepsilon n}(x+\beta) & , -\beta-\delta < x < -\beta \\ F'' \sin\kappa_n(x+a/2) & , -a/2 < x < -\beta-\delta \end{cases}$$

(The coefficients $B''_1, B''_2, C'', E''_1, E''_2$, and F'' are given in Appendix C)

Figure 29

LSE_{nm} Mode Function

are evident for the LSE_{20} mode (the first anti-symmetric in x mode).

Typical $e''_{y10}(x,y)$ distributions are shown in Figures 30 and 31 for an element operating at 2.5 GHz and 6.0 GHz, respectively. The element is a WR187 guide with .250" ($=\delta$) slabs of $\varepsilon_r = 9$ dielectric located .325" ($=\alpha$) from either narrow wall. At low frequency, the distribution is roughly uniform between slabs, with some field concentration in the vicinity of the interior air-dielectric interfaces. In the region $|x|>\beta+\delta$, the field behaves very nearly like $\cos(\Pi x/A)$. At 6 GHz, the $e'_{y10}(x,y)$ distribution is entirely different, showing well defined field concentration about the dielectric, with very low field strength in the air-filled regions. The distributions are roughly symmetric about the slabs, with non-zero field at the guide center. As the dielectric constant is increased the fields become more heavily concentrated in the dielectric, and, consequently, the field strength at the guide center approaches zero.

At 6 GHz, the antisymmetric LSE_{20} mode is also propagating, and all other modes are well beyond cut-off. The $e''_{y20}(x,y)$ distribution is shown overlayed on the $e''_{y10}(x,y)$ distribution in Figure 32. This comparison shows that the

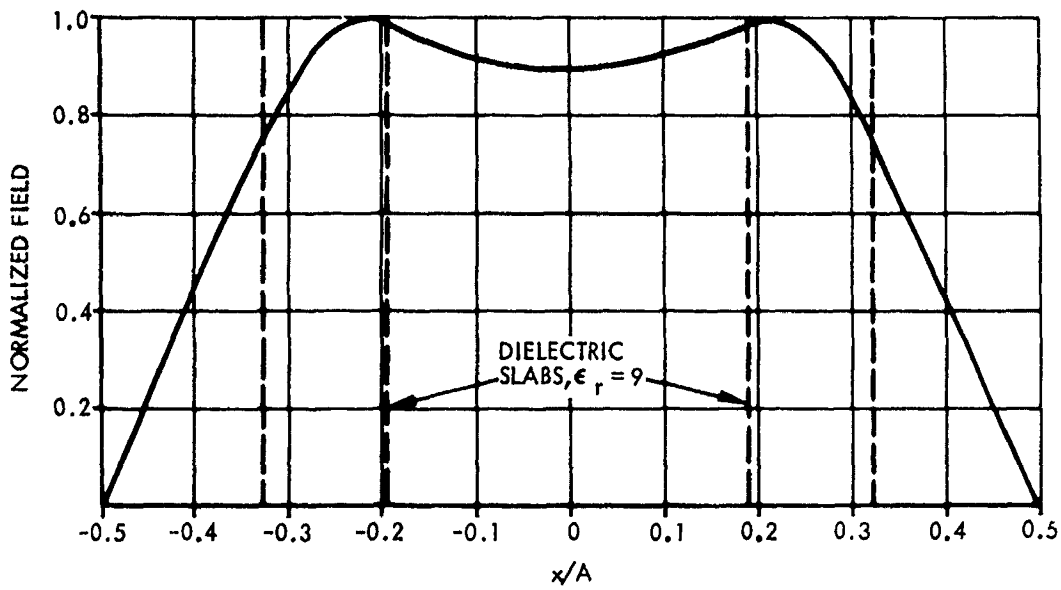

Figure 30. e_{y10} (x,y) Distribution for WR187 Bifurcated Guide With .250" Thick ϵ_r = 9 Loading. 2.5 GHz

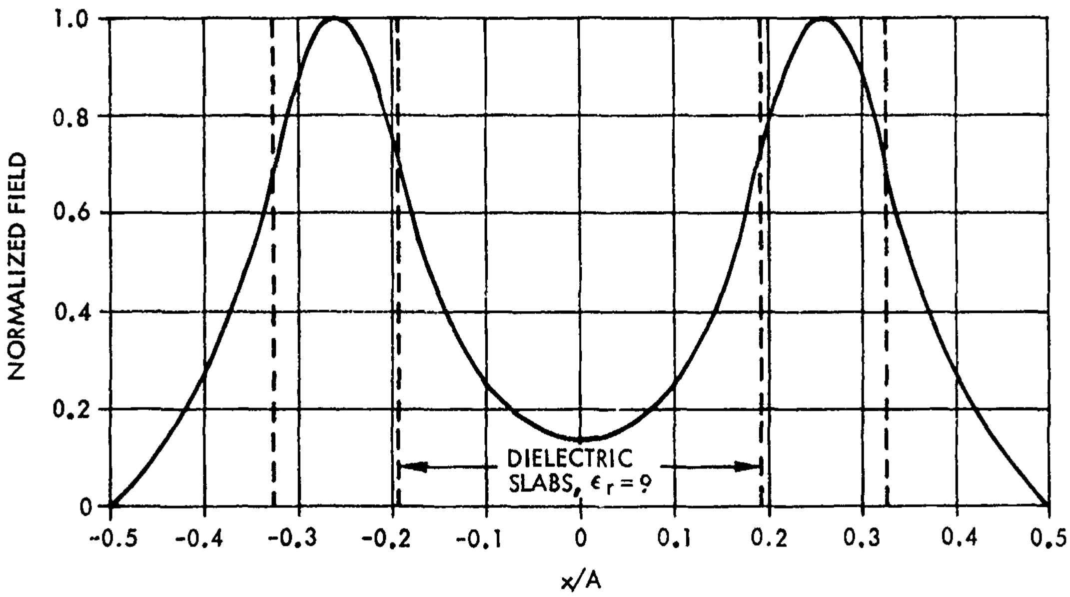

Figure 31. e_{y10} (x,y) Distribution for WR187 Bifurcated Guide With .250"Thick ϵ_r = 9 Loading. 6 GHz

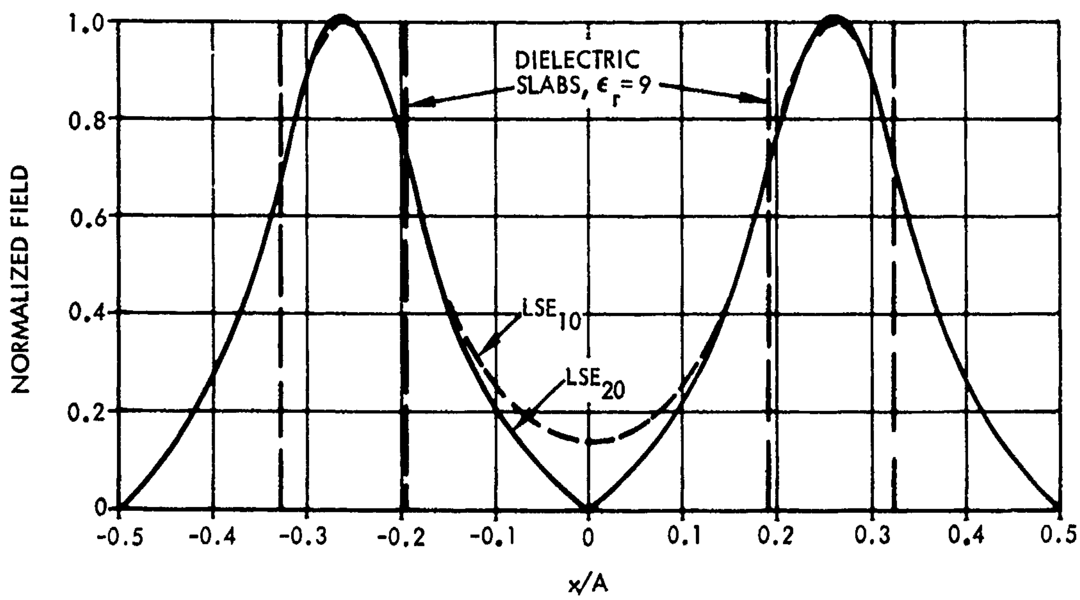

Figure 32. e_{y10} and e_{y20} (x,y) Distributions for WR187 Bifurcated Guide With .250" Thick ϵ_r = 9 Loading. 6 GHz

LSE_{10} and LSE_{20} modal field distributions are quite similar, differing by no more than a few percent in relative magnitude for $|x/A|>.15$, but having opposite symmetries. It is this high frequency propagation characteristic and the fact that $\gamma_{20}/\gamma_{10} \doteq 1.0$ for appropriately chosen dielectric constants and guide geometries which provide the unique dual frequency array element potential of the symmetric twin dielectric slab loaded rectangular waveguide. For, assuming the functions are exactly identical in magnitude and that $\gamma_{20}/\gamma_{10} = 1$, the LSE_{10} and LSE_{20} modes, by magnitude control only, may be excited such that two independent phase centers are located at roughly the positions of the slabs.

The similarity of the $e''_{y10}(x,y)$ and $e''_{y20}(x,y)$ distributions, and hence, the achieveable high frequency phase center independence, is directly related to dielectric constant for fixed geometry. As the dielectric constant is decreased, holding cross-section fixed, the LSE_{10} distribution approaches the TE_{10} distribution of empty guide; and the LSE_{20} approaches the empty guide TE_{20} distribution. These trends are evident in Figure 33, where the $e''_{y10}(x,y)$ and $e''_{y20}(x,y)$ distributions are shown overlayed for the WR187 guide with $\varepsilon_r = 5$ loading. The departure in magnitude

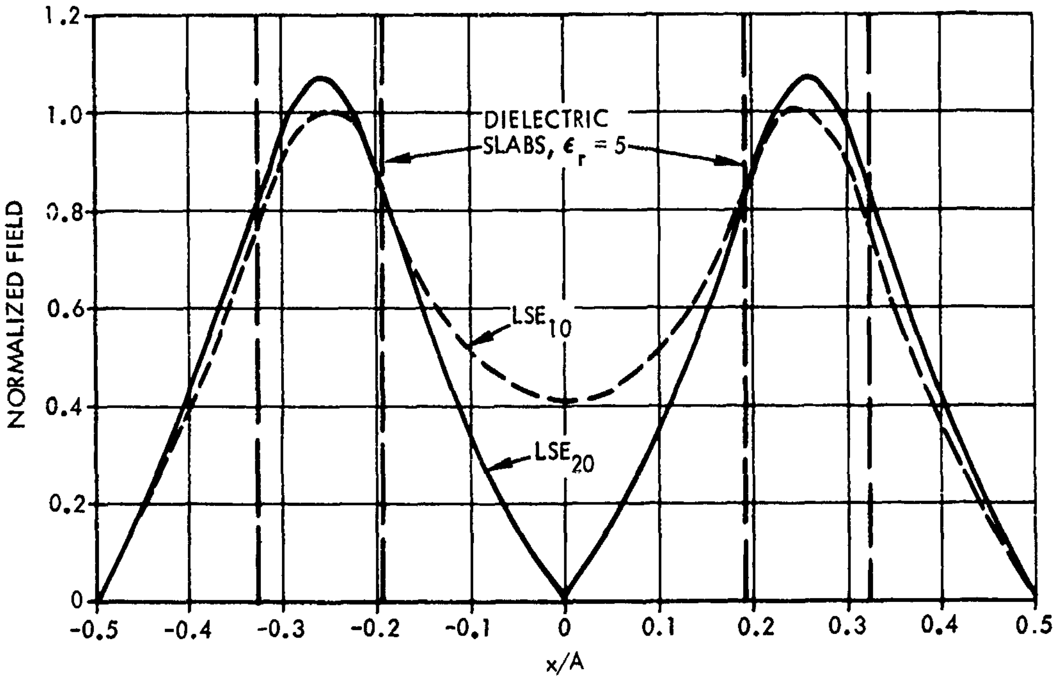

Figure 33. e_{y10} and e_{y20} (x,y) Distrubutions for WR187 Bifurcated Guide With .250" Thick ϵ_r = 5 Loading. 6 GHz

between the distributions is significantly greater for the lower dielectric constant than for the higher.

While the above discussion shows that there is a strong influence of dielectric constant on achieveable high frequency phase center independence, it should not be construed that large dielectric constant is generally preferable to low dielectric constant. In particular, it will be shown in section 4-1 that for certain geometries, dielectric constants on the order of $\varepsilon_r = 9$ may lead to large aperture reflections which are difficult, if not impossible, to match out.

3.2 Mode Spectrum

The modal spectrum of the symmetric twin dielectric slab loaded rectangular waveguide is obtained *via* a transverse resonance procedure. Representing the loaded guide as an E or H mode transmission line in x, as in Figure 27, and requiring that x = 0 be either an open or short circuit plane results in four dispersion relations, in x, of the form,

$$D(\kappa_n, \kappa_{\varepsilon n}) = 0. \tag{87}$$

where

$$\kappa_n^2 = k^2 - \left(\frac{m\Pi}{B}\right)^2 - \gamma_{nm}^2 \tag{88}$$

$$\kappa_{\varepsilon n}^2 = \kappa_n^2 + k_n^2(\varepsilon_r - 1) \tag{89}$$

$k = 2\Pi/\lambda$ is the free space wave number, $m\Pi/B$ is the y directed wave number, and γ_{nm} is the z directed wave-number. One dispersion relation is obtained for each symmetry condition, in x, of each modal subset. The four dispersion relations are given in Table 2. It should be noted that the forms given are computationally unstable due to both the various tangent evaluations,

Mode	Symmetry	Condition at x = 0	$D(\kappa,\kappa_\varepsilon)$
LSM	Symmetric	S.C. or PEC	$\varepsilon_r\kappa\tan\kappa\alpha + \kappa_\varepsilon \dfrac{\varepsilon_r\kappa\tan\kappa + \kappa_\varepsilon\tan\kappa_\varepsilon\delta}{\kappa_\varepsilon-\varepsilon_r\kappa\tan\kappa\beta\tan\kappa_\varepsilon\delta}$
LSM	Anti-Symmetric	O.C. or PMC	$\varepsilon_r\kappa\tan\kappa\alpha+\kappa_\varepsilon \dfrac{\kappa_\varepsilon\tan\kappa_\varepsilon\delta-\varepsilon_r\kappa\cot\kappa\beta}{\kappa_\varepsilon+\varepsilon_r\kappa\cot\kappa\beta\tan\kappa_\varepsilon\delta}$
LSE	Symmetric	O.C. or PMC	$\kappa_\varepsilon\tan\kappa\alpha+\kappa \dfrac{\kappa\tan\kappa\beta\tan\kappa_\varepsilon\delta-\kappa_\varepsilon}{\kappa_\varepsilon\tan\kappa_\varepsilon\delta+\kappa\tan\kappa\beta}$
LSE	Anti-Symmetric	S.C. or PEC	$\kappa_\varepsilon\tan\kappa\alpha+\kappa \dfrac{\kappa_\varepsilon\tan\kappa\beta+\kappa\tan\kappa_\varepsilon\delta}{\kappa-\kappa_\varepsilon\tan\kappa_\varepsilon\delta\tan\kappa\beta}$

Table 2, Dispersion Relations for Inhomogeneously Loaded Rectangular Waveguide and the indicated divisions. In practice, the expressions are converted to combinations of sines and cosines, and all divisions are removed.

In the LSE and LSM modal subsets, the mode indexing is (n,m). The first index, n, is associated with the infinite sequence of zeros of $D(\kappa,\kappa_\varepsilon)$ which are arrayed along the real κ_ε axis, as illustrated in Figure 34. The first zero is always associated with the even symmetry solution of the modal subset (i.e. open circuit symmetry for LSE modes; short circuit symmetry for LSM modes). Thereafter, the roots of the even and odd symmetry dispersion relations are interleaved. Hence, for even symmetry, n is always odd, and conversely. The second index, m, appears explicitly in the auxilliary dispersion equation, (88), and is directly interpreted as the order of the y variation of the modal field.

The potential of the symmetric twin dielectric slab loaded rectangular waveguide as a dual frequency array element arises, in part, due to the unique migration of the roots γ_{10} and γ_{20} with frequency. Figure 35 shows an LSE mode dispersion diagram for half height WR187 guide with $\varepsilon = 9$ loading. Only the (n,o), n = 1,2,3 and (n,1), n = 1,2 roots are shown, other LSE roots being considerably

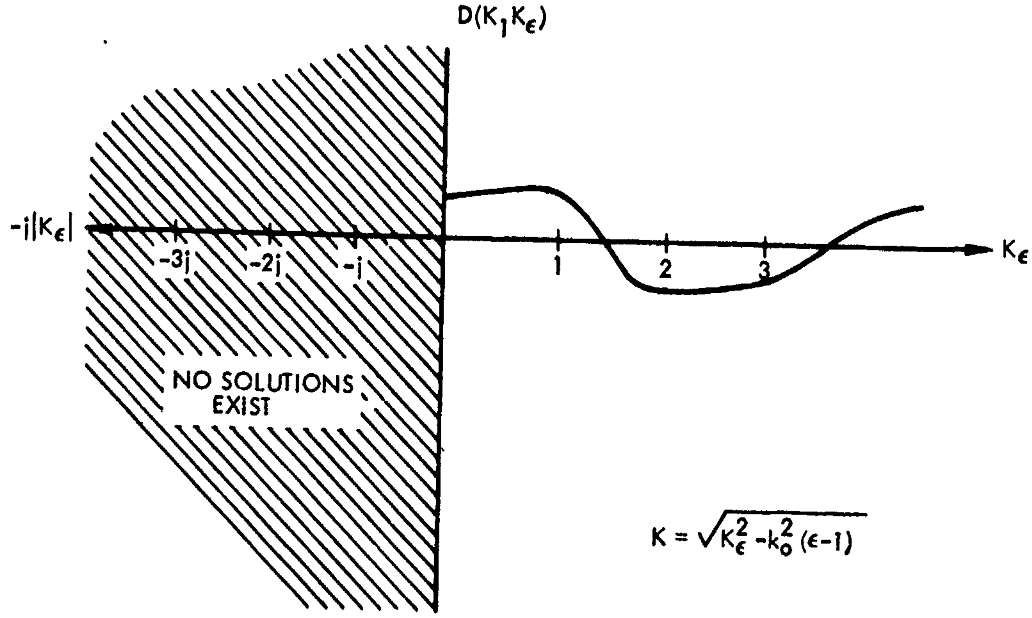

Figure 34. Disposition of Roots of $D(K,K_\epsilon)$ Along Real K_ϵ Axis

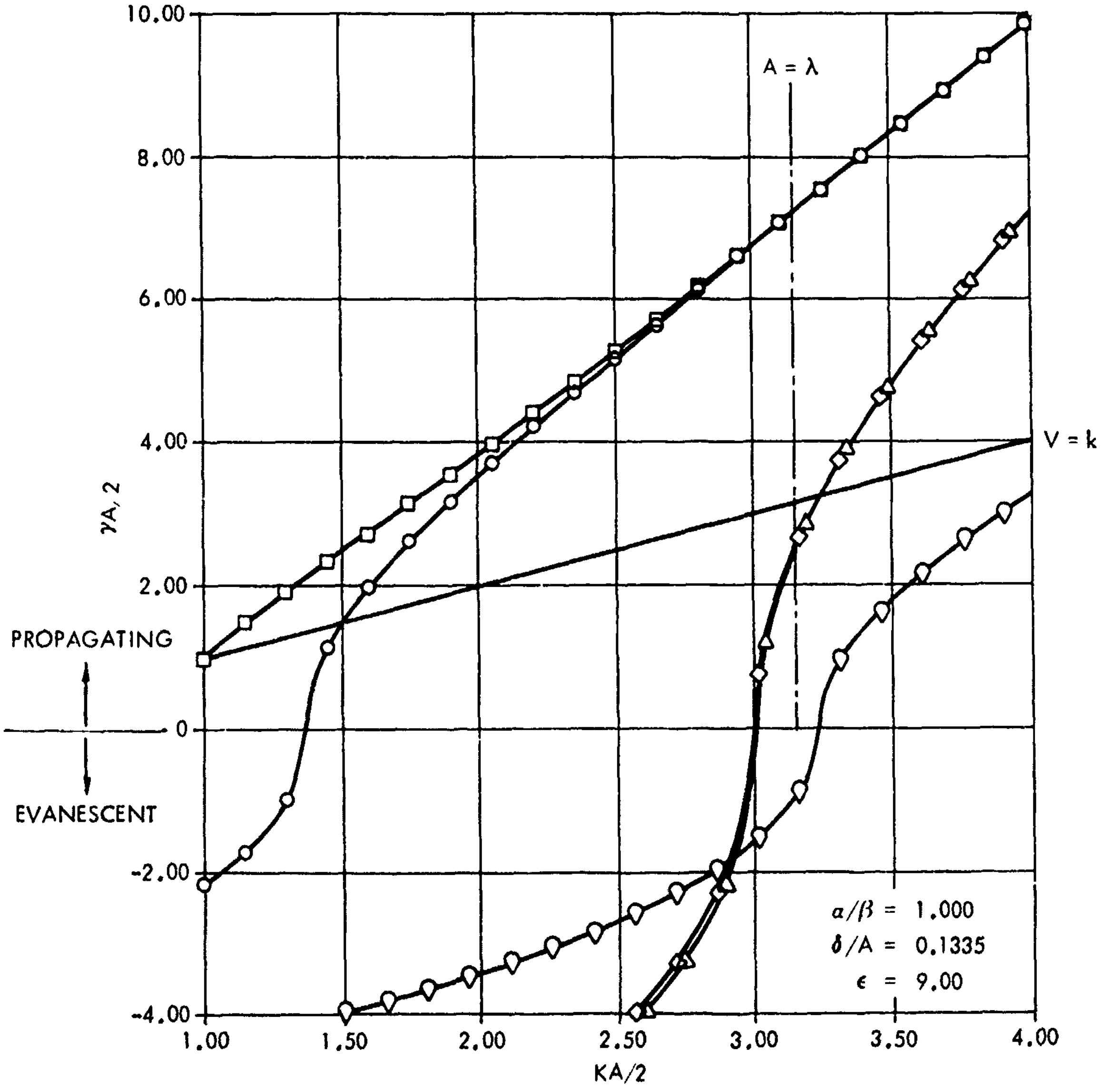

Figure 35. LSE Dispersion Diagram for Bifurcated WR187 Guide With 250" Thick ϵ_r = 9 Loading

more evanescent. For $kA/2 < 1.40$, only the LSE_{10} mode is propagating. As frequency is increased, the LSE_{20} mode begins to propagate, and γ_{20} rapidly approaches γ_{10}, the ratio γ_{20}/γ_{10} being nearly unity for $KA/2 > 2.5$. As frequency is further increased, the LSE_{11} and LSE_{21} modes begin to propagate, though they may, of course, be pushed further out by decreasing the guide height. The result is that over the range $2.5 < kA/2 < 3.0$, the propagating modes of the structure have virtually identical dispersion. Hence, if in this range, the LSE_{10} and LSE_{20} mode functions differs only in symmetry, as in Figure 32, the half height WR187 guide with $\varepsilon_r=9$ slab loading will support two independent phase centers over an 18% frequency band centered at $kA/2 = 2.75$; and over multiple guide wavelengths, $2\Pi/\gamma_{10}$, in z.

The dashed line, $\gamma = k$, in Figure 35 may be used to estimate the mismatch at the feedguide-free space interface for broadside excitation (only the LSE_{10} is excited). The modal admittance of the LSE_{10} mode is $\gamma_{10}/\omega\mu$, and the modal admittance of the dominant space harmonic is $k/\omega\mu$ at broadside. As an estimate, then, the reflection coefficient at the aperture will be in the neighborhood of

$$(90) \qquad |\Gamma| = \frac{Y_{10}-k}{Y_{10}+k}$$

for broadside excitation. For the WR187 guide with $\varepsilon_r=9$ loading, operating at KA/2 = 2.99, equation (4-39) gives $|\Gamma|$ = .383, whereas the exact value for a rectangular thin wall array of these guides is $|\Gamma|$ = .424. For the same guide operating at kA/2 = 1.25, equation (90) gives $|\Gamma|$ = .110, and the exact value is $|\Gamma|$ = .285. In both cases, the implication is that the aperture susceptance, which is ignored in (90), is significant. This is not entirely surprising, since it is well known* that equation (90) is exact for thin walled rectangular grid arrays of empty rectangular grid guide, for which the set of transverse wavenumbers of the feedguide is the set of transverse wavenumbers for the unit cell guide.

For fixed guide wall dimensions, the parameters which most strongly influence the dispersion curves are dielectric constant and slab thickness. The location of the slabs, denoted by the ratio α/β, has second order effects in the regions $.5 < \alpha/\beta \leq 2.0$. α/β ratios outside this region are not of interest due to the irregularly spaced high freq-

*See, for example, Amitay, Galindo, and Wu,(10) pg 132ff.

uency phase centers which would result.

Figures 36 through 39 are LSE dispersion diagrams for half height WR137 guide with δ = .250" and α/β = 1.00. The curves progress from loading of ε_r=3 to ε_r=9. As the loading increases, γ_{20} approaches γ_{10}, in general, and the trend is toward steeper slopes.

The migration of the LSE_{30} cutoff frequency toward lower frequency produces one of the critical trade-offs inherent to the design of the symmetric twin dielectric slab rectangular waveguide dual frequency array element. In general, the overriding array design criterion will be to minimize the number of radiators (or, equivalently maximize array cell size). Thus, for dual frequency operation, the high frequency band center operating point will be in the vicinity of $kA/2 = \Pi$. In this region, the higher dielectric constants (ε_r = 7,9) provide γ_{20}/γ_{10} ratios very close to unity, but the LSE_{30} mode is propagating. Since it is necessary to push this mode out, lower dielectric constant is required.

Similar results are obtained by holding ε_r fixed and varying only slab thickness, δ. Figures 40 through 43 are LSE dispersion diagrams for four slab thicknesses in half height WR137 guide. The dielectric constant is 5, and α/β = 1.00. In general, the behavior with thickness

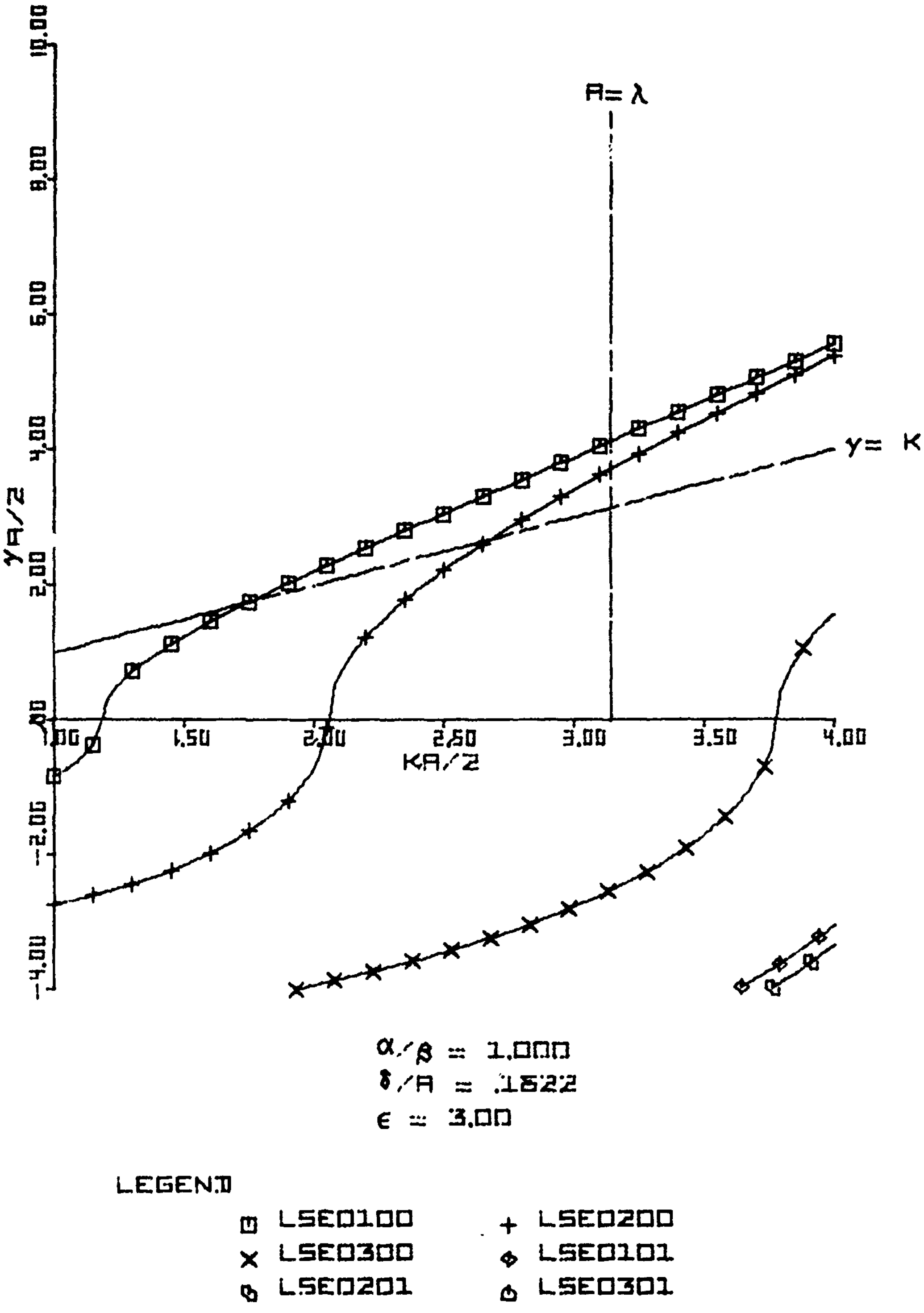

Figure 36. LSE Dispersion Diagram for Bifurcated WR137 Guide With 250" Thick $\epsilon_r = 3$ Loading

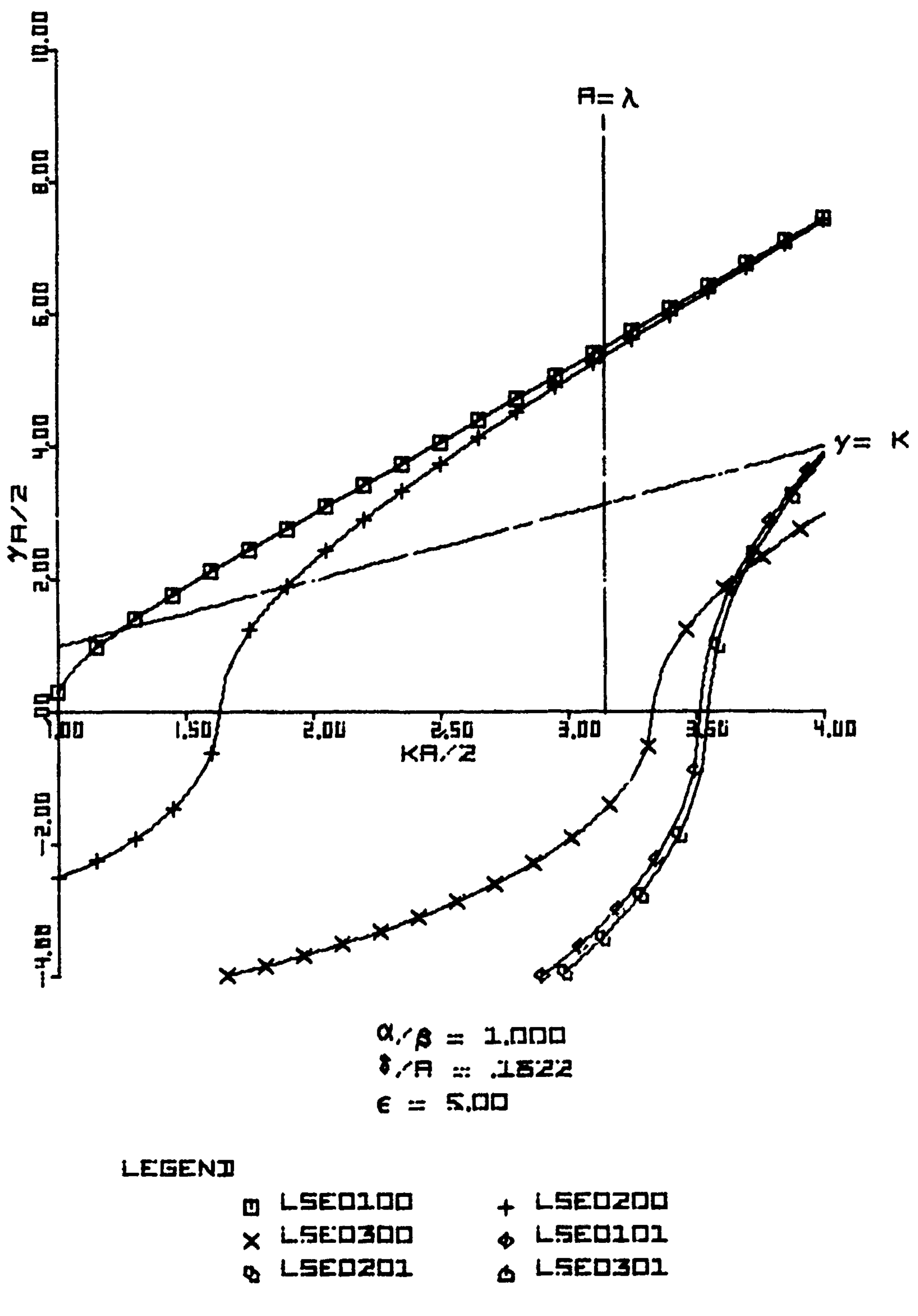

Figure 37. LSE Dispersion Diagram for Bifurcated WR137 Guide With .250" Thick ϵ_r = 5 Loading

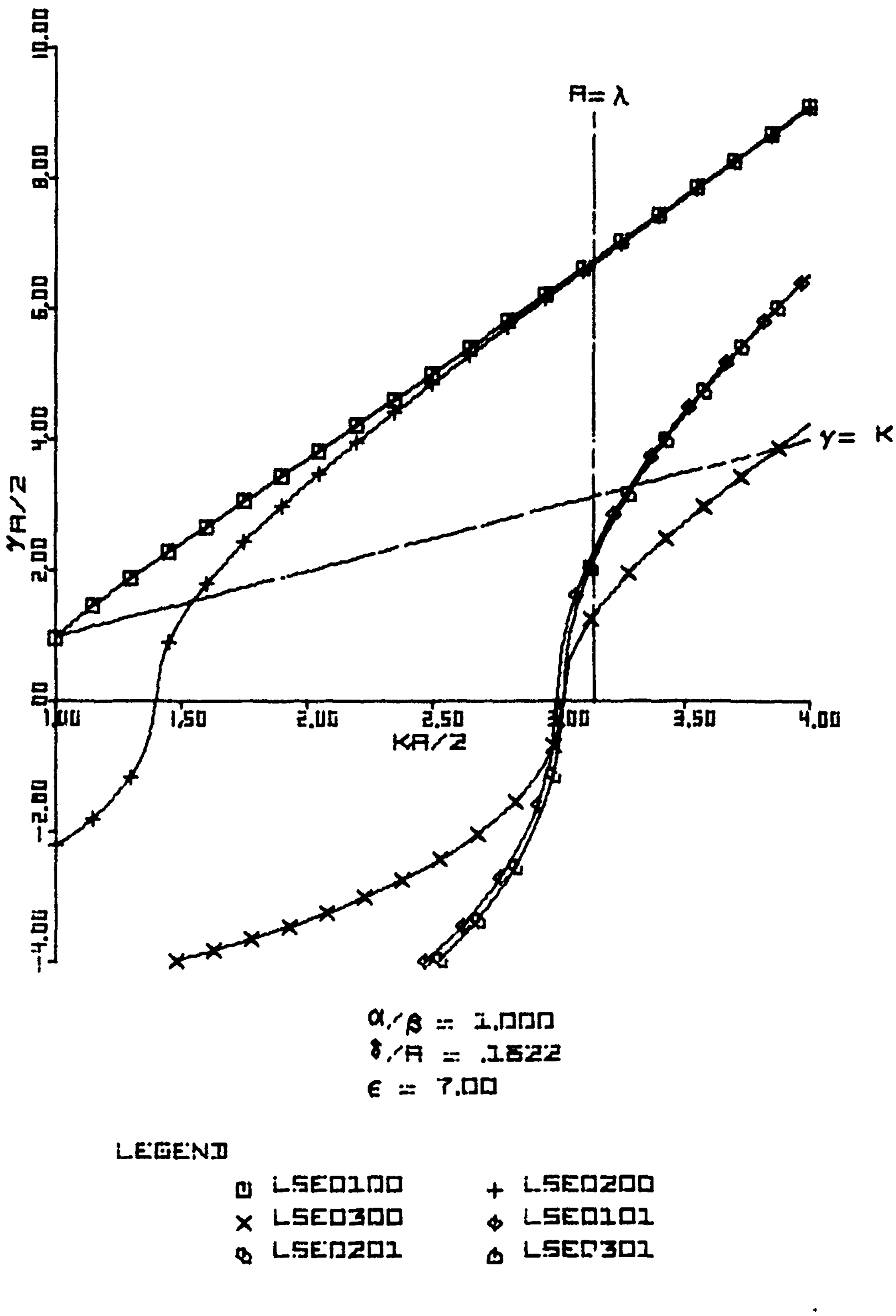

Figure 38. LSE Dispersion Diagram for Bifurcated WR137 Guide With .250" Thick ϵ_r = 7 Loading

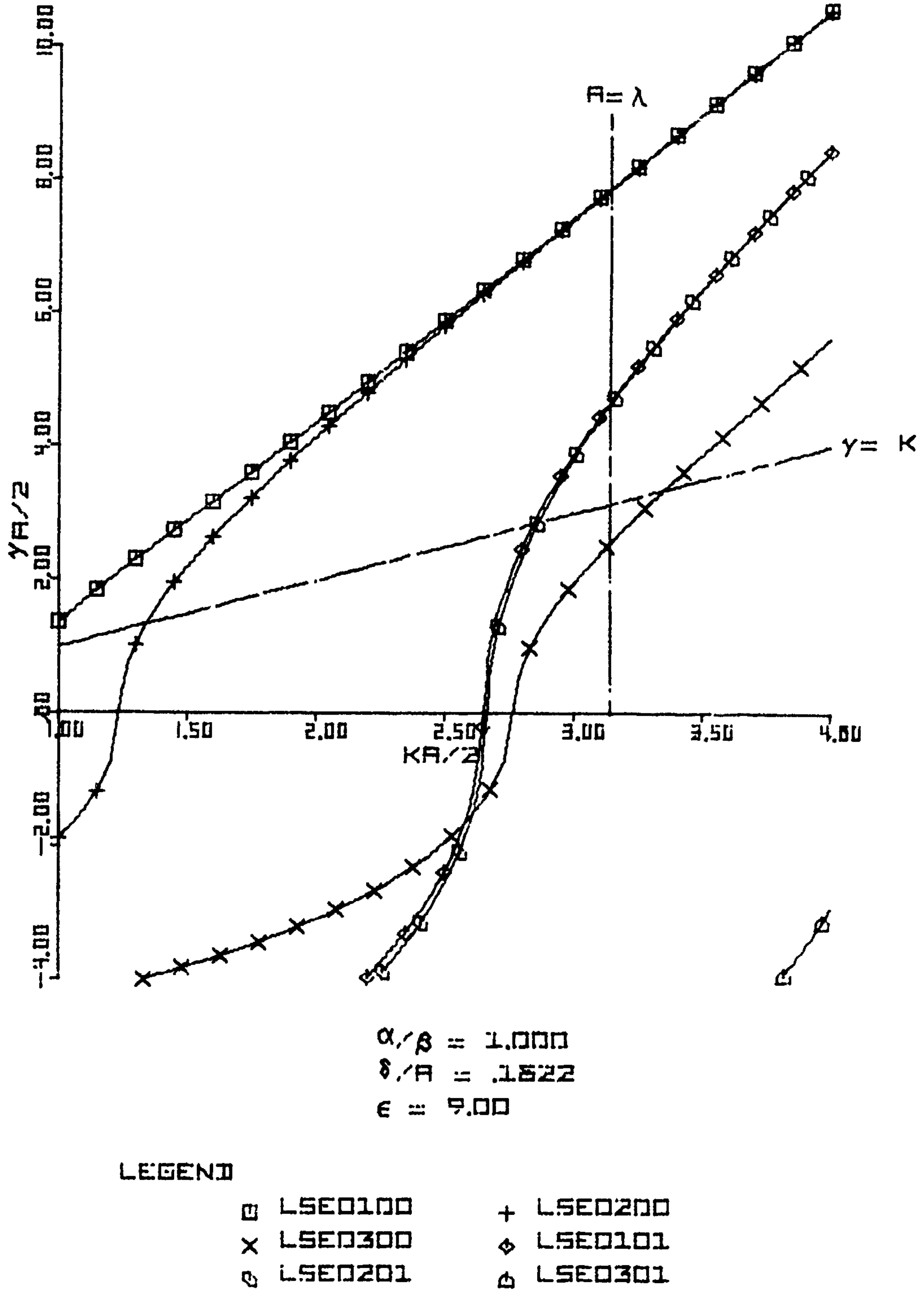

Figure 39. LSE Dispersion Diagram for Bifurcated WR137 Guide With .250" Thick ϵ_r = 9 Loading

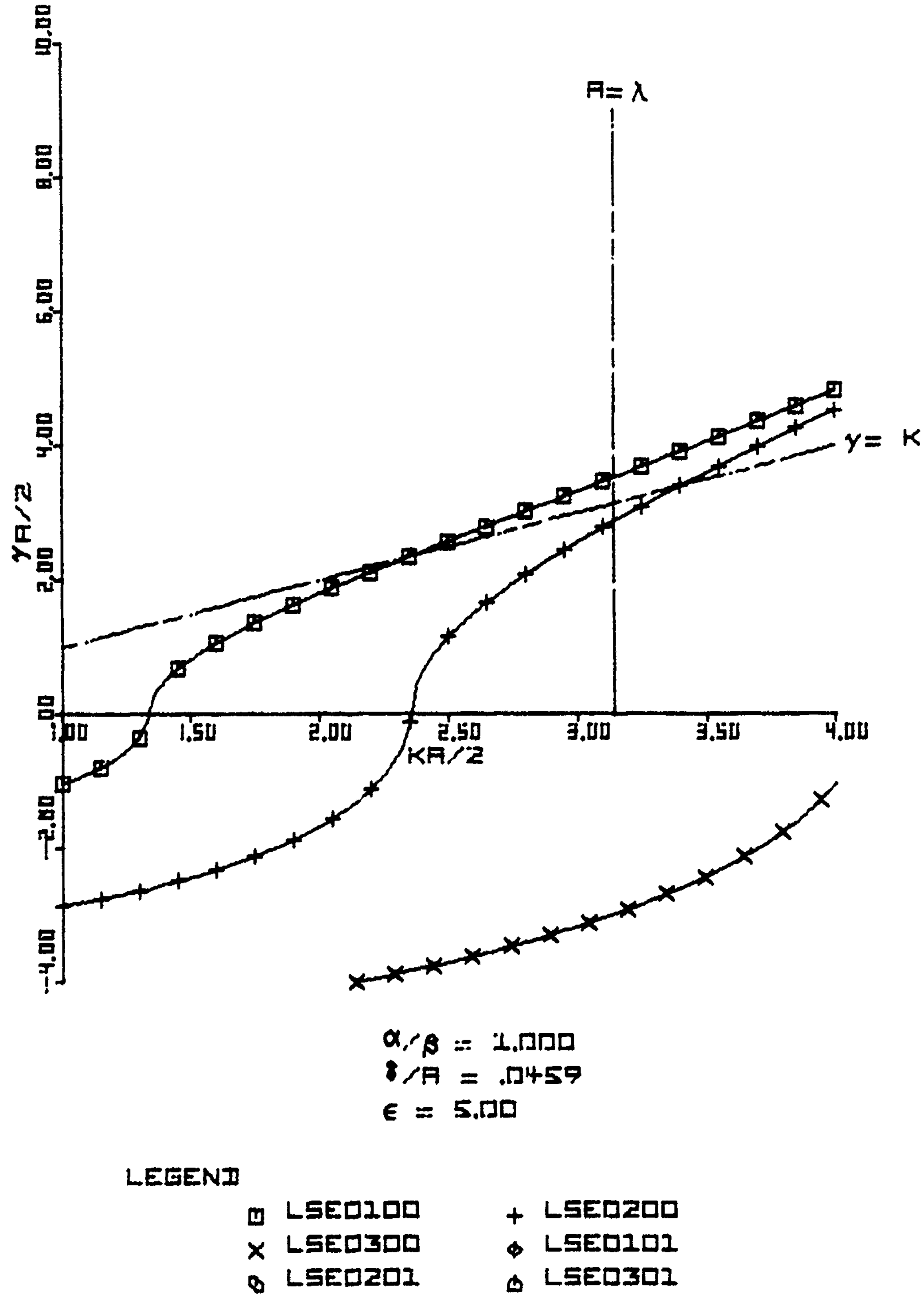

Figure 40. LSE Dispersion Diagram for Bifurcated WR137 Guide With .063" Thick $\epsilon_r = 5$ Loading

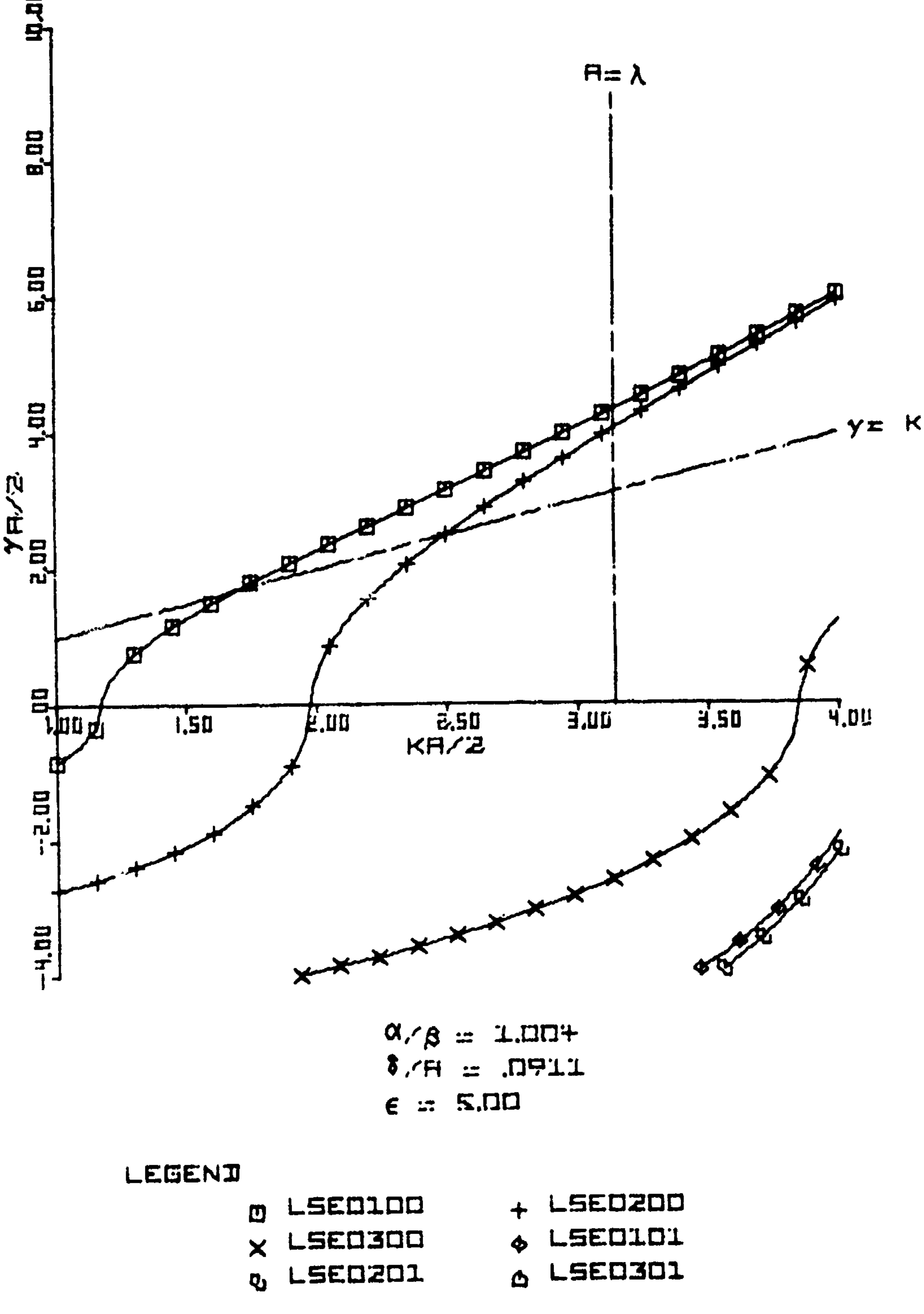

Figure 41. LSE Dispersion Diagram for Bifurcated WR137 Guide With .125" Thick ϵ_r = 5 Loading

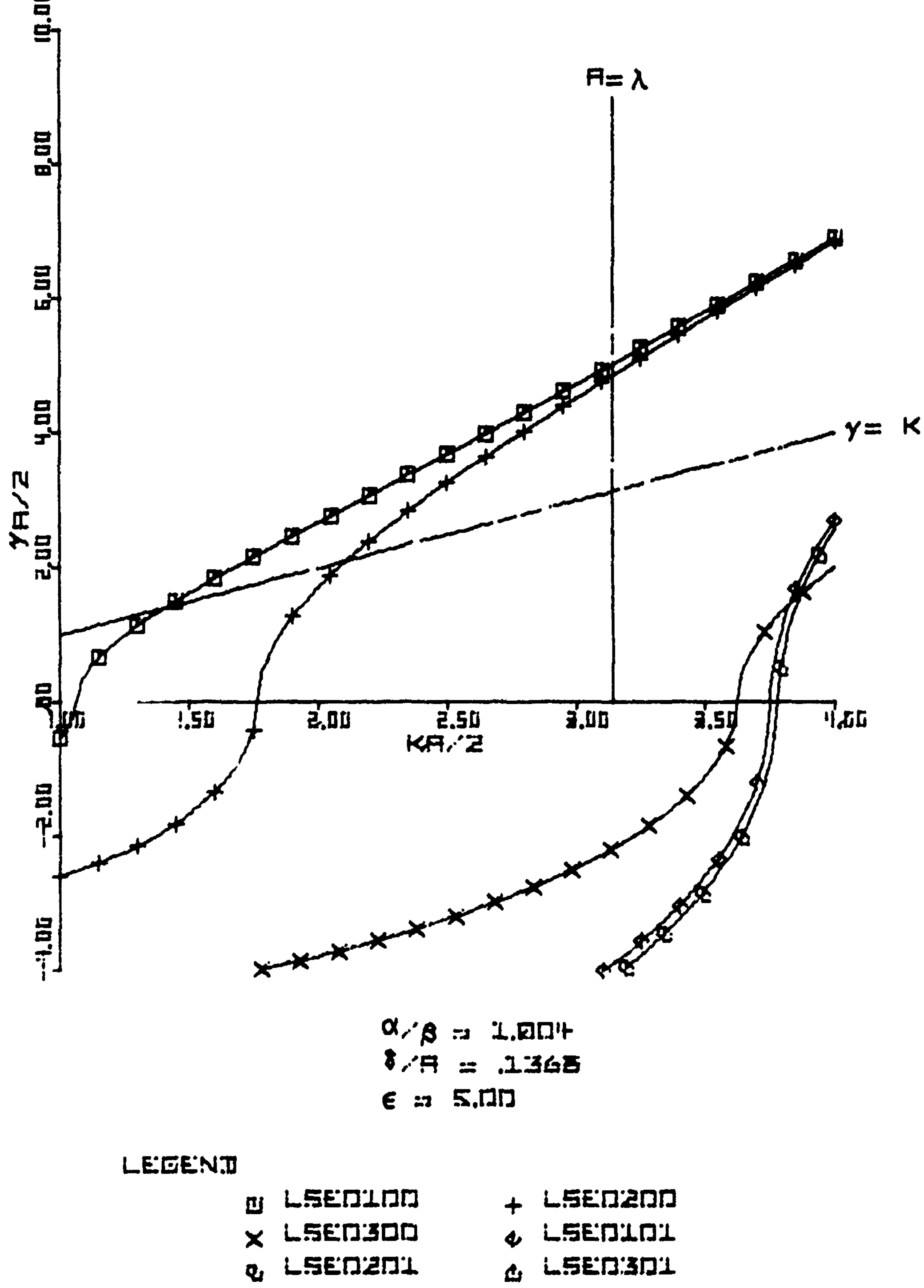

Figure 42. LSE Dispersion Diagram for Bifurcated WR137 Guide With .188" Thick ϵ_r = 5 Loading

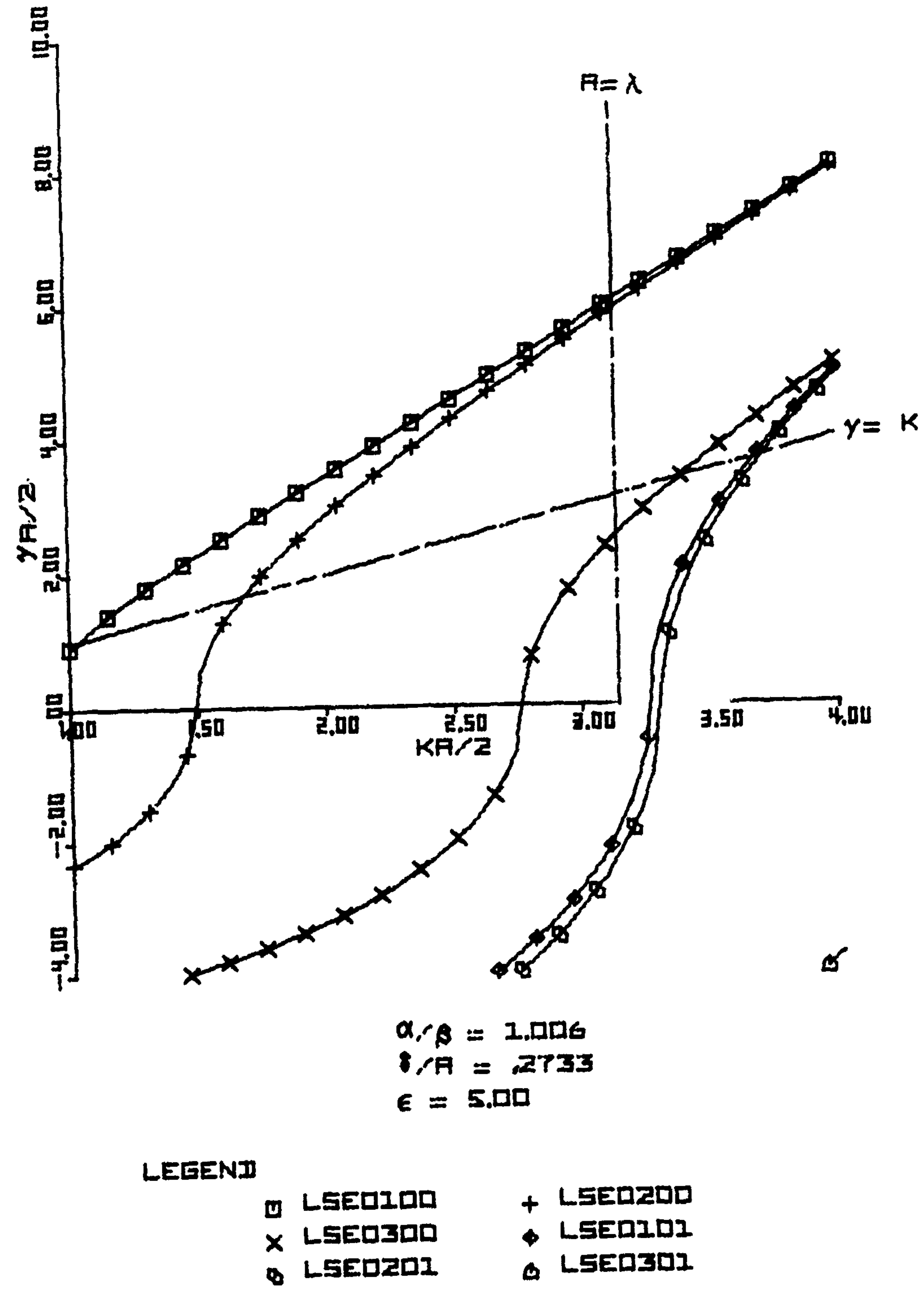

Figure 43. LSE Dispersion Diagram for Bifurcated WR137 Guide With .375" Thick ϵ_r = 5 Loading

is very like the behavior with ε_r. However, comparison of Figures 39 and 43 shows that high dielectric constant is preferable to extreme thickness. In the two figures, the LSE_{30} mode enters at roughly the same frequency, but the ratio of z directed wave numbers, γ_{20}/γ_{10}, is significantly nearer to unity for $\varepsilon_r=9$ than for $\varepsilon_r=5$.

4.0 ARRAY APERTURE DESIGN

In this section, the trade-offs leading to a practical array aperture design are presented for the hypothetical array performance given in Table 3. The operating bands are 15% centered at 4 and 8 GHz. Sixty degree (60^o) principle plane scan coverage is required. The array is to provide 30 db gain for 60^o principle plane scan at 4 GHz. The first sidelobe level is to be below 20 db and RMS sidelobe levels are to be below 35 db. Nominal feed losses of 1.5 db at 4 GHz and 2.8 db at 8 GHz are assumed. To reduce the inherent difficulties in matching out the aperture, an aperture mismatch loss at broadside of no greater than .6 db is required.

To provide the required performance, a Taylor, $\bar{n}=3$, 25 db SLL distribution is selected, resulting in an aperture gain of 37 db at 4 GHz.

The principle result of this section is the determination of an element/grid configuration which minimizes element count while holding high frequency grating lobe contributions to levels consistant with the sidelobe requirements.

Frequency	4,8 GHz $\pm$7.5%
Scan Coverage	$\pm 60^{\circ}$ in either principle plane
Aperture Gain @ 60° Principle Plane Scan	30 db @ 4 GHz
1st Sidelobe Level	20 db
RMS Sidelobe Level	35 db
Feed Losses	1.5 db @ 4 GHz
	2.8 db @ 8 GHz
Aperture Mismatch Loss @ 0° Scan	<.6 db in both bands

Table 3

Prescribed Array Performance

4.1 Aperture Design Trade-Offs

It is well-known[16] that an equilateral triangle lattice configuration minimizes element count for a given scan requirement. As a basis for comparison, it is therefore, convenient to first consider a lattice specifically taylored to minimize element count at low frequency. This lattice and the near-in grating lobe diagrams for 4 and 8 GHz are shown in Figure 44. The lattice base is 1.780" (.602λ @ 4 GHz).

It is immediately apparent from Figure 44c that the six near-in high frequency grating lobes will migrate well inside the coverage sector for all scan directions and pose a potential limitation on achieveable peak sidelobe level and main beam gain. This difficulty may be alleiviated somewhat by appropriate selection of the element configuration and high frequency excitation modifier, R, for the LSE_{20} mode as discussed in section 2.2. However, it should be noted that the six grating lobe locations actually represent twelve independent beams (six each E and H with respect

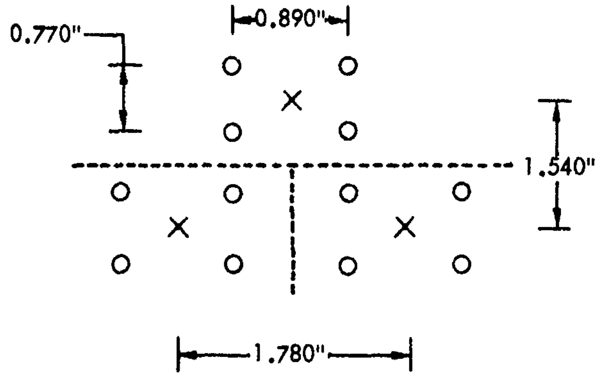

(a) Lattice Configuration Shown Low (x) and High (o) Frequency Centers

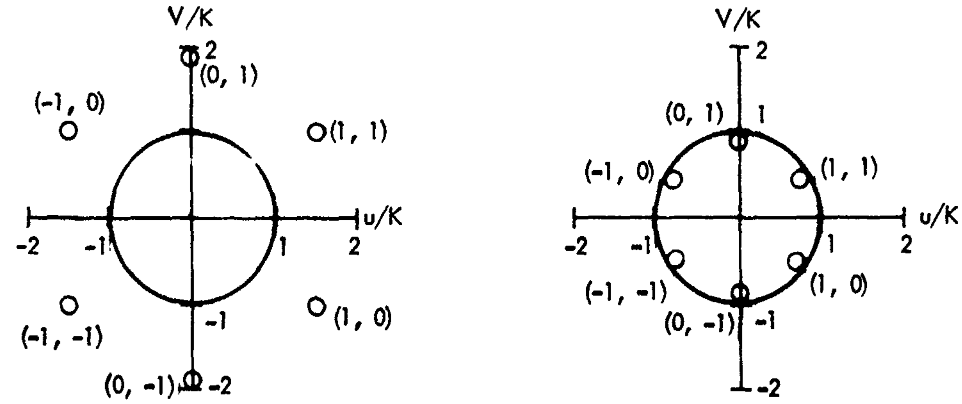

(b) Low Frequency Grating Lobe Diagram - $\lambda/_{Dx} = 1.66$, $\lambda/_{Dy} = 1.92$

(c) High Frequency Grating Low Diagram - $\lambda/_{Dx} = .83$, $\lambda/_{Dy} = .96$

Figure 44. Equilateral Triangle Lattice Configuration Which Minimizes Element Count @ 4 GHz

to the array normal). Since there are only nine design parameters (half aperture dimensions A and B; septum thickness; Δ; relative permittivity, ε; slab thickness, δ; ratio α/β; lattice spacings, d_x and d_y; and R), it is clear that there is insufficient control for the cancellation of all beams.

The only available means of cancelling the beams residing along the v axis, the (0,1) and (0,-1) lobes is to separate the half apertures by one half the y lattice spacing d_y, resulting in a scanning sub-array pattern with nulls coincident with the grating lobe. This coincidence is maintained for H-plane scanning, however degrades in all other scan planes due to the imbalance in half-aperture reflections induced by the phase taper. In the circumstance that the half apertures are spaced at less than 0.5 d_y, a significant fraction of the radiated power is delivered to the E-mode (0,1) and (0,-1) beams for all scan directions, including broadside. In calculations with the half apertures separated by 0.26 d_y, it was found that as much as 20% of the power was delivered to each of the two E-mode beams at broadside scan.

Cancellation of the remaining eight beams is a considerably more difficult problem, and turns out to be virtually impossible for this large lattice spacing. Again, effective reduction of radiated power into the unwanted lobes must be obtained by locating the null of a scanning subarray pattern at or near the grating lobe location. One subarray spacing has already been used to cancel the on axis lobes; the remaining degree of freedom is therefore, the x separation of the apparent high frequency phase centers. In the event that these separations can be extended to 0.5 d_x, good grating lobe rejection can be achieved. However, as a practical matter,such wide x displacements of apparent high frequency phase centers are not possible.

As was shown in section 3.2, a reasonable upper limit on aperture x dimension is in the vicinity of $A=\lambda$ at the center of the high frequency band for moderate relative permittivity loading ($\varepsilon_r \tilde{=} 5$). Larger aperture dimensions can be achieved by reducing the permittivity, or using very thin slabs; however, such an approach is generally counter-productive in that bandwidth is reduced and H-plane scan loss is increased at high frequency due to the widening dissimilarity between LSE_{10} and LSE_{20} modes which occurs for parameter variations in these directions. Consequently, in order to achieve the wide apparent phase center displacement for this grid, it is necessary to place the slabs very close to the narrow feedguide walls, giving α/β ratios of, typically, 0.56 to 0.62. This is not a very attractive solution since it produces considerable aperture field asymmetry about the apparent phase centers, thereby invalidating the primary assumption that the high frequency aperture distributions are roughly symmetric about these phase centers. As a practical matter, then, it is impossible to kill off the eight remaining beams.

The best result obtained for the 1.78" base equilateral grid are summarized in Table 4. The element dimensions are given in the table caption. Clearly, the 1.05 db power loss to the grating lobes is intolerable, and it is necessary to reduce the grid size significantly.

As mentioned above, cancellation of off-axis high frequency grating lobes requires that the apparent phase centers be separated by roughly 0.5 d_x. In addition, to maintain reasonable aperture field symmetry about these phase centers, ratios α/β should lie in the approximate range $0.8 < \alpha/\beta < 1.25$. Allowing for

	4 GHz	8 GHz
Broadside Reflection Loss (db)	1.18	1.05
*H-plane Scan Loss at 60° (db)	6.44	6.80
Power Loss to Grating Lobes (broadside scan)		1.05
Broadside Gain Loss (db)	1.18	2.43

Table 4

Performance of Dual Frequency Element in 1.78" Base Equilateral Traingular Grid at 4 and 8 GHz. A = 1.480", β = .412", δ = .358", d_x = 1.780", d_y = 1.540", α = .241", β = .301", δ = .198", ε_r = 5.0

*Includes cos θ beam broadening factor.

a wall thickness of 0.062", a practical set of element and grid x-dimensions is then A = 1.376", d_x = 1.500", and $\beta+\delta/2$ = .375", resulting in the specification of slab thickness, δ, as no greater than .130", or $\delta/A<.094$ and $\alpha/\beta<.835$. From Figures 36 through 43, it is seen that a relative permittivity of 5 will provide the desired feedguide characteristics in both frequency bands for this aperture size with $\alpha/\beta = 1$ and $\delta/A = .091$. Bringing the α/β ratio into the required range produces only a small perturbation on the dispersion curves shown in Figure 41. Consequently, the selection of α=.247", β=.309", and δ=.132" will provide the necessary control of off-axis grating lobes while keeping higher order feedguide modes well below cutoff. By requiring that the LSE_{11} mode be attenuated by 8 db per wavelength at the high end of the 8 GHz band, the y aperture dimensioned is obtained as B = .400".

The aperture/grid parameters determined so far guarantee some cancellation of the off-axis grating lobes, and it might be assumed that by reducing d_y for the original grid by the ratio 1.5/1.78 would result in an acceptable configuration, giving a 29%

increase in element count over the "optimum" number. Unfortunately this spacing is still on the large size and results in considerable power loss to the grating lobes at relatively small scan angles. It is therefore, necessary to further reduce the cell along the E-plane to $d_y = .960"$.

The final configuration, shown in Figure 45, with its low and high frequency grating lobe diagrams has a cell area roughly half that for the grid optimized for element count at low frequency, and results in an array of 2444 elements. With five phase shifters per element, this increase seems (at first glance) rather unattractive. However, this comparison is quite misleading. The twin dielectric slab dual frequency array element concept provides for simultaneous excitation by two entirely independent feed systems, and consequently the simultaneous radiation of two independent beams at two widely separated frequency bands. If the alternatives for multifrequency operation are considered, the dual frequency element is suddenly very attractive.

One such alternative is the use of wideband elements in the grid depicted in Figure 44 to obtain simultaneous aperture usage. The obvious disadvantage

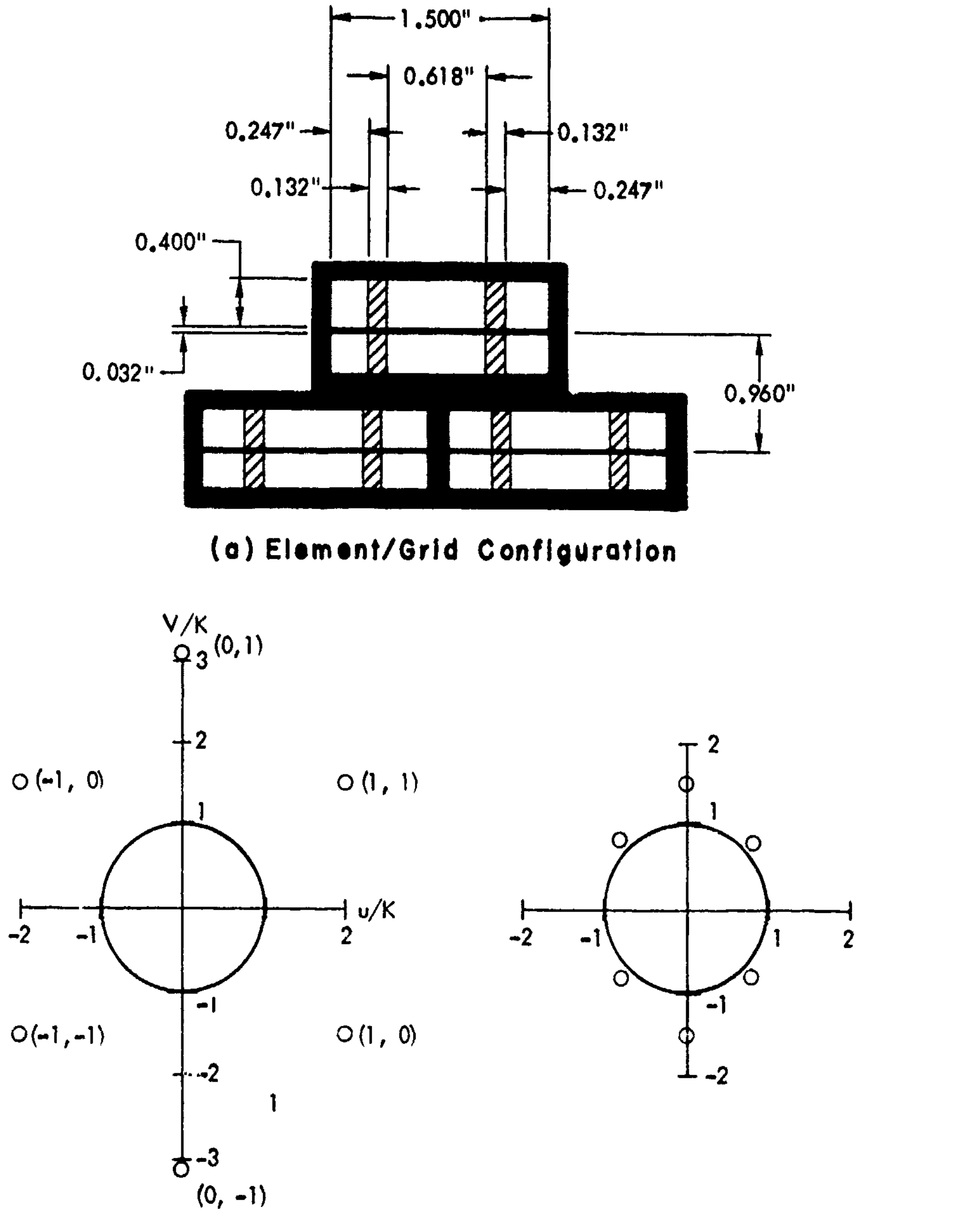

(a) Element/Grid Configuration

(b) Low Frequency Grating Lobe Diagram $\lambda/D_X = 1.96$ $\lambda/D_y = 3.07$

(c) High Frequency Grating Lobe Diagram - $\lambda/Dx = .98$, $\lambda/Dy = 1.54$

Figure 45. Triangular Grid Configuration for Dual Frequency Operation over 16% Bands Centered at 4 GHz and 8 GHz

of this scheme is that it requires eight phase shifters and four diplexers per element quartet or unit cell. In comparison with the dual frequency element, this configuration requires twice the number of low frequency controls, and half the number of high frequency controls per unit area of the array, plus diplexers.

A second alternative, in a broad sense, is to design two entirely independent single frequency systems. However, it is clear that only under very special circumstances could this system be considered a viable multifrequency concept.

Predicted principle scan plane performance for the configuration in Figure 45, is shown in Figures 46 through 54, at the end and midpoints of the 4 and 8 GHz bands. In these figures, the performance measure is taken as the power transmission coefficient into the radiating beam(s). Mainbeam scan loss is determined by adding $10 \log_{10} (\cos\theta)$ to the curve for the (0,0) beam.

Figures 46, 47, and 48 show E and H plane performance at the low end, middle, and high end of the 4 GHz band, respectively, for scan out to $\sin\theta=.975$.

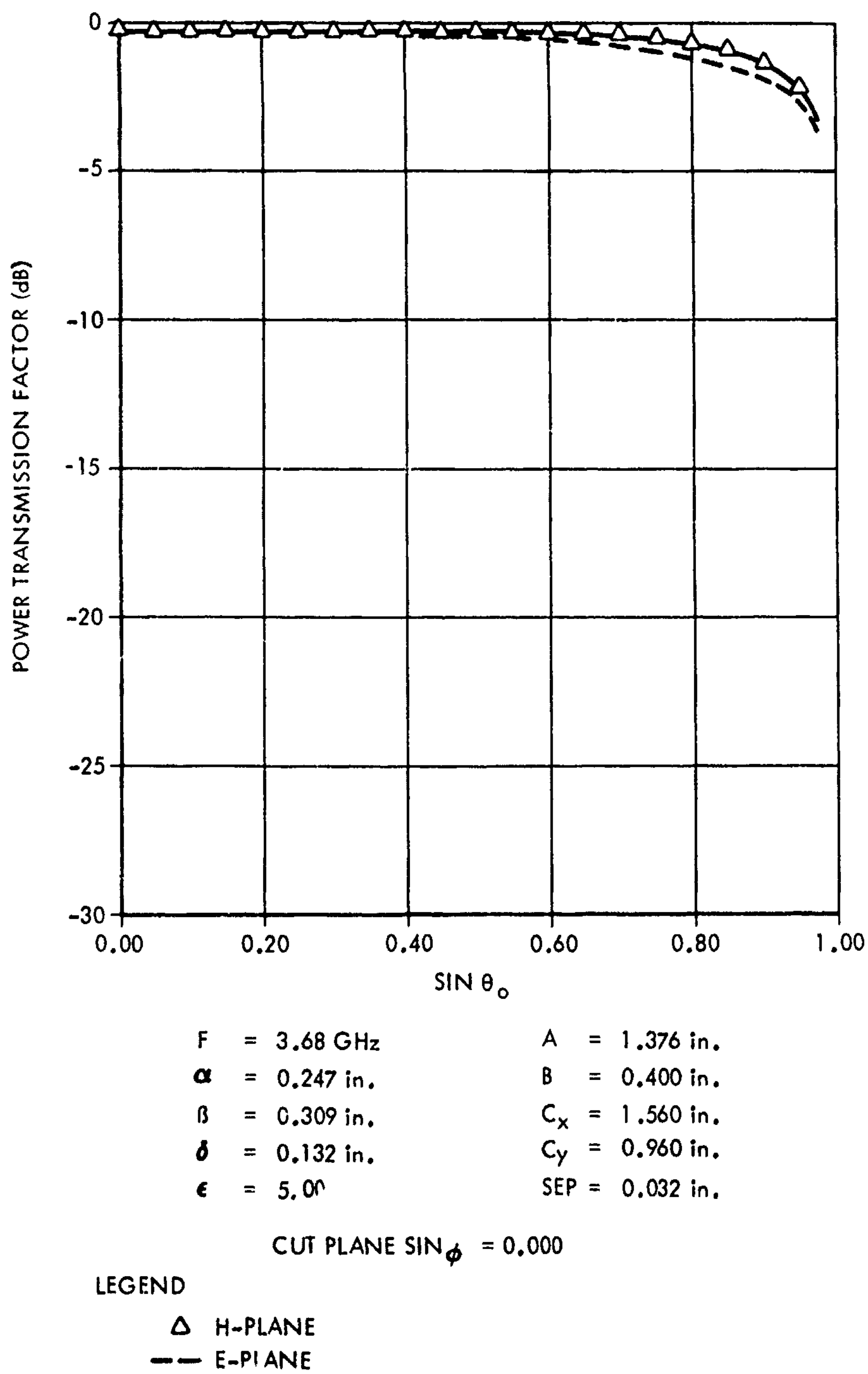

Figure 46. E- and H-Plane Performance of Designed Element, f =3.68 GHz

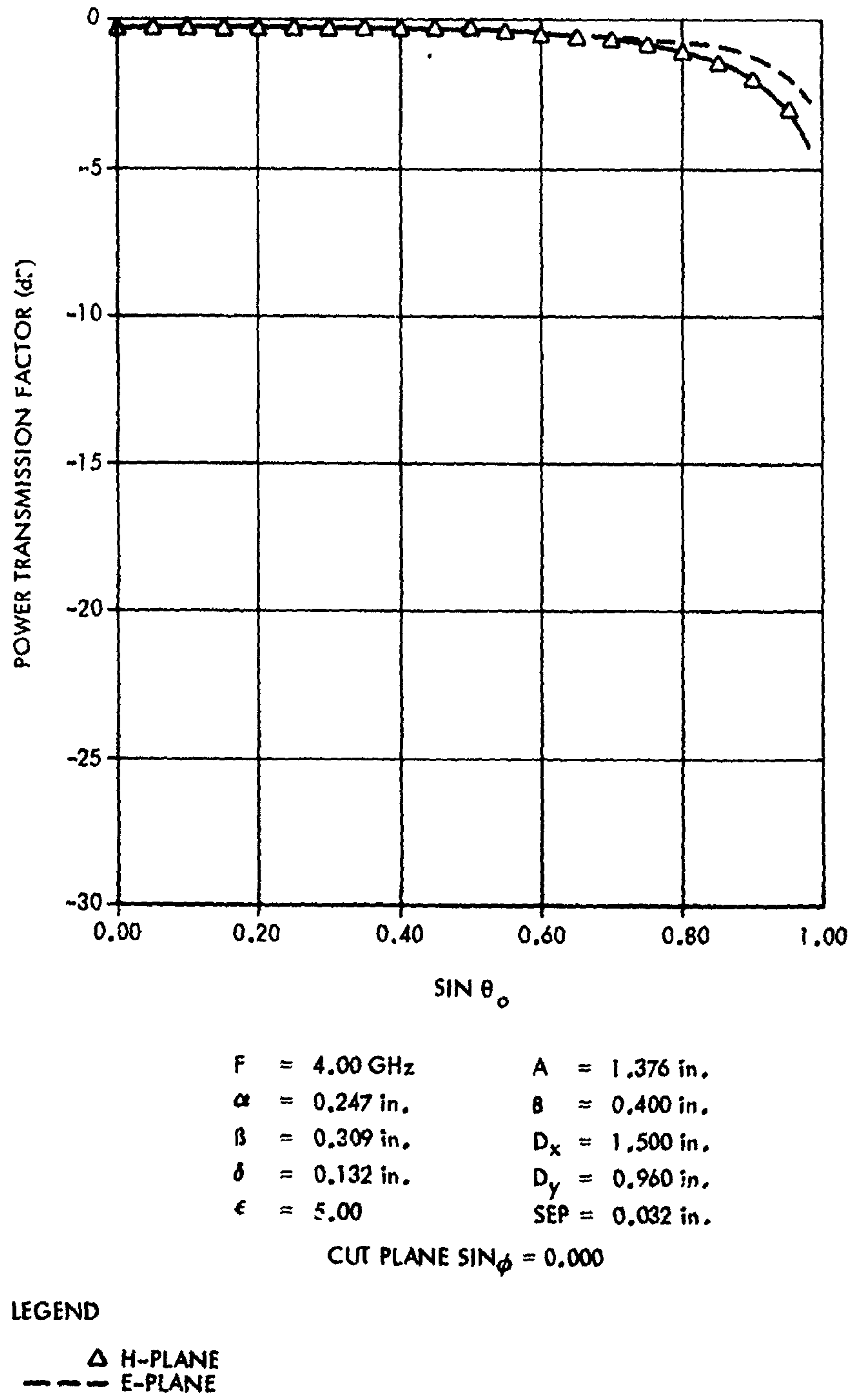

Figure 47. E- and H- Plane Performance of Designed Element, f = 4.0 GHz

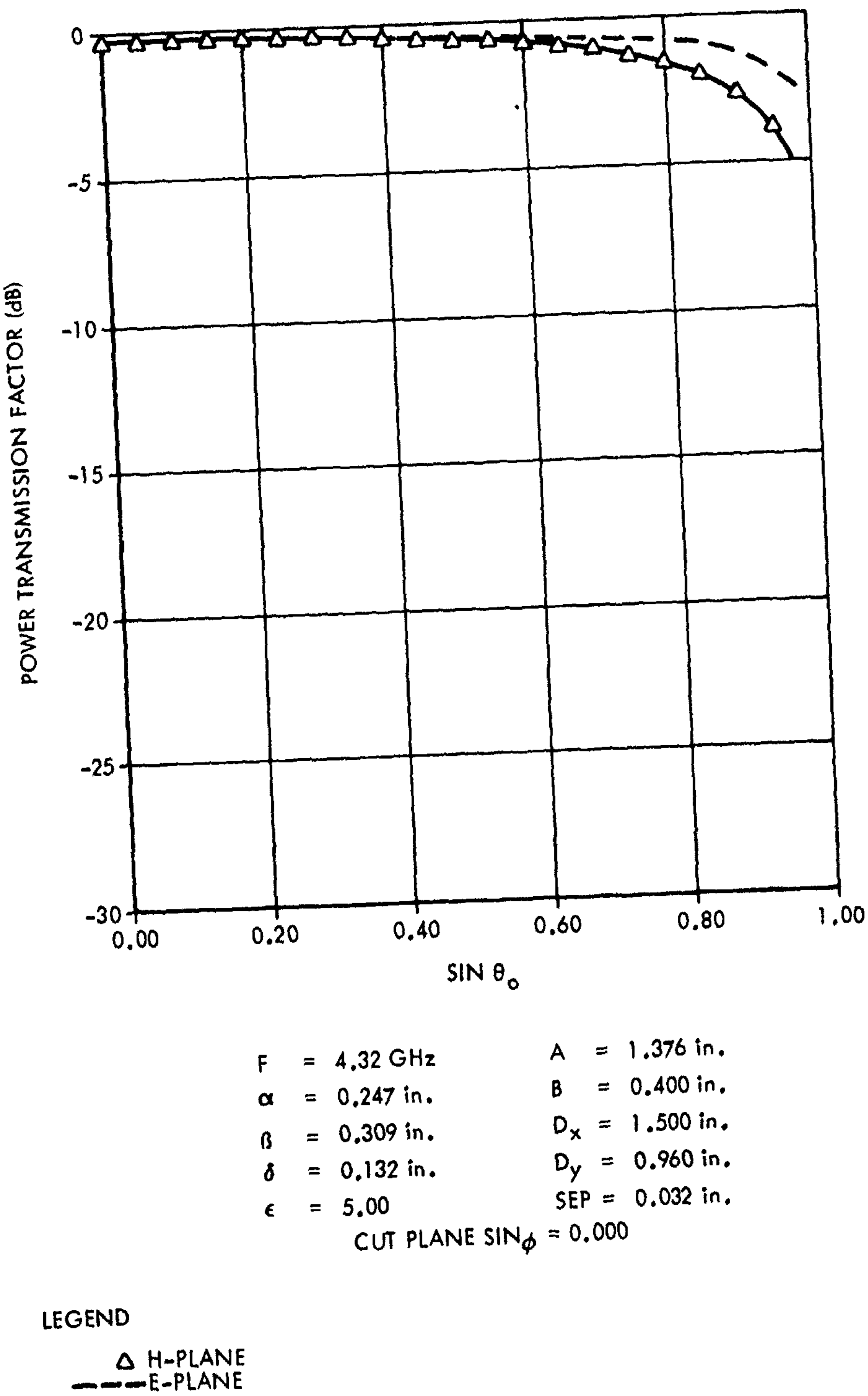

Figure 48. E- and H- Plane Performance of Designed Element, f = 4.32 GHz

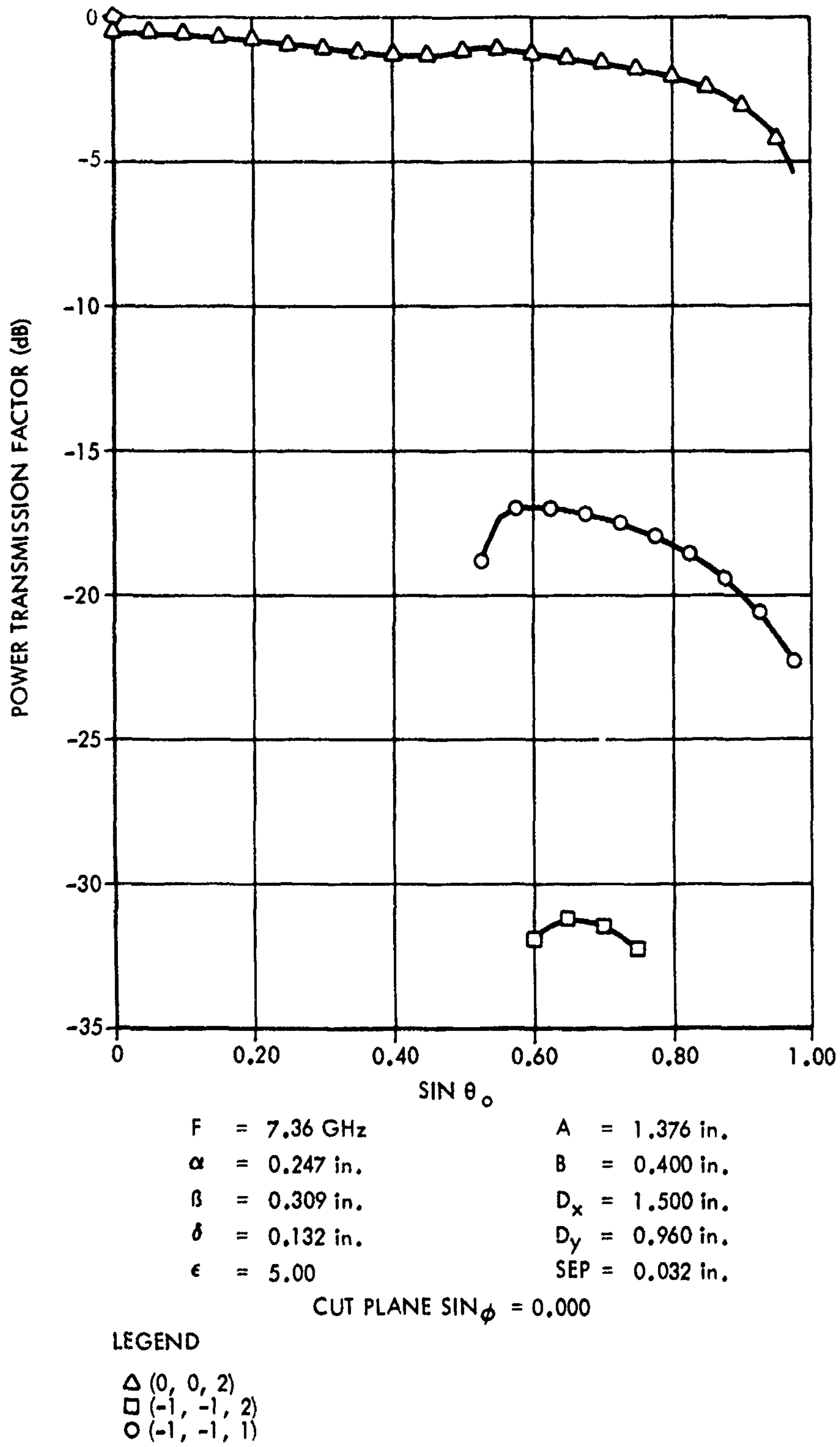

Figure 49. Propagating Beam Power Levels - H-Plane Scan, f = 7.36 GHz

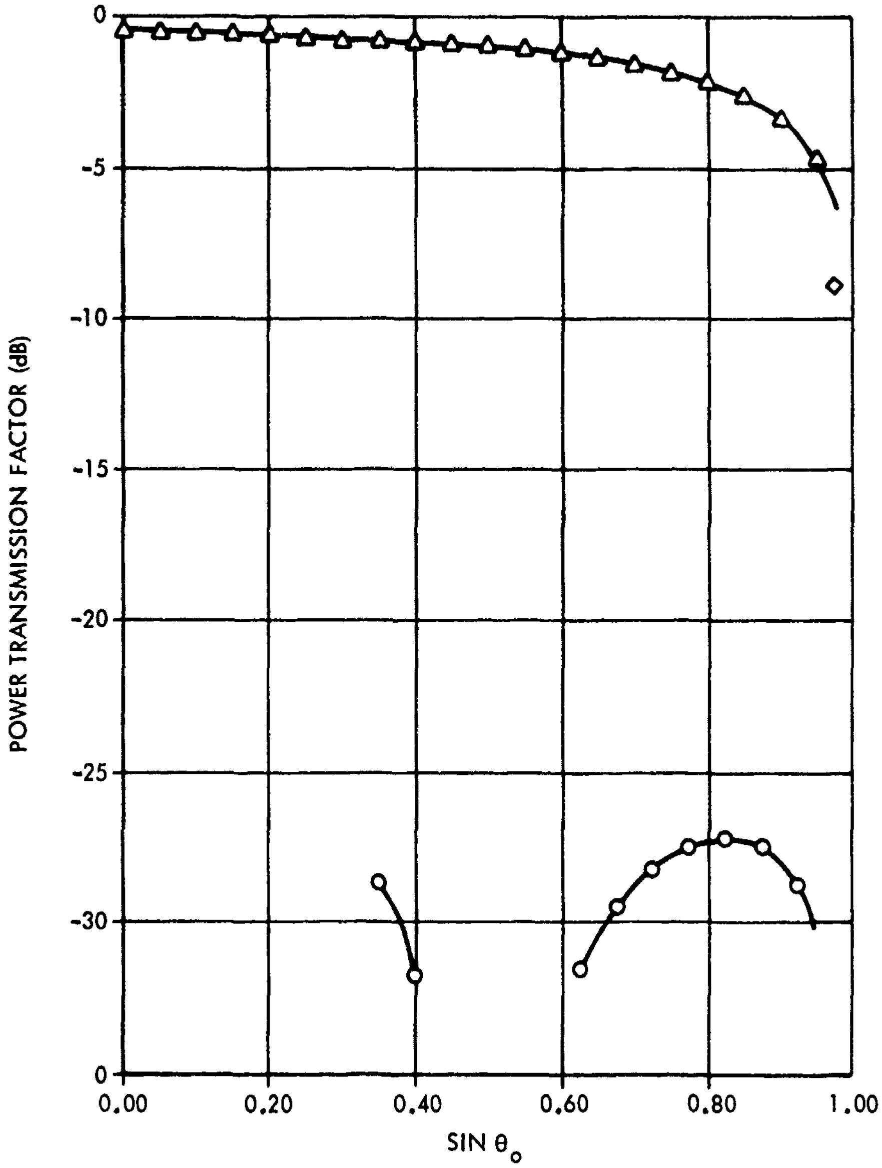

F = 8.00 GHz   A = 1.376 in.
α = 0.247 in.   B = 0.400 in.
β = 0.309 in. D_x = 1.500 in.
δ = 0.132 in. D_y = 0.960 in.
ϵ = 5.00   SEP = 0.032 in.
CUT PLANE SIN$_\phi$ = 0.000

LEGEND

△ (0, 0, 2)
○ (-1, -1, 1)
◇ (-2, -1, 2)

Figure 50. Propagating Beam Power Levels - H-Plane Scan
f = 8.0 GHz

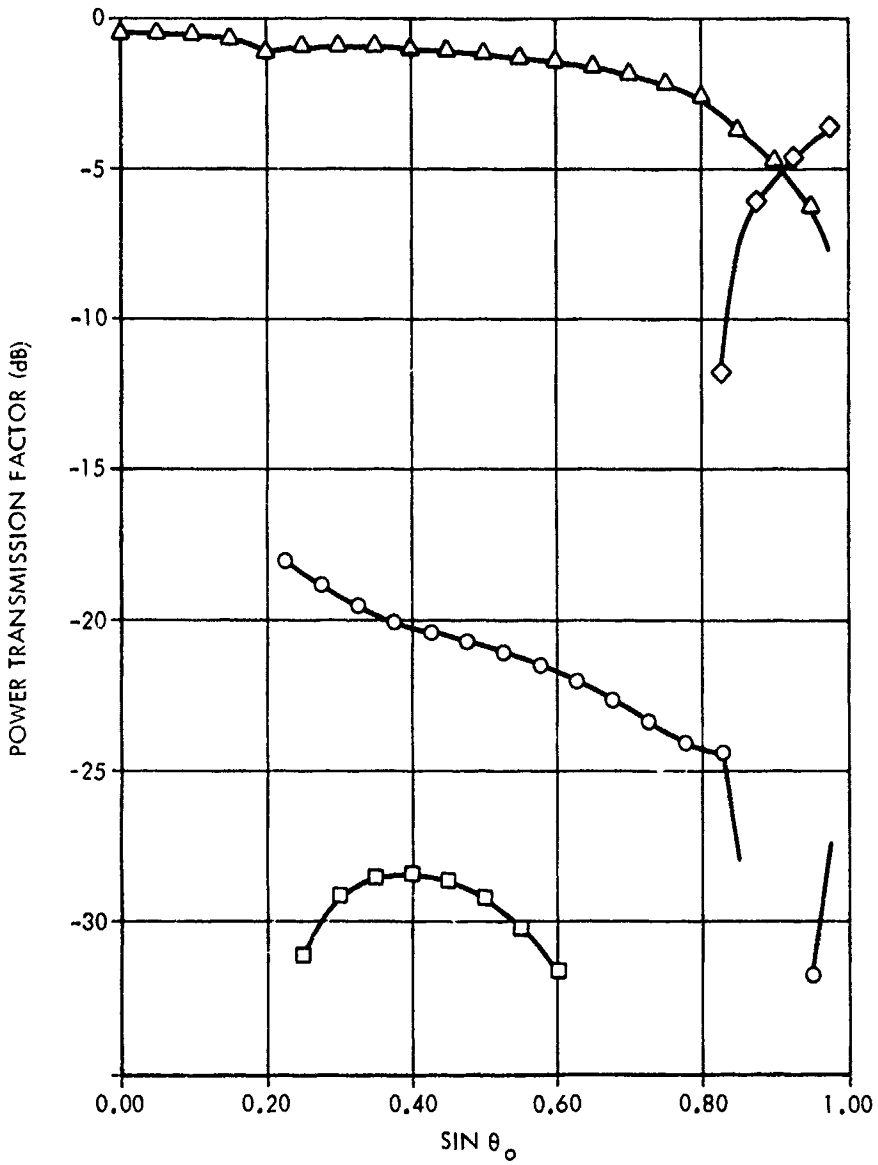

F - 8.64 GHz
α = 0.247 in.
β = 0.309 in.
δ = 0.132 in.
ε = 5.00

A - 1.376 in.
B = 0.400 in.
D_x = 1.500 in.
D_y = 0.960 in.
SEP = 0.032 in.

CUT PLANE SINϕ= 0.000

LEGEND

△ (0, 0, 2) ○ (-1, -1, 1)
□ (-1, -1, 2) ◇ (-2, -1, 2)

Figure 51. Propagating Beam Power Levels - H-Plane Scan, f = 8.64 GHz

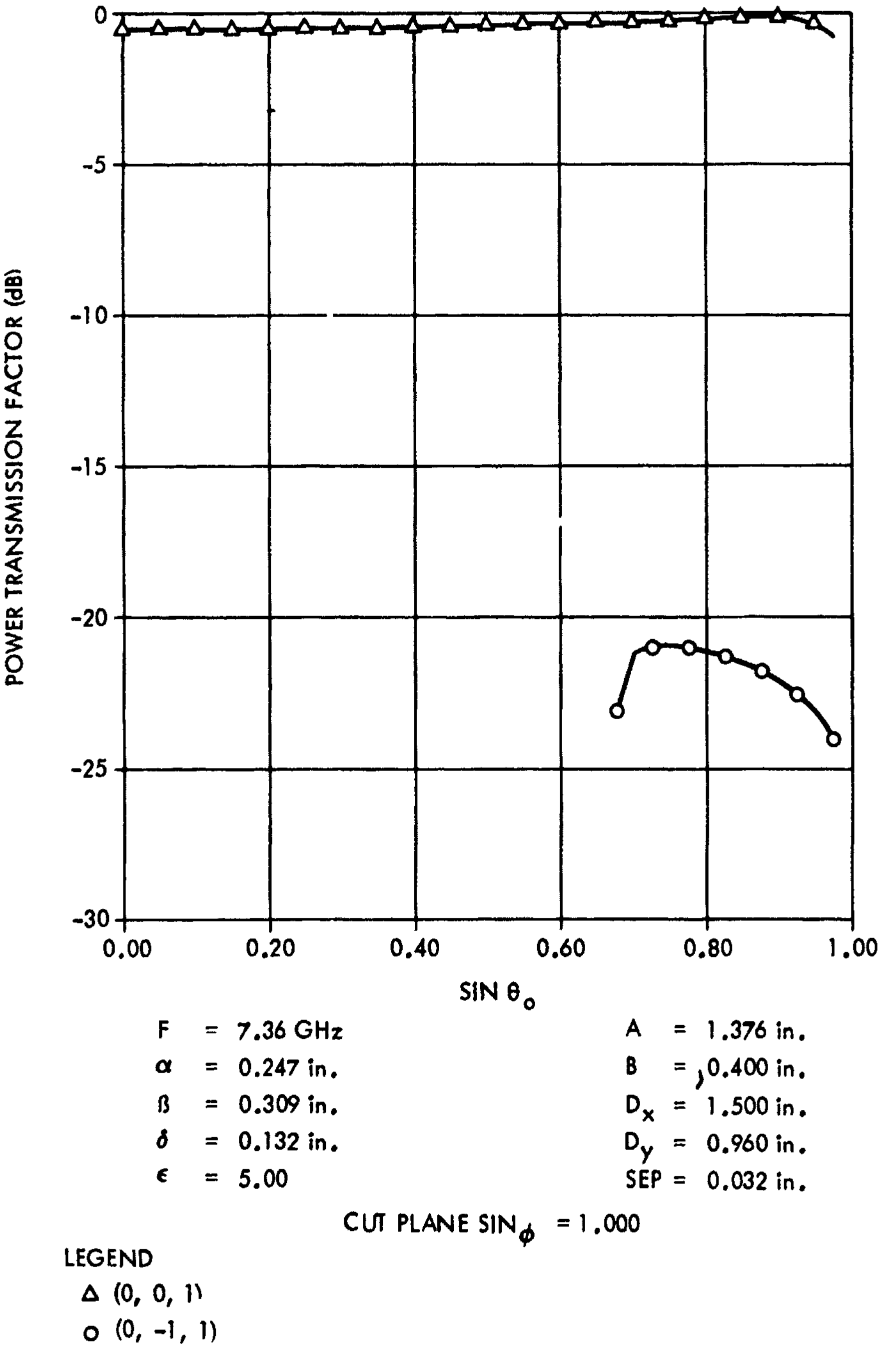

Figure 52. Propagating Beam Power Levels - E-Plane Scan, f = 7.36 GHz

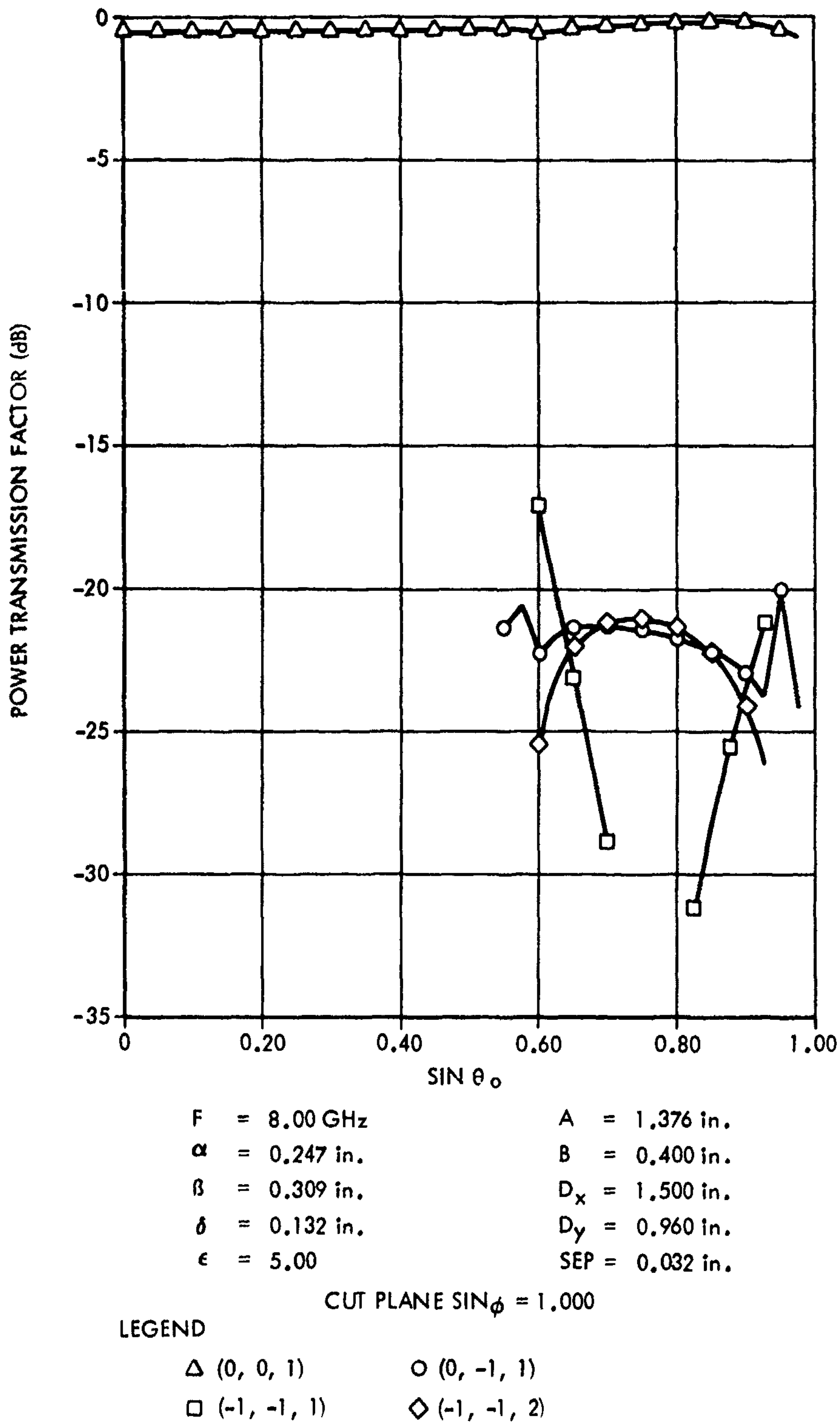

Figure 53. Propagating Beam Power Levels - E-Plane Scan, f = 8.0 GHz

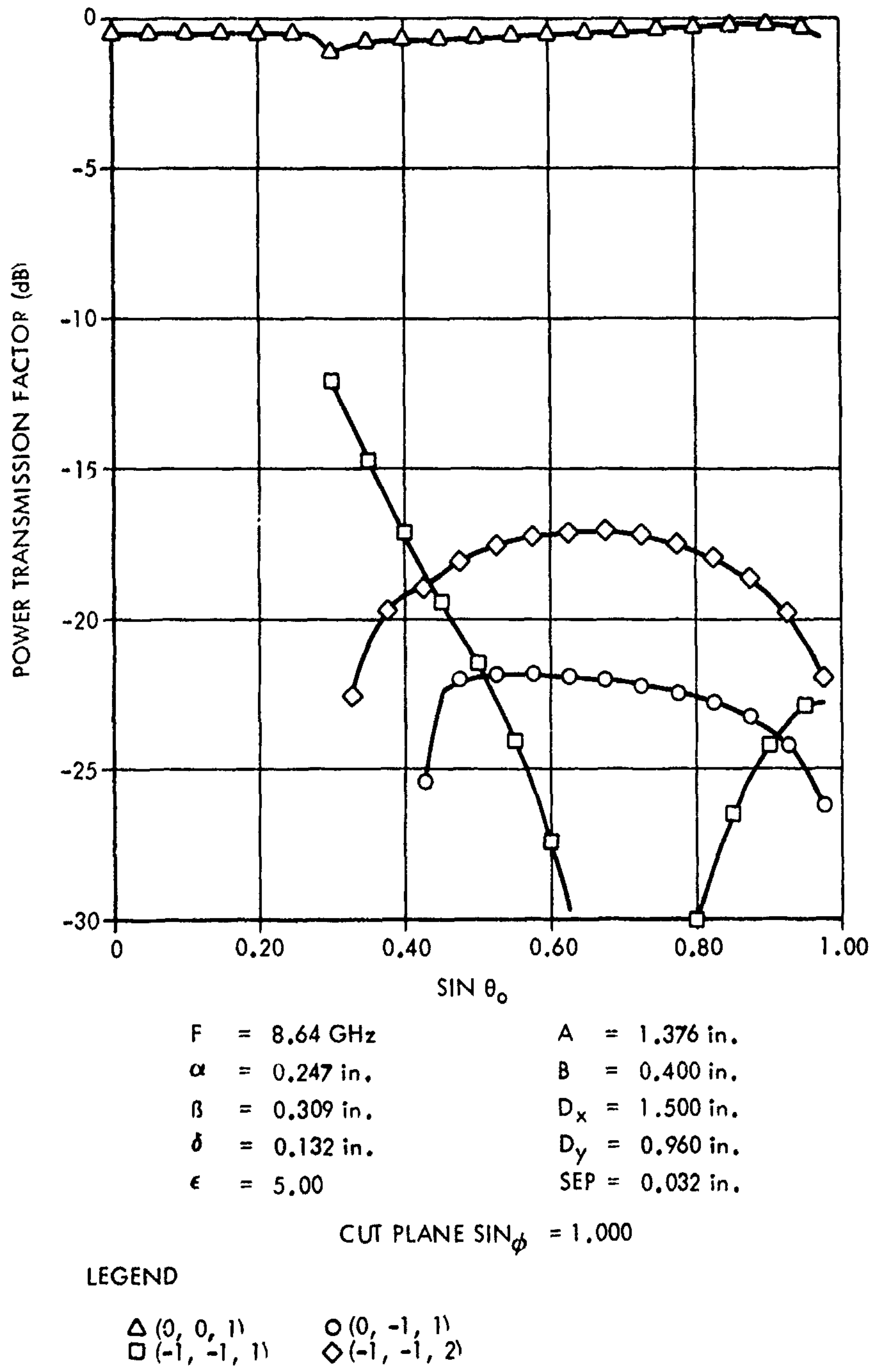

Figure 54. Propagating Beam Power Levels - E-Plane Scan
f = 8.64 GHz

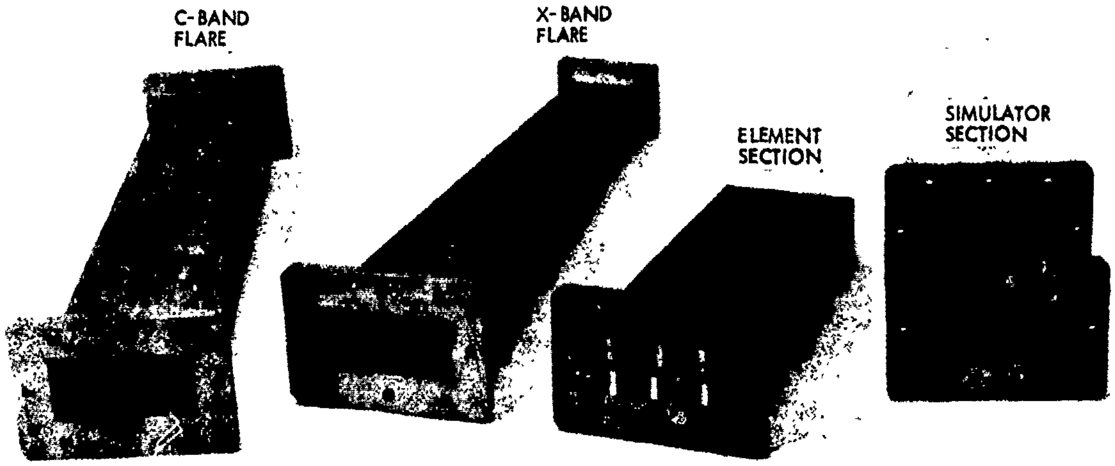

Figure 55. Waveguide Simulator for Designed Element

In this range, no grating lobes enter real space. Maximum broadside mismatch loss in this band is less than .3 db and is readily matched out by any number of means. The E-plane fall-off out to approximately 60° is somewhat better than might be expected for the subarray array factor at these spacings, and decreases at the upper end of the band. The H-plane fall-off is typical of a planar array of rectangular apertures.

Figures 49, 50 and 51 show the H-plane power levels in the propagating beams in the 8 GHz band. To evaluate the array characteristics over this band, the LSE_{10} and LSE_{20} feedguide modes are assumed to be generated $2\lambda_{g10}$ behind the aperture plane, where λ_{g10} is the LSE_{10} guide wavelength evaluated at 8 GHz. This long feedguide phase length results in considerable excitation of the (-1,-1) E-mode at the band extremes. Evidently, this path must be shortened for such wide band operation.

At midband, Figure 50, the (-1,-1) and (-1,0) grating lobes are well within the desired range of rms sidelobe level and will not result in any significant perturbation of the far-out sidelobe region. This level of cancellation is achieved using the modifier $R = 1.2 \exp(-j14^{\circ})$, which seems to also result in significant reduction of the H-mode (-1,-1) and (-1,0) beams at the band edges as seen in Figures 49 and 51. However, the modifier clearly has little effect on the E-mode beams, and these levels must be controlled by a proper choice of a feedguide phase length.

In Figure 51, it is seen that the (-2,-1) H-mode beam is heavily excited at the upper end of the band. However, this occurs only at the H-plane extreme of the scan volume, and will be of only minor consequence.

The 8 GHz band E-plane performance is shown in Figures 52 through 54. In general, the best performance occurs at the lower end of the band. Due to the choice of y lattice spacing, the grating lobes remain outside real space throughout most of the scan volume at this end of the band, and are only moderately excited upon entering. From the results at 8 and 8.64 GHz, it is clear that this is the most effective means of controlling spurious beam levels in this plane.

At the high end of the band, the (-1,-1) E and H mode beams are very heavily excited and will have considerable impact on the general sidelobe level for scanning beyond 25°. However, except for the small dips occuring near (-1,-1) lobe incipience, there is little effect on main beam gain. Again, as for the H-plane results, a general improvement in grating lobe levels may be expected for shorter feedguide phase lengths.

4.2 Experimental Evaluation of the Bifurcated Twin Dielectric Slab Loaded Rectangular Waveguide Dual Frequency Element

The dual frequency element design shown in Figure 45 was built and tested in H-plane waveguide simulators over an 8% frequency band centered at 4.6 GHz and a 16% band centered at 8 GHz. In general, the experimental results were in excellent agreement with predictions.

The simulators are shown in Figure 55. They are constructed of brass and are soft soldered. A single element section and parallel wall simulator section is used for both bands, resulting in near broadside simulation in the upper band, and wide angle scan simulation in the lower band. The parallel wall section has 2.250" x .960" cross-section and provides imaging as shown in Figure 56. In the low frequency band, only the TE_{10} mode propagates in the simulator. In the high frequency band, up to eight modes can propagate.

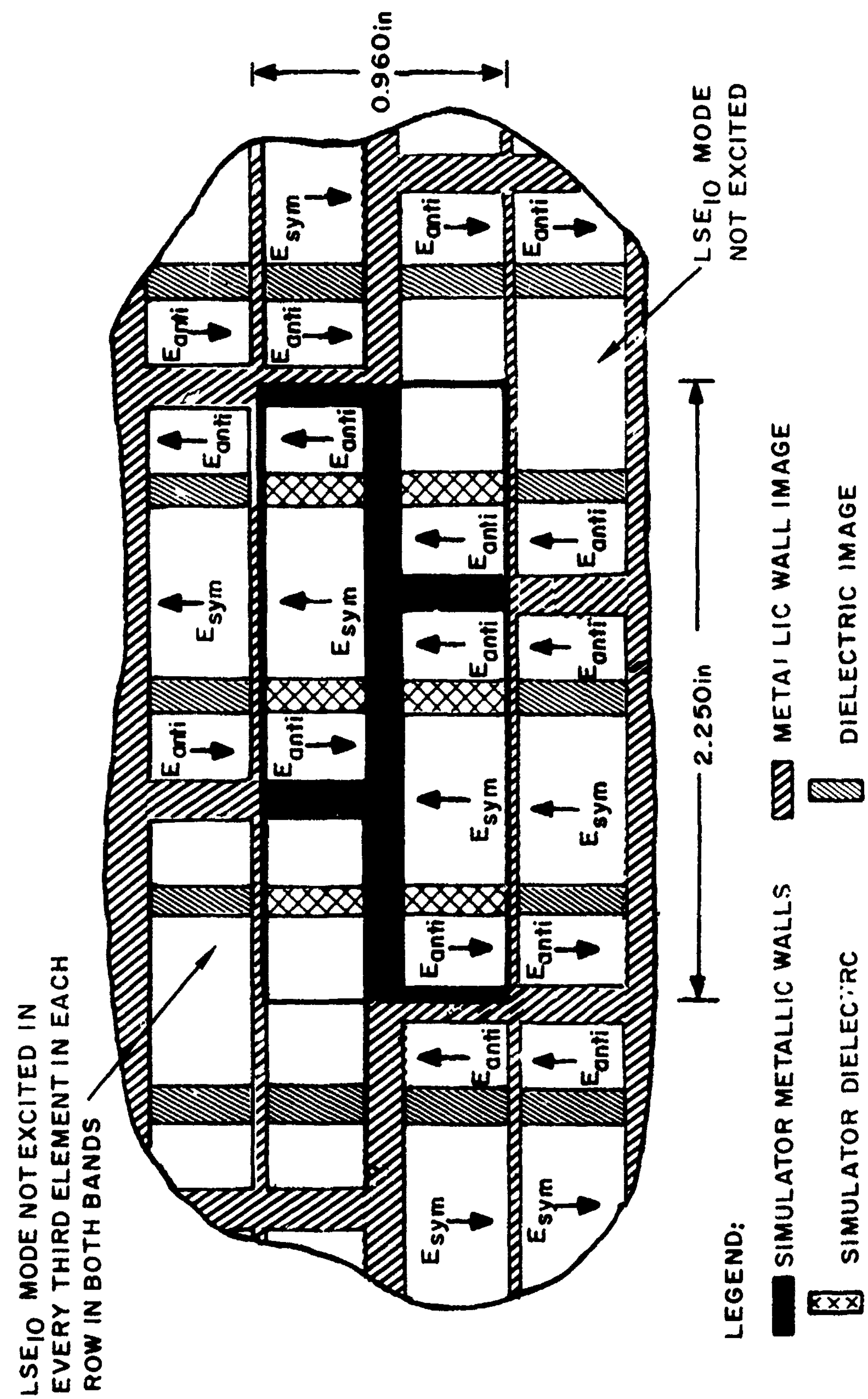

Figure 56. Simulator Imaging of Element Section

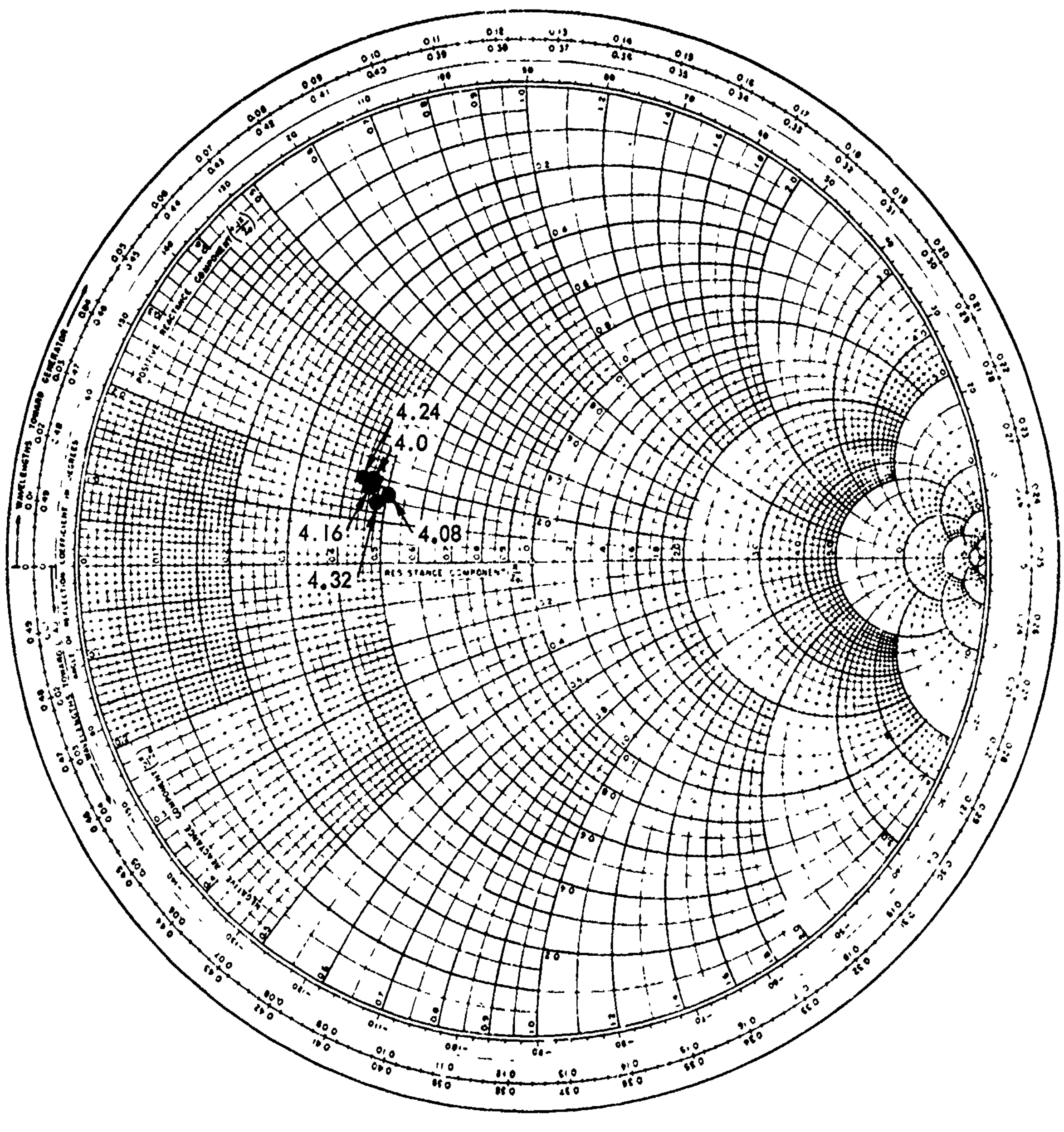

Figure 57. Measured Simulator Port, Impedance 4.0 - 4.32 GHz
Sampled in 80 MHz Increments

The element section, shown in Figure 56 with the simulator imaging, consists of two half elements and two quarter elements, resulting in 19.1^{o} and 41^{o} H-plane scan simulations at the centers of the high and low bands, respectively. The dielectric slabs are stycast HiK, $\varepsilon_r = 5$. The element section is 7.2" long ($2\lambda_g$ at 4 GHz), with tapered 3.6" 300Ω card loads inserted at the rear of the section on either side of the dielectric slabs and the feedguide mid-plane. The long tapers are necessary to eliminate rearward radiation and reduce reflections at the load discontinuities.

Figure 57, shows measured results in the upper half of the low frequency band. Results in the lower half of the band were not obtained due to the frequency limitation of the network analyzer. To ensure measurement accuracy, the experimental band was sampled discretely in 80 MHz increments, and a short circuit reference was established at each frequency step. Measured reflection coefficient magnitude is in the rance .34 to .41* with the peak and minimum at 4.24 and 4.08 GHz, respectively, and is typical of the variation in H-plane gain loss with scan observed in many broadside matched phased arrays. The phase of the reflection coefficient is nearly constant.

*For H-plane scan, it is permissible to represent feed-guide port pairs (upper and lower element halves) by a single "effective port". Consequently, the reflection coefficient magnitude at the simulator port is a factor of $\sqrt{2}$ greater than that in either half element.

Measured and predicted simulator results are shown in Figure 58. The calculated results lie well within the range of the measurements. Also shown in the figure is a least mean square straight line fit to the experimental data and $\sqrt{(1-\sqrt{\cos\theta})}$, where θ is the simulator angle. These two curves, in comparison with the predictions, show quite clearly that the analytical model provides an excellent description of the array. The scatter of experimental data about the theoretical results is due primarily to errors in element section fabrication which resulted in small air gaps between the feedguide broadwalls and the dielectric primarily in the interior of the section. By assuming a maximum reflection coefficient magnitude of 0.035 at the internal discontinuities, the discrepancies in the results are accounted for throughout the band.

In the 8 GHz band, up to eight waveguide modes will propagate in the simulator. Below 8.08 GHz, the first five simulator modes will propagate. However, for a properly fabricated element section, only the TE_{10} mode is excited. Above 8.08 GHz, three of the eight modes will be excited by the array interface. These

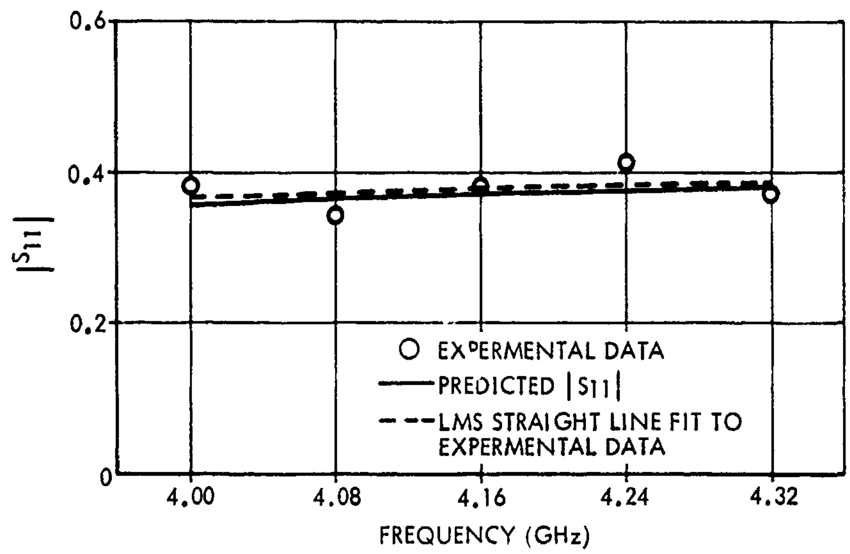

Figure 58. Comparison of Measured and Predicted Reflections Coefficient Magnitude at the Simulator Port, 4.0 - 4.32 GHz

are the TE_{10}, TE_{21}, and TM_{21} modes, corresponding to the (0,0); H mode (1,0) and (-1,-1); and E mode (1,0) and (-1,-1) beams, respectively.

The equivalent network representing the simulator discontinuity is a 3-port below 8.08 GHz, and a 5-port above 8.08 GHz. Consequently, below the (2,1) waveguide mode cut-off, the measured reflection coefficient at the simulator port is given as

$$(91)\quad |S_{11}|^2 = -1 + |S_{22}|^2 + |S_{33}|^2 + |S_{23}|^2\, Y_2/Y_3 + |S_{32}|^2\, Y_3/Y_2$$

where the ports are defined in Figure 59. Above the cut-off frequency, the simulator dominant mode self reflection term is complicated function of the self and cross coupling scattering parameters of the remaining ports in the network. Since, in the analysis presented here, the interface scattering blocks $\underline{\underline{S}}_{12}$ and $\underline{\underline{S}}_{22}$ are unnecessary for the determination of element performance, they are not calculated*, and it

*The calculation of $\underline{\underline{S}}_{12}$ and $\underline{\underline{S}}_{22}$ requires prohibitively large amounts of computer core. Roughly 120K, decimal, words are required for $\underline{\underline{S}}_{22}$ for the convergence radii considered here.

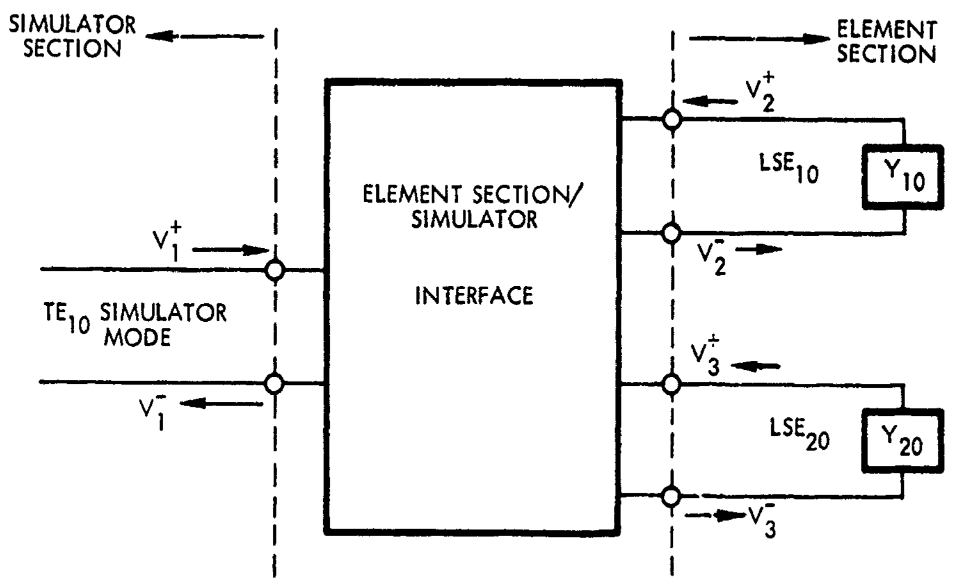

Figure 59. Port Definitions for 7.32 - 8.08 GHz Simulator

and it is therefore, not possible to compare theoretical and measured results above 8.08 GHz.

Measured results in the 7.32 to 8.64 GHz band are shown in Figure 60. As for the 4 GHz band, the experimental band was sampled discretely to ensure measurement accuracy. The sampling rate is roughly every 160 MHz, with an exact short circuit reference established for each sample point. The reflection coefficient magnitude is in the range .35 to .46, and the phase is nearly constant.

In the measurements, no attempt was made to load terminate the higher order modes of the simulator. This leads to an inherent error in the results which is associated with the reactive termination of the higher order modes by the simulator flare transition. This error should be insignificant for a reasonably well fabricated element section since the higher order beams are only weakly excited above 8.08 GHz. However, as discussed above, some irregularities in element section fabrication did occur, resulting in week excitation of the TE_{20} simulator mode.

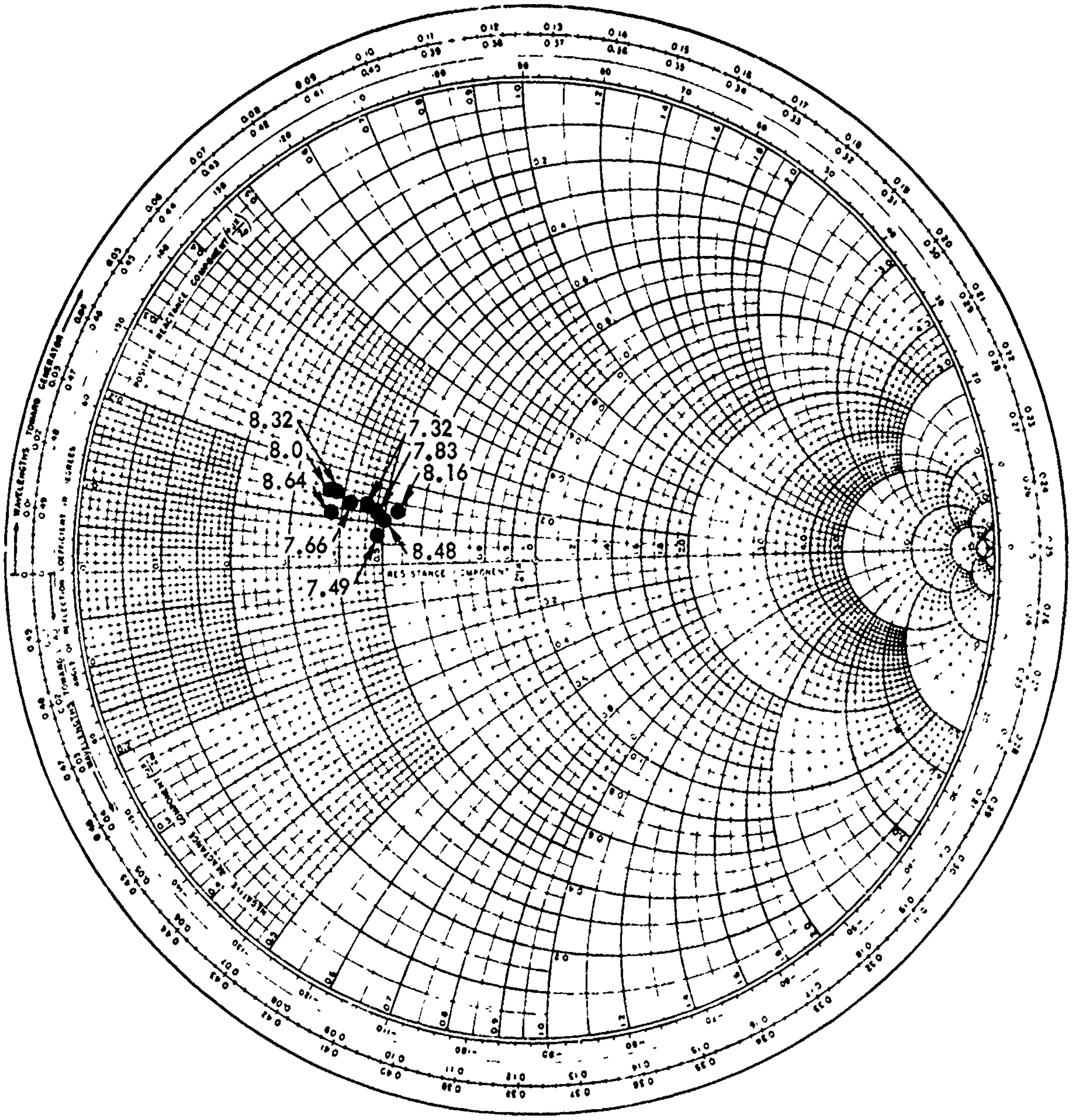

Figure 60. Measured Simulator Port Impedance 7.32 - 8.64 GHz
Sampled in 160 MHz Increments

A comparison of measured and predicted results in the 7.32 to 8.00 GHz region of the experimental band is shown in Figure 61. Also shown in the figure is a straight line least square fit to the experimental data. As in the 4 GHz band, the theoretical data falls within the range of the experimental results, and the least square fit has approximately the same slope and magnitude as the calculated curve. The maximum deviation of measured reflection coefficient from the theoretical value is .051 and occurs at 8 GHz.

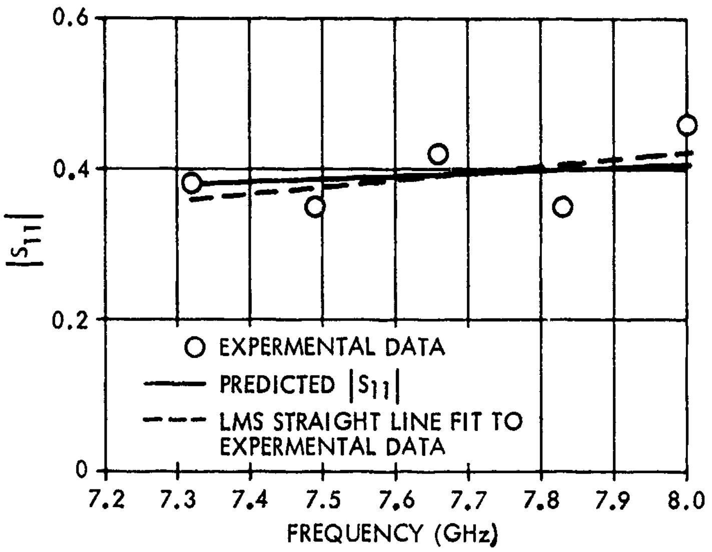

Figure 61. Comparison of Measured and Predicted Reflection Coefficient Magnitude at the Simulator Port, 7.32 - 8.00 GHz

5.0 ELEMENT EXCITER DESIGN

The design of an exciter for the slab loaded dual frequency element presents a particularly intriguing problem. As demonstrated in section 3, the dominant mode dispersion in the inhomogeneously loaded guide is roughly linear with frequency for practical element configurations. However, the slope of γ/k is, in general, considerably greater than unity. Consequently, the use of a bidirectional exciter, such as a stub or slot, requires load termination at the back of the feedguide to ensure proper aperture excitation, and results in a 3dB power loss.

5.1 Exciter Concept

A unique uni-directional exciter concept, shown in Figure 62, has been developed which alleviates this difficulty. The exciter consists of three stripline fed flared notch antennas,[2,3,4] configured to provide maxium coupling to the driven feedguide modes in either band. The center probe is the low frequency exciter, and is placed well in advance of the high frequency exciters (outer two probes) to maximize the low frequency isolation. The high frequency exciters butt directly into the dielectric slabs.

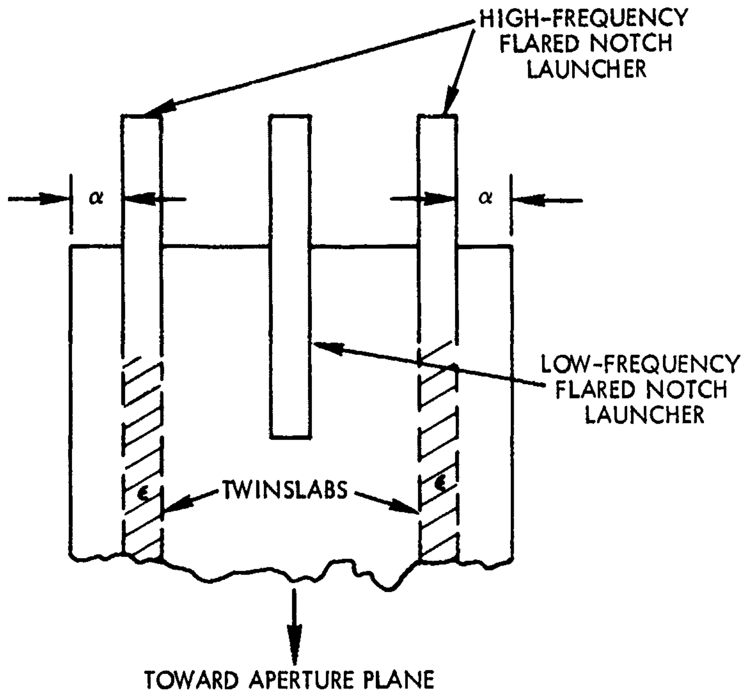

Figure 62. Stripline Fed Notch Exciter for Twin Dielectric Slab Loaded Rectangular Waveguide Dual Frequency Array Element

The basic exciter is shown in Figure 63. It is formed by symmetrically etching the outer conductor of symmetric stripline board to form flared notches which terminate with maximum aperture at the board edge and short circuit at the notch bottom. The stripline center conductor is configured to cross the notch region at a right angle to the notch center line, and terminates in an open circuit. By appropriately selecting the distance x_2, from the center conductor center line to the notch short circuit, and the distance y_2, from the notch edge to the center conductor open circuit, the exciter is matched in the feedguide environment over the operating band.

A particularly attractive feature of the flared notch exciter is that the stripline board is plugged into the back of the element. This considerably simplifies feed design. In addition, the phase shifter and exciter may be integrated into a single unit.

The exciter geometry shown in Figure 62 results in natural isolation between the low and high frequency probes in the low frequency band. Since the stripline outer conductor is etched only near the board edge, the center probe provides a short circuit bifurcation of the guide in the

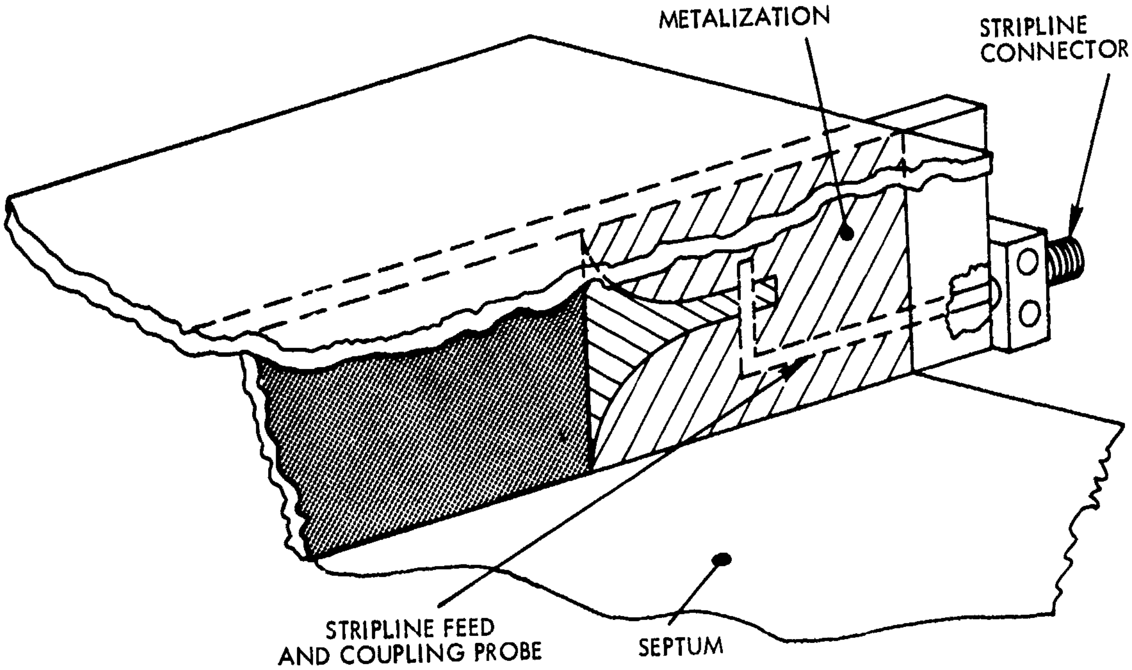

Figure 63. Basic Notch Exciter

vicinity of the high frequency probes. Consequently, the outer probes are in effectively below cut-off guide in the low frequency band, and their excitation is governed by the longitudinal separation between center probe notch bottom and leading edges of the outer probes.

In the high frequency band, the outer probes couple into the LSE_{10} mode of the loaded half width guide and some natural probe isolation is achieved due to the low field strength along the outer conductors of the center probe. However, the discontinuity at the center probe termination results in scattering back into the low frequency port. This difficulty may be removed by introducing an appropriately placed shorting stub along the low frequency probe center conductor, but the impact of this technique on high frequency aperture field distributions has not been determined and remains a design problem for future consideration.

5.2 Experimental Investigation of the Stripline Fed Flared Notch Exciter

Experimental investigation of the stripline fed flared notch exciter and exciter design were initiated during the contract period. In general, the anticipated results were obtained, and demonstrate the viability of the concept.

Notch exciter designs were developed to provide better than 2:1 VSWR looking into the load terminated feedguide over greater than 10% band widths, and greater than 50dB probe isolation in the low frequency band.

The baseline exciter design, a scaled version of a previously designed antenna element, is shown in Figure 64. The dielectric is Rexolite. The etched notch region has uniform width of .058" for a length of .154" from the notch short circuit, and then flares smoothly to a width of .400" at the board edge. The centerline of the stripline center conductor crosses the notch .135" from the short circuit. In the vicinity of the notch, the stripline impedance is 80 ohms, and transitions smoothly to 50 ohms at the connector junction. For the experimental investigation, only the center conductor open circuit location, y_2, was varied.

Five exciter elements, differing only in open circuit location, were fabricated and tested using an HP Automatic Network Analyzer (ANA). The values of y_2 for these elements, designated P1 through P5, are given in Table 5. In the 4GHZ band, exciter P5 produced the best overall match. In the 8 GHZ band, P1 gave best results.

Measured VSWR for the P5 exciter is shown in Figure 65.

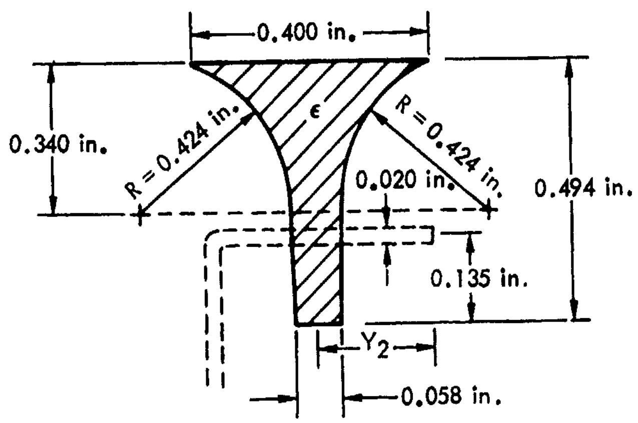

(a) Notch Detail

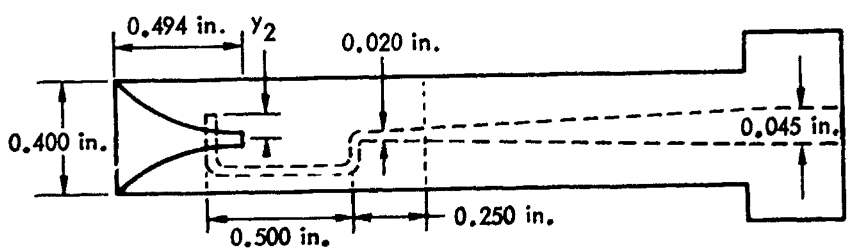

(b) Exciter Board

Figure 64. Baseline Notch Exciter Design

Exciter	Y_2
P1	0.070"
P2	0.090"
P3	0.110"
P4	0.130"
P5	0.150"

Table 5

Open Circuit Stub Lengths for Experimental Exciters

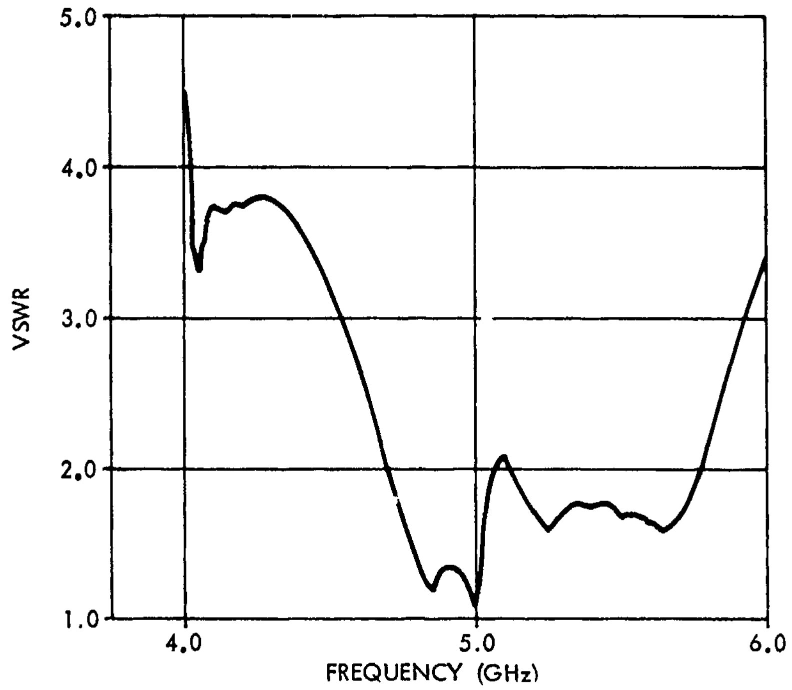

Figure 65. Measured VSWR for the P5 Exciter, 4 to 6 GHz

The measurement band is 4 to 6 GHZ. From 4 to 4.7GHZ, the exciter is poorly matched, and is operating in the vicinity of its low frequence cutoff.[4] From 4.7 GHZ to 5.75 GHZ, the mismatch is below 2:1. The low frequency cut-off phenomenon is known to occur when the open and short circuit stub lengths (x_2 and y_2 in Figure 64) become electrically short. Consequently, by increasing the notch depth and center conductor stub length, the exciter operating band may be readily reduced to the band of interest.

The ripple in the well-matched region of the experimental band may also be largely eliminated by judicious selection of the stub lengths. In the study of isolated notch antennas,[4] it was found that similar ripple in reflection coefficient occurred when the electrical lengths of the stubs were significantly different. Since the spectrum of guided waves in the region of the notch short circuit may be determined in a straight forward manner, the proper stub length ratio is obtainable by either analytical or experimental means.

Measured VSWR for the P1 exciter looking into load terminated half width loaded guide is shown in Figure 66. The measurement band is 7.5 to 8.5 GHZ. The match is below 2:1 throughout the band. It is evident from the figure that

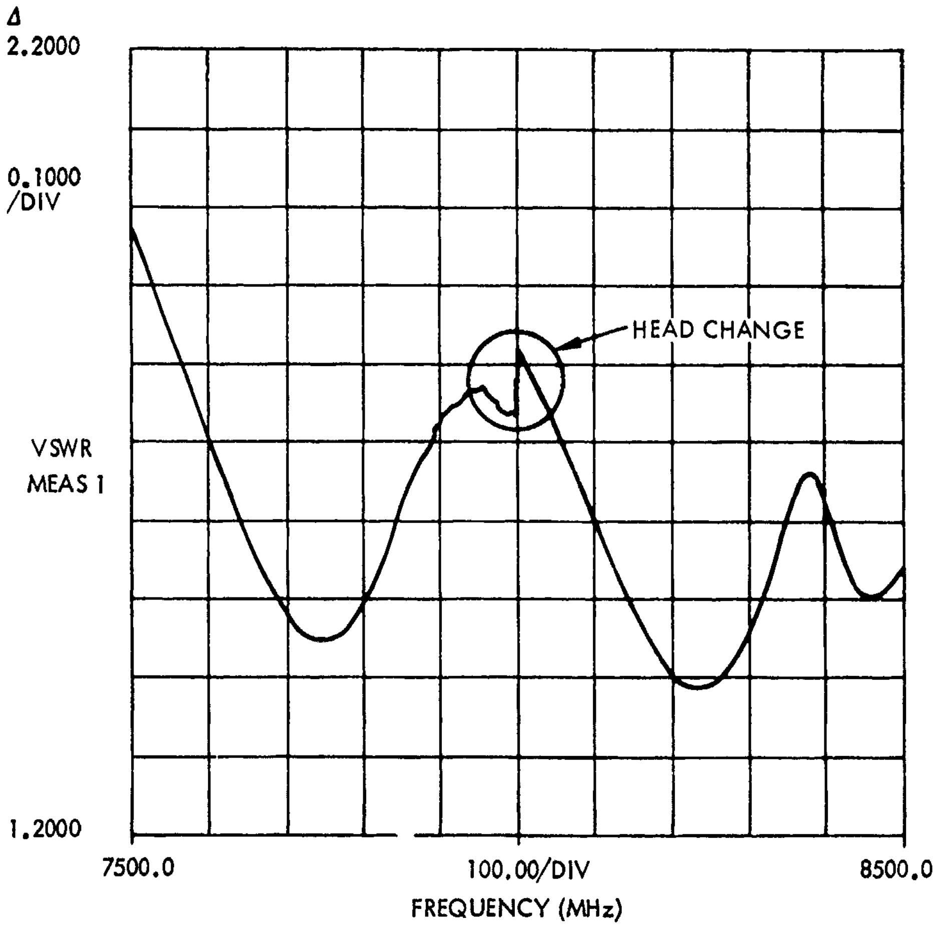

Figure 66. Measured VSWR for the P1 Exciter, 7.5 to 8.5 GHz

the low end of the experimental band is quite close to the low frequency cutoff for the exciter and that some stub lengthening is required to extend the bandwidth to cover the full 16% operating band. The discontinuity at 8 GHZ is due to the automatic head change on the ANA. While the ripple shown in the Figure is not large, some improvement can be achieved by adjusting the stub length ratio.

Probe isolation is determined by exciting a single high frequency probe in the three probe load terminated configuration and measuring return power in the center probe. In the high frequency band, the measured result corresponds, roughly, to equal excitation of LSE_{10} and LSE_{20} modes in the probe free region of the test device, and consequently is an improper excitation for high frequency operation. Below the loaded halfwidth guide cut-off frequency, the measurement approximates the band isolation at broadside.

Measured isolation from 3.5 to 8.5 GHZ is shown in Figure 67. The center probe is the P5 exciter and is inserted into the guide 1.80" beyond the P1 exciters. The high frequency exciters are butted against the dielectric slabs and arranged such that the slab and exciter midplanes are coplanar. Below 5.8GHZ (the halfwidth loaded guide cutoff frequency) the measured isolation is greater than 40dB, and

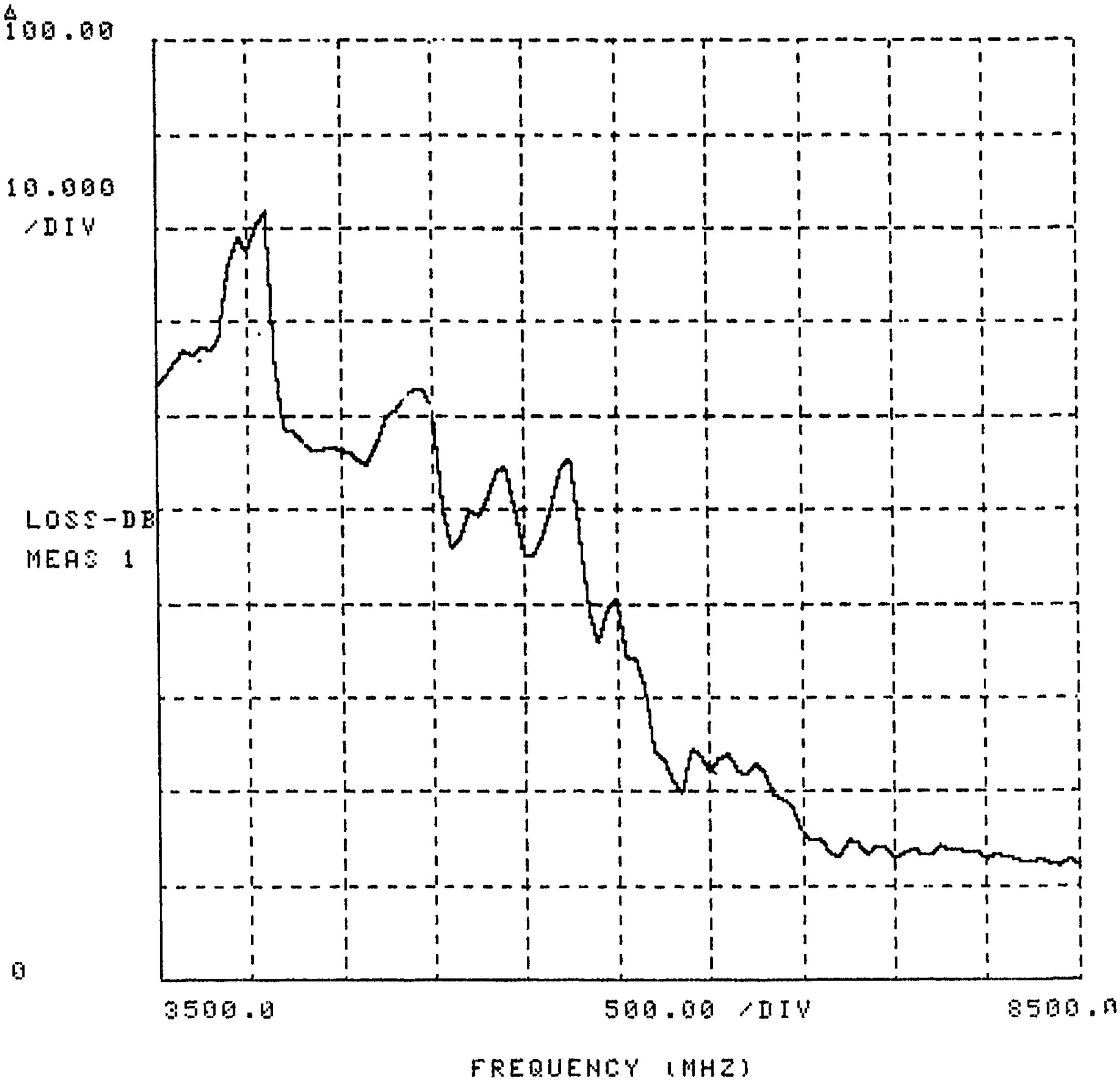

Figure 67. Measured Probe Isolation, 3.5 to 8.5 GHZ

exceeds 50dB from 3.5 to 5.0 GHZ. As anticipated, the isolation in dB shows a roughly linear decrease from 5.5 to 5.8 GHZ. Above 5.8 GHZ, the isolation rapidly degenerates to 12dB at 8.5 GHZ.

The weak isolation in the 7.5 to 8.5 GHZ band is due to the LSE_{10} mode constituant of the waveguide field in the plane of the center probe board edge. As was shown in section 3.2, the LSE_{10} relative modal electric field strength along the loaded guide centerline will be on the order of .3 to .4 for a slab relative permittivity of 5. Consequently, improved high frequency isolation can be obtained by either tapering the center probe board thickness near the edge, or by introducing an appropriately located shorting stub along the low frequency probe center conductor. In general, the first alternative seems best since it minimizes aperture perturbations, but may be impractical. The second approach has several difficulties associated with perturbations of the field at the radiating aperture, but is readily implemented. Clearly, the high frequency isolation presents a problem which will only be resolved through further study.

6.0 CONCLUSIONS

The bifurcated twin dielectric slab loaded rectangular wave guide has been shown to be a viable candidate as a dual frequency array element which results in a considerable reduction in electronic components relative to other multi-frequency aperture techniques. In comparison with wide band elements, the bifurcated twin dielectric slab loaded rectangular waveguide element requires 21% fewer controls per unit aperture area for equivalent scan and gain specifications.

To provide the multi-mode aperture control required for dual frequency operation, a unidirectional stripline fed notch exciter concept has been investigated which results in greater than 50dB isolation between high and low frequency probes in the low frequency operating band. Preliminary exciter designs have been shown to remain well matched over greater than 10% bandwidths.

An element design for operation over 16% frequency bands centered at 4 and 8 GHZ has been fabricated and tested in waveguide simulators. Measured results are in excellent agreement with theoretical predictions in the 4.0 to 4.32 GHZ and 7.32 to 8.08 GHZ bands. Measured results outside these bands were not obtained due to limitations of measurement equipment (below 4 GHZ) and computational practicallity (above 8.08 GHZ), but are expected to show similar close agreement with theory in small array testing.

APPENDIX A

EVALUATION OF THE $\varepsilon_{pqr,nm}$ FOR RECTANGULAR LATTICE

The coefficients $\varepsilon_{pqr,nm}$ are defined by the integral

$$\text{(A-1)} \qquad \varepsilon_{pqr,nm} = \int_{b_1}^{B+b_1} dy \int_{-A/2}^{A/2} dx \; \underline{e}^{p}_{nm}(x,y) \cdot \underline{e}^{*}_{a_{pqr}}(x,y)$$

where A is the x dimension of the guide, B is the y dimension of the guide, b_1 is the half-thickness of the septum, $\underline{e}^{p}_{nm}(x,y)$ is an LSM_{nm} (p = ') or LSE_{nm} (p = ") feedguide electric mode function, and $\underline{e}_{a_{pqr}}(x,y)$ is a cell guide electric mode function which is an E mode with respect to the array normal (r = 1) or an H mode (r = 2). By appropriate choice of ordering in both feedguide and cell guide regimes, single subscripts may be used to identify the modes. These indices are taken as i for the feedguide mode modes, and σ, for the cell modes, giving

$$\text{(A-2)} \qquad \varepsilon_{\sigma,i} = \int_{b_1}^{B+b_1} dy \int_{-A/2}^{A/2} dx \; \underline{e}_{i}(x,y) \cdot \underline{e}^{*}_{a_\sigma}(x,y)$$

Expressions for $\underline{e}_i(x,y)$ are given in chapter 3, and expressions for $\underline{e}_{a_\sigma}(x,y)$ are given in equation 8.

In all, there are eight forms of the integral $E_{\beta\sigma}$, corresponding to the possible inner products of feedguide and cell guide modes. These are:

1. LSM-Symmetric Modes with E-Modes
2. LSM-Symmetric Modes with H-Modes
3. LSM-Antisymmetric Modes with E-Modes
4. LSM-Antisymmetric Modes with H-Modes
5. LSE-Symmetric Modes with E-Modes
6. LSE-Symmetric Modes with H-Modes
7. LSE-Antisymmetric Modes with E-Modes
8. LSE-Antisymmetric Modes with H-Modes

Since the integrals possess many terms in common, these terms are defined first and will be used as simple variables to shorten the expressions. These terms are:

$$R_1 = \beta \frac{\sin(k_x+\kappa_i)\beta}{(k_{x\sigma}+\kappa_i)\beta}$$

$$R_2 = \beta \frac{\sin(k_{x\sigma}-\kappa_i)\beta}{(k_{x\sigma}-\kappa_i)\beta}$$

$$R_3 = \frac{\cos(k_{x\sigma}+\kappa_{\varepsilon i})\delta}{k_{x\sigma}+\kappa_{\varepsilon i}}$$

$$R_4 = \frac{\cos\ (k_{x\sigma}-\kappa_{\varepsilon i})^{\delta}}{k_{x\sigma}-\kappa_{\varepsilon i}}$$

$$R_5 = \delta \, \frac{\sin(k_{x\sigma}+\kappa_{\varepsilon i})\delta}{(k_{x\sigma}-\kappa_{\varepsilon i})\delta}$$

$$R_6 = \delta \, \frac{\sin(k_{x\sigma}-\kappa_{\varepsilon i})\delta}{(k_{x\sigma}-\kappa_{\varepsilon i})\delta}$$

$$R_7 = \frac{\cos(k_{x\sigma}-\kappa_i)\delta}{k_x + \kappa_i}$$

$$R_8 = \frac{\cos(k_{x\sigma}-\kappa_i)\delta}{k_x + \kappa_i}$$

$$R_9 = \alpha \, \frac{\sin(k_{x\sigma}-\kappa_i)\alpha}{(k_{x\sigma}-\kappa_i)\alpha}$$

$$R_{10} = \alpha \, \frac{\sin(k_{x\sigma}-\kappa_i)\alpha}{(k_{x\sigma}-\kappa_i)\alpha}$$

and $$S = \frac{e^{jk_{y\sigma}b_1}\left(1-e^{jk_{y\sigma}b}\cos m\Pi\right)}{\left(\frac{m\Pi}{B}\right)^2 - k_{y\sigma}^2}$$

The coefficients B'_1, B'_2, C', E'_1, E'_2, F', B''_1, B''_2, C'', E'_1, E''_2, F'', N'^{S}_{i}, N'^{A}_{i}, N''^{S}_{i}, and N''^{A}_{i} which appear in the following expressions are defined in Appendix D.

1. LSM-Symmetric Modes with E-Modes

$$E_{\sigma,i} = \frac{S}{N_i^{\prime s}\sqrt{c}\,|\underline{k}_{t\sigma}|}\ \{k_{x\sigma} I_1^{\prime} + k_{y\sigma} I_2^{\prime}\} \tag{A-3}$$

where

$$I_1^{\prime} = \frac{m\Pi}{B}\ \{R_1+R_2 + \frac{1}{\varepsilon_r} B_1^{\prime}\ [R_3+R_4 - \frac{2k_{x\sigma}}{k_{x\sigma}^2-\kappa_{\varepsilon i}^2}] \sin k_{x\sigma}\beta \tag{A-4}$$

$$+ \frac{1}{\varepsilon_r} B_1^{\prime}\ [R_5+R_6]\ \cos k_{x\sigma}\beta$$

$$+ \frac{1}{\varepsilon_r} B_2^{\prime}\ [\frac{2\kappa_{\varepsilon i}}{k_{x\sigma}^2 - \kappa_{\varepsilon i}^2} + R_3-R_4]$$

$$+ \frac{1}{\varepsilon_r} B_2^{\prime}\ [R_6-R_5] \sin k_{x\sigma}\beta$$

$$+ C^{\prime}[\frac{2k_{x\sigma}}{k_{x\sigma}^2-\kappa_i^2} - R_7-R_8] \sin k_{x\sigma}\frac{A}{2}$$

$$+ C^{\prime}\ [R_9+R_{10}] \cos k_{x\sigma}\frac{A}{2}\}$$

and

$$I_2^{\prime} = -\frac{m\Pi}{B}\ k_{y\sigma}\ \{\ \frac{\kappa_i}{k^2-\kappa_i^2}\ [R_2-R_1] \tag{A-5}$$

$$+ \frac{\kappa_{\varepsilon i} B_1^{\prime}}{k\varepsilon_r^2-\kappa_{\varepsilon i}^2}\ [R_4-R_3 - \frac{2\kappa_{\varepsilon i}}{k_{x\sigma}^2-\kappa_{\varepsilon i}^2}] \sin k_{x\sigma}\beta$$

$$+\frac{\kappa_{\varepsilon i} B_1'}{k_{\varepsilon_r}^2-\kappa_{\varepsilon i}^2}\,[R_6-R_5]\cos k_{x\sigma}\beta$$

$$+\frac{\kappa_{\varepsilon i} B_2'}{k_{\varepsilon_r}^2-\kappa_{\varepsilon i}^2}\,\left[\frac{2k_{x\sigma}}{k_{x\sigma}^2-\kappa_{\varepsilon i}^2}-R_3-R_4\right]\cos k_{x\sigma}\beta$$

$$+\frac{\kappa_{\varepsilon i}\, B_2'}{k_{\varepsilon_r}^2-\kappa_{\varepsilon i}^2}\,[R_5+R_6]\sin k_{x\sigma}\beta$$

$$+\frac{\kappa_i C'}{k^2-\kappa_i^2}\,\left[\frac{2\kappa_i}{k_{x\sigma}^2-\kappa_i^2}+R_7-R_8\right]\sin k_{x\sigma}\frac{A}{2}$$

$$+\frac{\kappa_i C'}{k^2-\kappa_i^2}\,[R_{10}-R_9]\cos k_{x\sigma}\frac{A}{2}\}$$

2. LSM Symmetric Modes with H-Modes.

$$E_{\sigma,i}=\frac{S}{N_1'^{S}\sqrt{c}\,|\underline{k}_{t\sigma}|}\{k_{y\sigma}I_1'-k_{x\sigma}I_2'\} \tag{A-6}$$

where I_1' and I_2' are defined in equations (A-4) and (A-5), respectively.

3. LSM-Antisymmetric Modes with E-Modes

(A-7) $$E_{\sigma,i} = \frac{S}{N_i^{!\,a}\sqrt{c}\,|\underline{k}_{t\sigma}|}\{k_{x\sigma}I_3' + k_{y\sigma}I_4'\}$$

where

$$I_3' = -j\,\frac{m\Pi}{B}\,\{R_2 - R_1 + \frac{1}{\varepsilon_r}\,E_1'\,[\frac{2k_{x\sigma}}{k_{x\sigma}^2 - \kappa_{\varepsilon i}^2} - R_3 - R_4]\cos k_{x\sigma}\beta$$

$$+ \frac{1}{\varepsilon_r}\,E_1'\;[R_5 + R_6]\sin k_{x\sigma}\beta$$

$$+ \frac{1}{\varepsilon_r}\,E_2'\;[\frac{2\kappa_{\varepsilon i}}{k_{x\sigma}^2 - \kappa_{\varepsilon i}^2} + R_3 - R_4]\sin k_{x\sigma}\beta$$

$$+ \frac{1}{\varepsilon_r}\,E_1'\;[R_5 - R_6]\cos k_{x\sigma}\beta$$

$$+ F'\;[R_7 + R_8 - \frac{2k_{x\sigma}}{k_{x\sigma}^2 - \kappa_i^2}\cdot]\cos k_{x\sigma}\frac{A}{2}$$

$$+ F'\;[R_9 + R_{10}]\sin k_{x\sigma}\frac{A}{2}$$

and

(A-9) $$I_4' = jk_{y\sigma}\frac{m\Pi}{B}\,\{\frac{\kappa_i}{k^2 - \kappa_i^2}\,[R_1 + R_2]$$

$$+ \frac{\kappa_{\varepsilon i}E_1'}{k^2\varepsilon_r - \kappa_{\varepsilon i}^2}\quad[\frac{2\kappa_{\varepsilon i}}{k_{x\sigma}^2 - \kappa_{\varepsilon i}^2} + R_3 - R_4]\cos k_{x\sigma}\beta$$

$$+ \frac{\kappa_{\varepsilon i} E_1'}{k^2 \varepsilon_r - \kappa_{\varepsilon i}^2} [R_6 - R_5] \sin k_{x\sigma}\beta$$

$$+ \frac{\kappa_{\varepsilon i} E_2'}{k^2 \varepsilon_r - \kappa_{\varepsilon i}^2} [R_3 + R_4 - \frac{2k_{x\sigma}}{k_{x\sigma}^2 - \kappa_{\varepsilon i}^2}] \sin k_{x\sigma}\beta$$

$$+ \frac{\kappa_{\varepsilon i} E_2'}{k^2 \varepsilon_r - \kappa_{\varepsilon i}^2} [R_5 + R_6] \cos k_{x\sigma}\beta$$

$$+ \frac{\kappa_i F'}{k^2 - \kappa_i^2} [R_8 - R_7 - \frac{2\kappa_i}{k_{x\sigma}^2 - \kappa_i^2}] \cos k_{x\sigma}\frac{A}{2}$$

$$+ \frac{\kappa_i F'}{k^2 - \kappa_i^2} [R_{10} - R_9] \sin k_{x\sigma}\frac{A}{2}\}$$

4. LSM-Antisymmetric Modes with H-Modes.

$$\text{(A-10)} \qquad E_{\sigma,i} = \frac{S}{N_i'^A \sqrt{c}|\underline{k}_{t\sigma}|} \{k_{y\sigma} I_3' - k_{x\sigma} I_4'\}$$

where I_3' and I_4' are defined in equations (A -8) and (A -9), respectively.

5. LSE-Symmetric Modes with E-Modes

$$(A\text{-}11)\qquad E_{y,i} = \frac{S}{N_i''^{S}\sqrt{c}\,|\underline{k}_{t\sigma}|}\,k_{y\sigma} I_5''$$

where

$$(A\text{-}12)\qquad I_5'' = jk_{y\sigma}\{R_2+R_1+B_2''\left[\frac{2\kappa_{\varepsilon i}}{k_{x\sigma}^2-\kappa_{\varepsilon i}^2}+R_3-R_4\right]\cos k_{x\sigma}\beta$$

$$+\ B_2''\ [R_6-R_5]\sin k_{x\sigma}\beta$$

$$+\ B_1''\ \left[R_3+R_4-\frac{2k_{x\sigma}}{k_{x\sigma}^2-\kappa_{\varepsilon i}^2}\right]\sin k_{x\sigma}\beta$$

$$+\ B_1''\ [R_5+R_6]\cos k_{x\sigma}\beta$$

$$+\ C''\ \left[R_8-R_7-\frac{2\kappa_i}{k_{x\sigma}^2-\kappa_i^2}\right]\cos k_{x\sigma}\frac{A}{2}$$

$$+\ C''\ [R_{10}-R_9]\sin k_{x\sigma}\frac{A}{2}\}$$

6. LSE-Symmetric Modes with H-Modes

$$(A-13) \qquad E_{\sigma,i} = \frac{S}{N_i''^{S} \sqrt{c}\,|\underline{k}_{t\sigma}|} \left(-k_{x\sigma} I_5''\right)$$

where I_5'' is defined in equation (A -12).

7. LSE-Antisymmetric Modes with E-Modes

$$(A-14) \qquad E_{\sigma,i} = \frac{S}{N_i''^{A} \sqrt{c}\,|\underline{k}_{t\sigma}|} \left(jk_{y\sigma} I_6''\right)$$

where

$$(A-15) \qquad I_6'' = jk_{y\sigma} \{R_2 - R_1 + E_2'' \left[R_4 - R_3 - \frac{2\kappa_{\varepsilon i}}{k_{x\sigma}^2 - \kappa_{\varepsilon i}^2}\right] \sin k_{x\sigma}\beta$$

$$+ E_2'' \left[R_6 - R_5\right] \cos k_{x\sigma}\beta$$

$$+ E_1'' \left[R_3 + R_4 - \frac{2k_{x\sigma}}{\kappa_{x\sigma}^2 - \kappa_{\varepsilon i}^2}\right] \cos k_{x\sigma}\beta$$

$$+ E_1'' \quad [-R_5 - R_6]\sin k_{x\sigma}\beta$$

$$+ F'' \quad [\frac{2\kappa_i}{k_{x\sigma}^2 - \kappa_i^2} + R_7 - R_8]\sin k_{x\sigma}\frac{A}{2}$$

$$+ F'' \quad [R_{10} - R_9]\cos k_{x\sigma}\frac{A}{2}$$

8. LSE-Antisymmetric Modes with H-Modes

(A-16) $$E_{\sigma,i} = \frac{S}{N_i''{}^A\sqrt{c}\,|\underline{k}_{t\sigma}|}\,(-jk_{x\sigma}I_6'')$$

where I_6'' is defined in equation (A -15)

APPENDIX B

DERIVATION OF DIFFERENTIAL EQUATION RELATING $\underline{e}$ AND $\underline{h}$

The homogeneous Maxwell field equations are

$$\text{(B-1)} \qquad \nabla \times \underline{E}\,(\underline{x}) = -j\omega\mu \underline{H}(\underline{x})$$

$$\text{(B-2)} \qquad \nabla \times \underline{H}\,(\underline{x}) = j\omega\varepsilon \underline{E}\,(\underline{x})$$

To separate out longitudinal components ($\underline{z}_o$ directed) take vector and scalar products of (B-1) and (B-2) with $\underline{z}_o$. Thus

$$\text{(B-3)} \qquad j\omega\mu \underline{H}(\underline{x}) \times \underline{z}_o = \underline{z}_o \times (\nabla \times \underline{E}(\underline{x})) = -\frac{\partial}{\partial z}\,\underline{E}(\underline{x}) + \nabla E_z(\underline{x})$$

$$= \frac{\partial}{\partial z}\,(\underline{z}_o E_z(\underline{x} + \hat{\underline{e}}(\underline{x})) + (\nabla_t + \underline{z}_o \frac{\partial}{\partial z}) E_z(\underline{x})$$

$$= \nabla_t E_z(\underline{x}) - \frac{\partial}{\partial z}\,\hat{\underline{e}}\,(\underline{x})$$

$$(B-4) \qquad -j\omega\mu H_z = \underline{z}_o \cdot (\nabla x \underline{E}(\underline{x})) = -\nabla_t \cdot (\underline{Z}_o x \underline{E}(\underline{x}))$$

where $\hat{\underline{e}}(\underline{x})$ is the tranverse to z electric field.

Similarly,

$$(B-5) \qquad j\omega\varepsilon \underline{Z}_o \times \underline{E}(\underline{x}) = \nabla_t H_z(\underline{x}) - \frac{\partial}{\partial z} \hat{\underline{h}}(\underline{x})$$

$$(B-6) \qquad j\omega\varepsilon E_z(\underline{x}) = \nabla_t \cdot (\underline{H} x \underline{Z}_o)$$

Substituting for $E_z(\underline{x})$ in (B-3) from (B-6) gives:

$$(B-7) \qquad -\frac{\partial}{\partial z} \hat{\underline{e}}(\underline{x}) = j\omega\mu [\overleftrightarrow{I} + \frac{\nabla_t \nabla_t}{k^2}] \cdot (\hat{\underline{h}}(\underline{x}) \times \underline{Z}_o)$$

Recognizing that

$$\hat{\underline{e}}(\underline{x}) = e^{-j\gamma z} \underline{e}(x,y)$$

$$\hat{\underline{h}}(\underline{x}) = e^{-j\gamma z} \underline{h}(x,y)$$

for uniform (in $\underline{z}_o$) media, (B-7) reduces to

$$\frac{\gamma}{\omega\mu}\,\underline{e}(x,y) = [\overleftrightarrow{I} + \frac{\nabla_t \nabla_t}{k^2}] \cdot (\underline{h}(x,y) \times \underline{z}_o) \tag{B-8}$$

And from (B-4) and (B-5)

$$\gamma\underline{h}(x,y) = \omega\epsilon\ [\overleftrightarrow{I} + \frac{\nabla_t \nabla_t}{k^2}] \cdot (\underline{z}_o \times \underline{e}(x,y)) \tag{B-9}$$

For the inhomogeneously filled, uniform in $\underline{z}_o$ waveguide, uncoupled modes will be either LSE ($e''_x \equiv 0$) or LSM ($h'_x \equiv 0$). For LSE modes, solution of (B-8) gives

$$e''_y(x,y) = -\frac{\omega\gamma\mu}{k^2 - k_x^2}\, h''_x(x,y)$$

e''_y is related to h''_x by an impedance. It is convenient, therefore, to define a modal admittance Y", such that

$$e''_y(x,y) = -h''_x(x,y)$$

and

$$\iint dA(\underline{h}_i \times \underline{z}_o) \cdot \underline{e}_j = \delta_{ij}$$

In this manner, (B-8) may be rewritten as

$$\text{(B-10)} \qquad \gamma Z'' \, \underline{e}''(x,y) = \omega\mu[\overleftrightarrow{I} + \frac{\nabla_t \nabla_t}{k^2}] \cdot (\underline{h}''(x,y) \, x \, \underline{z}_o)$$

Similarly

$$\text{(B-11)} \qquad \gamma Y' \underline{h}'(x,y) = \omega\varepsilon[\overleftrightarrow{I} + \frac{\nabla_t \nabla_t}{k^2}] \cdot (\underline{z}_o \; x \; \underline{e}'(x,y))$$

APPENDIX C

ORTHONORMALIZATION OF FEEDGUIDE MODE FUNCTIONS

Let $\underline{E}_n, \underline{H}_n$ and $\underline{E}_m, \underline{H}_m$ be linearly independent characteristic solutions of Maxwell's source free equations in the cylindrical guide shown in Figure D-1. The guide is uniform in z, resulting in z dependencies given by

$$e^{-j\gamma_n z}, \quad e^{-j\gamma_m z}$$

Assuming a lossless region, then the conjugates of the characteristic solutions are also solutions of Maxwell's Equations. Consider the curl equations

$$\text{(C-1a,b)} \qquad \nabla \times \underline{E}_n = -j\omega\mu \underline{H}_n \qquad\qquad \nabla \times \underline{E}_m^* = j\omega\mu \underline{H}_m^*$$

$$\text{(C-1c,d)} \qquad \nabla \times \underline{H}_n = j\omega\varepsilon \underline{E}_n \qquad\qquad \nabla \times \underline{H}_m^* = -j\omega\varepsilon \underline{E}_m^*$$

where * denotes conjugation. Taking scalar products of (C-1a,b) with $\underline{H}_m^*$ and $\underline{H}_n$, respectively, and adding, gives,

$$\text{(C-2)} \qquad \underline{H}_m^* \cdot \nabla \times \underline{E}_n + \underline{H}_n \cdot \nabla \times \underline{E}_m^* = 0$$

Similarly, from (C-1c,d)

(C-3) $$\underline{E}_m^* \cdot \nabla \times \underline{H}_m + \underline{E}_n \cdot \nabla \times \underline{H}_m^* = 0$$

Adding (C-2) and (C-3) and manipulating results in

(C-4) $$0 = \nabla_t \cdot (\underline{E}_m^* \times \underline{H}_n + \underline{E}_n \times \underline{H}_m^*) + \underline{z}_0 \frac{\partial}{\partial z} \cdot (\underline{E}_m^* \times \underline{H}_n + \underline{E}_n \times \underline{H}_m^*)$$

where ∇_t is the transverse gradient operator, and the longitudinal gradient has been specifically shown. Since the entire z dependence is embodied in the exponentials, (C-4) becomes

(C-5) $$\nabla_t \cdot (\underline{E}_m^* \times \underline{H}_n + \underline{E}_n \times \underline{H}_m^*) = j(\gamma_n - \gamma_m)\underline{z}_0 \cdot (\underline{E}_{t_m}^* \times \underline{H}_{t_n} + \underline{E}_{t_n} \times \underline{H}_{t_m}^*)$$

where the transverse field is indicated by the subscript t. In equation (C-5) the longitudinal components of the fields have been ignored on the right hand side due to the $\underline{z}_0 \cdot$ operator. Let

(C-6) $$\underline{E}_{t_n} = \underline{e}_n(x,y)\, e^{-j\gamma_n z}$$

and similarly for the other explicitly transverse field quantities (subscript t). Then, application of the divergence theorem (z-dependent integrals cancel out) results in

$$(C\text{-}7) \qquad (\gamma_n - \gamma_m) \iint_S \underline{z}_0 \cdot (\underline{e}_m^* \times \underline{h}_n + \underline{e}_n \times \underline{h}_m^*) d\sigma = 0$$

where S is the cylindrical cross-section and $d\sigma$ is the differential unit of transverse area.

The fields $\underline{E}_n$, $\underline{H}_n$, $\underline{E}_m$, and $\underline{H}_m$ are assumed to be linearly independent. Hence $\gamma_n \neq \gamma_m$, and (C-7) may be rewritten as

$$(C\text{-}8) \qquad \iint_S \underline{z}_0 \cdot (\underline{e}_m^* \times \underline{h}_n + \underline{e}_n \times \underline{h}_m^*) d\sigma = 0$$

Since the direction of propagation ($\pm z$) should not effect the result (C-8), consider the z dependencies

$$e^{-j\gamma_n z}, \quad e^{+j\gamma_m z}$$

Then, by entirely equivalent steps,

$$(C\text{-}9) \qquad (\gamma_n + \gamma_m) \iint_S \underline{z}_0 \cdot (\underline{e}_m^* \times \underline{h}_n - \underline{e}_n \times \underline{h}_m^*) d\sigma = 0$$

or, for $\gamma_n \neq -\gamma_m$,

$$(C\text{-}10) \qquad \iint_S \underline{z}_0 \cdot (\underline{e}_m^* \times \underline{h}_n - \underline{e}_n \times \underline{h}_m^*) d\sigma = 0$$

Adding and subtracting (C-8) and (C-9) results in

(C-11) $$\iint_S \underline{e}_m^* \cdot (\underline{h}_n \times \underline{z}_0)\,d\sigma = 0$$

(C-12) $$\iint_S \underline{e}_n \cdot (\underline{h}_m^* \times \underline{z}_0)\,d\sigma = 0$$

Equations (C-11) and (C-12) are the desired mode orthogonality relations.

In the instance that $\gamma_n = \gamma_m$, then, assuming the eigenvalues are not degenerate, equation (C-7) is satisfied independent of the value of the integral. From equation (C-10), with $m \to n$

(C-13) $$\underline{e}_n^* \times \underline{h}_n = \underline{e}_n \times \underline{h}_n^*$$

Substituting (C-13) into

(C-14) $$\iint_S \underline{z}_0 \cdot (\underline{e}_n^* \times \underline{h}_n + \underline{e}_n \times \underline{h}_n^*)\,d\sigma = \text{constant}$$

yields the desired mode function normalization integral

(C-15) $$\iint_S \underline{e}_n \cdot (\underline{h}_n^* \times \underline{z}_0)\,d\sigma = \text{constant}$$

If the constant in equation (C-15) is taken as 1, then in the field representations

$$\underline{E} = \sum_i V_i \underline{e}_i$$

$$\underline{H} = \sum_i I_i \underline{h}_i$$

$V_i I_i^*$ has units of power.

Using the expressions for $\underline{e}_i^r$ and $\underline{h}_i^r$ (r=',") from section 4 in equation (C-15) with unit constant, and rearranging results in the following integrals for the normalization constant N_i^r:

1. LSM symmetric modes (r=')

$$(N'^{s}_{nm})^2 = \int_{-A/2}^{A/2} dx \int_0^b dy \frac{1}{\epsilon_r(x)} \sin^2\frac{m\pi y}{b} |I'^{s}_n(x)|^2$$

$$= b\Big\{\frac{\beta}{2}S_1(2\kappa'\beta) + \frac{1}{\epsilon_r}B_1'^2\frac{\delta}{2}S_1(2\kappa'_\epsilon\delta)$$

$$+ \frac{1}{\epsilon_r}|B_2'|^2\frac{\delta}{2}S_2(2\kappa'_\epsilon\delta)\sigma(\kappa'_\epsilon)$$

$$-t(\kappa'_\epsilon)B_1'B_2'\delta S_3(\kappa'_\epsilon\delta)\sigma(\kappa'_\epsilon)$$

$$+|C'|^2\frac{\alpha}{2}S_1(2\kappa'\alpha)\Big\}$$

where

$$B_1' = \cos\kappa'\beta$$

$$B_2' = \frac{\epsilon_r\kappa'}{\kappa'_\epsilon}\sin\kappa'\beta$$

$$C' = \frac{\sin\kappa'\beta}{\sin\kappa'_\epsilon\alpha}[\cos\kappa'_\epsilon\delta + \frac{\kappa'_\epsilon}{\epsilon_r\kappa'}\cot\kappa'\beta\sin\kappa'_\epsilon\delta]$$

and

$$t(x) = \begin{cases} 1, & x=|x| \\ j, & x=-j|x| \end{cases}$$

$$\sigma(x) = \begin{cases} 1, & x=|x| \\ -1, & x=-j|x| \end{cases}$$

$$S_1(x) = \frac{\sin x}{x} + 1$$

$$S_2(x) = 1 - \frac{\sin x}{x}$$

$$S_3(x) = t(x)\frac{\sin^2 x}{x}$$

2. LSM antisymmetric modes (r=')

$$\begin{aligned}(N'^{a}_{nm}) &= \int_{-A/2}^{A/2} dx \int_{0}^{b} dy \frac{1}{\varepsilon_r(x)} \sin^2\frac{m\pi y}{b} |I'^{a}_{n}|^2 \\ &= b\Big\{\frac{\beta}{2}S_2(2\kappa'\beta) + \frac{1}{\varepsilon_r}|E'_1|^2\frac{\delta}{2}S_1(2\kappa'_\varepsilon\delta) \\ &\quad +\frac{1}{\varepsilon_r}|E'_2|^2\frac{\delta}{2}S_2(2\kappa'_\varepsilon\delta)\sigma(\kappa'_\varepsilon) \\ &\quad -\frac{\sigma(\kappa'_\varepsilon)}{\varepsilon_r}F\delta S_3(\kappa'_\varepsilon\delta) \\ &\quad +|F'|^2\frac{\alpha}{2}S_1(2\kappa'\alpha)\Big\}\end{aligned}$$

where

$$E'_1 = \sin\kappa'\beta$$

$$E'_2 = -\frac{\varepsilon_r\kappa'}{\kappa'_\varepsilon}\cos\kappa'\beta$$

$$F' = \frac{\cos\kappa'\beta}{\sin\kappa'\alpha}[\cos\kappa'_\varepsilon\delta - \frac{\kappa'_\varepsilon}{\varepsilon_r\kappa'}\tan\kappa'\beta\sin\kappa'_\varepsilon\delta]$$

$$F = \begin{cases} Re\{E'_1 E'^*_2\}, & \kappa'_\varepsilon = |\kappa'_\varepsilon| \\ \\ Im\{E'_1 E'^*_2\}, & \kappa'_\varepsilon = -j|\kappa'_\varepsilon| \end{cases}$$

3. LSE symmetric modes (r=")

$$(N''^s_{nm}) = \int_{-A/2}^{A/2} dx \int_0^b dy \cos^2\frac{m\pi y}{b}|V''^s_n(x)|^2$$

$$= r_m b\left\{\frac{\beta}{2}S_1(2\kappa''\beta) + B''^2_1\frac{\delta}{2}S_1(2\kappa''_\varepsilon\delta)\right.$$

$$+|B''_2|^2\frac{\delta}{2}S_2(2\kappa''_\varepsilon\delta)\sigma(\kappa''_\varepsilon)$$

$$-t(\kappa''_\varepsilon)B''_1B''_2\delta S_3(\kappa''_\varepsilon\delta)\sigma(\kappa''_\varepsilon)$$

$$\left.+|C''|^2\frac{\alpha}{2}S_2(2\kappa''\alpha)\sigma(\kappa'')\right\}$$

where

$$r_m = \text{Neumann factor} = \begin{cases} 1, & m\neq 0 \\ 2, & m=0 \end{cases}$$

$$B''_1 = \cos\kappa''\beta$$

$$B''_2 = \frac{\kappa''}{\kappa''_\varepsilon}\sin\kappa''\beta$$

$$C'' = \frac{\cos\kappa''\beta}{\sin\kappa''\alpha}\{\cos\kappa''_\varepsilon - \frac{\kappa''}{\kappa''_\varepsilon}\tan\kappa''\beta\sin\kappa''_\varepsilon\delta]$$

4. LSE antisymmetric modes (r=")

$$
(N''^{a}_{nm}) = \int_{-A/2}^{A/2} dx \int_{0}^{b} dy \cos^2\frac{m\pi y}{b} |V''^{a}_{n}(x)|^2
$$

$$
= r_m b \Big\{ \frac{\beta}{2} S_2(2\kappa''\beta)\sigma(\kappa'') + |E''_1|^2 \frac{\delta}{2} S_1(2\kappa''_\varepsilon\delta)
$$

$$
+ |E''_2|^2 \frac{\delta}{2} S_2(2\kappa''_\varepsilon\delta)\sigma(\kappa''_\varepsilon)
$$

$$
- F\delta S_3(\kappa''_\varepsilon\delta)
$$

$$
+ |F''|^2 \frac{\alpha}{2} S_2(2\kappa''\alpha) \Big\}
$$

where

$$
E''_1 = -\sin\kappa''\beta
$$

$$
E''_2 = \frac{\kappa''}{\kappa''_\varepsilon}\cos\kappa''\beta
$$

$$
F'' = -\frac{\sin\kappa''\beta}{\sin\kappa''\alpha}[\cos\kappa''_\varepsilon\delta + \frac{\kappa''}{\kappa''_\varepsilon}\cot\kappa''\beta\sin\kappa''_\varepsilon\delta]
$$

$$
F = \begin{cases} E''_1 E''_2, & \kappa'' = |\kappa''| \\ Re\{E''_1 E''^{*}_2\}, & \kappa'' = -j|\kappa''|,\ \kappa''_\varepsilon = |\kappa''_\varepsilon| \\ j0.5\{E''_1 - E''^{*}_1\}E''_2, & \kappa'' = -j|\kappa''|,\ \kappa''_\varepsilon = -j|\kappa''_\varepsilon| \end{cases}
$$

APPENDIX D

PROGRAM LISTINGS

This Appendix gives listings of all programs, and subprograms required to reproduce the numerical results presented in this report. In general, the listings are self-explanatory. The language is FORTRAN (extended) and the programs are designed to run on CDC 6600, 6700 and CYBER 73 series computers.

The Appendix has two subsections. The first gives listings of main programs. The second section gives listing of subroutines and function subprograms required for execution of the main programs.

D.1 Program Listings

```
      PROGRAM PLTPAT (INPUT,OUTPUT,TAPE5=INPUT,TAPE6=OUTPUT,TAPE4)
C
C      COMPUTATION OF BIFURCATED TWIN DIELECTRIC SLAB LOADED RECTANGULAR
C      WAVEGUIDE ARRAY ELEMENT RADIATION CHARACTERISTICS.
C
C      REQUIRES CALCOMP LIBRARY AND SUBROUTINES GIVEN IN APPENDIX D.2.
C
      DIMENSION POW(10,51),ST(51),S1I(2),S2I(2),MORD(20),IP(10),IQ(10),
     1IR(10),JJ(10)
      DIMENSION IBUF(1000)
      REAL K,KE,L
      INTEGER P1,Q1,TO(10),QO(10),RO(10),SIGO(10),SIG(20),SIG10(10)
      COMPLEX Y,YA,C10,C20,C1,C2,AJ,C3,R1,R2,C4
      COMPLEX S11(20,20),S21(250,20),VO
      COMMON /ARRAY/ AL,BL,DL,B1,SEPTL,TPI,EPS,S1(2),S2(2)
      COMMON /CNSRV/ Y(20),YA(250)
      COMMON /MODES/ K(20),KE(20),GAMMA(20),MODE1(20),ISYM(20),NN(20),
     1MM(20),MODORD(20)
      COMMON /PQ/ P1,Q1
      DATA TPI,C/6.2831853071796,11.8028526/
      DATA AJ/(0.,1.)/
      CALL PLOTS (IBUF,1000,4)
      KNT=0
C
C      INPUT>  FREQUENCY IN GHZ, F0#  RELATIVE SLAB PERMITTIVITY, EPS#
C      FEEDGUIDE HEIGHT, BD, IN INCHES# A(ALPHA), B(BETA), AND D(DELTA),
C      IN INCHES# AND APERTURE PLAN TO-REFFRENCE PLANE SEPARATION IN
C      FEEDGUIDE WAVELENGTHS, ALEN.
C
100   READ (5,800) F0,EPS,BD,A,B,D,SEP,ALEN
      IF (EOF(5).NE.0) GO TO 160
      A1=2.*(A+B+D)
      WRITE (6,900) F0,EPS,A1,BD,A,B,D,SEP,ALEN
C
C      INPUT>  LIMITS OF SAMPLED GRATING LOBE SPACE, P1 AND Q1
C
      READ (5,820) P1,Q1
C
C      INPUT> LATTICE VECTORS S1 AND S2, IN INCHES.
C
      READ (5,800) S1,S2
      DO 105 I=1,2
      S1I(I)=S1(I)
      S2I(I)=S2(I)
105   CONTINUE
      IGRD=1
      S=S1(1)*S2(1)+S1(2)*S2(2)
      IF (ABS(S).LT.1.E-10) IGRD=2
      DX=S1(1)
      DY=S2(2)
C
C      INPUT>  NUMBER OF MODES TO ESTABLISH ORDERING, NMODE1, #MAX OF
C      20## AND FREQUENCY BAND DESIGNATION, LOHI#=LO OR HI#.
C
      READ (5,810) NMODE1,LOHI
      IHLO=LOHI
      IF (SEP.GT.1.E-10) IHLO=2HLO
C
C      INPUT>  SINE SPACE SCAN RANGE AND INCREMENTS.
C
```

```
      READ (5,800) STHS,STHE,STHI,SPHS,SPHE,SPHI
      NTH=INT((STHE-STHS)/STHI+0.5)+1
      NPH=INT((SPHE-SPHS)/SPHI+0.5)+1
C
C      INPUT>  NUMBER OF FEEDGUIDE MODES TO BE USED FOR APERTURE FIELD
C      APPROXIMATION, NMODES# AND NUMBER OF BEAMS TO BE PLOTTED, LOBES.
C
      READ (5,820) NMODES,LOBES
      NM=NMODES+1
      DO 106 I=1,NMODES
C
C      INPUT>  NMODES FEEDGUIDE MODE DESIGNATIONS #E.G., LSE0100,
C      LSM0101, LSE0201#.
C
      READ (5,830) MORD(I)
106   CONTINUE
      IF (LOBES.EQ.0) GO TO 108
      IF (LOBES.GT.10) STOP 'LOBES>10'
C
C      INPUT>  #LOBES# BEAM DESIGNATIONS IN FORM P,Q,R
C
      DO 107 I=1,LOBES
      READ (5,820) TO(I),QO(I),RO(I)
      SIGO(I)=QO(I)+Q1+1+(TO(I)+P1)*(2*Q1+1)+(RO(I)-1)*(2*P1+1)*
     1(2*Q1+1)
107   CONTINUE
C
C      INPUT>  COMPLEX LSE0200 MODE VOLTAGE MODIFIER, R1# AND COMPLEX
C      UPPER ELEMENT HALF VOLTAGE MODIFIER, R2.
C
108   READ (5,800) R1,R2
      WRITE (6,904) R1,R2
      WRITE (6,910) S1,S2
      WRITE (6,915) P1,Q1,NMODES
      L=F0/C
      AL=A*L
      BL=B*L
      DL=D*L
      B1=BD*L
      SEPTL=SEP*L
C
C      COMPUTE DISPERSION RELATION AT CENTER BAND.
C
      CALL LSMLSE (NMODE1)
      ALEN=ALEN/(L*GAMMA(1))
      IF (ALEN.GT.1.E-05) ALEN1=ALEN
      ALEN=ALEN1
      C10=CEXP(AJ*TPI*GAMMA(1)*ALEN*L)
      C20=CEXP(AJ*TPI*GAMMA(2)*ALEN*L)
C
C      INPUT>  HALF BANDWIDTH (INTEGER) IN PERCENT, IBW# AND PERCENT
C      BANDWIDTH STEP, ISTEP.
C
      READ (5,820) IBW,ISTEP
      NBW=2*IBW+1
C
C      COMPUTE PERFORMANCE OVER BAND.
C
      DO 155 JBW=1,NBW,ISTEP
      BW=1.+0.01*(JBW-1-IBW)
```

```
      F=BW*F0
      IF (IBW.EQ.0) GO TO 109
      WRITE (6,905) BW,F,EPS,A1,BD,A,B,D,SEP,ALEN
109   L=F/C
      AL=A*L
      BL=B*L
      DL=D*L
      B1=BD*L
      SEPTL=SEP*L
      B11=0.5*(B1+SEPTL)
      IF (IBW.EQ.0) GO TO 1091
      CALL LSMLSE (NMODE1)
1091  C1=C10*CEXP(-AJ*TPI*GAMMA(1)*ALEN*L)
      C2=C20*CEXP(-AJ*TPI*GAMMA(2)*ALEN*L)
      DO 110 I=1,2
      S1(I)=S1I(I)*L
      S2(I)=S2I(I)*L
110   CONTINUE
      J=0
      DO 116 I=1,NMODES
115   J=J+1
      IF (MODORD(J).NE.MORD(I)) GO TO 115
      K(I)=K(J)
      KE(I)=KE(J)
      GAMMA(I)=GAMMA(J)
      NN(I)=NN(J)
      MM(I)=MM(J)
      MODE1(I)=MODE1(J)
      ISYM(I)=ISYM(J)
      MODORD(I)=MORD(I)
116   CONTINUE
      IWRITE=1
      CALL NORM (NMODES,IWRITE)
      SPH=SPHS-SPHI
      DO 150 IPH=1,NPH
      KNT=KNT+1
      DO 1164 I=1,10
      DO 1163 ITH=1,51
      POW(I,ITH)=-100.00
1163  CONTINUE
1164  CONTINUE
      SPH=SPH+SPHI
      CPH=SQRT(1.-SPH**2)
      STH=STHS-STHI
      IF (IHLO.EQ.2HLO) WRITE (6,920) SPH
      IF (IHLO.EQ.2HHI) WRITE (6,930) SPH
      J1=0
      KJ1=0
C
C      TAKE THETA CUTS.
C
      DO 140 ITH=1,NTH
      STH=STH+STHI
      ST(ITH)=STH
      CTH=SQRT(1.-STH**2)
      U=STH*CPH
      V=STH*SPH
      C3=CEXP(AJ*TPI*V*B11)
      C4=R2/C3
      C3=R2*C3
```

```
C
C      EVALUATE SCATTERING BLOCKS S11 AND S21
C
      CALL SCTMAT (IHLO,NMODES,U,V,S11,S21,NMOD,ISIG)
      J=J1
      KJ=KJ1
      DO 117 I=1,ISIG
      IF (REAL(YA(I)).LE.0.) GO TO 117
      IF (J1.EQ.0) GO TO 1162
      DO 1161 I1=1,J1
      IF (I.EQ.SIG(I1)) GO TO 117
1161  CONTINUE
1162  J=J+1
      IF (J.LE.10) GO TO 1165
      KJ=KJ+1
      SIG10(KJ)=I
1165  SIG(J)=I
117   CONTINUE
      J1=J
      J2=J
      IF (J2.GT.10) J2=10
      KJ1=KJ
      IF (LOHI.EQ.2HHI) GO TO 120
      P=2.*CABS(Y(1))
      PO=0.
C
C      COMPUTE POWER TRANSMISSION COEFFICIENTS FOR FIRST 10 PROPAGATING
C      BEAMS IN GRATING LOBE SEQUENCE, AT LOW FREQUENCY AND POWER
C      REFLECTION COEFFICIENTS.  P=INPUT POWER# PO=SUM OF REAL POWER IN
C      ALL BEAMS AND FEEDGUIDE MODES.
C
      DO 118 I=1,J1
      ISG=SIG(I)
      PT=(CABS(S21(ISG,1)+S21(ISG,NM))**2)*REAL(YA(ISG))/P
      S=REAL(YA(ISG))-1.0
      IPT=1
      IF (ABS(S).LT.1.E-10.AND.ABS(SPH*CPH).LT.1.E-10) IPT=IPT+1
      IF (ABS(SPH-1.).LT.1.E-10.AND.ISG.GT.ISIG/2) IPT=IPT-2
      IF (ABS(CPH-1.).LT.1.E-10.AND.ISG.LE.ISIG/2) IPT=IPT-2
      IPT=IABS(IPT)
      PT=IPT*PT
      PO=PO+PT
      IF (PT.LT.1.E-10) PT=1.E-10
      IF (I.GT.10) GO TO 118
      POW(I,ITH)=10.*ALOG10(PT)
118   CONTINUE
      PRU=(CABS(S11(1,1)+S11(1,NM))**2)*CABS(Y(1))/P
      PO=PO+PRU
      IF (PRU.LT.1.E-10) PRU=1.E-10
      PRU=10.*ALOG10(PRU)
      PRL=(CABS(S11(NM,1)+S11(NM,NM))**2)*CABS(Y(1))/P
      PO=PO+PRL
C
C      CHECK CONSERVATION OF ENERGY.  IPO AND IM ARE MINUS THE NUMBER OF
C      DIGITS TO WHICH CONSERVATION OF ENERGY IS APPROXIMATED BY
C      SOLUTION.
C
      PO=ALOG10(ABS(PO-1.0)+1.E-80)
      IPO=PO
      IF (IPO.LT.-99) IPO=-99
```

```
      IF (PRL.LT.1.E-10) PRL=1.E-10
      PRL=10.*ALOG10(PRL)
      CALL CONSRV (S11,S21,NMOD,ISIG,IM)
      WRITE (6,940) STH,PRU,PRL,IP0,IM,(POW(I,ITH),I=1,J2)
      GO TO 130
C
C      COMPUTE POWER TRANSMISION AND REFLECTION COEFFICIENTS AT HIG
C      FREQUENCY.
C
120   V2=TAN(0.25*TPI*S1(1)*U)
      V0=R1*V2
      V2=CABS(V0)
      P=CABS(Y(1))+CABS(Y(2))*V2**2
      IF (IHLO.NE.LOHI) GO TO 124
C
C      CASE 1>  INFINITESSIMALLY THIN SEPTUM AND RECTANGULAR GRID.
C
      P0=0.0
      DO 121 I=1,J1
      ISG=SIG(I)
      PT=REAL(YA(ISG))*(CABS(S21(ISG,1)+S21(ISG,2)*V0)**2)/P
      S=REAL(YA(ISG))-1.0
      IPT=1
      IF (ABS(S).LT.1.E-10.AND.ABS(SPH*CPH).LT.1.E-10) IPT=IPT+1
      IF (ABS(SPH-1.).LT.1.E-10.AND.ISG.GT.ISIG/2) IPT=IPT-2
      IF (ABS(CPH-1.).LT.1.E-10.AND.ISG.LE.ISIG/2) IPT=IPT-2
      IPT=IABS(IPT)
      PT=IPT*PT
      P0=P0+PT
      IF (PT.LT.1.E-10) PT=1.E-10
      IF (I.GT.10) GO TO 121
      POW(I,ITH)=10.*ALOG10(PT)
121   CONTINUE
      PR1=CABS(Y(1)*(S11(1,1)+S11(1,2)*V0)**2)/P
      P0=P0+PR1
      IF (PR1.LT.1.E-10) PR1=1.E-10
      PR1=10.*ALOG10(PR1)
      PR2=CABS(Y(2)*(S11(2,1)+S11(2,2)*V0)**2)/P
      P0=P0+PR2
C
C      CHECK CONSERVATION OF ENERGY.
C
      P0=ALOG10(ABS(P0-1.0)+1.E-80)
      IP0=P0
      IF (IP0.LT.-99) IP0=-99
      IF (PR2.LT.1.E-10) PR2=1.E-10
      PR2=10.*ALOG10(PR2)
      CALL CONSRV (S11,S21,NMOD,ISIG,IM)
      WRITE (6,940) STH,PR1,PR2,IP0,IM,(POW(I,ITH),I=1,J2)
      GO TO 130
C
C      CASE 2>  THICK SEPTUM OR TRIANGULAR GRID.
C
124   P=2.0*P
      P0=0.0
      DO 125 I=1,J1
      ISG=SIG(I)
      PT=REAL(YA(ISG))*CABS(((S21(ISG,1)*C4+S21(ISG,NM)*C3)*C1+
     1(S21(ISG,2)*C4+S21(ISG,NM+1)*C3)*C2*V0)**2)/P
      S=REAL(YA(ISG))-1.0
```

```
      IPT=1
      IF (ABS(S).LT.1.E-10.AND.ABS(SPH*CPH).LT.1.E-10) IPT=IPT+1
      IF (ABS(SPH-1.).LT.1.E-10.AND.ISG.GT.ISIG/2) IPT=IPT-2
      IF (ABS(CPH-1.).LT.1.E-10.AND.ISG.LE.ISIG/2) IPT=IPT-2
      IPT=IABS(IPT)
      PT=IPT*PT
      P0=P0+PT
      IF (PT.LT.1.E-10) PT=1.E-10
      IF (I.GT.10) GO TO 125
      POW(I,ITH)=10.*ALOG10(PT)
  125 CONTINUE
      PRU=CABS(Y(1)*((S11(1,1)*C4+S11(1,NM)*C3)*C1+(S11(1,2)*C4
     1+S11(1,NM+1)*C3)*C2*V0)**2)/P
      PRU=PRU+CABS(Y(2)*((S11(2,1)*C4+S11(2,NM)*C3)*C1+(S11(2,2)*C4
     1+S11(2,NM+1)*C3)*C2*V0)**2)/P
      P0=P0+PRU
      IF (PRU.LT.1.E-10) PRU=1.E-10
      PRU=10.*ALOG10(PRU)
      PRL=CABS(Y(1)*((S11(NM,1)*C4+S11(NM,NM)*C3)*C1+(S11(NM,2)*C4
     1+S11(NM,NM+1)*C3)*C2*V0)**2)/P
      PRL=PRL+CABS(Y(2)*((S11(NM+1,1)*C4+S11(NM+1,NM)*C3)*C1+
     1(S11(NM+1,2)*C4+S11(NM+1,NM+1)*C3)*C2*V0)**2)/P
      P0=P0+PRL
C
C      CHECK CONSERVATION OF ENERGY.
C
      P0=ALOG10(ABS(P0-1.0)+1.E-80)
      IP0=P0
      IF (IP0.LT.-99) IP0=-99
      IF (PRL.LT.1.E-10) PRL=1.E-10
      PRL=10.*ALOG10(PRL)
      CALL CONSRV (S11,S21,NMOD,ISIG,IM)
      WRITE (6,940) STH,PRU,PRL,IP0,IM,(POW(I,ITH),I=1,J2)
  130 CONTINUE
  140 CONTINUE
C
C      PRINT BEAM DESIGNATIONS.
C
      IQ1=2*Q1+1
      ISG=ISIG/2
      DO 141 I=1,J2
      DO 1410 I1=1,NOBES
      IF (SIG(I).NE.SIG0(I1)) GO TO 1410
      JJ(I1)=I
      GO TO 1411
 1410 CONTINUE
 1411 IR(I)=1
      IF (SIG(I).GT.ISG) IR(I)=2
      IP(I)=(SIG(I)-1-(IR(I)-1)*ISG)/IQ1-P1
      IQ(I)=SIG(I)-1-Q1-(IR(I)-1)*ISG-(IP(I)+P1)*IQ1
  141 CONTINUE
      WRITE (6,950) (IP(I),IQ(I),IR(I),I=1,J2)
      IF (KJ1.EQ.0) GO TO 143
      DO 142 I=1,KJ1
      IR(I)=1
      IF (SIG10(I).GT.ISG) IR(I)=2
      IP(I)=(SIG10(I)-1-(IR(I)-1)*ISG)/IQ1-P1
      IQ(I)=SIG10(I)-1-Q1-(IR(I)-1)*ISG-(IP(I)+P1)*IQ1
  142 CONTINUE
      WRITE (6,960) (IP(I),IQ(I),IR(I),I=1,KJ1)
```

```
143    IF (LOBES.EQ.0) GO TO 150
       IF (KNT.EQ.1) CALL PLOT (0.,.5,-3)
C
C       PLOT *LOBES* BEAMS
C
       CALL PLOT (0.,.2,2)
       ISTRT=1
       LOBE=MIN0(4,LOBES)
       CALL PLTCAL (A,B,D,F,EPS,A1,BD,DX,DY,SEP,POW,SIGO,LOBE,ISTRT,JJ,
      1ST,SPH,IGRD,NTH)
       IF (LOBES.LE.4) GO TO 150
       CALL PLOT (0.,.2,2)
       LOBE=MIN0(4,LOBES-4)
       ISTRT=5
       CALL PLTCAL (A,B,D,F,EPS,A1,BD,DX,DY,SEP,POW,SIGO,LOBE,ISTRT,JJ,
      1ST,SPH,IGRD,NTH)
       IF (LOBES.LE.8) GO TO 150
       CALL PLOT (0.,.2,2)
       LOBE=MIN0(2,LOBES-8)
       ISTRT=9
       CALL PLTCAL (A,B,D,F,EPS,A1,BD,DX,DY,SEP,POW,SIGO,LOBE,ISTRT,JJ,
      1ST,SPH,IGRD,NTH)
150    CONTINUE
155    CONTINUE
       GO TO 100
160    CALL PLOT (0.,.2,2)
       CALL PLOT (10.,0.,999)
       ENDFILE 4
       CALL EXIT
C
800    FORMAT (8F10.0)
810    FORMAT (I5,A2)
820    FORMAT (16I5)
830    FORMAT (A7)
900    FORMAT (1H1,46X,37HDUAL FREQUENCY ARRAY ELEMENT PATTERNS,///,
      15X,13HELEMENT DATA&,/,10X,5HF0 = ,F5.2,5X,6HEPS = ,F5.2,5X,4HA = ,
      2F5.3,5X,4HB = ,F5.3,/,10X,8HALPHA = ,F5.3,5X,7HBETA = ,F5.3,5X,
      38HDELTA = ,F5.3,5X,9HSEPTUM = ,F5.3,5X,14HALEN/LAMBDA = ,F5.3,/)
904    FORMAT (5X,18HVOLTAGE MODIFIERS&,/,10X,5HR1 = ,2F7.4,1HJ,5X,
      15HR2 = ,2F7.4,1HJ,/)
905    FORMAT (1H1,10X,7HCASE&  ,F4.2,2HF0,//,10X,4HF = ,F5.2,5X,
      16HEPS = ,F5.2,5X,4HA = ,F5.2,5X,4HB = ,F5.3,/,10X,8HALPHA = ,
      2F5.3,5X,7HBETA = ,F5.3,5X,8HDELTA = ,F5.3,5X,9HSEPTUM = ,F5.3,
      35X,7HALEN = ,F5.3,/)
910    FORMAT (5X,11HARRAY DATA&,/,10X,4HS1 =,F6.3,1H,,F5.3,5X,4HS2 =,
      1F6.3,1H,,F5.3)
915    FORMAT (10X,4HP1 =,I3,5X,4HQ1 =,I3,5X,8HNMODES =,I3,/,10X,
      124HALL DIMENSIONS IN INCHES,/)
920    FORMAT (1H1,5X,11HSIN(PHI) = ,F5.2,///,1X,7HSIN(TH),5X,3HPRU,5X,
      13HPRL,7X,3HIP0,2X,2HIM,3X,31HPOWER IN EXCITED BEAMS (DB) --A,//)
930    FORMAT (1H1,5X,11HSIN(PHI) = ,F5.2,///,1X,7HSIN(TH),5X,3HPR1,5X,
      13HPR2,7X,3HIP0,2X,2HIM,3X,31HPOWER IN EXCITED BEAMS (DB) --A,//)
940    FORMAT (2X,F5.2,4X,2(1X,F6.2,1X),3X,2(1X,I3,1X),10(1X,F6.2,1X))
950    FORMAT (/,5X,8HP,Q,R = ,26X,10(1X,I2,1H,,I2,1H,,I1))
960    FORMAT (//,5X,28HSPACE MODES NOT PRINTED ARE&,/,5X,8HP,Q,R = ,
      110(2(I2,1H,),I1,3X))
       END
**
```

```
      PROGRAM DESMOD (INPUT,OUTPUT,TAPF5=INPUT,TAPE6=OUTPUT,TAPE7)
C
C      COMPUTATION OF FIRST FOUR ROUTS OF SYMMETRIC AND ANTI-SYMMETRIC
C      LSE AND LSM MODE DISPERSION RELATIONS WITH M=0 FOR TWIN DIELECTRIC
C      SLAB LOADED RECTANGULAR WAVEGUIDE IN RANGE 1.LE.K*A/2.AND.
C      K*A/2.LE.4.
C
C      CREATES DATA FILE INPUT FOR PROGRAM DESGN.
C
      DIMENSION BB(16),G(16)
      REAL K(16),KA2
      COMMON /WAVGD/ A,B,D,B1,TPI,EPS
      DATA CPI,TPI/3.756964667,6.283185308/
C
C      INPUT>  A(ALPHA), B(BETA), AND D(DELTA), IN INCHES# GUIDE HEIGHT,
C      B1, IN INCHES# AND RELATIVE SLAB PERMITTIVITY, EPS.
C
100   READ (5,800) A,B,D,B1,EPS
      IF (EOF(5).NE.0) CALL EXIT
      AA=2.*(A+B+D)
      WRITE (6,910)
      WRITE (6,900) A,B,D,B1,EPS
      WRITE (7,900) A,B,D,B1,EPS
      EPSQ=SQRT(EPS-1.0)
      DO 110 I=1,16
      BB(I)=-EPSQ+1.E-10
110   CONTINUE
      KA2=.97
      DO 130 I=1,101
      KA2=KA2+0.03
      F=CPI*KA2/AA
      CALL FOURMDS (F,BB)
      DO 120 J=1,16
      K(J)=KA2*BB(J)
      T=KA2**2-K(J)*ABS(K(J))
      G(J)=SQRT(ABS(T))
      IF (T.LT.0.) G(J)=-G(J)
      BB(J)=BB(J)-1.0
      IF (BB(J).LT.-EPSQ) BB(J)=-EPSQ+1.E-10
120   CONTINUE
      WRITE (7,900) KA2
      WRITE (6,900) KA2
      WRITE (7,900) (K(J),J=1,16)
      WRITE (6,900) (G(J),J=1,16)
130   CONTINUE
      GO TO 100
C
800   FORMAT (8F10.0)
900   FORMAT (8F10.6)
910   FORMAT (1H1)
      END
```

```
      PROGRAM DESGN (INPUT,OUTPUT,TAPE5=INPUT,TAPE6=OUTPUT,TAPE10)
C
C      COMPUTATION OF BROADSIDE SCAN ELEMENT MISMATCH FOR INFINITE
C      ARRAY OF BIFURCATED TWIN DIELECTRIC SLAB LOADED RECTANGULAR
C      WAVEGUIDES   VS. K*A/2.  USE IN CONJUNCTION WITH PROGRAM DESMOD
C      WHICH CREATES TAPE10.
C
      DIMENSION NM(10),NE(10),T1(16),T(64),IMODE(2),PT(2),PTDB(2,101),
     1PR1(2),PR1DB(2),SS1(2),SS2(2)
      REAL K,KE,KA(101),M2B
      INTEGER P1,Q1,SYM(2)
      COMPLEX Y,YA,S11(20,20),S21(250,20)
      COMMON /ARRAY/ AL,BL,DL,B1L,SEPTL,TPI,EPS,S1(2),S2(2)
      COMMON /CNSRV/ Y(20),YA(250)
      COMMON /MODES/ K(20),KE(20),GAMMA(20),MODE1(20),ISYM(20),NN(20),
     1MM(20),MODORD(20)
      COMMON /PQ/ P1,Q1
      DATA TPI/6.2831853071796/
      DATA IMODE,SYM/3HLSM,3HLSE,1HA,1HS/
      IWRITE=0
C
C      INPUT>  SEPTUM THICKNESS, SEPT, IN INCHES*  AND LATTICE VECTORS
C      SS1 AND SS2 IN INCHES.
C
      READ (5,800) SEPT,SS1,SS2
C
C      INPUT>  NUMBER OF MODES FOR APERTURE FIELD APPROXIMATION*  AND
C      LIMITS OF SAMPLED GRATING LOBE SPACE, P1 AND Q1.
C
      READ (5,810) NMODES,P1,Q1
      MLO=1
      IF (SEPT.LT.1.E-10) MLO=2
      NO=NMODES+1
      NMODE=NMODES
100   READ (10,800) A,B,D,B1,EPS
      IF (EOF(10).NE.0) GO TO 190
      AA=2.*(A+B+D)
      WRITE (6,900) AA,B1,A,B,D,SEPT,EPS,NMODES,SS1,SS2,P1,Q1
      AP=2./(AA*TPI)
      WRITE (6,940)
      DO 180 IF=1,101
      READ (10,800) KA(IF)
      AP1=KA(IF)*AP
      AL=A*AP1
      BL=B*AP1
      DL=D*AP1
      B1L=B1*AP1
      M2B=(0.5/B1L)**2
      SEPTL=SEPT*AP1
      S1(1)=AP1*SS1(1)
      S1(2)=AP1*SS1(2)
      S2(1)=AP1*SS2(1)
      S2(2)=AP1*SS2(2)
      S12=S1(2)
      S22=S2(2)
      READ (10,800) (T1(I),I=1,16)
      IO=0
      DO 120 I=1,16
      T1(I)=T1(I)/KA(IF)
      MO=(I-1)/4+1
```

```
      M=-M0/3
      DO 110 J=1,4
      I0=I0+1
      M=M+1
      S=1.-M2B*M**2-T1(I)*ABS(T1(I))
      G=SQRT(ABS(S))
      IF (S.LT.0.) G=-G
      T(I0)=G
110   CONTINUE
120   CONTINUE
      J=1
130   X=-1.E+25
      DO 140 I=1,64
      IF (X.GT.T(I)) GO TO 140
      IA=1+(I-1)/16
      IB=(I-1-(IA-1)*16)/4+1
      IC=I-(IA-1)*16-(IB-1)*4
      ID=I
      X=T(I)
140   CONTINUE
      GAMMA(J)=X
      T(ID)=-1.E+30
      IE=4*(IA-1)+IB
      K(J)=T1(IE)
      G=EPS-1.+K(J)*ABS(K(J))
      S=SQRT(ABS(G))
      IF (G.LT.0.) S=-S
      KE(J)=S
      MODE=IA/3+1
      MODE1(J)=IMODE(MODE)
      MODE=MOD(IA,2)+1
      ISYM(J)=SYM(MODE)
      NM(IC)=NM(IC)+1-IA/3
      NE(IC)=NE(IC)+IA/3
      N2=(1-IA/3)*NM(IC)+(IA/3)*NE(IC)
      IC1=IC-IA/3
      NN(J)=N2
      MM(J)=IC1
      IF (IA.NE.3.OR.IC1.NE.0) GO TO 130
      ENCODE (10,910,MODORD(J)) MODE1(J),N2,IC1
      J=J+1
      IF (J.LE.NMODES) GO TO 130
      CALL NORM (NMODES,IWRITE)
      U=0.
      V=0.
      ISG=(3*P1+1)*(2*Q1+1)+Q1+1
      DO 170 ILO=MLO,MLU
      LOHI=2HLO
      IF (ILO.EQ.2) LOHI=2HHI
      IF (ILO.EQ.2) S1(2)=0.5*S12
      IF (ILO.EQ.2) S2(2)=0.5*S22
      CALL SCTMAT (LOHI,NMODE,U,V,S11,S21,NMOD,ISIG)
      IF (ILO.EQ.2) GO TO 150
      PT(ILO)=CABS(S21(ISG,1)+S21(ISG,N0))**2
      PT(ILO)=REAL(YA(ISG)/Y(1))*PT(ILO)
      IF (PT(ILO).LT.1.E-10) PT(ILO)=1.E-10
      PTDB(ILO,IF)=10.*ALOG10(PT(ILO))
      PR1(ILO)=0.5*CABS(S11(1,1)+S11(1,N0))**2
      IF (PR1(ILO).LT.1.E-10) PR1(ILO)=1.E-10
      PR1DB(ILO)=10.*ALOG10(PR1(ILO))
```

```
      PR2=0.5*CABS(S11(NO,1)+S11(NO,NO))**2
      IF (PR2.LT.1.E-10) PR2=1.E-10
      PR2DB=10.*ALOG10(PR2)
      GO TO 160
150   PT(ILO)=REAL(YA(ISG)/Y(1))*CABS(S21(ISG,1))**2
      PT(ILO)=2.*ABS(PT(ILO))
      IF (PT(ILO).LT.1.E-10) PT(ILO)=1.E-10
      PTDB(ILO,IF)=10.*ALOG10(PT(ILO))
      PR1(ILO)=CABS(S11(1,1))**2
      IF (PR1(ILO).LT.1.E-10) PR1(ILO)=1.E-10
      PR1DB(ILO)=10.*ALOG10(PR1(ILO))
160   CALL CONSRV (S11,S21,NMOD,ISIG,IM)
      IF (ILO.EQ.1) WRITE (6,950) KA(IF),LOHI,PT(ILO),PTDB(ILO,IF),
     1PR1DB(ILO),PR2DB,IM
      IF (ILO.EQ.2) WRITE (6,960) KA(IF),LOHI,PT(ILO),PTDB(ILO,IF),
     1PR1DB(ILO),IM
170   CONTINUE
180   CONTINUE
      GO TO 100
190   CALL EXIT
C
800   FORMAT (8F10.0)
810   FORMAT (16I5)
900   FORMAT (1H1,44X,42HDUAL FREQUENCY ARRAY ELEMENT DESIGN CURVES,
     1////,10X,13HELEMENT DATA&,/,15X,3HA =,F6.3,5X,3HB =,F6.3,5X,
     27HALPHA =,F6.3,5X,6HBETA =,F6.3,5X,7HDELTA =,F6.3,5X,
     38HSEPTUM =,F6.3,/,
     415X,5HEPS =,F5.2,5X,I2,6H MODES,//,10X,11HARRAY DATA&,/,
     515X,4HS1 =,F6.3,1H,,F5.3,5X,4HS2 =,F6.3,1H,,F5.3,5X,4HP1 =,I3,
     65X,4HQ1 =,I3,/,15X,24HALL DIMENSIONS IN INCHES)
910   FORMAT (A3,2I2.2)
930   FORMAT (2X,A7,3X,A6,2X,3F10.5,I4)
940   FORMAT (1H1,46X,38HPOWER TRANSMISSION FACTOR AT BROADSIDE,/,
     159X,12HVERSUS K*A/2,////,10H   K*A/2  ,10HEXCITATION,10H    PT
     2,10H  PT(DB)  ,10H  PR1(DB) ,10H  PR2(DB) ,10H    IM    ,/,
     310X,10H   TYPE   ,/)
950   FORMAT (3X,F5.2,6X,A2,4X,4(2X,F7.3,1X),I7)
960   FORMAT (3X,F5.2,6X,A2,4X,3(2X,F7.3,1X),10X,I7)
      END
**
```

D.2 Subroutine and Function Subprogram Listings

```
      SUBROUTINE LSMLSE (NMODES)
C
C       COMPUTE CHARACTERISTIC ROOTS OF DISPERSION RELATION FOR SYMMETRIC
C       INHOMOGENEOUSLY LOADED RECTANGULAR GUIDE.
C
C              DEFINITIONS&
C                     B         =    GUIDE NARROW DIMENSION DIVIDED BY
C                                    FREE SPACE WAVELENGTH
C                     EPS       =    RELATIVE DIELECTRIC CONSTANT OF
C                                    LOADING
C                     AL        =    DISTANCE FROM GUIDE WALL TO NEAREST
C                                    EDGE OF LOADING SLAB #WAVELENGTHS≠
C                     BL        =    DISTANCE FROM SLAB EDGE TO SYMMETRY
C                                    PLANE #WAVELENGTHS≠
C                     DL        =    SLAB THICKNESS #WAVELENGTHS≠
C                     SEPTL     =    SEPTUM THICKNESS WITH RESPECT TO FREE
C                                    SPACE WAVELENGTH
C                     TPI       =    6.2831.........
C                     S1        =    FIRST LATTICE VECTOR
C                     S2        =    SECOND LATTICE VECTOR
C                     K         =    X-DIRECTED WAVENUMBER IN AIR REGION OF
C                                    GUIDE WITH RESPECT TO FREE SPACE
C                                    WAVENUMBER
C                     KE        =    X-DIRECTED WAVENUMBER IN DIELECTRIC
C                                    REGION OF GUIDE WITH RESPECT TO FREE
C                                    SPACE WAVENUMBER
C                     GAMMA     =    LONGITUDINAL WAVENUMBER NORMALIZED TO
C                                    FREE SPACE WAVENUMBER --- ORDERED BY
C                                    INCREASING CUT-OFF FREQUENCY
C                     MODE1     =    MODE TYPE (I.E., LSE OR LSM)
C                     ISYM      =    SYMMETRY (I.E., S OR A)
C                     NN        =    X ORDERING PARAMETER
C                     MM        =    Y ORDERING PARAMETER
C                     MODORD    =    VECTOR CONTAINING MODE DESIGNATIONS --
C                                    ORDERED BY INCREASING CUT-OFF
C                                    FREQUENCY
C
C*********************************************************************
      DIMENSION GAM(4,10,11),IMODE(421),SO(4,10,11),SE(4,10,11),NM(11),
     1NE(11)
      REAL KAP,KAPE,M2B,K,KE,KINC
      COMMON /ARRAY/ AL,BL,DL,B,SEPTL,TPI,EPS,S1(2),S2(2)
      COMMON /MODES/ K(20),KE(20),GAMMA(20),MODE1(20),ISYM(20),NN(20),
     1MM(20),MODORD(20)
      A1=TPI*AL
      B1=TPI*BL
      D1=TPI*DL
      EPS1=EPS-1.
      EPSQ=SQRT(EPS1)
      M2B=(0.5/B)**2
C
C       COMPUTE K FOR M=0
C
      DO 180 MODE=1,4
      M4=1HS
      IF ((MODE/2)*2.EQ.MODE) M4=1HA
      M1=3HLSM
      IF (MODE.GT.2) M1=3HLSE
      M2=10
      IF (MODE.GT.2) M2=11
```

```
      M3=MODE/3
      KAP=-EPSQ+1.E-10
      MO=1
      M=MO-M3
      DO 160 N=1,11
      J=1/N
      S=1.01
      IF (KAP.LT.0.) S=0.99
      KAP=J*KAP+(1-J)*S*KAP
      KINC=0.314
      KAP=KAP-KINC
      I=0
100   KAP=KAP+KINC
      DIFF=DIFF1
      I=I+1
      KAPE=EPS1+KAP*ABS(KAP)
      S=SQRT(ABS(KAPE))
      IF (KAPE.LT.0.) S=-S
      KAPE=S
      DIFF1=DISP(MODE,KAP,KAPE,A1,B1,D1,EPS)
      IF (I.EQ.1) GO TO 120
      IF (KINC.LT.1.E-10) GO TO 130
      IF (ABS(DIFF*DIFF1).LE.1.E-10) GO TO 130
      IF (DIFF*DIFF1) 110,130,100
110   KAP=KAP-KINC
      KINC=0.5*KINC
      DIFF1=DIFF
      GO TO 100
120   DIFF=DIFF1
      GO TO 100
130   IF (ABS(DIFF).LT.ABS(DIFF1)) GO TO 140
      GO TO 150
140   KAP=KAP-KINC
      KAPE=EPS1+KAP*ABS(KAP)
      S=SQRT(ABS(KAPE))
      IF (KAPE.LT.0.) S=-S
      KAPE=S
150   SO(MODE,N,MO)=KAP
      SE(MODE,N,MO)=KAPE
      G=1.-M2B*M-ABS(KAP)*KAP
      S=SQRT(ABS(G))
      IF (G.LT.0.) S=-S
      GAM(MODE,N,MO)=S
160   CONTINUE
180   CONTINUE
C
C      INCLUDE Y (I.E., M) DEPENDENCE
C
      DO 183 MODE=1,4
      M3=MODE/3
      M2=10+M3
      DO 182 N=1,10
      KAP=SO(MODE,N,1)
      KAPE=SE(MODE,N,1)
      DO 181 MO=2,M2
      SO(MODE,N,MO)=KAP
      SE(MODE,N,MO)=KAPE
      M=(MO-M3)**2
      BML=M2B*M
      G2=-KAP*ABS(KAP)+1.0-BML
```

```
      GAM(MODE,N,M0)=SQRT(ABS(G2))
      IF (G2.LT.0.) GAM(MODE,N,M0)=-GAM(MODE,N,M0)
181   CONTINUE
182   CONTINUE
183   CONTINUE
      WRITE (6,900)
      DO 185 I=1,11
      NM(I)=0
      NE(I)=0
185   CONTINUE
      I=1
190   GAMMA(I)=-1.E+30
      DO 220 MODE=1,4
      M4=1HS
      IF ((MODE/2)*2.EQ.MODE) M4=1HA
      M1=3HLSM
      IF (MODE.GT.2) M1=3HLSE
      M2=10
      IF (MODE.GT.2) M2=11
      M3=MODE/3
      DO 210 M0=1,M2
      M=M0-M3
      DO 200 N=1,10
      IF (GAMMA(I).GT.GAM(MODE,N,M0)) GO TO 200
      GAMMA(I)=GAM(MODE,N,M0)
      ENCODE (10,910,IMODE(I)) M1,M4,N,M
      IA=MODE
      IB=N
      IC=M0
200   CONTINUE
210   CONTINUE
220   CONTINUE
C
C       ORDER MODES
C
      GAM(IA,IB,IC)=-1.E+38
      K(I)=SO(IA,IB,IC)
      KE(I)=SE(IA,IB,IC)
      M1=3HLSM
      IF (IA.GT.2) M1=3HLSE
      IF (IA.LT.3) NM(IC)=NM(IC)+1
      IF (IA.GT.2) NE(IC)=NE(IC)+1
      N2=NM(IC)
      IF (IA.GT.2) N2=NE(IC)
      IC1=IC-IA/3
      MODE1(I)=M1
      NN(I)=N2
      MM(I)=IC1
      ISYM(I)=1HS
      IF ((IA/2)*2.EQ.IA) ISYM(I)=1HA
      ENCODE (10,940,MODORD(I)) M1,N2,IC1
      WRITE (6,920) IMODE(I),MODORD(I),GAMMA(I),I
      I=I+1
      IF (I.LE.NMODES) GO TO 190
      SEC=SECOND(X)
      WRITE (6,930) SEC
      RETURN
C
900   FORMAT (1H1)
910   FORMAT (A3,A1,2I2.2)
```

```
920   FORMAT (5X,A8,5X,A7,5X,F10.5,5X,I5)
930   FORMAT (5X,F20.3, 8H SECONDS)
940   FORMAT (A3,2I2,2)
      END
••
```

```
      FUNCTION DISP(M,K,KE,A,B,D,ER)
C
C      COMPUTE DISPERSION RELATION D(K,KE) FOR ARBITRARY K AND KE
C
C            DEFINITIONS>
C                  M          =    MODE FUNCTION DESIGNATION = SEE CODE
C                  K          =    X=DIRECTED WAVENUMBER IN AIR REGION
C                                  WRT KO
C                  KE         =    X=DIRECTED WAVENUMBER IN DIELECTRIC
C                                  REGION WRT KO
C                  A          =    ALPHA/LAMBDAO
C                  B          =    BETA/LAMBDAO
C                  D          =    DELTA/LAMBDAO
C                  ER         =    RELATIVE PERMITTIVITY OF SLABS
C
C*************************************************************************
      REAL K,KE
      SA=SINC(K*A)
      CA=COSC(K*A)
      SB=SINC(K*B)
      CB=COSC(K*B)
      SD=SINC(KE*D)
      CD=COSC(KE*D)
      SKA=SXOX(K*A)*A
      SKB=SXOX(K*B)*B
      SKE=SXOX(KE*D)*D
      S1=SIGN(1.,K)
      S2=SIGN(1.,KE)
      GO TO (100,110,120,130), M
C
C      LSM SYMMETRIC MODES
C
100   DISP=ER*K*SA*S1*(CB*CD-ER*K*SB*S1*SKE)
      DISP=DISP+CA*(ER*K*SB*S1*CD+KE*SD*S2*CB)
      RETURN
C
C      LSM ANTI-SYMMETRIC MODES
C
110   DISP=ER*SA*S1*(SB*CD+ER*K*SKE*CB)+CA*(KE*SD*S2*SKB-ER*CD*CB)
      RETURN
C
C      LSE SYMMETRIC MODES
C
120   DISP=SKA*(KE*SD*S2*CB+K*SB*S1*CD)+CA*(K*SB*S1*SKE-CB*CD)
      RETURN
C
C      LSE ANTI-SYMMETRIC MODES
C
130   DISP=SKA*(CB*CD-KE*SKB*SD*S2)+CA*(SKB*CD+SKE*CB)
      RETURN
      END
**
```

```
      SUBROUTINE NORM (NMODES,IWRITE)
C
C      SUBROUTINE NORM COMPUTES THE FEEDGUIDE MODE NORMALIZATIONS, AND
C      VALUES FOR THE COEFFICIENTS APPEARING IN THE EXPRESSIONS FOR VHAT
C      AND IHAT *FOR WHICH SEE DOCUMENTATION*.
C
C      NOTE&  THE COEFFICIENTS B2P,E1P,E2P,FP,B2DP,CDP,E1DP,E2DP MAY BE
C      REAL OR IMAGINARY *NOT COMPLEX*.  ALL OTHER COEFFICIENTS ARE
C      ALWAYS REAL.  ALSO, NORMALIZATIONS CARRY AN ADDITIONAL 1/LAMBDA
C      DEPENDENCE WHICH CANCELS IN SCATTERING MATRIX COMPUTATIONS, BUT
C      NOT IN MODE FUNCTION COMPUTATUIONS.
C
C
C             DEFINITIONS>  SEE SUBROUTINE LSMLSE
C
C             SUFFIXES>
C                   P          =     PRIME (LSM MODES)
C                   DP         =     DOUBLE PRIME (LSE MODES)
C                   S          =     SYMMETRIC
C                   A          =     ANTI=SYMMETRIC
C***********************************************************************
      REAL KAP,KAPE,K,KE,NPS,NPA,NDPS,NDPA
      COMMON /ARRAY/ AL,BL,DL,B1L,SEPTL,TPI,EPS,SS1(2),SS2(2)
      COMMON /COEFS/ B1P(10),B2P(10),B1DP(10),B2DP(10),CP(10),CDP(10),
     1E1P(10),E2P(10),E1DP(10),E2DP(10),FP(10),FDP(10),NPS(10),NPA(10),
     2NDPS(10),NDPA(10),KOUNT(20)
      COMMON /MODES/ KAP(20),KAPE(20),GAM(20),MODE1(20),ISYM1(20),
     1NN(20),MM(20),MODORD(20)
      A=TPI*AL
      B=TPI*BL
      D=TPI*DL
      IF (IWRITE.EQ.1) WRITE (6,900)
      ILSMS=0
      ILSMA=0
      ILSES=0
      ILSEA=0
      DO 140 I=1,NMODES
      K=KAP(I)
      KE=KAPE(I)
      AK=K*A
      BK=K*B
      DKE=D*KE
      MODE=MODE1(I)
      ISYM=ISYM1(I)
      M=MM(I)
      IF (MODE.EQ.3HLSE) GO TO 110
C
C      LSM MODES
C
      IF (ISYM.EQ.1HA) GO TO 100
C
C      SYMMETRIC
C
      ILSMS=ILSMS+1
      KOUNT(I)=ILSMS
      B1P(ILSMS)=COSC(BK)
      B2P(ILSMS)=EPS*K*SINC(BK)/KE
      B2P(ILSMS)=B2P(ILSMS)*SIGN(1.,K)*SIGN(1.,KE)
      CP(ILSMS)=-SINC(BK)*(COSC(DKE)+COSC(BK)*SINC(DKE)/B2P(ILSMS))
      CP(ILSMS)=CP(ILSMS)/SINC(AK)
```

```
      ANORM=0.5*B1L*(BL*S1(2.*BK)+(DL*S1(2.*DKE)*B1P(ILSMS)**2+DL*S2(2.*
     1DKE)*SIGN(1.,KE)*B2P(ILSMS)**2)/EPS
     2-2.0*B1P(ILSMS)*B2P(ILSMS)*DL*S3(DKE)*SIGN(1.,KE)/EPS
     3+AL*S1(2.*AK)*CP(ILSMS)**2)
      NPS(ILSMS)=SQRT(ABS(ANORM))
      GO TO 130
C
C       ANTI-SYMMETRIC
C
100   ILSMA=ILSMA+1
      KOUNT(I)=ILSMA
      BL=BL*SIGN(1.,K)
      E1P(ILSMA)=SINC(BK)
      E2P(ILSMA)=-EPS*K*COSC(BK)/KE
      FP(ILSMA)=COSC(BK)*(COSC(DKE)-KE*TANT(BK)*SINC(DKE)*SIGN(1.,KE)/
     1(EPS*K))*SIGN(1.,K)/SINC(AK)
      F=E1P(ILSMA)*E2P(ILSMA)
      ANORM=0.5*B1L*(BL*S2(2.*BK)+DL*(S1(2.*DKE)*E1P(ILSMA)**2+
     1(S2(2.*DKE)*E2P(ILSMA)**2-2.*F*S3(DKE))*SIGN(1.,KE))/EPS+
     2AL*S1(2.*AK)*FP(ILSMA)**2)
      NPA(ILSMA)=SQRT(ABS(ANORM))
      BL=BL*SIGN(1.,K)
      GO TO 130
C
C       LSE MODES
C
110   RM=1.0
      IF (M.EQ.0) RM=2.0
      IF (ISYM.EQ.1HA) GO TO 120
C
C       SYMMETRIC
C
      ILSES=ILSES+1
      KOUNT(I)=ILSES
      B1DP(ILSES)=COSC(BK)
      B2DP(ILSES)=K*SINC(BK)*SIGN(1.,K)*SIGN(1.,KE)/KE
      CDP(ILSES)=COSC(BK)*(COSC(DKE)-K*TANT(BK)*SINC(DKE)*SIGN(1.,K)/KE)
     1*SIGN(1.,K)/SINC(AK)
      ANORM=0.5*RM*B1L*(BL*S1(2.*BK)+DL*(S1(2.*DKE)*B1DP(ILSES)**2+
     1SIGN(1.,KE)*(S2(2.*DKE)*B2DP(ILSES)**2-2.*B1DP(ILSES)*
     2B2DP(ILSES)*S3(DKE)))+AL*S2(2.*AK)*SIGN(1.,K)*CDP(ILSES)**2)
      NDPS(ILSES)=SQRT(ABS(ANORM))
      GO TO 130
C
C       ANTI-SYMMETRIC
C
120   ILSEA=ILSEA+1
      AL=AL*SIGN(1.,K)
      BL=BL*SIGN(1.,K)
      KOUNT(I)=ILSEA
      E1DP(ILSEA)=-SINC(BK)
      E2DP(ILSEA)=K*COSC(BK)/KE
      FDP(ILSEA)=-SINC(BK)*(COSC(DKE)+K*SINC(DKE)/(KE*TANT(BK)))/SINC(AK
     1)
      F=E1DP(ILSEA)*E2DP(ILSEA)
      ANORM=0.5*RM*B1L*(BL*S2(2.*BK)+DL*(S1(2.*DKE)*E1DP(ILSEA)**2+
     1SIGN(1.,KE)*((S2(2.*DKE)*E2DP(ILSEA)**2-2.0*F*S3(DKE))))+
     2AL*S2(2.*AK)*FDP(ILSEA)**2)
      NDPA(ILSEA)=SQRT(ABS(ANORM))
      AL=AL*SIGN(1.,K)
```

```
      BL=BL*SIGN(1.,K)
130   IF (IWRITE.EQ.0) GO TO 140
      WRITE (6,910) I,K,KE,GAM(I),MODORD(I),ANORM
140   CONTINUE
      RETURN
C
900   FORMAT (1H1,5H  I  ,10H     K    ,10H    KE    ,10H    GAM
     110H   MODE   ,10H  NORM**2 ,//)
910   FORMAT (1X,I3,1X,3F10.5,2X,A7,1X,F10.5)
      END
**
```

```
      SUBROUTINE SCTMAT (LOHI,NMODES,U0,V0,S11,S21,NMOD,SIG1)
C
C      SCTMAT COMPUTES THE FEEDGUIDE - FREE SPACE SCATTERING MATRIX
C      BLOCKS S11 AND S21 FOR AN INFINITE RECTANGULAR GRID ARRAY OF
C      TWIN DIELCTRIC SLAB LOADED RECTANGULAR WAVEGUIDES.
C      LATTICE VECTORS S1 AND S2
C
C      LOHI SPECIFIES WHICH FREQUENCY BAND ,LOHI=2HLO FOR LOW FREQUENCY
C      BAND# LOHI=2HHI FOR HIGH FREQUENCY BAND#.
C
C      NOTE&  IF THE SEPTUM THICKNESS IS NOT EQUAL TO THE WALL THICKNESS
C      LOHI=2HLO, AND THE HIGH AND LOW FREQUENCY UNIT CELLS ARE
C      IDENTICAL.
C
C
C             DEFINITIONS>
C                    LOHI        -     =2HLO, FOR TRIANGULAR GRID OR THICK
C                                      SEPTUM# =2HHI, FOR THIN SEPTUM, HIGH
C                                      FREQUENCY BAND, AND RECTANGULAR GRID
C                    NMODES      -     NUMBER OF FEEDGUIDE MODES USED TO
C                                      APPROXIMATE APERTURE FIELD
C                    U0          -     SIN(THETA)*COS(PHI)
C                    V0          -     SIN(THETA)*SIN(PHI)
C                    S11         -     FEEDGUIDE SELF REFLECTION SCATTERING
C                                      BLOCK
C                    S21         -     FEEDGUIDE TO SPACE MODE VOLTAGE
C                                      TRANSMISSION COEFFICIENT
C                    NMOD        -     NUMBER OF FEEDGUIDE MODES IN UNIT CELL
C                    SIG1        -     NUMBER OF SPACE MODES = 2*P1*Q1
C                    Y           -     FEEDGUIDE MODE ADMITTANCE
C                    YA          -     SPACE MODE ADMITTANCE
C                    *** FOR OTHER DEFINITIONS SEE SUB LSMLSE ***
C
C             SUFFIXES>  SEE SUBROUTINE NORM
C***********************************************************************
      DIMENSION AM(20)
      REAL KAP,KAPE,K,KE,NPS,NPA,NDPS,NDPA,KZ1,KT(250),KX(250),KY(250)
      COMPLEX KZ,AJ,COEFM(250),ESN(250,20),S11(20,20),Y,YA,EXPB1(250),
     1S21(250,20),EXPB(250),TRIP(20,20),INTGRL
      INTEGER P,Q,P1,Q1,SIG,SIG1,SIG2
      COMMON /ARRAY/ AL,BL,DL,BIL,SEPTL,TPI,EPS,S1(2),S2(2)
      COMMON /CNSRV/ Y(20),YA(250)
      COMMON /COEFS/ B1P(10),B2P(10),B1DP(10),B2DP(10),CP(10),CDP(10),
     1E1P(10),E2P(10),E1DP(10),E2DP(10),FP(10),FDP(10),NPS(10),NPA(10),
     2NDPS(10),NDPA(10),KOUNT(20)
      COMMON /COSSIN/ SKAPAL(20),CKAPAL(20),SKAPB(20),CKAPB(20),
     1SKAPD(20),CKAPD(20),SKXAL(250),CKXAL(250),SKXA(250),CKXA(250),
     2SKXB(250),CKXB(250),SKXD(250),CKXD(250)
      COMMON /MODES/ KAP(20),KAPE(20),GAM(20),MODE(20),ISYM(20),NN(20),
     1MM(20),MODORD(20)
      COMMON /PQ/ P,Q
      DATA AJ/(0.,1.)/
100   A=TPI*AL
      B=TPI*BL
      D=TPI*DL
      BB=TPI*BIL
      SEP=TPI*SEPTL
      EPSQ=1./TPI**2
      P1=2*P+1
      Q1=2*Q+1
```

```
      SIG1=2*P1*Q1
      SIG2=SIG1/2
      NMOD=NMODES
      IF (LOHI.EQ.2HLO) NMOD=2*NMODES
      DO 110 N=1,NMODES
      KE=KAPE(N)*D
      W=KAP(N)*A
      X=KAP(N)*B
      AM(N)=0.5*MM(N)/B1L
      T=GAM(N)/(1.-KAP(N)*ABS(KAP(N)))
      Y(N)=CMPLX(T,0.)
      IF (GAM(N).LT.0.) Y(N)=CMPLX(0.,T)
      IF (MODE(N).EQ.3HLSE) Y(N)=1./Y(N)
      SKAPAL(N)=SINC(W)
      CKAPAL(N)=COSC(W)
      SKAPB(N)=SINC(X)
      CKAPB(N)=COSC(X)
      SKAPD(N)=SINC(KE)
      CKAPD(N)=COSC(KE)
      IF (LOHI.EQ.2HHI) GO TO 110
      Y(N+NMODES)=Y(N)
110   CONTINUE
C
C      COMPUTE INVERSE LATTICE
C
      T=S1(1)*S2(2)-S2(1)*S1(2)
      CELLA=1./SQRT(ABS(T))
      T=1./T
      T1X=T*S2(2)
      T2X=-T*S1(2)
      T1Y=-T*S2(1)
      T2Y=T*S1(1)
      SIG=0
C
C      COMPUTE FREE SPACE WAVE NUMBERS AND WAVE ADMITTANCES
C
      DO 130 L=1,2
      L1=2-L
      RL1=L1
      L1=L-1
      RL2=L1
      DO 130 J1=1,P1
      J=J1-P-1
      U=U0+J*T1X
      V=V0+J*T1Y
      DO 130 K1=1,Q1
      SIG=SIG+1
      K=K1-Q-1
      KX(SIG)=U+K*T2X
      KY(SIG)=V+K*T2Y
      KZ1=1.-KX(SIG)**2-KY(SIG)**2
      AA=SQRT(ABS(KZ1))
      KZ=CMPLX(AA,0.)
      IF (KZ1.LT.0.) KZ=CMPLX(0.,-AA)
      KT(SIG)=SQRT(ABS(1.-KZ1))
      IF (AA.LT.1.E-10) GO TO 120
      YA(SIG)=RL1/KZ+RL2*KZ
      GO TO 130
120   YA(SIG)=RL2*KZ
130   CONTINUE
```

```
C
C       COMPUTE SINES AND COSINES OF KX*(ELEMENT DIMENSIONS)
C
      DO 140 SIG=1,SIG1
      T=KX(SIG)*A
      SKXAL(SIG)=SIN(T)
      CKXAL(SIG)=COS(T)
      T=KX(SIG)*D
      SKXD(SIG)=SIN(T)
      CKXD(SIG)=COS(T)
      T=KX(SIG)*B
      SKXB(SIG)=SIN(T)
      CKXB(SIG)=COS(T)
      T=KX(SIG)*(A+B+D)
      SKXA(SIG)=SIN(T)
      CKXA(SIG)=COS(T)
      T=KY(SIG)*BB
      EXPB1(SIG)=CEXP(AJ*T)
      T=KY(SIG)*(BB+SEP)
      EXPB(SIG)=CEXP(AJ*T)
140   CONTINUE
C
C       COMPUTE COUPLING COEFFICIENTS, ESN(SIG,N)
C
      DO 180 N=1,NMODES
      T=AM(N)**2
      T2=AM(N)
      IF (MM(N).EQ.0) T2=1.0
      DO 160 SIG=1,SIG1
      T1=ABS(KY(SIG))
      IF (ABS(T-T1**2).LT.1.E-10) GO TO 150
      COEFM(SIG)=(1.-EXPB1(SIG)*(-1.)**MM(N))*T2/(T-T1**2)
      IF (MODE(N).EQ.3HLSE) COEFM(SIG)=COEFM(SIG)*KY(SIG)/T2
      GO TO 155
150   COEFM(SIG)=0.5*AJ*BB
      IF (MM(N).EQ.0) COEFM(SIG)=2.*COEFM(SIG)
      IF (MODE(N).EQ.3HLSM) COEFM(SIG)=COEFM(SIG)*SIGN(1.,KY(SIG))
155   COEFM(SIG)=COEFM(SIG)*CELLA
160   CONTINUE
      DO 170 SIG=1,SIG1
      LR=1
      IF (SIG.GT.SIG2) LR=2
      ESN(SIG,N)=INTGRL(KX(SIG),KY(SIG),KT(SIG),LR,SIG,N)
      ESN(SIG,N)=FPSQ*COEFM(SIG)*ESN(SIG,N)
      IF (LOHI.EQ.2HHI) GO TO 170
      ESN(SIG,N+NMODES)=CONJG(EXPB(SIG))*ESN(SIG,N)
170   CONTINUE
180   CONTINUE
C
C       FORM SCATTERING MATRIX BLOCKS S11 AND S21
C
C
C       FORM MATRIX TRIPLE PRODUCT
C            MAT(TRIP)=MAT(CONJG(ESN))*MAT(YA)*MAT(ESN)
C       AND MATRIX FOR INVERSION,
C                      DIAG(Y)+MAT(TRIP)
C
      DO 210 IA=1,NMOD
      DO 200 IB=1,NMOD
      TRIP(IA,IB)=(0.,0.)
```

```
      S11(IA,IB)=(0.,0.)
      IF (IA.EQ.IB) S11(IA,IB)=2.*Y(IA)
      DO 190 SIG=1,SIG1
      TRIP(IA,IB)=TRIP(IA,IB)+CONJG(ESN(SIG,IA))*YA(SIG)*ESN(SIG,IB)
190   CONTINUE
200   CONTINUE
210   CONTINUE
      DO 220 IA=1,NMOD
      TRIP(IA,IA)=Y(IA)+TRIP(IA,IA)
220   CONTINUE
C
C      CSIMEQ RETURNS MAT(S11+DEL(I,J)) WHERE DEL(I,J) IS THE KRONECKER
C      DELTA FUNCTION
C
      CALL CSIMEQ (TRIP,NMOD,S11,NMOD,KS)
C
C      SOLVE
C                 MAT(S21)=MAT(ESN)*MAT(S11+DEL(I,J))
C
      DO 250 SIG=1,SIG1
      DO 240 IB=1,NMOD
      S21(SIG,IB)=(0.,0.)
      DO 230 IA=1,NMOD
      S21(SIG,IB)=S21(SIG,IB)+ESN(SIG,IA)*S11(IA,IB)
230   CONTINUE
240   CONTINUE
250   CONTINUE
C
C      SOLVE
C                       MAT(S11)=MAT(S11+DEL(I,J))
C
      DO 260 IA=1,NMOD
      S11(IA,IA)=S11(IA,IA)-1.0
260   CONTINUE
      RETURN
      END
**
```

```
      COMPLEX FUNCTION INTGRL (KX,KY,KT,LR,SIG,N)
C
C      FUNCTION INTGRL COMPUTES THE INTEGRAL (IN X) PORTION OF THE
C      COUPLING COEFFICIENTS, ESN(SIG,N)
C
C      NOTE>  MNEMONICS ARE CHOSEN TO COINCIDE WITH NOTATION IN REPORT
C
C             DEFINITIONS>
C                    KX        -      X-DIRECTED WAVENUMBER OF LOBE WRT KO
C                    KY        -      Y-DIRECTED WAVENUMBER OF LOBE WRT KO
C                    KT        -      TRANSVERSE WAVENUMBER OF LOBE WRT KO
C                    LR        -      =1, FOR E-MODES= =2, FOR H-MODES
C                    SIG       -      NUMBER OF GRATING LOBE IN INTERNAL
C                                     ORDERING
C                    N         -      NUMBER OF APERTURE MODE IN INTERNAL
C                                     ORDERING
C                    *** FOR OTHER DEFINITIONS SEE SUB LSMLSE ***
C
C             SUFFIXES>  SEE SUBROUTINE NORM
C*************************************************************************
      COMPLEX R1,R2,R3,R4,R5,R6,R7,R8,R9,R10,AJ,Z1,Z2,Z3,Z4,Z5,Z6,TT,TU,
     1TV,TU1,TV1,I1P,I2P
      REAL KX,KY,KT,K,KE,NPS,NPA,NDPS,NDPA,KAP,KAPE
      INTEGER SIG
      COMMON /ARRAY/ AL,BL,DL,B1L,SEPTL,TPT,EPS,S1(2),S2(2)
      COMMON /COEFS/ B1P(10),B2P(10),B1DP(10),B2DP(10),CP(10),CDP(10),
     1E1P(10),E2P(10),E1DP(10),E2DP(10),FP(10),FDP(10),NPS(10),NPA(10),
     2NDPS(10),NDPA(10),KOUNT(20)
      COMMON /COSSIN/ SKAPAL(20),CKAPAL(20),SKAPB(20),CKAPB(20),
     1SKAPD(20),CKAPD(20),SKXAL(250),CKXAL(250),SKXA(250),CKXA(250),
     2SKXB(250),CKXB(250),SKXD(250),CKXD(250)
      COMMON /MODES/ KAP(20),KAPE(20),GAM(20),MODE1(20),ISYM1(20),
     1NN(20),MM(20),MODORD(20)
      EQUIVALENCE (R1,A1),(R2,A2),(R3,A3),(R4,A4),(R5,A5),(R6,A6),
     1(R7,A7),(R8,A8),(R9,A9),(R10,A10),(Z1,B1),(Z2,B2),(Z3,B3),(Z4,B4),
     2(Z5,B5),(Z6,B6)
      DATA AJ/(0.,1.)/
      DATA SQR2/1.41421356237309/
C
C      INITIALIZE TEMPORARY STORAGE
C
      R1=(0.,0.)
      R2=(0.,0.)
      R3=(0.,0.)
      R4=(0.,0.)
      R5=(0.,0.)
      R6=(0.,0.)
      R7=(0.,0.)
      R8=(0.,0.)
      R9=(0.,0.)
      R10=(0.,0.)
      Z1=(0.,0.)
      Z2=(0.,0.)
      Z3=(0.,0.)
      Z4=(0.,0.)
      Z5=(0.,0.)
      Z6=(0.,0.)
      M=KOUNT(N)
      K=KAP(N)
      KE=KAPE(N)
```

```
      MODE=MODE1(N)
      ISYM=ISYM1(N)
      ALR=LR
      ALR=1.5-ALR
      IKT=0
      IF (KT.LT.1.E-10) IKT=1
C
C      COMPUTE TERMS COMMON TO ALL INTEGRALS
C
C      KAP IMAGINARY
C
      IF (K.GT.0.) GO TO 100
      TU=AJ*K/(1.-K*ABS(K))
      TU1=AJ
      R1=(SKXB(SIG)*CKAPB(N)+AJ*SKAPB(N)*CKXB(SIG))/(KX+AJ*K)
      R2=(SKXB(SIG)*CKAPB(N)-AJ*SKAPB(N)*CKXB(SIG))/(KX-AJ*K)
      R7=(CKXAL(SIG)*CKAPAL(N)+AJ*SKXAL(SIG)*SKAPAL(N))/(KX-AJ*K)
      R8=(CKXAL(SIG)*CKAPAL(N)-AJ*SKXAL(SIG)*SKAPAL(N))/(KX+AJ*K)
      R9=(SKXAL(SIG)*CKAPAL(N)-AJ*SKAPAL(N)*CKXAL(SIG))/(KX-AJ*K)
      R10=(SKXAL(SIG)*CKAPAL(N)+AJ*SKAPAL(N)*CKXAL(SIG))/(KX+AJ*K)
C
C      KAPE TERMS
C
100   T=ABS(KX)
      TV=KE/(EPS-KE**2)
      TV1=(1.0,0.)
      IF (ABS(T-KE).GT.1.E-15) GO TO 110
      R3=(1.E+27,0.)
      IF (KX.LT.0.) A3=(CKXD(SIG)*CKAPD(N)+SKXD(SIG)*SKAPD(N))/(KX-KE)
      R4=(1.E+27,0.)
      IF (KX.GT.0.) A4=(CKXD(SIG)*CKAPD(N)-SKXD(SIG)*SKAPD(N))/(KX+KE)
      A5=TPI*DL
      IF (KX.LT.0.) A5=(SKXD(SIG)*CKAPD(N)-CKXD(SIG)*SKAPD(N))/(KX-KE)
      A6=TPI*DL
      IF (KX.GT.0.) A6=(SKXD(SIG)*CKAPD(N)+CKXD(SIG)*SKAPD(N))/(KX+KE)
      GO TO 120
110   A3=(CKXD(SIG)*CKAPD(N)+SKXD(SIG)*SKAPD(N))/(KX-KE)
      A4=(CKXD(SIG)*CKAPD(N)-SKXD(SIG)*SKAPD(N))/(KX+KE)
      A5=(SKXD(SIG)*CKAPD(N)-CKXD(SIG)*SKAPD(N))/(KX-KE)
      A6=(SKXD(SIG)*CKAPD(N)+CKXD(SIG)*SKAPD(N))/(KX+KE)
C
C      KAP REAL
C
120   IF (K.LT.0.) GO TO 140
      TU=K/(1.-K**2)
      TU1=(1.0,0.)
      IF (ABS(T-K).GT.1.E-15) GO TO 130
      A1=TPI*BL
      IF (KX.GT.0.) A1=(SKXB(SIG)*CKAPB(N)+SKAPB(N)*CKXB(SIG))/(KX+K)
      A2=TPI*BL
      IF (KX.GT.0.) A2=(SKXB(SIG)*CKAPB(N)-SKAPB(N)*CKXB(SIG))/(KX-K)
      R7=(1.E+27,0.)
      IF (KX.LT.0.) A7=(CKXAL(SIG)*CKAPAL(N)+SKXAL(SIG)*SKAPAL(N))/(KX-K
     1)
      R8=(1.E+27,0.)
      IF (KX.GT.0.) A8=(CKXAL(SIG)*CKAPAL(N)-SKXAL(SIG)*SKAPAL(N))/(KX+K
     1)
      A9=TPI*AL
      IF (KX.LT.0.) A9=(SKXAL(SIG)*CKAPAL(N)-CKXAL(SIG)*SKAPAL(N))/(KX-K
     1)
```

```
      A10=TPI*AL
      IF (KX.GT.0.) A10=(SKXAL(SIG)*CKAPAL(N)+CKXAL(SIG)*SKAPAL(N))/(KX+
     1K)
      GO TO 140
130   A1=(SKXB(SIG)*CKAPB(N)+SKAPB(N)*CKXB(SIG))/(KX+K)
      A2=(SKXB(SIG)*CKAPB(N)-SKAPB(N)*CKXB(SIG))/(KX-K)
      A7=(CKXAL(SIG)*CKAPAL(N)+SKXAL(SIG)*SKAPAL(N))/(KX-K)
      A8=(CKXAL(SIG)*CKAPAL(N)-SKXAL(SIG)*SKAPAL(N))/(KX+K)
      A9=(SKXAL(SIG)*CKAPAL(N)-CKXAL(SIG)*SKAPAL(N))/(KX-K)
      A10=(SKXAL(SIG)*CKAPAL(N)+CKXAL(SIG)*SKAPAL(N))/(KX+K)
140   A11=2.*KX/(KX**2-KE*ABS(KE))
      A12=2.*KE/(KX**2-KE*ABS(KE))
      A13=2.*KX/(KX**2-K*ABS(K))
      A14=2.*K/(KX**2-K*ABS(K))
      IF (MODE.EQ.3HLSE) GO TO 320
      IF (ISYM.EQ.1HA) GO TO 230
C
C      LSM - SYMMETRIC   AND   LSE - ANTISYMMETRIC
C
145   IF (A3.GT.1.E+25.OR.A4.GT.1.E+25) GO TO 150
      Z1=(R3+R4-A11)*SKXB(SIG)
      Z2=(TV1*A12-R3+R4)*CKXB(SIG)
      Z3=(R3-R4-TV1*A12)*SKXB(SIG)
      Z4=(A11-R3-R4)*CKXB(SIG)
      GO TO 180
150   IF (A3*A4.GT.1.E+50) GO TO 170
      IF (A4.GT.1.E+25) GO TO 160
      B1=-SKAPD(N)**2/KE
      B2=B1
      B1=B1*SKXB(SIG)
      B2=B2*CKXB(SIG)
      B3=-B1
      B4=-B2
      GO TO 180
160   B1=SKAPD(N)**2/KE
      B2=-B1
      B1=B1*SKXB(SIG)
      B2=B2*CKXB(SIG)
      B3=B1
      B4=B2
      GO TO 180
170   B1=0.
      B2=0.
      B3=0.
      B4=0.
180   IF (A7.GT.1.E+25.OR.A8.GT.1.E+25) GO TO 190
      Z5=(A13-R7-R8)*SKXA(SIG)
      Z6=(TU1*A14-R7+R8)*SKXA(SIG)
      GO TO 220
190   IF (A7*A8.GT.1.E+50) GO TO 210
      IF (A8.GT.1.E+25) GO TO 200
      B5=SKXAL(SIG)*SKAPAL(N)**2/K
      B6=-B5
      GO TO 220
200   B5=-SKXAL(SIG)*SKAPAL(N)**2/K
      B6=B5
      GO TO 220
210   B5=0.
      B6=0.
220   IF (MODE.EQ.3HLSE) GO TO 340
```

```
      TT=(1.,0.)
      I1P=R1+R2+(B1P(M)*(Z1+(R5+R6)*CKXB(SIG))
     1+TT*B2P(M)*(Z2+(R5-R6)*SKXB(SIG)))/EPS
     2+CP(M)*(Z5+(R9+R10)*CKXA(SIG))
      I2P=TU*(R2-R1)+TV*(B1P(M)*(Z3+(R5-R6)*CKXB(SIG))
     1+B2P(M)*(Z4+(R5+R6)*SKXB(SIG)))+TU*CP(M)*(Z6+(R9-R10)*CKXA(SIG))
C
C       LSM - SYMMETRIC
C
C
C       WITH E-MODES
C
      INTGRL=KX*I1P-I2P*KY**2
C
C       WITH H-MODES
C
      IF (LR.EQ.2) INTGRL=KY*I1P+KX*KY*I2P
      IF (IKT.EQ.1) INTGRL=I1P/SQR2
      IF (IKT.EQ.0) INTGRL=INTGRL/KT
      INTGRL=INTGRL/NPS(M)
      RETURN
C
C       LSM - ANTISYMMETRIC   AND   LSE - SYMMETRIC
C
230   IF (A3.GT.1.E+25.OR.A4.GT.1.E+25) GO TO 240
      Z1=(A11-R3-R4)*CKXB(SIG)
      Z2=(TV1*A12-R3+R4)*SKXB(SIG)
      Z3=(TV1*A12-R3+R4)*CKXB(SIG)
      Z4=(R3+R4-A11)*SKXB(SIG)
      GO TO 270
240   IF (A3*A4.GT.1.E+50) GO TO 260
      IF (A4.GT.1.E+25) GO TO 250
      B1=SKAPD(N)**2/KE
      B2=-B1
      B1=B1*CKXB(SIG)
      B2=B2*SKXB(SIG)
      B3=-B1
      B4=B2
      GO TO 270
250   B1=-SKAPD(N)**2/KE
      B2=B1
      B1=B1*CKXB(SIG)
      B2=B2*SKXB(SIG)
      B3=B1
      B4=-B2
      GO TO 270
260   B1=0.
      B2=0.
      B3=0.
      B4=0.
270   IF (A7.GT.1.E+25.OR.A8.GT.1.E+25) GO TO 280
      Z5=(R7+R8-A13)*CKXA(SIG)
      Z6=(R7-R8-TU1*A14)*CKXA(SIG)
      GO TO 310
280   IF (A7*A8.GT.1.E+50) GO TO 300
      IF (A8.GT.1.E+25) GO TO 290
      B5=-CKXA(SIG)*SKAPAL(N)**2/K
      B6=-B5
      GO TO 310
290   B5=CKXA(SIG)*SKAPAL(N)**2/K
```

```
      B6=B5
      GO TO 310
300   B5=0.
      B6=0.
310   IF (MODE.EQ.3HLSE) GO TO 330
      I1P=R2-R1+TU1*(E1P(M)*(Z1+(R5+R6)*SKXB(SIG))
     1+TV1*E2P(M)*(Z2-(R5-R6)*CKXB(SIG))*SIGN(1.,KE))/EPS
     2+TU1*FP(M)*(Z5+(R9+R10)*SKXA(SIG))
      I2P=TU*(R1+R2)+TV*TU1*(E1P(M)*(Z3+(R5-R6)*SKXB(SIG))
     1+TV1*E2P(M)*(Z4+(R5+R6)*CKXB(SIG))*SIGN(1.,KE))
     2+TU*TU1*FP(M)*(Z6+(R9-R10)*SKXA(SIG))
C
C       LSM - ANTISYMMETRIC
C
C       WITH E-MODES
C
      INTGRL=AJ*(-KX*I1P+I2P*KY**2)
C
C       WITH H-MODES
C
      IF (LR.EQ.2) INTGRL=AJ*(-KY*I1P-KX*KY*I2P)
      IF (IKT.EQ.1) INTGRL=-AJ*I1P/SQR2
      IF (IKT.EQ.0) INTGRL=INTGRL/KT
      INTGRL=INTGRL/NPA(M)
      RETURN
320   IF (ISYM.EQ.1HS) GO TO 230
      IF (ISYM.EQ.1HA) GO TO 145
330   I1P=R1+R2+TV1*B2DP(M)*(Z3+(R5-R6)*SKXB(SIG))
     1+B1DP(M)*(Z4+(R5+R6)*CKXB(SIG))+TU1*CDP(M)*(Z6+(R9-R10)*SKXA(SIG))
C
C       LSE - SYMMETRIC
C
C
C       WITH E-MODES
C
      INTGRL=AJ*I1P*KY
C
C       WITH H-MODES
C
      IF (LR.EQ.2) INTGRL=-AJ*KX*I1P
      IF (IKT.EQ.1) INTGRL=SQR2*AJ*ALR*I1P
      IF (IKT.EQ.0) INTGRL=INTGRL/KT
      INTGRL=INTGRL/NDPS(M)
      RETURN
340   I1P=R2-R1+TU1*(TV1*E2DP(M)*(Z3+(R5-R6)*CKXB(SIG))*SIGN(1.,KE)
     1-E1DP(M)*(Z4+(R5+R6)*SKXB(SIG)))+FDP(M)*(Z6+(R9-R10)*CKXA(SIG))
C
C       LSE - ANTISYMMETRIC
C
C
C       WITH E-MODES
C
      INTGRL=-I1P*KY
C
C       WITH H-MODES
C
      IF (LR.EQ.2) INTGRL=KX*I1P
      IF (IKT.EQ.1) INTGRL=-SQR2*ALR*I1P
      IF (IKT.EQ.0) INTGRL=INTGRL/KT
      INTGRL=INTGRL/NDPA(M)
```

```
      RETURN
      END
```

```
      SUBROUTINE CONSRV (S11,S21,NMOD,ISIG,IM)
C
C      CONSERVATION OF ENERGY CHECK
C
C      NOTE>  DOES NOT GUARANTEE THAT ANSWER IS CORRECT.  ONLY GUARANTEES
C      SELF-CONSISTENCY.
C
C            DEFINITIONS>
CC                 S11       -    FEEDGUIDE SELF-REFLECTION SCATTERING
C                                 BLOCK
C                  S21       -    FEEDGUIDE TO SPACE MODE VOLTAGE
C                                 TRANSMISSION COEFFICIENT
C                  NMOD      -    NUMBER OF FEEDGUIDE MODES IN UNIT CELL
C                  IM        -    MINUS THE NUMBER OF DIGITS TO WHICH
C                                 CONSERVATION OF ENERGY IS APPROXIMATED
C                                 BY SOLUTION
C
C*********************************************************************
      INTEGER SIG
      COMPLEX S11(20,20),S21(250,20),S(20,20),Y,YA
      COMMON /CNSRV/ Y(20),YA(250)
      IM=-10000
      DO 150 IA=1,NMOD
      DO 140 IB=1,NMOD
      S(IA,IB)=(0.,0.)
      DO 100 SIG=1,ISIG
      S(IA,IB)=S(IA,IB)+S21(SIG,IA)*CONJG(YA(SIG)*S21(SIG,IB))
100   CONTINUE
      DO 110 NN=1,NMOD
      DELR=0.
      DELS=0.
      IF (NN.EQ.IA) DELR=1.
      IF (NN.EQ.IB) DELS=1.
      S(IA,IB)=S(IA,IB)-(DELR+S11(NN,IA))*CONJG(Y(NN)*(DELS-S11(NN,IB)))
110   CONTINUE
      A=CABS(S(IA,IB))
      IF (A.GT.1.E-20) GO TO 120
      I=-1000
      GO TO 130
120   I=ALOG10(A)
130   IM=MAX0(I,IM)
140   CONTINUE
150   CONTINUE
      RETURN
      END
**
```

```
      SUBROUTINE PLTCAL (A,B,D,F,EPS,A1,B1,DX,DY,SEP,PT,S0,LOBE,ISTRT,
     1JJ,ST,SPH,IGRD,NTH)
C
C       CALCOMP PATTERN PLOTTING ROUTINE
C       MAX OF 10 CURVES, 51 POINTS EACH.
C
C               DEFINITIONS>
C                       A          =     ALPHA
C                       B          =     BETA
C                       D          =     DELTA
C                       F          =     FREQUENCY (GHZ)
C                       EPS        =     RELATIVE PERMITTIVITY OF SLABS
C                       A1         =     X-DIMENSION OF GUIDE
C                       B1         =     Y-DIMENSION OF GUIDE
C                       DX         =     X GRID SPACING
C                       DY         =     Y GRID SPACING
C                       SEP        =     SEPTUM THICKNESS
C                       PT         =     POWER TRANSMISSION COEFFICIENT
C                       S0         =     LOBE NUMBER IN INTERNAL ORDERING
C                       LOBE       =     NUMBER OF BEAMS TO BE PLOTTED
C                       ISTRT      =     ARRAY PICKUP VALUE FOR CURRENT PAGE
C                       JJ         =     LOBE SELECTION VECTOR
C                       ST         =     SIN(THETA) ARRAY
C                       SPH        =     SIN(PHI) OF PLOT
C                       IGRD       =     GRID TYPE
C                       NTH        =     NUMBER OF POINTS TO BE PLOTTED
C***********************************************************************
      DIMENSION PT(10,51),JJ(10),ST(51),ST1(51),P(51)
      INTEGER S0(10)
      L=1
      IF (NTH.GE.21) L=2
      CALL AXIS (2.,3.,1H ,-1,5.,0.,0.,0.2)
      CALL SYMBOL (4.3,2.6,.10,3HSIN,0.,3)
      CALL GREEK (4.6,2.55,.15,0.,8)
      CALL SYMBOL (4.7,2.5,0.07,1H0,0.,1)
      CALL IAXIS (2.0,3.0,30HPOWER TRANSMISSION FACTOR (DB),30,6.,90.,
     1-30.,5.)
      IF (IGRD.EQ.1) CALL SYMBOL (3.75,9.6,.1,15HTRIANGULAR GRID,0.,15)
      IF (IGRD.EQ.2) CALL SYMBOL (3.75,9.6,.1,16HRECTANGULAR GRID,0.,16)
      CALL PLOT (2.,3.,-3)
      I3=ISTRT-1
      DO 100 I2=1,LOBE
      I3=I3+1
      I4=JJ(I3)
      N1=NTH
      N=0
      I1=1
90    DO 91 I=I1,NTH
      IF (PT(I4,I).GT.-32.4999) GO TO 92
      N=I
91    CONTINUE
92    N=N+1
      IF (N.GT.NTH) GO TO 96
      DO 93 I=N,NTH
      IF (PT(I4,I).LE.-32.499999) GO TO 94
      N1=I
93    CONTINUE
94    N2=N1-N+1
      DO 95 I=N,N1
      P(I)=PT(I4,I)
```

```
      ST1(I)=ST(I)
95    CONTINUE
      P(N1+1)=-30.0
      P(N1+2)=5.0
      ST1(N1+1)=0.
      ST1(N1+2)=0.2
      CALL LINE (ST1(N),P(N),N2,1,L,I2+1)
      IF (N1.EQ.NTH) GO TO 96
      I1=N1+1
      GO TO 90
96    CONTINUE
100   CONTINUE
      CALL PLOT (-2.,0.,-3)
      CALL SYMBOL (2.5,-.75,.1,4HF = ,0.,4)
      CALL NUMBER (999.,999.,.1,F,0.,2)
      CALL SYMBOL (999.,999.,.1,4H GHZ,0.,4)
      CALL SYMBOL (5.5,-.75,.1,4HA = ,0.,4)
      CALL NUMBER (999.,999.,.1,A1,0.,3)
      CALL SYMBOL (999.,999.,.1,4H IN.,0.,4)
      CALL GREEK (2.5,-1.05,.15,0.,1)
      CALL SYMBOL (2.75,-1.0,.1,2H= ,0.,3)
      CALL NUMBER (999.,999.,.1,A,0.,3)
      CALL SYMBOL (999.,999.,.1,4H IN.,0.,4)
      CALL SYMBOL (5.5,-1.,.1,4HB = ,0.,4)
      CALL NUMBER (999.,999.,.1,B1,0.,3)
      CALL SYMBOL (999.,999.,.1,4H IN.,0.,4)
      CALL GREEK (2.5,-1.30,.15,0.,2)
      CALL SYMBOL (2.75,-1.25,.1,2H= ,0.,3)
      CALL NUMBER (999.,999.,.1,B,0.,3)
      CALL SYMBOL (999.,999.,.1,4H IN.,0.,4)
      CALL SYMBOL (5.5,-1.25,.1,1HD,0.,1)
      CALL SYMBOL (999.,-1.30,.07,1HX,0.,1)
      CALL SYMBOL (999.,-1.25,.1,3H = ,0.,3)
      CALL NUMBER (999.,999.,.1,DX,0.,3)
      CALL SYMBOL (999.,999.,.1,4H IN.,0.,4)
      CALL GREEK (2.5,-1.55,.15,0.,4)
      CALL SYMBOL (2.75,-1.50,.1,2H= ,0.,3)
      CALL NUMBER (999.,999.,.1,D,0.,3)
      CALL SYMBOL (999.,999.,.1,4H IN.,0.,4)
      CALL SYMBOL (5.5,-1.5,.1,1HD,0.,1)
      CALL SYMBOL (999.,-1.55,.07,1HY,0.,1)
      CALL SYMBOL (999.,-1.5,.1,3H = ,0.,3)
      CALL NUMBER (999.,999.,.1,DY,0.,3)
      CALL SYMBOL (999.,999.,.1,4H IN.,0.,4)
      CALL GREEK (2.5,-1.80,.15,0.,5)
      CALL SYMBOL (2.75,-1.75,.1,2H= ,0.,3)
      CALL NUMBER (999.,999.,.1,EPS,0.,2)
      CALL SYMBOL (5.5,-1.75,.1,6HSEP = ,0.,6)
      CALL NUMBER (999.,999.,.1,SEP,0.,3)
      CALL SYMBOL (999.,999.,.1,4H IN.,0.,4)
      CALL SYMBOL (3.5,-2.,.1,14HCUT PLANE  SIN,0.,14)
      CALL GREEK (4.9,-2.05,.15,0.,21)
      CALL SYMBOL (4.95,-2.0,.1,3H = ,0.,3)
      CALL NUMBER (999.,999.,.1,SPH,0.,3)
      CALL SYMBOL (1.5,-2.25,.1,6HLEGEND,0.,6)
      CALL SYMBOL (1.75,-2.45,.1,2,0.,-1)
      CALL GREEK (2.25,-2.5,.15,0.,18)
      CALL SYMBOL (2.35,-2.5,.1,3H = ,0.,3)
      AS=SO(ISTRT)
      CALL NUMBER (999.,999.,.1,AS,0.,0)
```

```
      IF (LOBE.LT.2) GO TO 110
      CALL SYMBOL (5.,-2.45,.1,3,0.,-1)
      CALL GREEK (5.5,-2.5,.15,0.,18)
      CALL SYMBOL (5.6,-2.5,.1,3H = ,0.,3)
      AS=SO(ISTRT+1)
      CALL NUMBER (999.,999.,.1,AS,0.,0)
      IF (LOBE.LT.3) GO TO 110
      CALL SYMBOL (1.75,-2.70,.1,4,0.,-1)
      CALL GREEK (2.25,-2.75,.15,0.,18)
      CALL SYMBOL (2.35,-2.75,.1,3H = ,0.,3)
      AS=SO(ISTRT+2)
      CALL NUMBER (999.,999.,.1,AS,0.,0)
      IF (LOBE.LT.4) GO TO 110
      CALL SYMBOL (5.,-2.7,.1,5,0.,-1)
      CALL GREEK (5.5,-2.75,.15,0.,18)
      CALL SYMBOL (5.6,-2.75,.1,3H = ,0.,3)
      AS=SO(ISTRT+3)
      CALL NUMBER (999.,999.,.1,AS,0.,0)
110   CALL PLOT (8.5,-3.0,-3)
      RETURN
      END
**
```

```
      SUBROUTINE FOURMDS (F,BB)
C
C      SPECIAL DISPERSION RELATION SOLVER FOR RAPID COMPUTATION OF
C      ELEMENT MISMATCH AT BROADSIDE.
C
C            DEFINITIONS>
C                       F          -     FREQUENCY IN GHZ
C                       BB         -     X-DIRECTED WAVENUMBER VECTOR
C                       A          -     ALPHA
C                       B          -     BETA
C                       D          -     DELTA
C                       BBB        -     GUIDE HEIGHT
C                       TPI        -     6.2831......
C                       EPS        -     RELATIVE PERMITTIVITY OF SLABS
C***********************************************************************
      DIMENSION BB(1)
      REAL K,KE,KINC
      COMMON /WAVGD/ A,B,D,BBB,TPI,EPS
      DATA C/11.8028526/
      TPIL=TPI*F/C
      EPS1=EPS-1.0
      A1=TPIL*A
      B1=TPIL*B
      D1=TPIL*D
      L=0
      DO 170 MODE=1,4
      DO 160 N=1,4
      L=L+1
      J=1/N
      S=1.01
      IF (K.LT.0.) S=0.99
      K=J*BB(L)+(1-J)*S*K
      KINC=0.314
      K=K-KINC
      I=0
100   K=K+KINC
      DIFF=DIFF1
      I=I+1
      KE=EPS1+K*ABS(K)
      S=SQRT(ABS(KE))
      IF (KE.LT.0.) S=-S
      KE=S
      DIFF1=DISP(MODE,K,KE,A1,B1,D1,EPS)
      IF (I.EQ.1) GO TO 120
      IF (KINC.LE.1.E-10) GO TO 130
      IF (ABS(DIFF*DIFF1).LE.1.E-10) GO TO 130
      IF (DIFF*DIFF1) 110,130,100
110   K=K-KINC
      KINC=0.5*KINC
      DIFF1=DIFF
      GO TO 100
120   DIFF=DIFF1
      GO TO 100
130   IF (ABS(DIFF).LT.ABS(DIFF1)) GO TO 140
      BB(L)=K
      GO TO 160
140   K=K-KINC
      BB(L)=K
160   CONTINUE
```

```
170   CONTINUE
      RETURN
      END
**
```

```
      SUBROUTINE KBET (NMODES)
C
C      SPECIAL SUBROUTINE FOR CREATING LSE(N,0) AND LSE(N,1) K-BETA
C      DIAGRAMS
C
C             DEFINITIONS>
C                    NMODES    -    DUMMY ARGUMENT
C                    BG        -    NORMALIZED LONGITUDINAL WAVENUMBER
C                    KA        -    K*A/2
C                    IMODE     -    MODE DESIGNATIONS
C                    A         -    ALPHA/LAMBDAO
C                    B         -    BETA/LAMBDAO
C                    D         -    DELTA/LAMBDAO
C                    BB        -    (GUIDE HEIGHT)/LAMBDAO
C                    TPI       -    6.2831......
C                    EPS       -    RELATIVE PERMITTIVITY OF SLABS
C*********************************************************************
      DIMENSION GAM(2,2,2),S0(2,2,2),SF(2,2,2)
      REAL K0,KA,K,KE,M2B,KINC
      COMMON /KBETA/ BG(6,101),KA(101),IMODE(6)
      COMMON /WAVGD/ A,B,D,BB,TPI,EPS
      DATA C/11.8028526/
      AA=A+B+D
      F0=C/(TPI*AA)
      DF=0.03*F0
      NF=101
      EPS1=EPS-1.0
      EPSQ=SQRT(EPS1)
      F=F0-DF
      WRITE (6,900) (IMODE(I),I=1,6)
      DO 200 IF=1,NF
      F=F+DF
      K0=TPI*F/C
      KA(IF)=K0*AA
      A1=K0*A
      B1=K0*B
      D1=K0*D
      M2B=(0.5*C/(BB*F))**2
      DO 180 MODE=1,2
      M1=MODE+2
      K=-EPSQ+1.E-10
      M0=1
      DO 160 N=1,3
      J=1/N
      S=1.01
      IF (K.LT.0.) S=0.99
      K=J*K+(1-J)*S*K
      KINC=0.314
      K=K-KINC
      I=0
100   K=K+KINC
      DIFF=DIFF1
      I=I+1
      KE=EPS1+K*ABS(K)
      S=SQRT(ABS(KE))
      IF (KE.LT.0.) S=-S
      KE=S
      DIFF1=DISP(M1,K,KE,A1,B1,D1,EPS)
      IF (I.EQ.1) GO TO 120
      IF (KINC.LT.1.E-10) GO TO 130
```

```
      IF (ABS(DIFF*DIFF1).LE.1.E-10) GO TO 130
      IF (DIFF*DIFF1) 110,130,100
110   K=K-KINC
      KINC=0.5*KINC
      DIFF1=DIFF
      GO TO 100
120   DIFF=DIFF1
      GO TO 100
130   IF (ABS(DIFF).LT.ABS(DIFF1)) GO TO 140
      GO TO 150
140   K=K-KINC
      G=EPS1+K*ABS(K)
      S=SQRT(ABS(G))
      IF (G.LT.0.) S=-S
      KE=S
150   SO(MODE,N,MO)=K
      SE(MODE,N,MO)=KE
      G=1.0-K*ABS(K)
      S=SQRT(ABS(G))
      IF (G.LT.0.) S=-S
      GAM(MODE,N,MO)=S*KA(IF)
160   CONTINUE
180   CONTINUE
      II=0
      DO 190 I1=1,2
      DO 190 I=1,2
      II=II+1
      IF (II.EQ.4) GO TO 190
      BG(II,IF)=GAM(I,I1,1)
      K=SO(I,I1,1)
      G2=-K*ABS(K)+1.0-M2B
      G=SQRT(ABS(G2))*KA(IF)
      IF (G2.LT.0.) G=-G
      BG(II+3,IF)=G
190   CONTINUE
      WRITE (6,910) KA(IF),(BG(I,IF),I=1,6)
200   CONTINUE
C
900   FORMAT (1H1,5X,10H   KA/2    ,10H%GAMMA*A/2 ,/15X,6(2X,A7,1X),//)
910   FORMAT (8X,F5.2,2X,6(2X,F6.3,2X))
      END
**
```

```
      SUBROUTINE LSEMOD (N)
C
C      COMPUTE LSE MODE FUNCTION FY(X)
C
C            DEFINITIONS>  SEE SUBROUTINE LSMLSE
C**************************************************************************
      DIMENSION VX(101)
      REAL KAP,KAPE,NPS,NPA,NDPS,NDPA
      COMMON /ARRAY/ AL,BL,DL,BIL,SEPIL,TPI,EPS,S(4)
      COMMON /COEFS/ B1P(10),B2P(10),B1DP(10),B2DP(10),CP(10),CDP(10),
     1F1P(10),F2P(10),E1DP(10),E2DP(10),FP(10),FDP(10),NPS(10),NPA(10),
     2NDPS(10),NDPA(10),KOUNT(20)
      COMMON /MODES/ KAP(20),KAPE(20),GAM(20),MODE(20),ISYM(20),NN(20),
     1MM(20),MODORD(20)
      M=MM(N)
      A=TPI*(AL+BL+DL)
      XDEL=0.02*A
      B=-TPI*BL
      D=-TPI*(BL+DL)
      N1=KOUNT(N)
      B1=-50.*B/A
      D1=-50.*D/A
      IF (ISYM(N).EQ.1HA) GO TO 140
      X=-1.02*A
      DO 130 I=1,51
      X=X+XDEL
      Y=ABS(X)
      IF (X.GT.D) GO TO 110
      VX(I)=CDP(N1)*SINC(KAP(N)*(X+A))*SIGN(1.,KAP(N))/NDPS(N1)
      VX(102-I)=VX(I)
      GO TO 130
110   IF (X.GT.B) GO TO 120
      T=KAPE(N)*(B-X)
      VX(I)=(B1DP(N1)*COSC(T)-B2DP(N1)*SINC(T))/NDPS(N1)
      VX(102-I)=VX(I)
      GO TO 130
120   VX(I)=COSC(KAP(N)*Y)/NDPS(N1)
      VX(102-I)=VX(I)
130   CONTINUE
      GO TO 180
140   X=-1.02*A
      DO 170 I=1,51
      X=X+XDEL
      Y=ABS(X)
      IF (X.GT.D) GO TO 150
      VX(I)=FDP(N1)*SINC(KAP(N)*(X+A))/NDPA(N1)
      VX(102-I)=-VX(I)
      GO TO 170
150   IF (X.GT.B) GO TO 160
      T=KAPE(N)*(B-X)
      VX(I)=(E1DP(N1)*COSC(T)-E2DP(N1)*SINC(T))/NDPA(N1)
      VX(102-I)=-VX(I)
      GO TO 170
160   VX(I)=-SINC(KAP(N)*Y)/NDPA(N1)
      VX(102-I)=-VX(I)
170   CONTINUE
C
C      CALL PRINT/PLOT ROUTINE
C
180   CALL PRNT (VX,3HLSF,B1,D1)
```

```
      RETURN
      END
```

```
      SUBROUTINE LSMMOD (N)
C
C      COMPUTE LSM MODE FUNCTION HY(X)
C
C            DEFINITIONS>  SEE SUBROUTINE LSMLSE
C*************************************************************************
      REAL KAP,KAPE,NPS,NPA,NDPS,NDPA,IX(101)
      COMMON /ARRAY/ AL,BL,DL,B1L,SEPTL,TPI,EPS,S(4)
      COMMON /COEFS/ B1P(10),B2P(10),B1DP(10),B2DP(10),CP(10),CDP(10),
     1E1P(10),E2P(10),E1DP(10),E2DP(10),FP(10),FDP(10),NPS(10),NPA(10),
     2NDPS(10),NDPA(10),KOUNT(20)
      COMMON /MODES/ KAP(20),KAPE(20),GAM(20),MODE(20),ISYM(20),NN(20),
     1MM(20),MODORD(20)
      M=MM(N)
      A=TPI*(AL+BL+DL)
      XDEL=0.02*A
      B=-TPI*BL
      D=-TPI*(BL+DL)
      N1=KOUNT(N)
      B1=-50.*B/A
      D1=-50.*D/A
      IF (ISYM(N).EQ.1HA) GO TO 140
      X=-1.02*A
      DO 130 I=1,51
      X=X+XDEL
      Y=ABS(X)
      IF (X.GT.D) GO TO 110
      IX(I)=CP(N1)*COSC(KAP(N)*(X+A))/NPS(N1)
      IX(102-I)=IX(I)
      GO TO 130
110   IF (X.GT.B) GO TO 120
      T=KAPE(N)*(B-X)
      IX(I)=(B1P(N1)*COSC(T)-B2P(N1)*SINC(T))/NPS(N1)
      IX(102-I)=IX(I)
      GO TO 130
120   IX(I)=COSC(KAP(N)*Y)/NPS(N1)
      IX(102-I)=IX(I)
130   CONTINUE
      GO TO 180
140   X=-1.02*A
      DO 170 I=1,51
      X=X+XDEL
      Y=ABS(X)
      IF (X.GT.D) GO TO 150
      IX(I)=FP(N1)*COSC(KAP(N)*(X+A))/NPA(N1)
      IX(102-I)=-IX(I)
      GO TO 170
150   IF (X.GT.B) GO TO 160
      T=KAPE(N)*(B-X)
      IX(I)=(E1P(N1)*COSC(T)-E2P(N1)*SINC(T))/NPA(N1)
      IX(102-I)=-IX(I)
      GO TO 170
160   IX(I)=SINC(KAP(N)*Y)/NPA(N1)
      IX(102-I)=-IX(I)
170   CONTINUE
C
C      CALL PRINT/PLOT ROUTINE
C
180   CALL PRNT (IX,3HLSM,B1,D1)
      RETURN
```

FND

```
      SUBROUTINE PRNT (VX,IM,B1,D1)
C
C      PRINT/PLOT ROUTINE FOR MODE FUNCTIONS
C
C             DEFINITIONS>
C                    VX          =     MODE AMPLITUDE
C                    IM          =     MODE TYPE
C                    B1          =     NORMALIZED DIELECTRIC BOUNDARY POINT
C                    D1          =     NORMALIZED DIELECTRIC BOUNDARY POINT
C*********************************************************************
      DIMENSION VX(1),IX(101),IP(102),IC(50)
      INTEGER DOT,BLANK,PLUS,ZERO,SLASH
      DATA DOT,BLANK,PLUS,MINUS,ZERO,SLASH/1H.,1H ,1H+,1H-,1H0,1H\/
      IF=3HE-Y
      IF (IM.EQ.3HLSM) IF=3HH-Y
      IBL=B1
      IDL=D1
      IBR=52+IBL
      IBL=52-IBL
      IDR=52+IDL
      IDL=52-IDL
      XMAX=0.
      DO 100 I=1,101
      T=ABS(VX(I))
      XMAX=AMAX1(XMAX,T)
100   CONTINUE
      WRITE (6,900) IM,IF
      DO 110 I=1,21
      WRITE (6,910) (JJ-51,VX(JJ),JJ=I,101,21)
110   CONTINUE
      DO 120 I=1,101
      T=50.*VX(I)/XMAX+0.25*SIGN(1.,VX(I))
      IX(I)=T
120   CONTINUE
      WRITE (6,920) XMAX
      IP(1)=DOT
      DO 130 I=2,102
      IP(I)=BLANK
130   CONTINUE
      IP(IDL)=SLASH
      IP(IBL)=SLASH
      IP(IBR)=SLASH
      IP(IDR)=SLASH
      DO 180 I=1,51
      I1=I-1
      IB=100-2*I1
      B=0.01*IB
      N=0
      DO 140 JJ=1,101
      IT=51-IABS(IX(JJ))
      IF (IT.NE.I) GO TO 140
      N=N+1
      IC(N)=JJ+1
      IP(JJ+1)=PLUS
      IF (IX(JJ).LT.0) IP(JJ+1)=MINUS
      IF (IX(JJ).EQ.0) IP(JJ+1)=ZERO
140   CONTINUE
      IF ((I1/10)*10.EQ.I1) GO TO 150
      WRITE (6,930) (IP(JJ),JJ=1,102)
      GO TO 160
```

```
150   WRITE (6,940) H,(IP(JJ),JJ=1,102)
160   IF (N.EQ.0) GO TO 180
      DO 170 JJ=1,N
      IB=IC(JJ)
      IP(IB)=BLANK
170   CONTINUE
      IP(IDL)=SLASH
      IP(IBL)=SLASH
      IP(IBR)=SLASH
      IP(IDR)=SLASH
180   CONTINUE
      WRITE (6,950) (I-51,I=1,101,20)
      RETURN
C
900   FORMAT (1H1,5X,A3,8H MODE, (,A3,18H COMPONENT)*LAMBDA,//,
     15(10H  100*X/A ,10H V*LAMBDA ),/)
910   FORMAT (5(3X,I4,3X,F8.4,2X))
920   FORMAT (1H1,10X,7HVMAX = ,F10.6,//)
930   FORMAT (10X,102A1)
940   FORMAT (5X,F5.2,102A1)
950   FORMAT (11X,1H*,10(10H.........*),/,10X,I3,5(17X,I3),/,58X,
     17H100*X/A)
      END
**
```

```
      SUBROUTINE GREEK (X,Y,H,T,M)
C
C      SUBROUTINE TO PLOT GREEK CHARACTERS
C
C            DEFINTIONS>
C                   X        =    X LOCATION OF CHARACTER
C                   Y        =    Y LOCATION OF CHARACTER
C                   H        =    CHARACTER HEIGHT
C                   T        =    PLOTTING ANGLE
C                   M        =    CHARACTER NUMBER (SEQUENCE IS GREEK
C                                 ALPHABET)
C*********************************************************************
      DIMENSION K(120),L(25)
      DATA K/7741,4225,1504,211,2144,4577,1526,3645,3477,1434,4342,3121,
     11277,7704,1522,7710,2245,7724,1312,2132,3315,1626,3577,7703,3377,
     23515,402,1131,7711,2131,1336,3525,1677,7701,1314,377,1335,4420,
     37715,1425,3544,4313,1221,3142,4377,7725,1121,2277,7711,1577,4513,
     44177,7701,2577,1625,3141,2477,4432,3177,1221,3277,7705,1511,3435,
     57710,2031,1102,1304,1525,3477,1333,7713,2434,4342,3121,1213,7703,
     61454,7744,3077,1024,1324,3443,3212,7754,2413,1221,3142,4334,7703,
     71434,3377,2410,7703,1424,1120,3041,5477,7720,3577,3424,1312,2131,
     84243,3477,4477,414,3040,7710,2477,515,312,2233,4577,7714,302,1131,
     94243,3477,2123/
      DATA L/1,7,14,16,24,29,34,39,46,49,53,57,62,65,72,77,82,85,90,94,
     199,106,109,115,121/
      CALL CALCMP (XF,YF,IDUM,-4)
      HX=H*XF/6.0
      HY=H*YF/6.0
      TT=0.0174533*T
      S=SIN(TT)
      C=COS(TT)
      CHX=C*HX
      SHX=S*HX
      CHY=C*HY
      SHY=S*HY
      IZ=99
      IA=L(M)
      IB=L(M+1)-1
      CALL CALCMP (X,Y,00,1)
      DO 3 I=IA,IB
      J=K(I)/100
      DO 3 II=1,2
      IX=J/10
      IF (IX-7) 2,1,2
1     IZ=00
      GO TO 3
2     IY=J-10*IX
      CALL CALCMP (X+CHX*IX-SHY*IY,Y+CHY*IY+SHX*IX,IZ,1)
      IZ=99
3     J=K(I)-100*J
      CALL CALCMP (X+C*H*XF,Y+S*H*XF,00,1)
      RETURN
      END
**
```

```
      SUBROUTINE  AXIS(XPAGE,YPAGE,IBCD,NCHAR,AXLEN,ANGLE,FIRSTV,DELTAV)
C           CONTAINS CALLS TO CALCMP INSTEAD OF PLOT
C           CONTAINS IAXIS ENTRY POINT - WRITES VALUES IN INTEGER FORMAT
C.....       XPAGE,YPAGE  COORDINATES OF STARTING POINT OF AXIS, IN INCHES
C.....       IBCD         AXIS TITLE.
C.....       NCHAR        NUMBER OF CHARACTERS IN TITLE. + FOR C.C-W SIDE.
C.....       AXLEN        FLOATING POINT AXIS LENGTH IN INCHES.
C.....       ANGLE        ANGLE OF AXIS FROM THE X-DIRECTION, IN DEGREES.
C.....       FIRSTV       SCALE VALUE AT THE FIRST TIC MARK.
C.....       DELTAV       CHANGE IN SCALE BETWEEN TIC MARKS ONE INCH APART
      DIMENSION   IBCD(1)
15    NDEC=2
      INT=2
      GO TO 8
C
      ENTRY IAXIS
C
      IF (ABS(DELTAV).LT.1.) GO TO 15
      NDEC=-1
      INT=1
8     KN=NCHAR
      VIEW=1.
      A=1.0
      IF(KN)1,2,2
1     A=-A
      KN=-KN
2     EX=0.0
      ADX=ABS(DELTAV)
      IF(ADX)3,7,3
3     IF(ADX-99.0)6,4,4
4     ADX=ADX/10.0
      EX=EX+1.0
      GO TO 3
5     ADX=ADX*10.0
      EX=EX-1.0
6     IF(ADX-0.1)5,7,7
7     XVAL=FIRSTV*10.0**(-EX)
      ADX=DELTAV*10.0**(-EX)
      STH=ANGLE*0.0174533
      CTH=COS(STH)
      STH=SIN(STH)
      CTHTIC=CTH*VIEW
      STHTIC=STH*VIEW
      DXB=-0.1
      POSN=.15
      IF(VIEW.LT..9)POSN=.25
      DYB=POSN*A-0.05
      XN=XPAGE+DXB*CTH-DYB*STH
      YN=YPAGE+DYB*CTH+DXB*STH
      NTIC=AXLEN+1.0
      NT=NTIC/2
      DO  20  I=1,NTIC
      DXN=0.
      DYN=0.
      GO TO (9,10),INT
9     NEG=0
      IF(XVAL.LT.0.)NEG=1
      AXVAL=ABS(XVAL)
      NDIG=2-NEG
      IF(AXVAL.GE.9.5)NDIG=1-NEG
```

```
      IF(AXVAL.GE.99.5)NDIG=0
      DXN=NDIG*0.045*CTH
      DYN=NDIG*0.045*STH
10    CALL NUMBER (XN+DXN,YN+DYN,0.105,XVAL,ANGLE,NDEC)
      XVAL=XVAL+ADX
      XN=XN+CTHTIC
      YN=YN+STHTIC
      IF(NT)20,11,20
11    Z=KN
      IF(EX)12,13,12
12    Z=Z+7.0
13    DXB=-.07*Z+AXLEN*0.5*VIEW
      POSN=.325
      IF(VIEW.LT..9)POSN=.425
      DYB=POSN*A-0.075
      XT=XPAGE+DXB*CTH-DYB*STH
      YT=YPAGE+DYB*CTH+DXB*STH
      CALL  SYMBOL(XT,YT,0.14,IBCD,ANGLE,NC)
      IF(EX)14,20,14
14    Z=KN+2
      XT=XT+Z*CTH*0.14
      YT=YT+Z*STH*0.14
      CALL  SYMBOL(XT,YT,0.14,3H*10,ANGLE,3)
      XT=XT+(3.0*CTH-0.8*STH)*0.14
      YT=YT+(3.0*STH+0.8*CTH)*0.14
      CALL  NUMBER(XT,YT,0.07,EX,ANGLE,-1)
20    NT=NT-1
      CALL  CALCMP(XPAGE+AXLEN*CTHTIC,YPAGE+AXLEN*STHTIC,0,1)
      DXB=-0.07*A*STH
      DYB=+0.07*A*CTH
      A=NTIC-1
      XN=XPAGE+A*CTHTIC
      YN=YPAGE+A*STHTIC
      DO  30  I=1,NTIC
      CALL  CALCMP(XN,YN,99,1)
      CALL  CALCMP(XN+DXB,YN+DYB,99,1)
      CALL  CALCMP(XN,YN,0,1)
      XN=XN-CTHTIC
      YN=YN-STHTIC
30    CONTINUE
      RETURN
      END
**
```

```
      SUBROUTINE  CSIMEQ(A,N,B,M,KS)
C      SCREEN.CSIMEQ
C       CDC6700***CSIMEQ
C
C     PURPOSE
C        OBTAIN SOLUTION OF A SET OF SIMULTANEOUS LINEAR EQUATIONS,
C        AX=B
C
C     USAGE
C        CALL CSIMEQ(A,N,B,M,KS)
C
C     DESCRIPTION OF PARAMETERS
C        A - MATRIX OF COEFFICIENTS STORED COLUMNWISE. THESE ARE
C            DESTROYED IN THE COMPUTATION.  THE SIZE OF MATRIX A IS
C            N BY N.
C        B - MATRIX OF ORIGINAL CONSTANTS (LENGTH N BY M). THESE ARE
C            REPLACED BY FINAL SOLUTION VALUES, MATRIX X.
C        N - NUMBER OF EQUATIONS
C        M - NUMBER OF SETS OF SOLUTIONS
C        KS - OUTPUT DIGIT
C            0 FOR A NORMAL SOLUTION
C            1 FOR A SINGULAR SET OF EQUATIONS
C
C     REMARKS
C        MATRIX A MUST BE GENERAL.
C        IF MATRIX IS SINGULAR, SOLUTION VALUES ARE MEANINGLESS.
C
C     METHOD
C        METHOD OF SOLUTION IS BY ELIMINATION USING LARGEST PIVOTAL
C        DIVISOR. EACH STAGE OF ELIMINATION CONSISTS OF INTERCHANGING
C        ROWS WHEN NECESSARY TO AVOID DIVISION BY ZERO OR SMALL
C        ELEMENTS.
C        THE FORWARD SOLUTION TO OBTAIN VARIABLE N IS DONE IN
C        N STAGES. THE BACK SOLUTION FOR THE OTHER VARIABLES IS
C        CALCULATED BY SUCCESSIVE SUBSTITUTIONS.  FINAL SOLUTION
C        VALUES ARE DEVELOPED IN VECTOR B, WITH VARIABLE 1 IN B(1),
C        VARIABLE 2 IN B(2),........, VARIABLE N IN B(N).
C        IF NO PIVOT CAN BE FOUND EXCEEDING A TOLERANCE OF 0.0,
C        THE MATRIX IS CONSIDERED SINGULAR AND KS IS SET TO 1. THIS
C        TOLERANCE CAN BE MODIFIED BY REPLACING THE FIRST STATEMENT.
C
C     ...............................................................
C
C
C     FORWARD SOLUTION
C
      COMPLEX     A,B,BIGA,SAVE
      DIMENSION A(20,20),B(20,20)
      TOL=0.0
      KS=0
      DO 200 J=1,N
      BIGA=(0.,0.)
C
C     SEARCH FOR MAXIMUM COEFFICIENT IN COLUMN
C
      DO 120 I=J,N
      IF(CABS(BIGA)-CABS(A(I,J)))110,120,120
  110 BIGA=A(I,J)
      IMAX=I
  120 CONTINUE
```

```
C
C     TEST FOR PIVOT LESS THAN TOLERANCE (SINGULAR MATRIX)
C
      IF(ABS(REAL(BIGA))+ABS(AIMAG(BIGA))-TOL)130,130,140
130   KS=1
      RETURN
C
C     INTERCHANGE ROWS IF NECESSARY
C
140   CONTINUE
      DO 150 I=J,N
      SAVE=A(J,I)
      A(J,I)=A(IMAX,I)
      A(IMAX,I)=SAVE
C
C     DIVIDE EQUATION BY LEADING COEFFICIENT
C
      A(J,I)=A(J,I)/BIGA
150   CONTINUE
      DO 160 I=1,M
      SAVE=B(J,I)
      B(J,I)=B(IMAX,I)
      B(IMAX,I)=SAVE
160   B(J,I)=B(J,I)/BIGA
C
C     ELIMINATE NEXT VARIABLE
C
      IF(J-N)170,210,170
170   J1=J+1
      DO 200 I=J1,N
      DO 180 K=J1,N
180   A(I,K)=A(I,K)-A(J,K)*A(I,J)
      DO 190 K=1,M
190   B(I,K)=B(I,K)-B(J,K)*A(I,J)
200   CONTINUE
C
C     BACK SOLUTION
C
210   NY=N-1
      DO 220 L2=1,NY
      J=N-L2
      JY=J+1
      DO 220 K=1,M
      DO 220 L=JY,N
220   B(J,K)=B(J,K)-A(J,L)*B(L,K)
      RETURN
      END
 **
```

```
      FUNCTION SINC(X)
      IF (X.LT.0.) GO TO 100
      SINC=SIN(X)
      RETURN
100   SINC=SINH(X)
      RETURN
      END
**
```

```
      FUNCTION COSC(X)
      IF (X.LT.0.) GO TO 100
      COSC=COS(X)
      RETURN
100   COSC=COSH(X)
      RETURN
      END
**
```

```
      FUNCTION TANT(X)
      IF (X.LT.0.) GO TO 100
      TANT=TAN(X)
      RETURN
100   TANT=TANH(X)
      RETURN
      END
```

```
      FUNCTION S1(X)
      IF (ABS(X).GT.1.E-15) GO TO 100
      S1=2.0
      RETURN
100   S1=SINC(X)/X+1.0
      RETURN
      END
```

```
      FUNCTION S2(X)
      IF (ABS(X).GT.1.E-15) GO TO 100
      S2=0.
      RETURN
100   S2=1.0-SINC(X)/X
      RETURN
      END
**
```

```
      FUNCTION S3(X)
      IF (ABS(X).GT.1.E-15) GO TO 100
      S3=0.0
      RETURN
100   S3=(SINC(X)**2)/ABS(X)
      RETURN
      END
••
```

```
      FUNCTION SXOX(X)
      SXOX=1.0
      IF (ABS(X).LT.1.E-10) RETURN
      SXOX=SINC(X)/X
      RETURN
      END
```

```
      FUNCTION TXOX (X)
      IF (ABS(X).GT.1.E-15) GO TO 100
      TXOX=1.0
      RETURN
100   TXOX=TANT(X)/X
      RETURN
      END
**
```

REFERENCES

1. R. J. Mailloux, Dual Band Phased Array Elements, U.S. Pat. No. 3882505, May 6, 1975.

2. Lewis, L.R., M. Fassett, and C.J. Hunt, "A Broadband Stripline Array Element," IEEE/AP-S Symposium, June 1974, Atlanta, GA.

3. Lewis, L.R., J.H. Pozgay, and A. Hessel, "Design and Analysis of Broadband Notch Antennas and Arrays," IEEE/AP-S International Symposium, October 1976, Amherst, MA.

4. Lewis, L.R. and J.H. Pozgay, Broadband Antenna Study, Final Report AFCRL-TR-75-0178, March 1975.

5. Lewis, L.R., A. Hessel, and G.H.Knittel, "Performance of a Protruding Dielectric Waveguide Element in a Phased Array," IEEE Trans. Antennas and Propagation, AP-20, No. 6, November 1972, pp 712-722.

6. Marcuwitz, N., Waveguide Handbook, Dover, 1965

7. Private communication from R.J. Mailloux

8. Wu, C.P. and V. Galindo, "Properties of a Phased Array of Rectangular Waveguides with Thin Walls" IEEE Trans. Antennas and Propagation, AP-14, No. 2, March 1966, pp.163-172.

9. Galindo, V. and C.P. Wu, "Numerical Solutions for an Infinite Phased Array of Rectangular Waveguides with Thick Walls," IEEE Trans. Antennas and Propagation, AP-14, No. 2, March 1966, pp. 149-158

10. Amitay, N., V. Galindo, and C.P. Wu, The Theory and Analysis of Phased Array Antennas, Wiley, New York, C1972, p.208

11. Diamond, B.L., "Resonance Phenomena in Waveguide Arrays," Proc. PTGAP International Symposium, Ann Arbor, Mich., October 1967, pp.110 - 115.

12. Seckelmann, R., "Propagation of TE Modes in Dielectric Loaded Waveguides," IEEE Trans Microwave Theory and Techniques, MTT-14, No. 11, November 1966, pp. 518 - 527.

13. Tsandoulas, G.N., D.H. Temme, and F.G. Willwerth, "Longitudinal Section Mode Analysis of Dielectrically Loaded Rectangular Waveguides with Application to Phase Shifter Design," IEEE Trans Microwave Theory and Techniques, MTT-18, No. 2, February 1970, pp.88-95.

REFERENCES (cont.)

14. Findakly, T.K. and H.M. Haskal, "On the Design of Dielectric Loaded Waveguides," IEEE Trans Microwave Theory and Techniques, MTT-24, No. 1, January 1976, pp.39 - 43

15. Collin, R.E., Field Theory of Guided Waves, McGraw-Hill, New York, 1960.

16. Lecture Notes for Microwave Journal Intensive Course in Practical Phased Array Systems, Lecture 4.

METRIC SYSTEM

BASE UNITS:

Quantity	Unit	SI Symbol	Formula
length	metre	m	...
mass	kilogram	kg	...
time	second	s	..
electric current	ampere	A	...
thermodynamic temperature	kelvin	K	...
amount of substance	mole	mol	..
luminous intensity	candela	cd	..

SUPPLEMENTARY UNITS:

plane angle	radian	rad	...
solid angle	steradian	sr	. .

DERIVED UNITS:

Acceleration	metre per second squared	.	m/s
activity (of a radioactive source)	disintegration per second		(disintegration)/s
angular acceleration	radian per second squared	...	rad/s
angular velocity	radian per second	.	rad/s
area	square metre	.	m
density	kilogram per cubic metre		kg/m
electric capacitance	farad	F	A·s/V
electrical conductance	siemens	S	A/V
electric field strength	volt per metre		V/m
electric inductance	henry	H	V·s/A
electric potential difference	volt	V	W/A
electric resistance	ohm		V/A
electromotive force	volt	V	W/A
energy	joule	J	N·m
entropy	joule per kelvin	...	J/K
force	newton	N	kg·m/s
frequency	hertz	Hz	(cycle)/s
illuminance	lux	lx	lm/m
luminance	candela per square metre	..	cd/m
luminous flux	lumen	lm	cd·sr
magnetic field strength	ampere per metre		A/m
magnetic flux	weber	Wb	V·s
magnetic flux density	tesla	T	Wb/m
magnetomotive force	ampere	A	.
power	watt	W	J/s
pressure	pascal	Pa	N/m
quantity of electricity	coulomb	C	A·s
quantity of heat	joule	J	N·m
radiant intensity	watt per steradian	.	W/sr
specific heat	joule per kilogram-kelvin	.	J/kg·K
stress	pascal	Pa	N/m
thermal conductivity	watt per metre-kelvin	..	W/m·K
velocity	metre per second	...	m/s
viscosity, dynamic	pascal-second		Pa·s
viscosity, kinematic	square metre per second	..	m/s
voltage	volt	V	W/A
volume	cubic metre		m
wavenumber	reciprocal metre	..	(wave)/m
work	joule	J	N·m

SI PREFIXES:

Multiplication Factors	Prefix	SI Symbol
1 000 000 000 000 = 10^{12}	tera	T
1 000 000 000 = 10^{9}	giga	G
1 000 000 = 10^{6}	mega	M
1 000 = 10^{3}	kilo	k
100 = 10^{2}	hecto*	h
10 = 10^{1}	deka*	da
0.1 = 10^{-1}	deci*	d
0.01 = 10^{-2}	centi*	c
0.001 = 10^{-3}	milli	m
0.000 001 = 10^{-6}	micro	μ
0.000 000 001 = 10^{-9}	nano	n
0.000 000 000 001 = 10^{-12}	pico	p
0.000 000 000 000 001 = 10^{-15}	femto	f
0.000 000 000 000 000 001 = 10^{-18}	atto	a

* To be avoided where possible